Anthropogenic impacts on convective storms over the South African Highveld

H Havenga

orcid.org/0000-0002-9238-0295

Thesis accepted in fulfilment of the requirements for the degree *Doctor of Philosophy in Science with Environmental Sciences* at the North-West University

Promoter:	Prof RP Burger
Co-promoter:	Prof SJ Piketh

Graduation May 2022

22743529

Whether I dedicate this to weather,
or whether I dedicate this to whatever,
only time will tell whether studying the weather,
was worth it or not.

Abstract

Convective events over the South African Highveld are a frequent and often dangerous summer weather phenomenon. Features such as aerosols, land-use, and thermodynamics, which humans can unintentionally modify, change the nature of convective events. Radar data indicates that convective weather has a strong diurnal signal. The Highveld experiences the most severe convective weather in the late afternoon, and November has the highest number convective events. Media reports indicate that rainfall is the most impactful convective weather event over the region followed by hail. The number of reported heavy rainfall events suggests an increase in frequency of these events from the 1980's, while hail reports for the same time have remained fairly consistent. Objective clustering methods indicate that both events are directly linked to characteristic mid- and early summer circulation patterns respectively. During mid-summer, tropical systems displace the westerlies and rainfall is the most significant event. During early summer, the presence of the westerlies at 500 hPa enhances conditional instability and wind shear, and favours hail formation. Simulations show that under high CCN loads, storms are less severe and less hail and precipitation reaches the surface. A high CCN environment results in a persistent stable layer that inhibits convection. A green city scenario simulates the most severe convective storms with the highest persistent CAPE and accumulated hail. Increased latent heat and local moisture could enhance precipitation processes under this scenario. Under low vegetation scenarios, there is a decrease in surface hail and rainfall and events are characteristics of tropical, short-lived, isolated thunderstorms. Trends show that the Highveld is favouring tropical circulation types more frequently. The thermodynamic environment shows signs of increasing instability and decreasing wind shear, characteristic of tropical storms. These observed changes are consistent with current projections of anthropogenic climate change.

Keywords: *numerical weather prediction, severe weather, convective permitting modelling, weather modification*

Contents

		Page
Contents		**I**
List of Figures		**III**
List of Tables		**VII**
List of Abbreviations		**VIII**
Preface		**XIII**
1	**Introduction and literature review**	**2**
	Defining convective weather events	5
	Climatology of significant convective weather in South Africa	10
	Atmospheric aerosols	14
	Numerical weather prediction in cloud-aerosol research	26
	Cloud-aerosol applications in weather modification	29
	Local-scale urban heat island effects	31
	Aims and objectives	32
2	**Data and methods**	**34**
	The Highveld region	34
	Weather and climate data	35
	WRF configuration and setup	50
	Limitations of the study	55
	Conclusion	58
3	**The nature of convective weather events over the Highveld**	**59**
	Introduction	59
	Radar derived convective storm characteristics	59
	Diurnal characteristics of radar observed convective events	63
	Cumulus characteristics during the summer	65
	Radar derived precipitation characteristics	70
	Conclusion	76
4	**The significance of convective weather events**	**77**
	Introduction	77
	Overview of significant weather in Highveld	78
	An analysis of convective storm reports	80
	Conclusion	84
5	**The synoptic and thermodynamic environment of significant convective weather events**	**85**
	Introduction	85
	Severe storm environments	85
	Synoptic environments favouring significant events	87
	Objective clustering of synoptic patterns associated with significant events	95

Thermodynamic conditions associated with significant events 104
Wind profile of significant events 108
Conclusion 115
6 Small scale impacts on radar derived convective events 117
Introduction 117
Spatio-temporal characteristics of convective storms 118
Impacts of topography and land-use on convective storms 120
Conclusion 139
7 CCN and land-use impacts on convective weather 142
Introduction 142
Case study overview 143
Simulation results 152
Changes to the local thermodynamic environment 163
Future convective environments over urban Gauteng 169
Conclusion 171
8 Summary and conclusions 173
References 178
Appendix 196

List of Figures

Page

1.1 The global risk landscape . . . 3
1.2 The relationship between hail probability and observational area . . . 4
1.3 Urban sprawl in Johannesburg, Gauteng, from 2001 to 2017 . . . 5
1.4 The characteristic time and space scales of weather events . . . 7
1.5 Spatio-temporal uncertainties of Extreme Event Attribution . . . 11
1.6 Circulation types over South-Africa . . . 12
1.7 Density of thunderstorm and hail events over South-Africa . . . 13
1.8 Continental and maritime clouds characteristics . . . 16
1.9 Vapour pressure curve . . . 19
1.10 The thermodynamic evolution in clean and polluted environments . . . 20
1.11 Rainfall pathways in pristine and polluted environments . . . 21
1.12 Components of radiative forcings . . . 23
1.13 Highveld CCN concentrations . . . 25
1.14 The parameterisation of cloud microphysics . . . 26
1.15 Droplet concentration in modelled clean and polluted environments . . . 28
1.16 Future convective storm scenarios . . . 29
1.17 The heat island over Johannesburg . . . 32

2.1 Study area: the Highveld . . . 35
2.2 SAWS infrastructure . . . 36
2.3 SAWS stations within the Irene Radar range . . . 37
2.4 Stations with publicly available data . . . 38
2.5 Stations with publicly available data in the Irene Radar range . . . 39
2.6 Radiosonde data availability from the IGRA . . . 40
2.7 Number of valid soundings for coinciding severe storm reports . . . 41
2.8 IGRA sounding availability in South-Africa . . . 42
2.9 SANLC and reclassified land cover maps . . . 50
2.10 Topography characteristics in the radar radius . . . 51
2.11 WRF Domains . . . 56

3.1 Convective storms frequency by month . . . 61
3.2 Relative monthly occurrence of convective events by mean reflectivity . . . 62
3.3 Relative monthly occurrence of convective events by maximum reflectivity . . . 63
3.4 Convective storms frequency by hour . . . 64
3.5 Monthly and diurnal characteristics of events over 35dBZ . . . 64
3.6 Cloud base, top and dBZ correlation . . . 65
3.7 NDJFM cloud base diurnal characteristics . . . 66
3.8 NDJFM cloud top diurnal characteristics . . . 67

3.9 The size distribution of radar-derived events . . . 67
3.10 NDJFM mean storm motion . . . 69
3.11 Cloud structure, precipitation and dBZ correlation . . . 70
3.12 The probability distribution of radar-derived rain rates . . . 71
3.13 Radar-derived precipitation rates . . . 72
3.14 Rain rate and cloud top correlation plot . . . 72
3.15 Frequency distribution of extreme convective events . . . 74
3.16 The mean size of extreme convective events . . . 75
3.17 Hail mass aloft and cloud top box and whiskers plot . . . 75
3.18 Rain rate and cloud top box and whiskers plot . . . 76

4.1 Weather reports in South-Africa from 1647 to 2018 . . . 78
4.2 Weather reports over the Highveld . . . 79
4.3 Monthly occurance of severe weather . . . 79
4.4 Cost of significant weather as documented in media . . . 80
4.5 Frequency of severe and non-severe convective events . . . 81
4.6 Monthy reports of convective weather events . . . 82
4.7 Hail and flash flood occurrences . . . 82
4.8 Number of hail and rainfall reports per decade . . . 83
4.9 Number of hail and rainfall reports per year . . . 83

5.1 The integration of observations . . . 86
5.2 ERA5 synoptic conditions associated with severe hail reports . . . 90
5.3 ERA5 synoptic conditions associated with severe rain reports . . . 91
5.4 ERA5 synoptic conditions associated with severe thunderstorm reports . . . 92
5.5 ERA5 synoptic conditions associated with severe lightning reports . . . 93
5.6 ERA5 synoptic conditions associated with severe tornado reports . . . 94
5.7 Synoptic conditions under which all significant convective events occur in . . . 96
5.8 Synoptic conditions under which significant hail events occur in . . . 98
5.9 Synoptic conditions under which significant rain events occur in . . . 99
5.10 Synoptic conditions under which significant thunderstorm events occur in . . . 100
5.11 Synoptic conditions under which significant lightning events occur in . . . 102
5.12 Synoptic conditions under which significant tornado events occur in . . . 103
5.13 IGRA profiles associated with convective weather reports, by month . . . 105
5.14 IGRA profiles associated with convective weather reports by event type . . . 106
5.15 Temperature at 500 hPa for reported severe events . . . 107
5.16 Wind speed and direction from reported events by month . . . 110
5.17 Wind speed and direction from reported events by event . . . 113
5.18 Bulk wind shear for reported severe convective events . . . 115
5.19 CAPE/Wind shear relationship for reported severe convective events . . . 115

6.2 Density of storms within the Irene radar range . . . 118
6.3 Density of storms within the Irene radar range, by month . . . 119
6.4 Density of storms over surface differentiating elevations . . . 120

6.5 Complex and simple terrain profiles of Pilanesberg and Legonyane 121
6.6 Observed dBZ characteristics over complex vs simple terrain 122
6.7 Cloud characteristics over complex vs simple terrain 122
6.8 Lightning characteristics over complex vs simple terrain 123
6.9 Orographic profile east and west of the Magaliesberg mountain 124
6.10 Orographically induced cloud characteristics between two regions 125
6.11 Orographic effect on storm intensity 126
6.12 Lightning activity along an orographic feature 126
6.13 Radar data points per category 127
6.14 Land-use characteristics in the radar radius 128
6.15 Urban elevation profile 129
6.16 SANLC categories in the urban analysis 129
6.17 Cloud top height in Johannesburg and surrounding areas 130
6.18 Reflectivity characteristics in Johannesburg and surrounding areas 130
6.19 Rain rate characteristics in Johannesburg and surrounding areas 131
6.20 Lightning activity in Johannesburg and surrounding areas 132
6.21 Cloud top height in and around informal settlements 133
6.22 Reflectivity characteristics in and around informal settlements 134
6.23 Rain rate characteristics in and around informal settlements 134
6.24 Lightning activity in and around informal settlements 135
6.25 Cloud top height in and around industrial complex 136
6.26 Reflectivity characteristics in and around industrial complex 137
6.27 Mean wind direction and speed 137
6.28 Rain rate characteristics in and around industrial complex 138
6.29 Lightning activity in and around industrial complex 139

7.1 28/11/2013 Observational data: Synoptic analysis 145
7.2 28/11/2013 Observational data: Thermodynamic analysis 147
7.3 28/11/2013 Observational data: SAWS surface station data 147
7.4 28/11/2013 Observational data: Radar derived cloud and wind characteristics . 149
7.5 28/11/2013 Observational data: Radar data for 0500-1300 SAST 150
7.6 28/11/2013 Observational data: Radar data for 1400-2200 SAST 151
7.7 28/11/2013 Observational data: Weak eco region 152
7.8 28/11/2013 WRF control run: Synoptic scale simulation 153
7.9 28/11/2013 WRF control run: SkewT analysis 154
7.10 28/11/2013 WRF control run: Radar and cloud cross sections 155
7.11 28/11/2013 WRF results: modified land-use parameters 156
7.12 Land cover differences in an urban and township area in Johannesburg 158
7.13 28/11/2013 WRF results: Reflectivity 159
7.14 28/11/2013 WRF results: Rain number concentration 160
7.15 28/11/2013 WRF results: Ice number concentration 161
7.16 28/11/2013 WRF results: Simulated hail 162
7.17 28/11/2013 WRF results: Simulated accumulated rainfall and hail 163

7.18 1000 UTC Simulated thermodynamic profile 165
7.19 1200 UTC Simulated thermodynamic profile 166
7.20 1400 UTC Simulated thermodynamic profile 167
7.21 1600 UTC Simulated thermodynamic profile 168
7.22 Trends of selected radiosonde variables 170

List of Tables

Page

1.1 Orlanski (1975)'s scales of the atmosphere 8

2.1 Weather reports from in the Highveld with valid radiosonde soundings 41
2.2 SANCL land-use dataset categories 1-37 48
2.3 SANCL land-use dataset categories 38-73 49
2.4 WRF configuration 52
2.5 WRF case study modifications 55
2.6 MODIS 21 class land-use categories 57

5.1 The mean of convective parameters during severe reports by month 104
5.2 The mean observed convective parameters during severe reports by event 106

List of Abbreviations

AER Aerosol Modified Simulation Run. 155–157, 160–168, 171

AERONET Aerosol Robotic Network. 22

AOD Aerosol Optical Depth. 22

ARREX Aerosol Recirculation and Rainfall Experiment. 16, 24, 25, 54

ATC Air Traffic Control. 61

AVHRR Advanced Very High RadiometeR. 30

AWS Automatic Weather Stations. 9, 35, 143

BC Black Carbon. 22, 24, 27, 54

CALIPSO Cloud-Aerosol Lidar and Infrared Pathfinder Satellite Observations. 22

CAPE Convective Available Potential Energy. 14, 18, 40, 46, 86–93, 95, 104–107, 114–116, 145–147, 153, 154, 164–171

CBD City Central Business District. 46, 47, 176

CCN Cloud Condensation Nuclei. 3, 4, 14–19, 22, 24, 25, 27, 30–34, 54, 55, 58, 135, 137, 138, 142–144, 152, 154, 155, 157–165, 167–169, 171–173, 176, 177

CHIRPS Climate Hazards Group Infrared Precipitation with Station dataset. 9

CIN Convective Inhibition. 17, 86, 104, 146, 164, 175

CMORPH Climate Prediction Center Morphing Method. 9

CNTRL Control Simulation Run. 155, 157, 160, 161

COSMO Consortium for Small-scale Modeling. 143

CP Convective Parameters. 39, 104–107, 169, 175

CPM Convective Permitting Models. 4, 6, 8–10, 26, 29, 33, 51, 142, 143

dBZ Decibels Relative to Z. 5, 42, 43, 56, 60–68, 70–74, 76, 117, 120–124, 126, 129, 130, 133, 134, 136, 147, 148, 150, 151, 157, 158, 176

DJF December, January and February. 14

DNS Directed Numerical Simulation. 9

EARLINET European Aerosol Research Lidar Network. 22

ECMWF European Centre for Medium-Range Weather Forecasts. 45, 52

EEA Extreme Event Attribution. 10, 11

ENSO El Niño-Southern Oscillation. 87

EUR Euro. 6

FOKR Foote Kraus Index. 73, 74, 76, 148

GCM Global Circulation Models. 6–11, 50

GFS Global Forecasting System. 8

GHCN Global Historical Climate Network Daily. 35–38

GISTEMP GISS Surface Temperature Analysis. 37

GOCART Goddard Chemistry Aerosol Radiation and Transport. 27, 54

GRNCITY Green City Simulation Run. 55, 155, 157–168, 171

GSOD Global Surface Summary of the Day. 35, 36, 38

HDF Hail Day Frequency. 12

HI High-Impact Weather. 6

ICN Ice Condensation Nuclei. 4, 14, 15, 19, 22, 24, 25, 27, 30, 31, 54

IGRA Integrated Global Radiosonde Archive. 35–39, 42, 85, 115, 173

IMERG Integrated Multisatellite Retrievals for GPM. 9

IPCC Intergovernmental Panel on Climate Change. 22, 23, 25

IR Infrared. 144, 153

ISS International Space Station. 43, 60, 61, 63, 64, 121, 123, 124, 132, 134, 135, 139

ITCZ Inter-Tropical Convergence Zone. 11, 14, 18, 87, 95–97, 104, 110, 119, 144, 145

LAI Leaf Area Index. 55, 156–158

LCL Lifting Condensation Level. 17, 40, 104–106, 146

LES Large Eddy Simulations. 9

LFC Level of Free Convection. 17, 40, 104–106

LiDAR Light Detection and Ranging. 22

LIS Lightning Imaging Sensor. 43, 58, 60, 61, 64, 121, 123, 134, 135, 139

LSM Land Surface Model. 52, 53

LWC Liquid Water Content. 27, 28

MCC Mesoscale Convective Complex. 6, 8, 45, 68, 170

METROMEX Metropolitan Meteorological Experiment. 4, 31, 32, 46, 143

MetUM Met Office Unified Model. 9, 143

MODIS Moderate Resolution Imaging Spectroradiometer. 22, 47, 52–54, 56

MPLNET NASA Micro Pulse Lidar Network. 22

MSLP Mean Sea Level Pressure. 36, 46, 87, 95, 115, 144, 153

MVD Median Volume Diameter. 27, 28

N_c Number Concentration. 16, 22, 24, 25, 27, 28, 52, 54, 154, 157, 159–161, 169

NASA National Aeronautics and Space Administration. 37

NCAR National Center for Atmospheric Research. 51, 52

NDJFM November, December, January, February, and March. 40, 43, 46, 64–66, 68, 70, 71, 74, 84, 85, 87, 89, 104–108, 111, 114, 118, 121, 123, 126, 128, 132, 135, 139, 169

NOAA National Oceanic and Atmospheric Administration. 8, 35, 38, 146

NRL Naval Research Laboratory. 30

NWP Numerical Weather Prediction. 4, 6–9, 17, 22, 25–28, 31, 33, 41, 42, 58, 86, 140, 142, 169, 172

NWU North-West University. 51

PBL Planetary Boundary Layer. 9, 51, 54, 136, 166

PCA Principle Component Analysis. 46, 87, 95, 97, 101, 103, 116

PHIPS Particle Habit Imaging and Polar Scattering Probe. 8

POAM Polar Ozone and Aerosol Measurement. 30

POLCITY Polluted City Simulation Run. 54, 55, 155, 156, 158–165, 167, 169

QC Quality Control. 39, 40, 45

RCM Regional Climate Models. 6, 8, 9, 85

RH Relative Humidity. 17–19

RRTMG Rapid Radiative Transfer Model Global. 52

SA South Africa. 2, 3, 8–14, 16, 18, 20, 24, 25, 29, 32–36, 40, 42–48, 50–52, 60, 71, 78, 84, 87–92, 95–101, 114, 117, 122, 123, 142–145, 156–158, 173

SAFARI-2000 Southern African Regional Science Initiative. 24, 25, 54, 55

SANLC South African National Land-Cover. 46, 47, 50, 57, 126, 129, 132, 139

SAST South African Standard Time. 63, 64, 68, 71, 144, 146, 147, 150–152, 162

SAWS South-African Weather Service. 9, 34–38, 42–44, 63, 65, 78, 146

SCP Supercell Composite Parameter. 146

SHIP Significant Hail Parameter. 146

SOI Southern Oscillation Index. 87

SOMs Self Organizing Maps. 14, 95

SON September, October and November. 14

SRH Storm Relative Helicity. 145–147

SSA Single-Scattering Albedo. 22

SSS Storm-Structure-Severity. 73, 148

SST Sea Surface Temperature. 35

STP Significant Tornado Parameter. 146

TAMSAT Tropical Applications of Meteorology using Satellite and Ground-Based Observations. 9

TC Tropical Cyclone. 6, 11

TITAN Thunderstorm Identification Tracking Analysis and Now Casting. 42, 43, 59, 146

TRMM Tropical Rainfall Measurement Mission. 43, 60, 61, 63, 64, 121, 123, 124, 132, 134, 135, 139

TTT Tropical Temperate Trough. 86, 89, 93, 95–101, 118, 119, 144, 145, 175

UHI Urban Heat Island. 3, 10, 31, 32, 46, 55, 155, 156, 158, 164, 167, 169, 176

USA United States of America. 4, 9, 13, 14, 27–29, 46, 61, 77, 88, 106, 146

UTC Coordinated Universal Time. 38, 40, 52, 63–66, 68, 71, 76, 122, 123, 144, 146–149, 152–154, 157, 160–168, 174

VIL Vertically Integrated Liquid. 148

WEF World Economic Forum. 2, 3, 5

WER Weak Echo Region. 148, 152, 154

WO Weather Office. 36

WPS WRF Pre-Processing System. 52, 53

WRF The Weather Research and Forecasting Model. 4, 24, 27, 28, 34, 50–56, 58, 142–144, 152–154, 156, 157, 159, 173, 176

WRF-Chem The Weather Research and Forecasting Model Coupled with Chemistry. 26

ZAR South-African Rand. 6, 45, 79, 80, 96, 143, 148, 174

Preface

The South-African Highveld arguably has the finest winters in the world. It's location beneath the descending leg of the Hadley cell means that a very characteristic continental high-pressure prevails for much of April to August. While the nights are cool to cold, with temperatures dipping slightly below freezing on some occasions, the days are perfect. Mild temperatures, clear blue skies, and no winds. On most days jeans and a t-shirt will do in the noon. Nevertheless, these fine conditions do not last. With the onset of summer in October, cumulus clouds become an ever-present sight in the afternoon. Initially, these are not very threatening, but as November comes along, cumulus clouds very quickly become cumulus *mediocris*, and then cumulus *congestus*, and on any given day, residents of the area can start to see something ominous developing on the horizon as the mighty and powerful cumulonimbus clouds start thundering in the distance. Those unprepared, and unaware, in the path of this mighty cumulonimbus cloud will soon be exposed to nature's most dramatic theatre.

A snippet of my 3-minute thesis talk for our faculty in 2019. The scene is dramatic, but I got second place...

It's November, and summer has commenced. The sun rises over the Highveld, it's a warm morning, and the sky is blue, blue as only the African sky can be. The air is calm, and the atmosphere is stable. A farmer looks in the distance. He can sense what's coming. He's sensed it before. He says a prayer and starts his day. Hoping to be spared. In Johannesburg, a businessman sits in traffic. It's 8 am, and the weather report comes on the radio. The South- African Weather Service has issued a warning. Thunderstorms are expected in the afternoon, with a high chance of hail, lightning and flash floods. He looks at the blue sky and forgets it. The day passes.

Around 4 pm, winds and rains shake the farmhouse! The thunder is deafening! Within twenty minutes, the storm has passed. This time, the farmer was spared. Good rains for the fields, he thinks. The storm reaches Johannesburg an hour later. Its rush hour! The storm grows! Rainfall gushes on the paved roads with nowhere to go! Water rises rapidly! Large hail begins to fall! No structure is spared! Our businessman cannot leave the office. The city is in chaos.

I find it fascinating that the term *Holism* was defined by a South African, Jan Smuts, nearly 100 years ago (Smuts, 1926). In the most basic terms, Holism tells that the whole is greater than the sum of its parts. In this study, we attempted to analyse some complex parts of such a complex system that my final answer to the finding on *"what man's impact is"*, is that *I don't know*. It would be foolish to admit otherwise or pretend that I found some secret to severe weather that has eluded people much smarter than me over the last however many years. But is this reason to despair? To give up to the notion of the absurd, that we can never really know, and what does knowledge even matter? No dear reader. This is exciting. The absurd is terrific and gives me meaning to pursue the seemingly *unpersueable*, because why not? We have nothing to lose so. We might as well try.

I wonder if I'm like those who see faces in random objects, rock formations, clouds... However, in my case, the face is a pattern. Am I? Are we, as scientists, looking for patterns in chaos when there is none? This question boggles me on a deep level. Is it easier to simplify a problem to an easy, explainable theory, or are we too scared to admit the role of chaos and dumb luck? No two clouds are the same. No two cities are the same. No two square millimetres of the earth are the same... I wonder if I look for a correlation, a pattern because admitting there might not be one goes against all scientific ethos (Nature, 2019; Nuzzo, 2014; Wasserstein et al., 2019).

Driving back from Johannesburg this morning, I heard the weather forecast on SAFM. One word comes up frequently today, *isolated*. Consider the word *isolated* when Gauteng is 18176 km^2, Mpumalanga 76485 km^2, Limpopo 125775km^2, North-West 104882 km^2, Free-State 129825 km^2, Northern Cape 372889 km^2, and KwaZulu-Natal 94361 km^2. The uncertainty of thunderstorm prediction remains one of the most challenging meteorological exercises to this day.

The above-mentioned provinces all had a chance of thunderstorms today and the parts of regional forecast from by the SA Weather Service reads as follows:

"**THE REGIONAL WEATHER FORECAST FOR TODAY: 2021-03-23 ISSUED AT 05:00 SAST BY THE SOUTH AFRICAN WEATHER SERVICE. THIS FORECAST WILL BE UPDATED AT 16:00 SAST.**

1. GAUTENG: Partly cloudy and warm with isolated showers and thundershowers.

2. MPUMALANGA: Cloudy in the east with drizzle and fog along the escarpment, otherwise partly cloudy and warm with isolated afternoon showers and thundershowers.

3. LIMPOPO: Cloudy in the east with drizzle and fog along the escarpment, otherwise partly cloudy and warm with isolated showers and thundershowers.

4. NORTH-WEST PROVINCE: Fine and warm, becoming partly cloudy in the afternoon with showers and thundershowers.

5. FREE STATE: Fine and warm, becoming partly cloudy in the late afternoon with showers and thundershowers in the northern parts.

6. NORTHERN CAPE: Fine and warm, becoming partly cloudy in the afternoon with showers and thundershowers except the west and south.

...

10. KWAZULU-NATAL: Cloudy with isolated afternoon showers and thundershowers except in the afternoon."

So everyone, continue with your current work. This isn't an exact science so, we have to wait and see what the meteorologist tells us. They're a bit uncertain where the storms will be. - An engineer on weather

I was lucky to be part of the CU Boulder Aerospace Engineering team during the **TORUS** project (Targeted Observation by Radars and UAS of Supercells) in 2019. This is a memorable quote to the engineering students by one of the head engineers after sitting in a morning weather briefing in Colby, Kansas. Frew et al. (2020) provides an overview of the team that I was part of and the work we did. A special thanks here to the whole CU Boulder team. I made lifelong friends and lived the dream of so many other weather enthusiasts while doing ground-breaking science. See below for some pictures of the campaign.

Figure 1: *Some instruments that were used during the TORUS campaign. From the top left NOAA mobile mesonet, some cumulonimbus clouds and me holding the RAAVEN UAS developed by CU Boulder, NOAA Nexrad Real-Time Radar Data, University of Nebraska Lincoln Mobile Mesonet. Bottom left NOAA P3 manned aircraft, and Oklahoma State university mobile mesonet, LIDAR and Radiosonde vehicle. Photos Henno Havenga*

I was also lucky to visit the University of North Dakota and join Dr David Dalene on the Naval Research Laboratory (NRL) project. During this time, I was exposed to the fantastic team at Weather Modification International (WMI), the extraordinary Dr Martin Schnaiter, and his wife, Dr Emma Järvinen. We kitted WMI's Lear Jet and flew in thunderstorm anvils in Titusville, Florida to characterise ice crystals in these anvils. This was quite the experience and not for the faint-hearted. David allowed me to stay in his house, drink all his coffee, taught me how to set up a jet full of instruments, and see cumulonimbus clouds as few ever do. Martin and Emma, who build the excellent PHIPS instrument, taught me much about cloud-ice processes over many converstations after successful flights in Florida.

Figure 2: *These pictures were taken during the preparation of the CAPE FIELD EXPERIMENTS (CAPEX2019). Top left, in Fargo, North Dakota, while preparing the WMI Lear Jet for the project. Top centre, on the way to Florida, we see towering cumulus clouds in the distance. Top right, myself during a flight, making sure all data streams come in as we expect. Bottom, getting ready for deployment with cumulonimbus visible in the background.*

Parts of this thesis has been presented in various forms over the last four years, and I am lucky to have two publications with me as a co-author. Numerous other publications have visualisations and data analysis I assisted in creating, however, these were on the basis of good faith and do not carry my name in any way or form. The following is a brief list of publications and peer reviewed conference proceedings during my time as a graduate student:

- Havenga, H., Burger, R.P, Piketh, S.J. and Botha, G. 2021. Severe convective storm characteristics under varied urbanization scenarios. South-African Atmospheric Society Annual Conference. Virtual Conference. (2nd place, best student presentation)
- Botha, G., Burger, R., and Havenga, H. 2021. Improving radar-derived Spatio-temporal characterisation of particulate matter plumes using weather radar observations. South-African Atmospheric Society Annual Conference. Virtual Conference.
- Sokhi, R.S., Singh, V., Querol, X., Finardi, S., Targino, A.C., de Fatima Andrade, M., Pavlovic, R., Garland, R.M., Massagué, J., Kong, S. Baklanov, A., Havenga, H. et al. 2021. A global observational analysis to understand changes in air quality during exceptionally low anthropogenic emission conditions. Environment international, 157, p.106818.
- Frew, E.W., Argrow, B., Borenstein, S., Swenson, S., Hirst, C.A., Havenga, H. and Houston, A. 2020. Field observation of tornadic supercells by multiple autonomous fixed-wing unmanned aircraft. Journal of Field Robotics, 37(6), pp.1077-1093.
- Botha, G., Burger R., and Havenga H. 2020. Improving radar-derived rainfall estimates for extreme events on the South African Highveld. South-African Atmospheric Society

Annual Conference. COVID19, Virtual Conference.

- Havenga, H., Burger, R.P. and Piketh S.J. 2019. Exploring Unintended Anthropogenic Impacts On Severe Weather over the South African Highveld. European Geosciences Union General Meeting. Vienna, Austria.
- Davies, S., Burger, R.P. and Havenga, H. 2018. The Evaluation of Thermodynamic Indices and Thunderstorm Occurrences over Gauteng South Africa. Society of South African Geographers Annual Conference 2018.
- Havenga, H., Burger, R.P. and Piketh S.J. 2018. The Trends of Thermodynamic Indices over Irene, Gauteng. South-African Atmospheric Society Annual Conference. Durban, South-Africa.

There are people in my life that deserve a special mention. My supervisors, Prof Roelof and Prof Stuart, who made everything possible. When I went to Roelof's office during the honours selection process and asked if I can do my honours under them, he asked me if I know what Linux is, and I replied, "a computer game?". He was happy enough, and here we are seven years later. Roelof and Stuart introduced me to everyone in their field without hesitation. Through them, I could travel the world and no amount of thanks will ever be enough. Dr Cindy Bruyere at NCAR, who allowed me to run WRF on the Cheyenne system. And most of all, to my family. For just, well, being family, and supporting me to be a student without hesitation or protest for a decade.

This degree is basically a philosophy degree, as the *Ph*D implies, and it has been interesting to think deeply about the problems still faced in our science during this study. My deviation from the traditional preface and the scrabble of thoughts I wrote down should show you how much I grapple with the uncertainty.

When I started this academic journey, I thought that numbers do not lie and that science is an absolute truth. What I did not account for is the assumptions we make in our quantification of the truth, how language (be that the language of physics or the language I write this thesis in) limits me based on the current rules and descriptions, and how hard it is to put this tacit knowledge out there as truth - when I do not know what I do not yet know. I have to acknowledge that I barely scratched the surface of the limitations we face, from assumptions instruments make when taking measurements, to gaps in data that we fill with assumptions, to the assumptions we make to build a general model that is *good enough*. Based on current assumptions. I would not say there is not an objective truth (sorry Nietzsche), but with every PhD or paper, a new question arises, and I hope someone can take this piece of work and ask a new set of questions in the future, bringing us closer to that objective truth.

On the day I finalised this thesis a ridging high-pressure system and well defined tropical trough resulted in an influx of surface moisture over central South-Africa. At 500 hPa, flow was predominantly meridional, enhancing instability and favoring large scale uplift. As I sit here, small hail and heavy rainfall is pouring down. A fitting day.

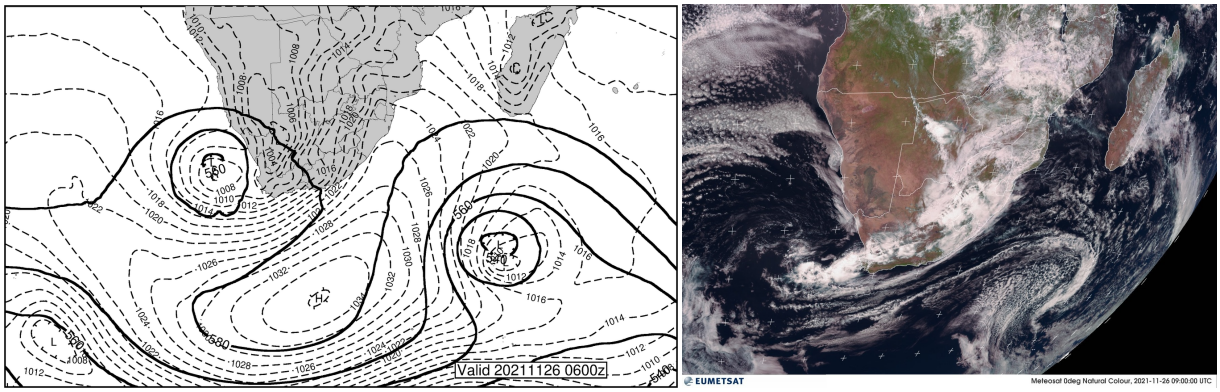

Figure 3: *26 November 2021*

I declare that this thesis has been composed solely by myself and that it has not been submitted in any previous application for a degree. Except where stated otherwise by reference or acknowledgment, the work presented is entirely my own.

Henno Havenga
26 November 2021

"... Bye bye December African rain –
The long gone summer has passed
And I hear the owls calling my name
The firelight has danced it's last
Across your face my friend
And though I love you
I somehow know this is going to be the end
Now the sun has disappeared
And all that remains
An old tin mug and a photograph
So wipe away those tears and remember the good times ..."
– Juluka, December African Rain

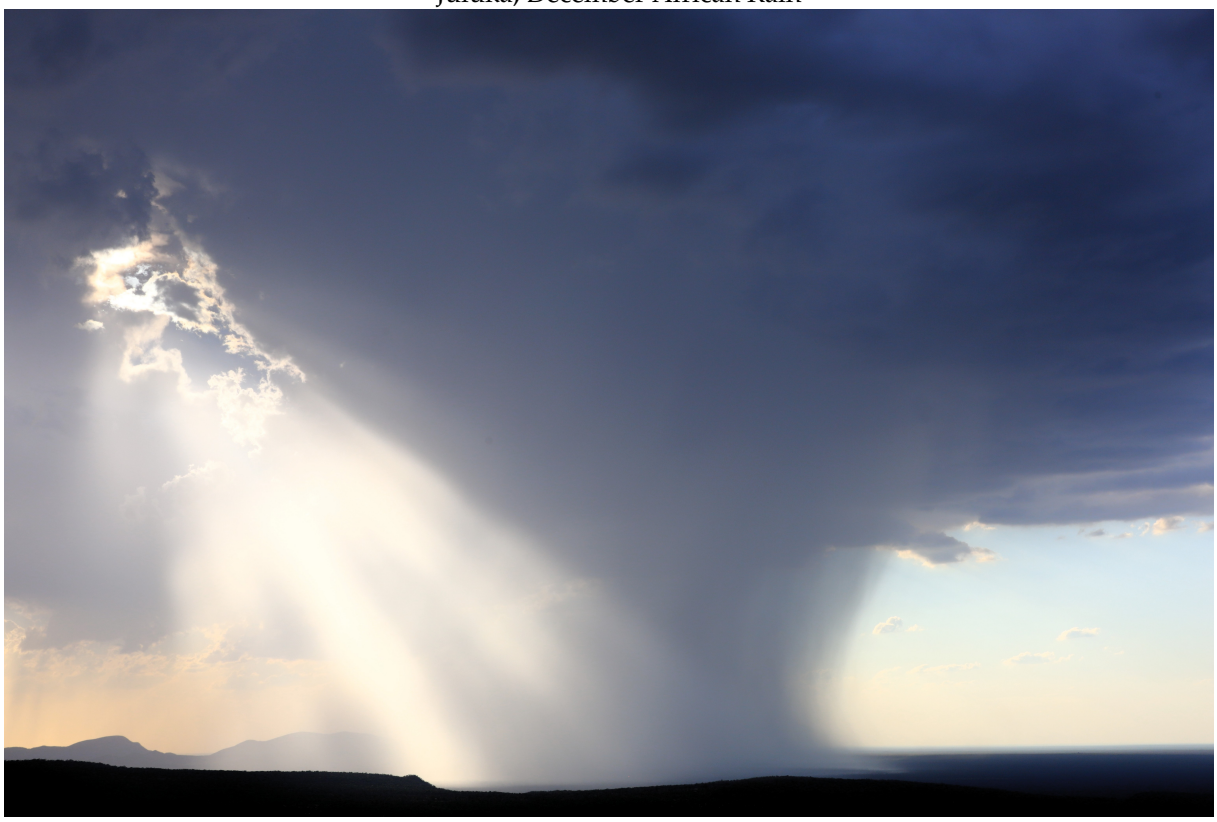

Crepuscular rays shine through an isolated thunderstorm during a summer afternoon.
Photo: Henno Havenga, Marakele National Park, December 2018

Chapter 1
Introduction and literature review

"Extreme weather phenomena has become a daily event"
French President Macron, United Nations General Assembly, 2018

With this documents initial writing, the World Economic Forum (WEF) released its global risk report (WEF, 2018), which paints a picture of the changing challenges we face. While related economic crises dominated in 2008 – 2011, from 2012, the risks posed by nature, climate, and weather have been of more significant concern (Figure 1.1). The WEF defines extreme weather as *"floods and storms"* causing *"major property, infrastructure and environmental damage as well as loss of human life caused by extreme weather events"* (WEF, 2018, Pp.60). As we will detail in the rest of this document, these events are exceptionally hard to predict more than one or two days in advance. In South Africa (SA), we often experience such events in the form of lightning, flash floods, hail and, on rare occasions, tornadoes. What is more worrying is that these events often happen over the Gauteng province, the economic hub of Africa and the most densely populated province in the country. In addition to this, there are legal commitments by the South-African government to conduct risk reduction planning under climate change scenarios as seen in the Drought Management Plan (2005), National Climate Change Adaptation Strategy (2016) and the National Development Plan (2017) (Wright et al., 2021). These factors, which will be discussed in detail later on, enforce the need to understand the impact of significant weather in order to make targeted and deliberate decisions.

Looking at the research conducted by AghaKouchak et al. (2020); Carte and Held (1978); Martins et al. (2017) into the variability of weather events and the fact that there is an increasingly urbanised population in SA and around the world, we can see that we are increasing our exposure to such events (Figure 1.2). This effect is also known as compound or cascading events, according to AghaKouchak et al. (2020). Figure 1.2 by Carte and Held (1978) also provides a good representation of the effect of an increasing area and the likelihood of significant weather exposure. As the size of an occupied area, or development increases, the chances of damage from a storm increases concurrently, a somewhat logical conclusion. What makes the illustration by Carte and Held (1978) so valuable is that the research was done around the Gauteng area, where the population has significantly increased and continues to do so yearly. Consider the satellite image (Figure 1.3) of Alexandra, a settlement in Johannesburg, where we observe a drastic increase in development from 2001 – 2017. Areas that were once farmland are now either residential or industrial complexes. Considering the scale of convective storms (described in detail in later sections), storms that could have passed without any *impact* may now have a high cost associated with human and property loss which would not have been observed before 2001. Martins et al. (2017) observed a similar trend in his examination of hail events in rural Brazil, where the number of reported weather events rose along with increasingly densely populated areas. Considering that the most expensive day for insurances in SA was a hailstorm on 28 November 2013 in Gauteng (Barry, 2014; Cover, 2013; Eliseev, 2013; Rahlaga, 2013; TimesLive, 2013), research into significant convective weather events must be embraced. Studies predict temperature increases over Gauteng, which could favour increasing convective conditions

The global risk landscape (WEF, 2018)

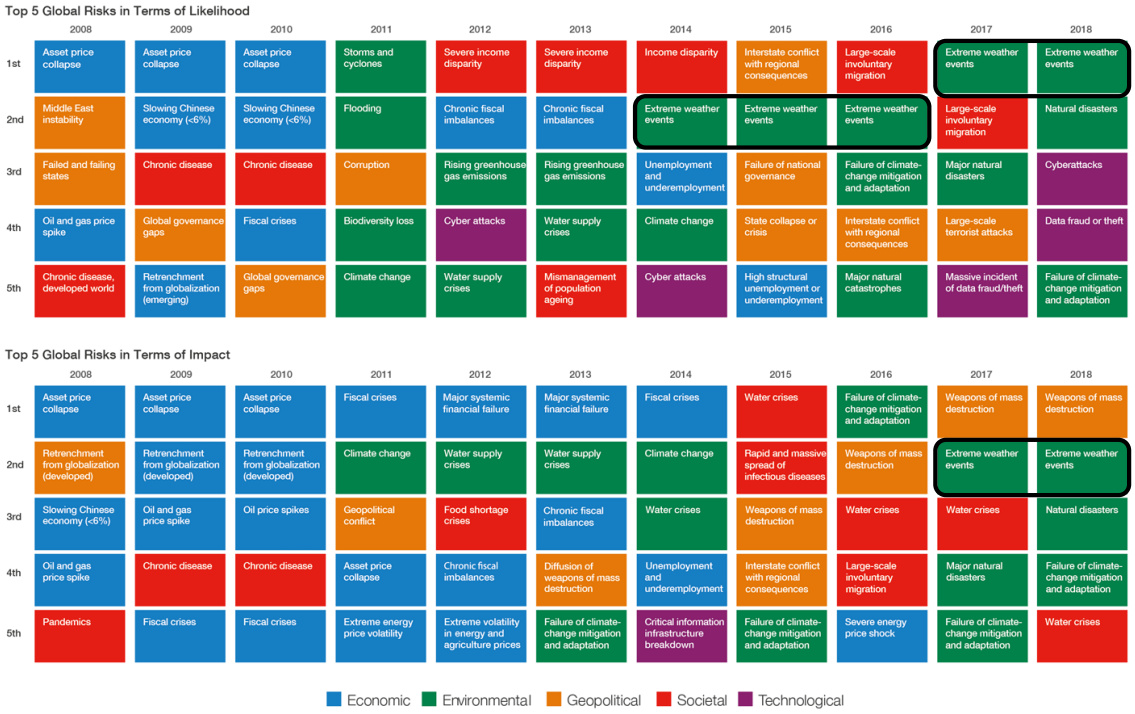

Figure 1.1: *The evolving risk landscape report by WEF (2018) paints a picture of the changing challenges we face. Weather and climate-related risks, highlighted in black, serve as the motivation behind the work done here. Over the last three years, severe weather has become our most important challenge and is likely affected by anthropogenic climate change resulting in a warmer, more convective favourable atmosphere. The most damaging weather events in SA have resulted from convective driven phenomenons such as hail and flash floods.*

(IPCC, 2007; Kruger and Sekele, 2013; Piketh et al., 2014) – possibly indicating that the local risk landscape is similar to the global outlook as depicted by the WEF.

The effects of population growth extend further than that. The increase in aerosols from industries, fires, traffic and domestic fuel burning has implications in cloud-aerosol interactions, cloud condensation nuclei (CCN) properties and precipitation formation (Changnon, 1992a; Changnon et al., 1977; Fan et al., 2018, 2016; Huff, 1973; Kerminen et al., 2018; Kingfield et al., 2018; Liu and Niyogi, 2019; Rosenfeld et al., 2014). Effects like the Urban Heat Island (UHI), soil moisture content and surface albedo are other variables that impact clouds' complex dynamical and physical properties. These features are already poorly understood in the SA, and global context and specific research into them is necessary. Dagan et al. (2016) summarises the impact of urban expansion and aerosol changes under two major themes: 1) global climate change affecting the atmospheric thermodynamic profile, and 2) the growth of the global industry changing the global aerosol budget. This thesis will clarify that these two themes have an interconnected relationship as we attempt to understand convective storms and their characteristics in various spatio-temporal settings, including in urban areas and areas with complex and simple topographies. A new and integrated data assimilation method is needed that accounts for processes on all scales and in the SA context to improve our country's forecasts and modelling capacity.

Hard to predict weather events (driven by convective processes and associated with hail, thunderstorms, flash floods, strong winds and tornadoes in the context of this study) lead to severe damage in a localised area within a short period, and often this impact is most damaging in densely populated cities. However, the cities themselves might impact the storm's physical and dynamical evolution, possibly even enhancing convective processes and precipitation. This question around the impact of urban environments on precipitation processes and storm dynamics is not new. The Metropolitan Meteorological Experiment (METROMEX) field campaigns in St. Louis, MO area were the first major attempt to better understand this effect. The research found an increase in precipitation of up to 25% around a 50 km city radius (Changnon, 1992a; Changnon et al., 1977; Kingfield et al., 2018; Liu and Niyogi, 2019). Most early studies relied on point measurements from rain gauge networks, and while providing accurate measurements, the total rainfall over an urban area could have been underestimated by relying on a spatially isolated rain gauge network (Kingfield et al., 2018). According to Kingfield et al. (2018), new technologies, such as satellite and radar have allowed us to overcome some of these spatial uncertainties, and work around these initial experiments continues till this day in the United States of America (USA). Studies in Houston, TX and Atlanta, GA have found an increase in precipitation in and downwind of urban areas (Kingfield et al., 2018). With recent developments in high-resolution numerical weather prediction (NWP) models, it is possible to simulate convective clouds explicitly and change the aerosol profile to match CCN, ice condensation nuclei (ICN), general pollution, and dust profiles in and around various cities, in order to examine changes in cloud dynamics and microphysics. These advances can help us to better understand the various impacts that might change cloud and rainfall processes on a local-scale.

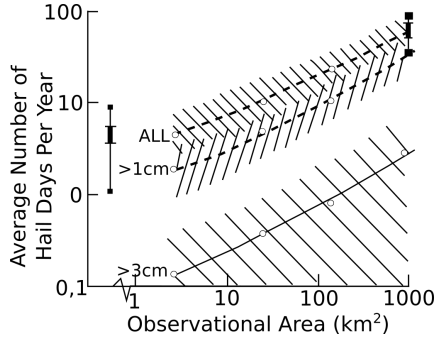

Figure 1.2: *The relationship between hail probability and observational area from Carte and Held (1978) illustrates how the probability of exposure increases with an increasing area.*

Study outline

This introduction is followed by a review of the relevant literature, thereafter the data, methods and limitations of the current study is discussed, followed by the results and discussion. The results attempt to answer the main aim of the thesis: **What are the impacts of CCN and land-use modifications on convective weather events over the Highveld?** The study will use a suite of data and methods, ranging from radar data, media reports, weather stations, reanalysis data and high resolution NWP. More specifically the study will characterise the nature of convective events across scales, the significance to the region, and how storm characteristics vary under different land-use types. Finally a high resolution convective permitting models (CPM) model, The Weather Research and Forecasting Model (WRF), is employed to simulate various urban and CCN modifications to examine changes in storm dynamics.

The premise of this study is to understand the impact that humans might have on convective weather events and subsequently the impact we will experience as a result of changes to these events. However the definition impact itself is complex and subjective. Recent research by

Urban sprawl in Johannesburg, Gauteng from 2001 – 2017

(a) *2001* **(b)** *2017*

Figure 1.3: *The urban sprawl image in Johannesburg, Gauteng from 2001 – 2017 shows the increasing risk exposure faced in areas where events may have had no impact in the past. This is directly related to Figure 1.2 as detailed by Carte and Held (1978) where the exposure to events increases as the observational area increases. Map data: ©2018 Google, Maxar Technologies, Landsat/Copernicus. Images used under Google Earth attribution guidelines. These images can be used purposes such as research, education, film and nonprofit use without needing permission.*

McPhillips et al. (2018) highlights that across the disciplines of Earth science, engineering, social science, and ecology the definition of impact varies widely. McPhillips et al. (2018) found that 27% of papers defined extreme or impactful weather events similar to that of the WEF definition mentioned in the first paragraph, with the addition that these events occur along the extreme end of the normal distribution. The study examines all convective storms with a Decibels Relative to Z(dBZ) ≥ 35 in the radar analysis, but in the synoptic and thermodynamic analysis only significant events are examined. In this context a significant event has to comply with the following criteria, first the event has to be associated with convective activity, i.e. thunderstorm, hail, tornado, lightning and heavy rainfall and it had to be documented. This has several advantages, but also several disadvantages. The advantage is that we examine events that had some anthropogenic impact, and this justifies the explicit use of all events that caused damage or loss of life as this is significant for the public. However, these events might not be dynamically severe events, and herein lies the major disadvantage of this definition. For example, a tornado that occurred over an uninhabited landscape with no impact, or an unusual Highveld snowstorm is not examined. In this regard the definition for a impact/hazard/significant/extreme event in the field of Earth science as defined by McPhillips et al. (2018) is applicable in this study as well, i.e. "a natural event that has the potential for a significant impact on humans, infrastructure, or the environment". It is then valuable to examine one of these impactful events that occurred on the extreme event of the normal distribution, and how small scale changes could alter the eventual characteristics of this storm specifically related to the impact we might experience on the surface.

Defining convective weather events

Around the world, convective weather events have often been the cause for a region's, and in many cases, a country's, most expensive natural disaster. Hail events contributed 55% of all total payouts after a storm in Munich, Germany; the same was seen in Denver, Colorado, and

in Sydney, Australia, when 50% and 43% of all payouts was attributed to a single storm (Hohl et al., 2002). In Europe, a hailstorm in 2013 caused an estimated EUR 2.8 billion in damages (Punge and Kunz, 2016), while another hailstorm in the same year was labelled Africa's most expensive single-day insurance loss at ZAR 1.6 billion (Barry, 2014; Cover, 2013; ENCA, 2013; Rahlaga, 2013; Sawdis, 2013). According to Jahn (2015), the impacts of such events can come either as direct losses, indirect losses, or non-market losses. The most common of these are direct losses as a result of damaged property. Events also lead to non-workdays, repair costs and delays, reflected as indirect losses. The damage resulting from an convective event can also be hard to measure in monetary value, such as when historical or cultural sights are damaged. The fact that a convective event such as a hailstorm can cause such damage with little or no warning justifies the need to focus research on understanding the complexities of these events on all scales to limit future losses. The following section will define convective weather events as used in this study and examine the spatio-temporal complexities associated with these events on various scales.

In the context of this study only convective events and environments will be examined; however, much of the methodology could be applied to other weather phenomena. Some terms that might be used interchangeably in this context are high-impact (HI) weather events, severe weather events and extreme weather events. These terms refer to weather events associated with convective instability – summer weather generated by surface heating on a spatio-temporal scale of $\leq 10^6$m and ≤ 1 day, respectively (Orlanski, 1975; Tippett et al., 2015). This includes events ranging from cumulus cells and tornadoes on the lower space-time scale to supercell events, cloud clusters and in some cases, tropical cyclones (TC) on the upper space-time scale. The scale within which these events fall is illustrated in Figure 1.4, adapted from Barry and Chorley (2009). What is important to note in this Figure is that large, synoptic-scale systems are important drivers of events that occur on the smaller-scale (Tippett et al., 2015), and are important to consider when examining the occurrence of smaller scale events. Two types of synoptic-scale forcing can be mentioned, weak and strong synoptic forcing. In the case where the synoptic forcing is weak, the impact of larger circulation is often not as pronounced; here isolated thunderstorms driven by local-scale convection comes to mind[1]. Whereas a supercell, or mesoscale convective complex systems (MCC), are strongly impacted by synoptic scale flow to drive the event (Lin et al., 2011).

Another popular scale used to define atmospheric phenomena is that of Orlanski (1975). This scale divides various phenomena into the definite spatio-temporal categories as detailed in Table 1.1. Using the Orlanski (1975) scale, convective weather as we defined it falls within the meso-γ and the upper end of the micro-α scale range, between 2-20 km in space and between 30 min to 12 hours in the time, similar to other definitions of convective storms. The Orlanski (1975) scale is used to describe scales in NWP, as discussed in the following subsection.

Scales in numerical weather prediction

Three broad categories of models exist in the field of atmospheric sciences and NWP. These include global circulation models (GCM), regional climate models (RCM), and CPM, Each of

[1]but the fact that the synoptic forcing is weak is also an important synoptic-scale consideration

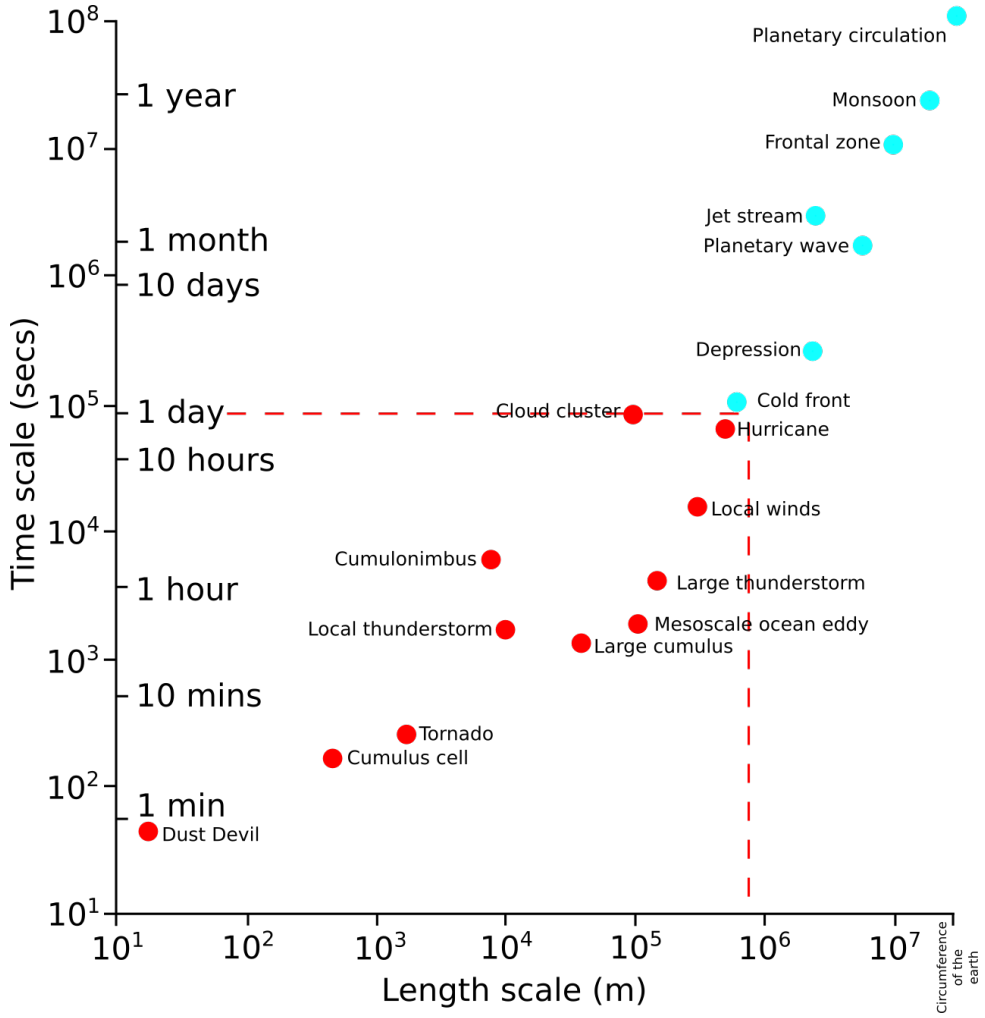

Figure 1.4: *The Figure adapted from Barry and Chorley (2009) indicates the spatio-temporal scale of different weather phenomenons. In the context of this study, convective events fall within spatio-temporal scale of* $\leq 10^6 m$ *and* ≤ 1 *day and are indicated here by the red demarcation. Events indicated in cyan (●) are essential drivers for these smaller-scale events but do not constitute the primary investigation of this thesis. These drivers include the easterly disturbances during summer and westerly waves that drive local-scale weather during winter.*

these NWP models are based on a characteristic space and timescale, each described hereafter.

GCM are used to simulate global circulation features, including events such as planetary circulation and large cyclonic systems that fall under the macro-α and -β scale as described in table 1.1. GCM, however, are not able to resolve local-scale features with great accuracy as computational resources cannot explicitly model various complex physical processes. To overcome these complexities, parameterisation schemes are extensively utilised in GCM (Dedekind et al., 2013), and refer to the simplified physical representation of various processes to improve model runtime. The drawback of parameterisation is that this simplification often leads to considerable uncertainty in the model output, especially when examining small scale events. GCM are not often used to simulate small scale events; as a result, the value of GCM in its current form lies in the ability to simulate past and future climates using parameterisation schemes. The most significant limitation is a lack of understanding and resources to directly model various atmospheric processes on a small scale, such as cloud-aerosol interaction, ice characteristics in clouds,

Table 1.1: *Scales in the atmosphere by Orlanski (1975). The scales defined here are used as a cornerstone in our understanding of atmospheric processes throughout the rest of the study.*

Macro -		Meso -			Micro -		
α, $\geq$ 10,000km	β, 2000km $\leqslant$ 10,000km	α, 200km $\leqslant$ 2000km	β, 20km $\leqslant$ 200km	γ, 2km $\leqslant$ 20km	α, 2km $\leqslant$ 200m	β, 200m $\leqslant$ 20m	γ, $\leq$ 20m
General circulation	Synoptic cyclones	Fronts	Mountain winds	Thunderstorm	Tornadoes	Plumes	Turbulance
$\geq$ 1 week		1 week $\leqslant$ 1 hour			1 hour $\leqslant$ 1 sec		

and clouds' impact on the radiation budget. This means significant discrepancies often exists between various GCM models and reality. For instance, Järvinen et al. (2018) estimated that a previous lack of accurate cloud-ice data meant GCM models were underestimating the cooling effect of ice in the order of -1.12 Wm^2. This was estimated after the novel measurement of cloud-ice using the high-resolution Particle Habit Imaging and Polar Scattering (PHIPS) probe (Abdelmotaleb et al., 2016; Schnaiter et al., 2018).

When moving down in scale to the meso-α and β scale range, RCM comes into play. These models can resolve larger local-scale circulation (Kapsch et al., 2012), even accurately resolving MCC in some cases (Wheatley and Stensrud, 2010). Compared to GCM, these models are computationally more expensive but are generally only used for simulations that run a couple of days in advance and over a limited area. Parameterisation schemes are still employed in RCM models, with similar uncertainties as GCM in accurately resolving clouds and their primary and secondary effects (discussed later) (Laprise, 2008). Models such as National Oceanic and Atmospheric Administration (NOAA)'s global forecasting system (GFS) are examples of regional-scale models. These model are run on the global domain, but only for a couple of days in advance. Advances in computing power have allowed these models to incorporate computationally expensive parameterisation schemes in recent times[2]. Areas where RCM still lacks include localised microphysics and where small scale convection needs to be modelled. Modelling convection explicitly on a day to day basis is not necessarily impossible, but because the model is set up for operational runs and initialised a couple of times a day the computational power currently required for CPM runs slows down NWP systems. A general now-casting model also employs a *best-case* setup for the whole domain and does not account for local-scale characteristics, for example, weekly changes in surface roughness of rural areas in SA. This is where CPM's role in atmospheric research becomes apparent as it allows researchers to refine convective processes in space and time, and as a function of other inputs.

CPM has been a significant development in NWP research and applications. CPM simulations fall into the lower meso-β, meso-γ and upper micro-α range. On this scale, it has proven advantages and computationally possible to explicitly simulate convection, along with refined land surface schemes and local aerosol characteristics. Because CPM are computationally expensive to run, CPM is used for case studies or in an operational setting a few hours in advance. Convective permitting has become synonymous with high resolution runs where convective parameterisation is turned off during model runtime, and convective processes can be fully resolved with a microphysics scheme. In the past, this was computationally expensive (Prein et al., 2015, 2013). The advantage of using this method is the accurate representation of small meso-γ scale events such as localised thunderstorms and supercells (Pal et al., 2019; Prein et al., 2016). Yano et al. (2018), however states that we should be aware of the limitations of CPM as

[2]and will continue to improve as the code, our understanding, and processing power become more efficient

the explicit simulation of convection is only one part of the problem. There is still a lack in parameterisation schemes, ranging from radiation to microphysics, to capture the complexity of the physical processes and their interaction with the larger climate, land-surface features. Yano et al. (2018)'s statement regarding this is interesting;

> *"... we know the microphysics too well, and we have to somehow simplify it for it to be included in operational NWP models while maintaining a reasonable model run speed."*
> (Yano et al., 2018)

Interestingly, there has been a significant focus on the explicit simulation of convection (also apparent in this study). However, at the same time, we still use parameterisation in the same models for other processes. One example is a recent study by Qian et al. (2020) where the authors found a notable improvement in the simulation of summer precipitation when irrigation was accounted for. This specific study examined irrigation in the USA mid-west, a region similar to our farming provinces in terms of summer convective storms and the use of irrigated farming. The small scale impact of irrigation on convective thunderstorms highlights how complex the land-atmosphere interaction is. Even if we understand it well theoretically, we have yet to effectively incorporate all the complexities in models, such as the effect of irrigation on the microphysics of clouds (Yano et al., 2018).

A lesser-used NWP technique is large eddy simulations (LES), where updrafts and downdrafts can be simulated. More precisely the large eddies in the boundary layer can be resolved and there is no requirement of a planetary boundary layer (PBL) parameterisation. This scale falls entirely in the Micro-α, β and γ scale range. Simulations are typically run on grid scales of 25-100m vertically and horizontally (Seinfeld et al., 2016). To resolve even smaller features, Directed Numerical Simulation (DNS) modelling can model turbulent flow on a fine grid scale, however, DNS scale has yet to used extensively in cloud dynamics. These types of simulations can be helpful to resolve shallow cumulus convection in a one-dimensional column or to resolve urban canopy layer features and examine the effect of buildings on airflow (Seinfeld et al., 2016). These models often form the basis for the inclusion of more detailed physics in the GCM, RCM and CPM.

Active research into higher resolution, most notably CPM simulations, in SA has only recently been undertaken. Work by Keat et al. (2019); Stein et al. (2019) and the South-African Weather Service (SAWS) made use of the Met Office Unified Model (MetUM) to simulate and validate CPM runs for Southern Africa in collaboration with the UK Met Office and other partners. The authors' simulated case studies at 4 km, 1.5 km and 300 m for severe convective events over the Highveld. Using automatic weather stations (AWS) data and remote sensing data from the Irene S-Band radar, along with satellite precipitation estimates from the Tropical Applications of Meteorology using Satellite and Ground-Based Observations (TAMSAT), Integrated Multisatellite Retrievals for GPM (IMERG), Climate Prediction Center Morphing Method (CMORPH), Climate Hazards Group Infrared Precipitation with Station dataset (CHIRPS), and CloudSat; the authors were able to identify model biases in the onset, initiation of convection, and the intensity of precipitation compared to the observational data. In both studies, the most significant uncertainty was the early onset of precipitation in the models. The use of radar data to verify

the CPM model runs is valuable. The current study conceptualised a similar idea to better understand the difference in convective cloud characteristics of rural and urban areas in the same region. Current models provide us with great insight into storms physics and dynamics, and the models can be used to simulate idealised cases of weather events by *tuning* the model to our needs and closer to the observed weather; this has allowed us to simulate case studies under different atmospheric conditions with the goal of understanding the anthropogenic impact on weather events.

The scale of climate change

Meaningful conversations around the effect of climate change on local-scale weather have been at the forefront of discussion in recent times. For example, in Southern Africa the effect of climate change on tropical cyclones was a major topic in media after the Fitchett (2018) publication. While the conversation is important and a theme of this study, care should be taken not to hastily link a single event to climate change when examining the occurrence of small scale events such as thunderstorms. Attributing any individual event to anthropogenic change remains a challenging task, primarily due to the problem of scale described in the previous sections. In this regard, the field of Extreme Event Attribution (EEA) is a relatively new branch in the Atmospheric Sciences that aims to quantitatively understand the effect of climate change and anthropogenic forcing on individual events, as discussed in detail by Swain et al. (2020). Using weather models and observational data has proven valuable, but as Swain et al. (2020) states, small scale events such as thunderstorms are not yet resolved by any GCM. Figure 1.5 adapted by Swain et al. (2020) from National Academies of Sciences. (2016) indicates exactly how small scale event attribution to human forcing has proven problematic since the fields emergence. Figure 1.5 shows how there is low confidence, or rather considerable uncertainty, in the actual attribution of climate change to the occurrence of small scale extreme events.

This *problem of scale* discussed in the above section has to be kept in mind throughout the rest of the study. We try to understand interactions between the space and time complexities of severe weather while being careful not to attribute any individual event to a changing climate. The following section will describe SA climatology as related to convective weather events. Following the discussion on climatology and convective weather, we move down in scale to introduce cloud-aerosols, cloud formation, and the direct and indirect impacts of aerosols on radiation, weather and climate, and the UHI.

Climatology of significant convective weather in South Africa

SA's location in the mid-latitudes between 21°S – 35°S and 15°E – 35°E means it is affected by several key circulation patterns as illustrated in Figure 1.6a. The descending column of the Hadley cell means the country is characterised by subsidence throughout the year, but most notably during winter months when a continental high-pressure system dominates daily weather over much of the interior of SA. Minimal mixing occurs, and the winter Highveld days are mostly sunny with a polluted boundary layer due to the stable atmosphere (Broccardo, 2015; Tyson and Preston-Whyte, 2000). During this time, rainfall is only prevalent in the South-Western Cape due to extra-tropical disturbances from the dominant westerly waves. In the Western Cape severe

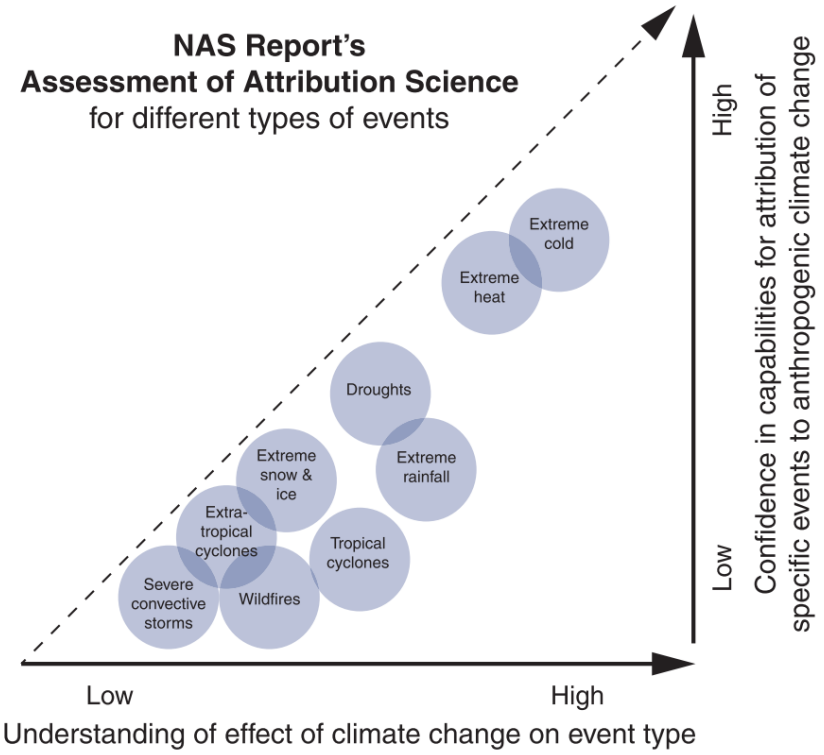

Figure 1.5: *The uncertainty of scale also has major implications for the attribution of individual events to anthropogenic forcing. As National Academies of Sciences. (2016); Swain et al. (2020) shows in the above Figure, EEA on a fine scale is still not well understood whereas larger synoptic scale events resolved by GCM can to a large degree of certainty be linked to possible anthropogenic forcing such as climate change.*

weather manifests itself as winter rainfall and snow in some areas of the Province (Nicholson, 2000). Nevertheless; this rainfall seldom extends over the interior of SA. In rare cases, cut-off low systems can harness themselves over SA, leading to cold and rainy conditions in what is otherwise a summer rainfall region (Tyson and Preston-Whyte, 2000).

Although the continental high-pressure system is semi-permanent over SA, summer circulation is dominated by easterly disturbances. The easterly disturbance is influenced by the annual north–south movement of the inter-tropical convergence zone (ITCZ). The tropical easterly forcing brings about warm and moist air from the equatorial latitudes, resulting in conditions favouring convective thunderstorms. These events are the dominant rain-bearing systems for central SA during this time (Tyson and Preston-Whyte, 2000). Convective thunderstorms are also associated with hail, flash floods and lightning (Figure 1.6b), which has resulted in various economic losses around the country. Over the central interior of SA, Blamey et al. (2016); Dyson (2009, 2013) describes the early summer months (October – November) as the most favourable for weather associated with a convective environment. This early summer convection is enhanced with the still present extra-tropical/mid-latitude systems, in contrast with the east coast, where convective storm environments are most prevalent during mid-summer (December – January). Other significant, heat-driven weather events such as TCs are rare over mainland SA, and if they move over the subcontinent, they often cause flooding over the northeastern parts of the country during summer. In exceptional cases, like TC Elaine that occurred in 2000, TCs can move as far as Namibia - possibly with La Niña years (Reason and Keibel, 2004).

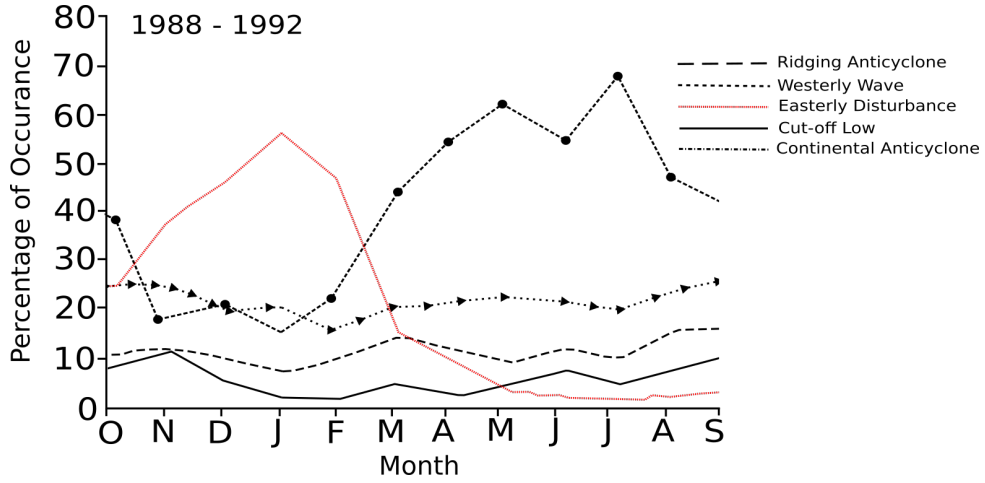

(a) *The dominant circulation types over SA from (Tyson and Preston-Whyte, 2000) illustrate the main circulation patterns that impact SA throughout the year. The most dominant is the continental anticyclone, due to the country's position in the middle latitudes and the subsequent effect of the subsiding Hadley cell.*

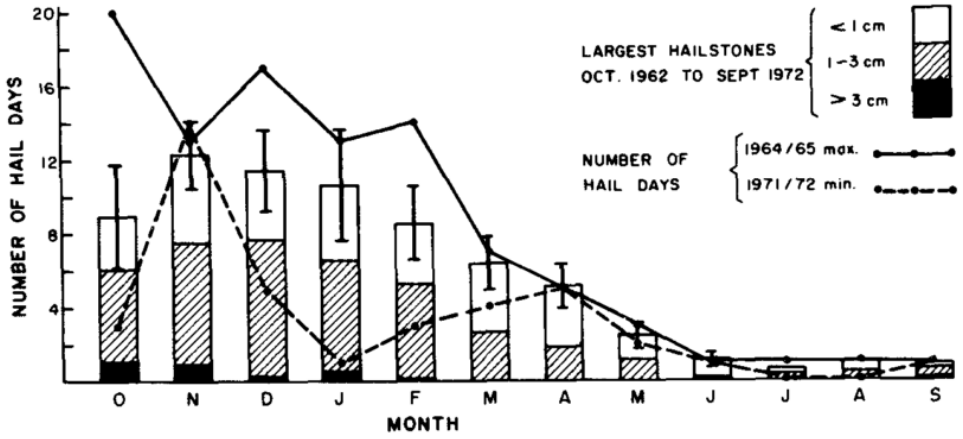

(b) *Carte and Held (1978)'s work on the variability of hail events over the Highveld provides detailed information on the monthly variation of this phenomenon; this has also proved valuable in research regarding convective events in general.*

Figure 1.6: *In the top Figure, the dominant circulation patterns that occur over SA is visable. Relevant to this study is the presence of the easterly disturbance, highlighted in red. The easterly disturbance manifests itself from September/October until late February, which, as shown in the bottom Figure, is when convective weather over the Highveld is most prevalent.*

In Figure 1.7, the results show the high concentration of convective events associated with hail and thunderstorms over central SA and the Highveld. When examining the hail day frequency (HDF) over the Highveld in detail, as seen in Figure 1.6b after Carte and Held (1978), the monthly variation in hail events is also clearly visible and supports later findings by Blamey et al. (2016); Dyson (2009, 2013). From October, there is an increase in the number of hail events, and during this time, the largest hailstones are also observed. November is the month with the most recorded number of hail events over the Highveld. As seen in Figure 1.7c Blamey et al. (2016), on severe convective environments; we can see that the density of severe environments is the most concentrated over the Highveld during November, also supported by Carte and Held (1978)'s original work. A feature not so apparent that might have an impact on the initiation of convection is the apparent dry line along the western interior of SA. The dry line, moisture

boundary, separates dry air from the Karoo/west coast region and the moist air that is advected from the tropics and the Indian ocean, in Tyson and Preston-Whyte (2000) this feature is defined as a moisture front. A similar feature exists in the USA known as the dry line. Along the dry line, or moisture front, convective initiation occurs frequently and can lead to tornadogenisis over the area (Mitchell and Schultz, 2020). The impact of the dry line on severe convection in SA is apparent in the occurrence of tornado events as was documented by DAbreton (1991); De Coning and Adam (2000); Lekoloane et al. (2021).

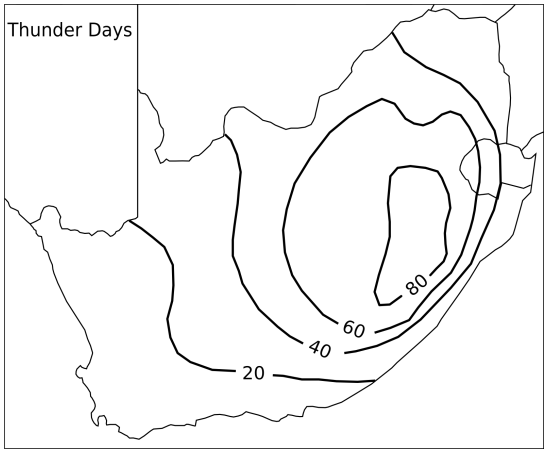

(a) *Spatio distribution of thunderstorms over SA*

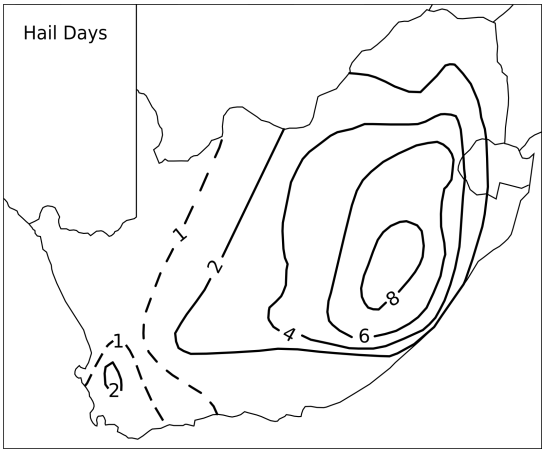

(b) *Spatio distribution of hail events over SA*

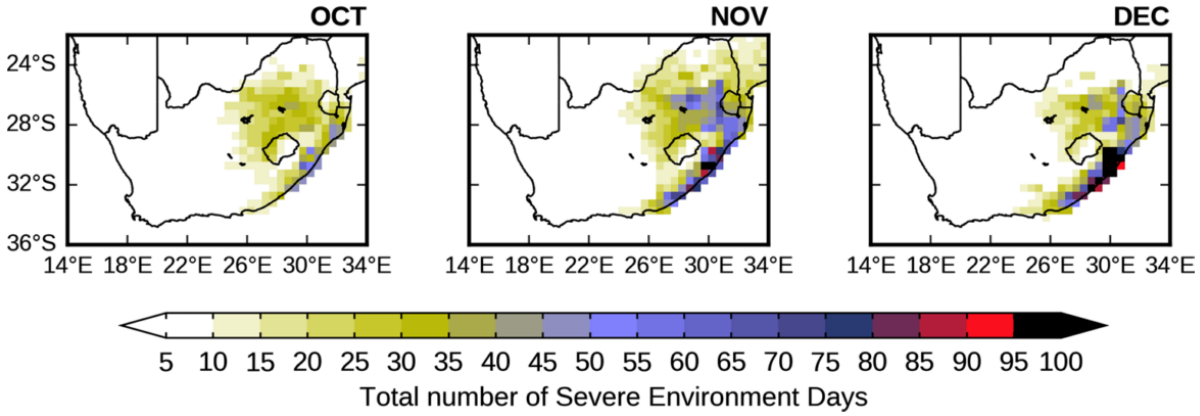

(c) *The recent examination of severe storm environments over SA by Blamey et al. (2016) is shown here.*

Figure 1.7: *Schulze (1965)'s work shows the spatial density of two convective environments, notably thunderstorms, left, and hail events, right. Events are generally distributed along the same pattern across SA, and this is expected as these events occur concurrently. The highest number of events occur in central SA over the Drakensberg mountains and the Highveld region. Note that the more recent examination supports that the above maps were redrawn from (Schulze, 1965). This is supported by the more recent examination by Blamey et al. (2016). This is seen in the bottom Figure. The central interior of SA is the area where the environment favours convective storms.*

The changing convective storm landscape

Under changing climate conditions the nature of convective events over the Highveld region is expected to change (Piketh et al., 2014). Using ERA5 reanalysis data, Taszarek et al. (2021) found there has been a significant decrease in the severe storm environment over the Highveld region, with the overall storm environment remaining the same. Notable was the changes in the

position of the westerlies that is observed to move poleward and a overall decrease in Convective Available Potential Energy (CAPE). However, local radiosonde data over Irene shows a slight increase in environments favorable for convective weather. This also highlights the limitations of using large scale reanalysis data to derive local scale conditions. Kruger and Nxumalo (2017) showed an overall increase rainfall over the central interior of South-Africa. These changes also show that high rainfall events (rain days over 10mm, 20mm and 25mm) during September, October and November (SON), December, January and February (DJF) are increasing.

To understand the environments favorable for convective storms remains a complex problem. The major challenges are related to the scale of the weather event studied, which in the case of convection can be ≤ 20 km, and the apparent link to larger scale environments. In the climatology section above this is also apparent, without the advection of moisture from the ITCZ and ridging anticyclone (large scale), or the westerlies driving conditional instability and wind shear conditions for convective storm development would be non existent. At the same time, small scale heating, moisture, topography and land-use play a role in the local convective landscape.

Several studies have proposed clustering solutions to examine the possible environments (weather types) local scale events such as convective storms occur in, and to examine the increase or decrease in these weather types under climate change conditions. To this end Insua-Costa et al. (2021); Lemus-Canovas et al. (2021); Lemus-Canovas, Lopez-Bustins, Trapero and Martin-Vide (2019); Prein et al. (2016, 2017) used objective clustering solutions to derive the environments weather events (severe events) occur under. These proved valuable in several aspects, first they showed the number of synoptic patterns that can be responsible for a significant event type, i.e. 9 synoptic types can be associated with torrential rain in the Pyrenees (Lemus-Canovas et al., 2021), or in the case of Prein et al. (2016) where it was found that the patterns associated with drought in the west coast (USA) is becoming more prevalent.

In SA, the use of Self Organizing Maps (SOMs) techniques (Sheridan and Lee, 2011) have been utilised to understand heavy rainfall events (Dyson, 2015; Engelbrecht et al., 2015; Wolski et al., 2018), synoptic variability (Engelbrecht et al., 2017; Quagraine et al., 2019; Wolski et al., 2018) and fog events (Van Schalkwyk and Dyson, 2013). These studies do add value in the understanding of the variability of synoptic conditions associated with complex local scale events. In the case of the Highveld Dyson (2015); Wolski et al. (2018), focussed on the rainfall in the direct area over Gauteng, and Wolski et al. (2018) found that CAPE did not show a significant correlation to rainfall in the SOM weather types identified as important to rainfall in the region.

Atmospheric aerosols

The formation of clouds in the atmosphere depends on the initial presence of a CCN and ICN on which water vapour can condensate to form droplets, or on which ice formation is triggered. This simple explanation requires a more in-depth discussion, as the simple presence of an aerosol that acts as a CCN and/or ICN creates some of the most complex and least-understood feedback mechanisms in nature, directly and indirectly.

An *aerosol* is defined as a particle with a size order of 0.001-1μm suspended in the atmosphere. The terminal velocity of this particle is generally not adequate to fall to the Earth's surface immediately (Wallace and Hobbs, 2006), and they remain suspended in the atmosphere. Aerosol

sources can be natural and anthropogenic, and the lifetime of aerosols vary depending on the aerosols size distributions. Three characteristic sizes are defined in literature; Aitken nuclei (ultra-fine, 0.001-0.1μm), large aerosols (accumulation mode, 0.1-1.0μm) and giant aerosols (coarse-mode, $\geq 1\mu$m) (Devara and Manoj, 2013; Wallace and Hobbs, 2006).

The first and most prominent of these three different aerosols is Aitken aerosols. These particles are derived from anthropogenic and natural sources, including incomplete combustion, fires (Ross et al., 2003), gas to particle conversion, and biogenic and biological sources (Li, Lau, Ramanathan, Wu, Ding, Manoj, Liu, Qian, Li, Zhou et al., 2016). Aitken particle's lifetime in the atmosphere is highly variable, but in the order of ≤ 1 day according to Wallace and Hobbs (2006). Larger particles quickly remove them through processes such as coagulation. Coagulation refers to a method of particle growth where droplets grow by capturing smaller particles as they move through the atmosphere (Ross et al., 2003).

Large aerosols originate through various pathways. First, growth through coagulation is possible; as the particles move through the atmosphere, they interact with other Aitken particles to grow. Secondly, growth through condensation can occur on the surface of the aerosol to increase its size. Anthropogenic sources of large aerosols can include the incomplete combustion of fossil fuels. Finally, the natural occurrence of large particles such as nitrates and sulfates adds to the concentration in the atmosphere (Ross et al., 2003). According to Andreae and Rosenfeld (2008); Wallace and Hobbs (2006) these aerosols have a longer lifetime in the order of hours to days and as a result can be transported vast distances.

Giant aerosols are also anthropogenically and naturally emitted into the atmosphere, typically from windblown dust and emissions from industries. These particles are, however large and heavy, and fall back to the surface relatively quickly (Ross et al., 2003).

The various types of aerosols discussed here is only an introduction to aerosols and their characteristics. In the context of this study, it is essential to understand that the size, lifetime, chemical composition, and spatial extent of aerosols impact droplet size distribution, concentration and precipitation processes. Aerosols further impact clouds and the radiation budget, and there is still a large gap in our understanding of the impact of aerosols on global heating/cooling. The following section expands on these topics by examining the aerosol-cloud life cycle, which then expands into a discussion on the direct and indirect impacts that clouds and aerosols have on the Earth's climate.

The aerosol and convective cloud life cycle

We can look to nature first to understand the possible impacts of anthropogenic CCN and ICN on clouds. Spatially there exists a difference in the properties of maritime and continental clouds (Rosenfeld and Lensky, 1998). The same theories can also be used to understand the effects of anthropogenic aerosol loading in the atmosphere. Continental clouds are composed of more aerosols as there exists more dust, soot from fires, and other aerosol sources. In comparison, in the maritime environment, thought of as a *clean* environment, we see less of the above particles that act as possible CCN/ICN. Over maritime environments, the aerosols present are mostly salts originating from the oceans (Squires, 1958a,b; Wallace and Hobbs, 2006). This difference between the continental and maritime environment's aerosol profile, has contrasting effects on

the properties of clouds, and hydrometeors[3], in the clouds as illustrated in Figure 1.8a. This is also true for the SA landscape, the Aerosol Recirculation and Rainfall Experiment (ARREX) program conducted in-situ observations of cloud droplet concentrations between the Highveld and coastal areas. In Figure 1.8b, the difference between the Highveld (continental), and coastal cloud droplet concentration is shown.

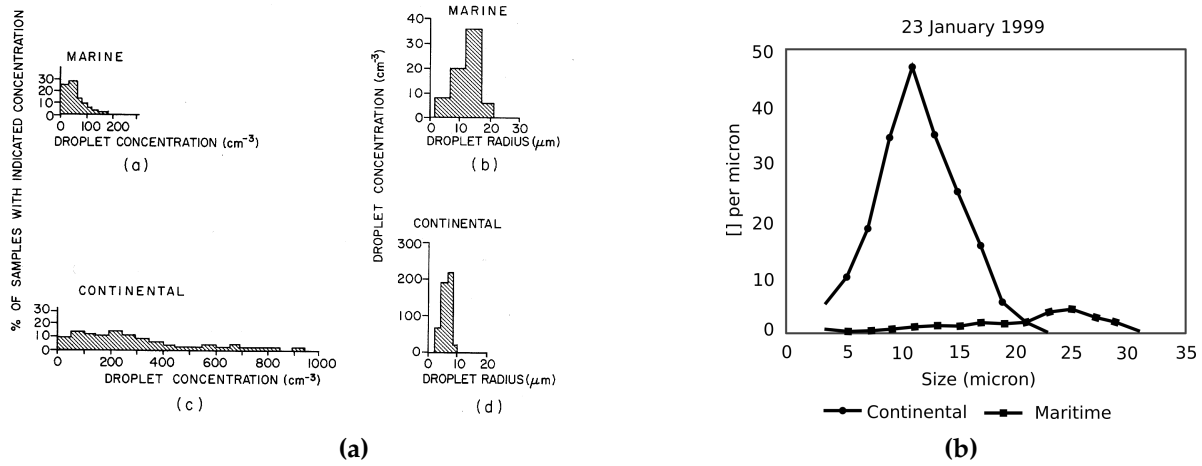

Figure 1.8: *Continental and maritime clouds show vastly different characteristics in their droplet concentration and size distribution. Continental clouds show a larger droplet concentration, but a smaller droplet size due to the abundance of possible CCN sources in inland areas. Maritime clouds have smaller droplet concentrations but larger droplet sizes. Figure a is from Wallace and Hobbs (2006) and based on the novel research by Squires (1958a,b). In Figure b (adapted from Terblanche et al. (2000)), the droplet concentration as measured by Terblanche et al. (2000) is shown, similar to Figure a, there is a distinctive difference in the droplet characteristics between clean and polluted environments, and Terblanche et al. (2000) confirms this for the SA landscape as well.*

The difference between continental and maritime cloud properties subsequently changes the surface precipitation of areas where these clouds are present (Fan et al., 2018, 2016; Rosenfeld et al., 2014). Continental clouds are characterised by a higher droplet Number Concentration (N_c) but smaller mean diameter. The assumption is that the higher number concentration of CCN means that CCN activation takes place earlier in the life of the cloud, allowing for more droplets to form. Because the hydrometeors are smaller than they would be in a maritime environment, they do not precipitate as readily. They have a longer lifetime in the cloud, affecting freezing, growth, and precipitation characteristics in the continental cloud life cycle (Fan et al., 2016). In maritime clouds, pristine clouds, a smaller droplet concentration but with a larger droplet diameter is observed. Fan et al. (2016) speculates that CCN are more efficiently activated, but due to the larger size distribution, the particles precipitate earlier, and hence clouds in the maritime region have a shorter lifetime.

[3]According to AMS (2016) hydrometeor refers to *"Any product of condensation or deposition of atmospheric water vapour, whether formed in the free atmosphere or at the Earth's surface; also, any water particle blown by the wind from the Earth's surface."*, this term will be used throughout the document to refer to rain and ice in the atmosphere

The rising parcel of air

To better understand the general formation of clouds[4], the thermodynamic processes, where a rising parcel of air reaches saturation in the presence of a CCN, needs to be discussed and considered further on. This process is also vital for understanding NWP parameterisation, droplet and ice formation, and precipitation. Favorable conditions for convective events require three basic ingredients according to Arnold (2008); Schultz et al. (2000), these include *lift, instability, and moisture*. Apart from these three basic ingredients, several other important features enhance the potential for severe storm development, but similarly various other thermodynamic processes can inhibit convective storm development, as will be discussed here.

The formation of clouds starts with the evaporation of water from the surface of the Earth, typically through convection. When evaporation occurs, water changes phases from a liquid to a gas. When this happens, the gaseous water exists in a dry parcel of air until condensation occurs. The ratio of dry air (m_d) and water vapour (m_v) can be calculated using the mixing ratio (w) equation 1.1,

$$w \equiv \frac{m_v}{m_d} \tag{1.1}$$

The parcel of dry air will then rise into the atmosphere while cooling down ($-\frac{dT}{dz}$) at the dry adiabatic lapse rate (Γ =1°C 100m^{-1}) expressed using equation 1.2 (Wallace and Hobbs, 2006),

$$-(\frac{dT}{dz})_{\text{dry parcel}} = \frac{g}{C_p} \equiv \Gamma_d \tag{1.2}$$

Where C_p = heat of air at a specific temperature and g = gravity constant 9.8 m/s^2. This process is also reversible when a parcel of air subsides and warms (Tyson and Preston-Whyte, 2000). If the parcels of air cool down and the pressure drops with respect to the environment, saturation is bound to occur. Based on the vapour pressure curve, as illustrated in Figure 1.9, we can see the direct relationship between pressure and temperature on saturation. However, there are some thermodynamic processes that can slow or completely inhibit this process, and this is stable layers in the atmosphere (or convective inhibition (CIN)) (Arnold, 2008). For CIN to be overcome, a parcel of air must have enough energy to break through this stable layer, or a parcel of warm moist air can be forced above the stable layer through frontal lifting, surface convergence or topographical features. Once the parcel of air (that is still moist and unstable with respect to the surrounding environment) breaks through the CIN and a parcel typically becomes saturated, and can rise further into the troposphere.

When saturation occurs, the relative humidity (RH) in the atmosphere is 100%, and thermodynamically this is known as the lifting condensation level (LCL). From here, the parcel will further rise wet adiabatically (also known as the level of free convection (LFC)) into the atmosphere. It is seldom that vapour spontaneously changes from a gas into a liquid droplet. For the saturation process to occur, a CCN is required under normal circumstances[5]. The atmosphere's

[4]Referring here to mixed-phase clouds where liquid and ice hydrometeors coexist

[5]Saturation can also happen under supersaturation conditions when the RH is greater than 100%

composition is rarely free from aerosols and CCN, and two types of aerosol mixing states exist according to Seinfeld et al. (2016). The first is in a homogeneous aerosol environment, and this would be known as an *internally mixed* state. In contrast, an atmosphere with varying aerosol compositions would be known as an *externally mixed* state (Seinfeld et al., 2016).

Now the parcel of air has reached the saturation phase and CCN activation has taken place, in what can be assumed to be an *externally mixed* state. The discussion can now examine growth, phase changes and eventual fallout of particles through precipitation processes. Although saturation was discussed previously as a precursor for condensation to occur on a surface, vapour can condensate on some particles below 100% RH. These particles, known as hygroscopic, or water-soluble particles, are highly attracted to vapour in the atmosphere and fall within the Aitken range.

After CCN activation takes place, small *drizzle type* droplets start to form. These tiny droplets remain suspended in the atmosphere and grow through collision-coalescence in the warm rain process (Dyson, 2013; Rosenfeld, Woodley, Lerner, Kelman and Lindsey, 2008). Thermodynamically the parcel of air will rise wet adiabatically (Γ′) after saturation takes place. This can be expressed as,

$$-\frac{dT}{dz} = \Gamma_d + \frac{L}{C_p}\frac{dx_s}{dz} = \Gamma' \tag{1.3}$$

Where L=latent heat of condensation and dx_s=the saturation mixing ration. If the droplets remain suspended below the freezing level (0°C), they will remain in a liquid state and only fall to the atmosphere when the terminal velocity exceeds, according to Stokes Law, that of the updrafts. This processes is known as warm-cloud precipitation (Li, Lau, Ramanathan, Wu, Ding, Manoj, Liu, Qian, Li, Zhou et al., 2016; Tyson and Preston-Whyte, 2000). If the droplets are displaced higher into the atmosphere, ice processes start to occur above the freezing level. The pathways to ice formation in clouds are not straightforward. Droplets can and do remain in a liquid state well below 0°C (Rosenfeld and Woodley, 2000).

For a parcel of air to rise to above the freezing level during convective storm development, conditional instability and adequate CAPE is needed. In SA these conditions are typically present during early summer when there is still a influence from the westerly wave systems above 500 hPa (Dyson, 2013). Here Schultz et al. (2000)'s three ingredients (*lift, instability, and moisture*) is realised, and results in SA most severe thunderstorms. During early summer there is an influx of moisture from the ITCZ which shifts south, above SA during this time. Surface moisture is advected over the interior in the form of easterly waves and lows, and ridging high pressure systems over the east coast. The importance of the ridging anticyclone has been highlighted in recent research by Ndarana et al. (2021). Two types of ridging anticyclone can impact weather over SA, namely type S (south of 40°S) and type N (north of 40°S). Type N events, typically live longer and result in increased moisture and rainfall over the escarpment. Due to the presence of these moisture rich systems over the subcontinent, another important ingredient for severe storm development is realised and this is wind shear (Brooks et al., 1994; Dyson, 2013; Sherburn and Parker, 2014; Taszarek, Kendzierski and Pilguj, 2020). Due to the differential winds between the surface (easterly) and at 500 hPa (westerly), storm rotation is enhanced.

If the parcel is then lifted high enough through the processes described above, the initial process of ice formation can occur through homogeneous nucleation, heterogeneous nucleation, contact nucleation and direct conversion (Andreae and Rosenfeld, 2008; Tyson and Preston-Whyte, 2000). In temperatures warmer than the homogeneous freezing level (≥ -38°C), ice particles can form in the presence of an ICN in the process known as heterogeneous freezing. These particles are rare (Andreae and Rosenfeld, 2008; Rosenfeld and Woodley, 2000) and encompass ≤ 10^6 of aerosol particles in the atmosphere. Particles that act as ICN include already present ice in the cloud that can accelerate ice formation through contact and collision mechanisms (Andreae and Rosenfeld, 2008). Homogeneous ice nucleation can also lead to the growth of ice particles. During this process, ice particles form spontaneously from a liquid state without the presence of an ICN. Homogeneous ice nucleation occurs in a supercooled environment at temperatures below -38°C, known as the homogeneous freezing level (Andreae and Rosenfeld, 2008; Rosenfeld and Woodley, 2000). Rosenfeld and Woodley (2000) found homogeneous freezing to be the dominant ice formation process in deep convective clouds during an *in-situ* cloud measurement campaign conducted in Texas, USA. Bühl et al. (2019) investigated the extent to which updrafts impact the displacement of ICN and CCN. The study showed that increased updrafts could enhance displacement of CCN/ICN and result in enhanced cooling and hence more efficient freezing

The continued growth and precipitation of the ice particles can be explained through the Bergeron process.[6] (Korolev, 2007). Once ice is formed droplets will gravitate towards the ice particles due to the differential vapour pressure of ice and liquid water. A high vapour pressure field exists around a droplet, while a low vapour pressure field exists around the ice particle. In a mixed-phase cloud, the ice particle will grow while droplets shrink for as long as droplets are present in the cloud. However, the particles increase in size and weight, and can melt or grow through collision processes as they move between different temperature gradients until the eventual precipitation/wet-deposition to the surface (Bühl et al., 2019; Korolev, 2007).

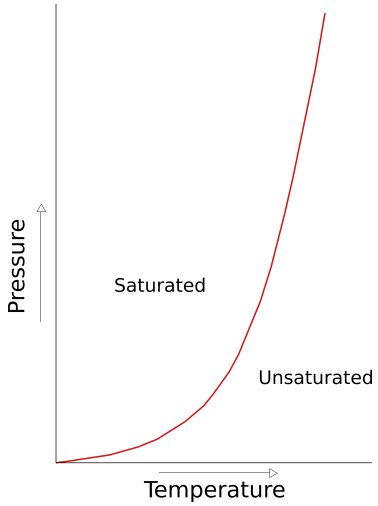

Figure 1.9: *The vapour pressure curve shows the direct relationship between pressure and temperature in relationship to the saturation ratio in the atmosphere. Gaseous water vapour will condense onto a surface when RH of 100% is reached.*

This thermodynamic evolution, and subsequent changes to the environmental temperature and water mixing ratio (q_v[g/kg]), as a function of increased pollution, was simulated by Dagan et al. (2016) as seen in Figure 1.10. Dagan et al. (2016) examined the specific impacts of varying aerosol concentrations (cm^3) representative of clean (5cm^3), mild (50 cm-250 cm^3) and heavy (2000 cm^3) polluted environments and the temporal changes to these conditions respectively. At different vertical levels, the effects of aerosols on the thermodynamic environment differ substantially, affecting rainfall suppression and enhancement (Dagan et al., 2016). In clean environments, maximum cloud tops were

[6]Also known as the Wegener-Bergeron-Findeisen process

relatively short-lived (cloud tops decreased T10), and throughout the simulation water vapour remained high in the model's vertical profile. When aerosols were increased, cloud lifetime seemed to increase as well. Cloud tops remained at a fairly constant height in the polluted runs, not precipitating as readily as the clean run. According to Dagan et al. (2016), the delayed precipitation indicates that rain formation could be suppressed when the aerosol concentration is high, similar to the findings of Fan et al. (2018, 2016).

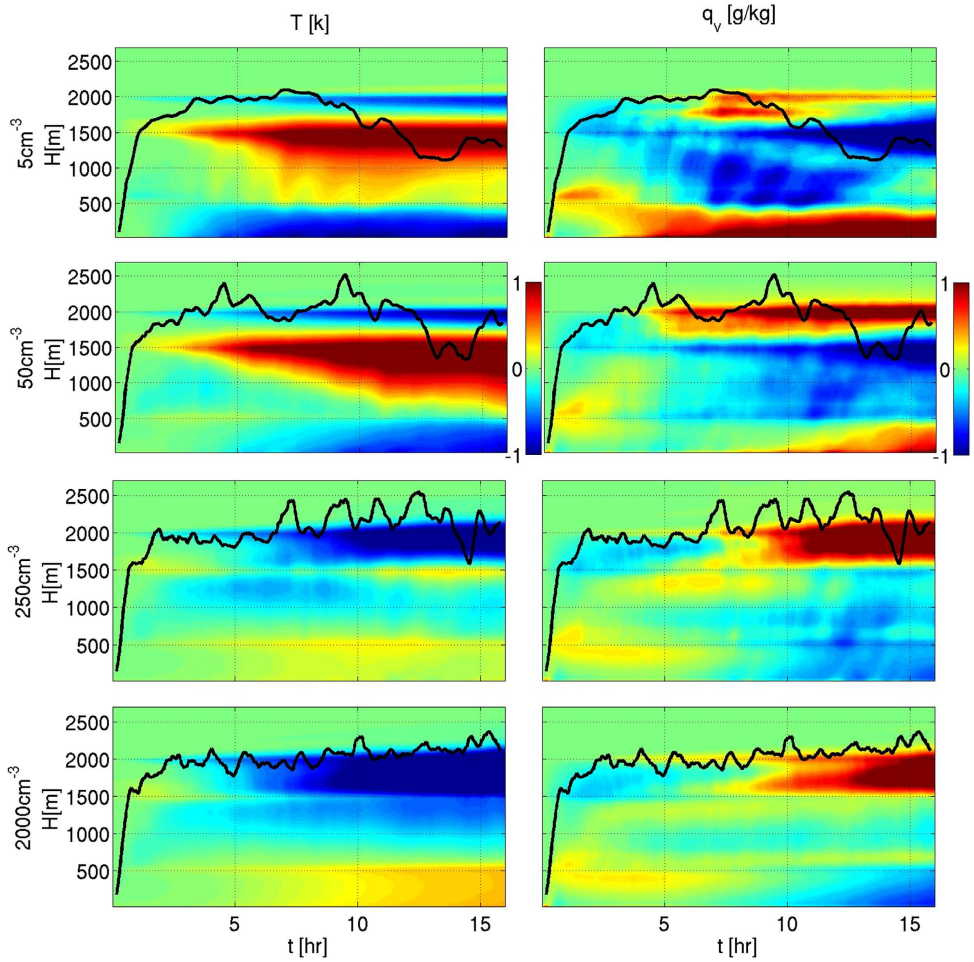

Figure 1.10: *Dagan et al. (2016)'s examination of cloud aerosol interactions over oceans and between clean and polluted environments shows how aerosols change the vertical temperature and mixing ratio ($q_v[g/kg]$) of the atmosphere over time. The black line indicates the average cloud top height, and Dagan et al. (2016) speculates that polluted conditions lead to the suppression of rainfall formation.*

Rosenfeld, Lohmann, Raga, O'Dowd, Kulmala, Fuzzi, Reissell and Andreae (2008)'s schematic, as indicated in Figure 1.11, shows a possible pathway to the effects of increased aerosols on clouds, and the eventual precipitation of hail and ice to the surface. Rosenfeld, Lohmann, Raga, O'Dowd, Kulmala, Fuzzi, Reissell and Andreae (2008)'s paper speculates that in pristine environments larger droplets will from during the growing phase of convection, subsequently, these droplets will be heavier and precipitate to the surface earlier. In contrast, polluted environments will have a higher number of droplets which are smaller in size (supported by Figure 1.8). These smaller droplets remain suspended in the atmosphere for longer and might reach higher levels, possibly delaying precipitation. This delay might increse severity and characteristics of precipitation over SA. Rosenfeld, Lohmann, Raga, O'Dowd, Kulmala, Fuzzi, Reissell

and Andreae (2008) and Pante et al. (2021); Solmon et al. (2021); Tosca et al. (2015) note that the increase in aerosols will result in heating of the lower troposphere, however, the papers differ in their findings on the eventual precipitation reaching the surface. Rosenfeld, Lohmann, Raga, O'Dowd, Kulmala, Fuzzi, Reissell and Andreae (2008) speculates that the heating of the lower troposphere might be enhancing the Asian Monsoon, while Pante et al. (2021); Solmon et al. (2021); Tosca et al. (2015) found evidence of lower tropospheric heating by aerosols to prevent convection and decrease precipitation over regions of west- and south-west Africa.

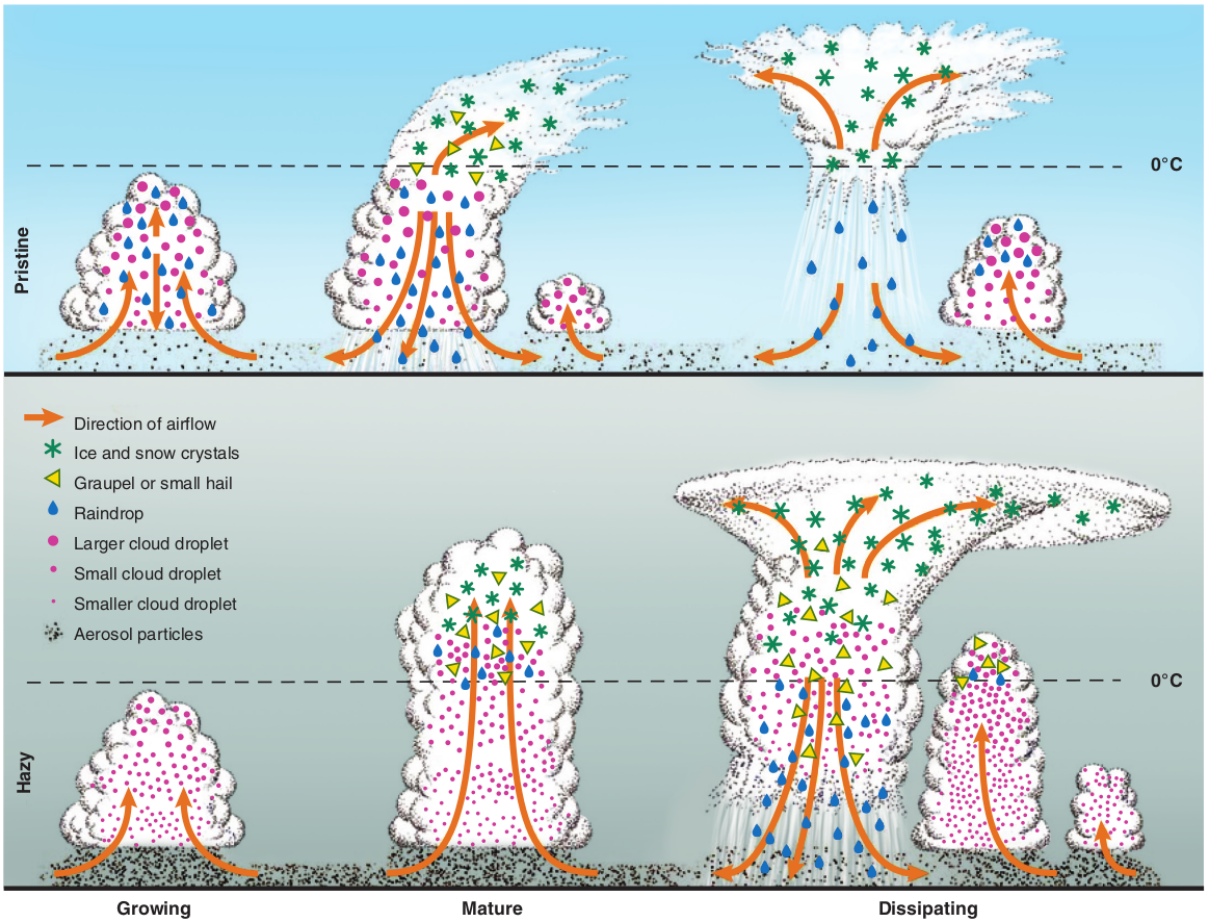

Figure 1.11: *Rainfall pathways in pristine and polluted environments by Rosenfeld, Lohmann, Raga, O'Dowd, Kulmala, Fuzzi, Reissell and Andreae (2008) shows the possible effects of increased aerosols on precipitation in these two contrasting environments. The paper speculates that polluted environments might also lead to lower troposphere heating, similar to findings from Pante et al. (2021); Solmon et al. (2021); Tosca et al. (2015).*

As described by the above processes and interactions, the eventual formation of clouds can lead to varied effects on surface precipitation. In large cumulonimbus/supercell mixed-phase clouds, ice such as hail and graupel, and rainfall can lead to localised damage over a region. Not only are the clouds and aerosols essential for precipitation, but both these processes impact local and the larger-scale radiation budget as well (Li, Lau, Ramanathan, Wu, Ding, Manoj, Liu, Qian, Li, Zhou et al., 2016). Aerosols, clouds and the hydrometeors in the atmosphere–absorb, reflect and refract sunlight (Ross et al., 2003) in exciting ways, as discussed in the next section.

Radiative impacts of clouds and aerosols

Two primary heating and cooling mechanisms affected by aerosols, include cloud albedo and the greenhouse effect. This happens through scattering, absorption, radiation, and changes to cloud microphysics (Penner et al., 2001; Ross et al., 2003). These effects can be separated into two distinct categories, direct and indirect (Penner et al., 2001; Ross et al., 2003). These two categories were theorised by Albrecht (1989); Atwater (1970); Twomey (1974, 1977), where they noted that pollution and natural aerosols could alter the Earth's cloud cover and radiation budget on the local and global scale (Li, Lau, Ramanathan, Wu, Ding, Manoj, Liu, Qian, Li, Zhou et al., 2016).

The direct effect refers to the scattering and absorption properties and radiative changes caused by aerosols. This effect is mostly determined by the aerosol composition and optical characteristics (Penner et al., 2001). The size distribution of aerosols play a significant part in the above-mentioned effects. According to Penner et al. (2001), large aerosols (accumulation aerosols) have the most significant impact on the radiative feedback as they have the highest scattering efficiency. According to Yu et al. (2006), three methods are predominantly used to determine the aerosol direct effect. The first is deriving aerosol optical depth (AOD) from a vertical column of air using satellite data from platforms such as MODerate resolution Imaging Spectroradiometer (MODIS) and Cloud-Aerosol Lidar and Infrared Pathfinder Satellite Observations (CALIPSO) or surface-based measurements from instruments such as the Raman Light Detection and Ranging (LiDAR), NASA Micro Pulse Lidar Network (MPLNET), European Aerosol Research Lidar Network (EARLINET), and AErosol RObotic NETwork (AERONET). Secondly, by using single-scattering albedo (SSA), researchers can measure the relative importance of aerosol scattering and absorption through the scattering and extinction coefficient of aerosols (Yu et al., 2006). Finally, by measuring the scattering intensity and direction of aerosols through a method known as the phase function. Using the three methods, as detailed by Yu et al. (2006), has been a significant advancement in understanding the radiative properties of aerosols

Myhre et al. (2013); Stocker et al. (2013)'s work in Intergovernmental Panel on Climate Change (IPCC)'s 5 assessment report highlights the direct heating and cooling properties as a function of cloud aerosol interactions. A net cooling effect of -0.9Wm^{-2} is observed, mainly by aerosol's direct reflectance of incoming solar radiation and indirect changes in cloud albedo. Recent research, however, suggests that the net cooling effect could be underestimated by as much as -1Wm^{-2} due to cloud-ice structures that are not well parameterised in NWP (Järvinen et al., 2018). Heat absorbing aerosols lead to an estimated 0.4Wm^{-2} increase in surface heating through changes in the albedo of snow cover according to the report. This is due to the deposition of soot and black carbon (BC) on snow, which increases the absorption of surfaces with a traditionally high albedo (Myhre et al., 2013; Stocker et al., 2013). The heating and cooling effects described above can be seen in Figure 1.12.

The indirect forcing caused by aerosols is classified into the first and second indirect effects, the Twomey and Albrecht effect respectively (Albrecht, 1989; Twomey, 1974, 1977). The indirect effects are related to CCN/ICN changes that occur after clouds have formed. The first indirect effect, the Twomey effect (Twomey, 1974, 1977), refers to the direct changes of aerosols on cloud albedo. Twomey (1974, 1977) hypothesised that clouds in a *natural* environment would have a lower albedo due to the low number concentration of large raindrops in the clouds, which

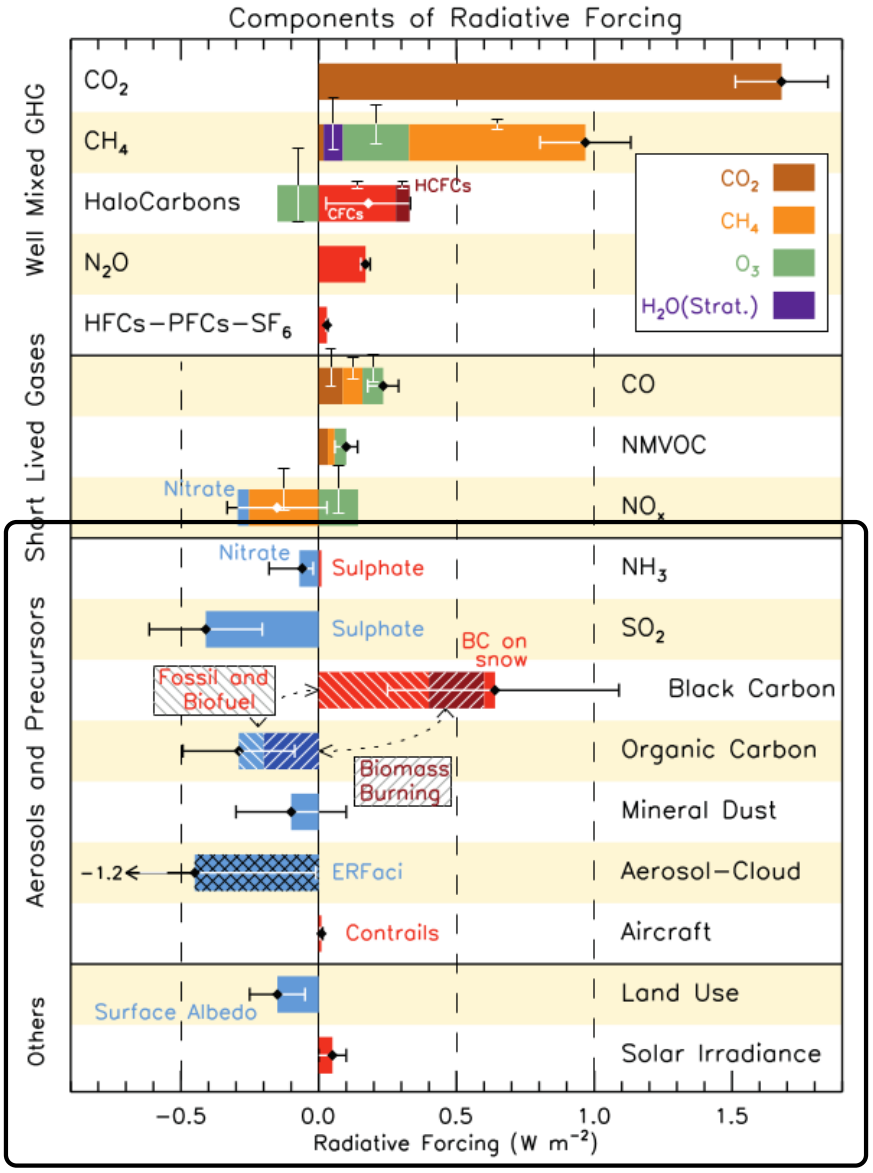

Figure 1.12: *Aerosols play a role in the global heating and cooling mechanisms, as seen in the above Figure from the IPCC's 5 Assessment report (Myhre et al., 2013; Stocker et al., 2013). The report estimates that aerosols-cloud interactions (outlined in the Figure) are responsible for a net cooling of -0.9Wm^{-2}. Heat absorbing aerosols lead to an estimated 0.4Wm^{-2} increase through changes in the albedo of snowpacks and an increase in heat-absorbing aerosols in the atmosphere (Myhre et al., 2013; Stocker et al., 2013).*

are not efficient in the reflectance of incoming solar radiation. In contrast, clouds in *polluted* environments will have a higher albedo due to a larger N_c of tiny droplets, increasing the cloud's surface area and subsequently increasing the reflectance according to Twomey (1974, 1977). The second indirect, the Albrecht, effect (Albrecht, 1989) builds on Twomey (1974, 1977)'s ideas by examining the effects of aerosol N_c on precipitation processes. According to Albrecht (1989), clouds in a *natural* environment will be more efficient, and precipitation will occur more readily. This, however, means that clouds that already have a lower albedo due to the Twomey effect are also short-lived. Meanwhile, *polluted* clouds are not as effective in precipitating and will have a longer lifetime while having a higher albedo and hence an increase in surface cooling (Albrecht, 1989).

The impact of aerosols, particles only a couple of μm in size, on the Earth's radiation budget and precipitation processes is particularly complex. The direct and indirect effects of aerosols can cause both heating and cooling. Rainfall can either be suppressed under certain circumstances or enhanced. Modelling these interactions has also proved complex, mostly because the interactions are necessarily simplified to a great degree, as touched on in the earlier sections. New in-situ measurements have shown that we might even be underestimating the effects of these particles on global cooling. In the context of the current study, these processes are fundamental to understanding unintended rainfall enhancement, or suppression, over the Highveld, where pollution and continental effects may play a massive role in the microphysics of these clouds. Due to the importance of convective weather as the primary rain-bearing system over the region, the study will focus on these summer rainfall systems and our unintended modification through changes to the aerosol properties of the atmosphere over the Highveld.

Highveld aerosol characteristics

In-situ studies of aerosol concentration over Southern Africa, specifically the Highveld, were conducted on a large scale during the Southern African Regional Science Initiative (SAFARI-2000) and ARREX campaigns in the late 90s and early 00s. The studies provided valuable information on the seasonal characteristics of aerosols, and CCN particles, across the region. Ross et al. (2003); Terblanche et al. (2000)'s research proves valuable in this study. CCN measurements taken during these campaigns can be used to force models with local-scale conditions accurately. Ross et al. (2003) documented CCN concentrations for the Highveld is a factor of 2 higher than the WRF aerosol aware scheme default setup (300cm^3 compared to 680cm^3 for the industrialised Highveld in the late dry season). In Figure 1.13, Ross et al. (2003) observed CCN concentration for different areas of the Highveld as taken during various flight observations over the region. The decrease in the CCN from the lower PBL up to the top of the flight altitude is vital to consider, as the number concentration of particles decrease from the surface to the upper troposphere, and assuming a fixed concentration for the whole column during model runtime will not represent local-scale conditions.

The primary sources of aerosols over the Highveld are from localized emissions by industries, through biomass burning, regional dust, and the recirculation of aerosols over the subcontinent (Piketh, Annegarn and Tyson, 1999; Ross et al., 2003). Industries are a major contributor of CCN. CCN from industries occurs in the form of sulphur, a highly hygroscopic compound with a long lifetime in the atmosphere. Sulphur is also an enormously effective scattering aerosol, leading to changes in the radiation budget (Myhre et al., 2013; Ross et al., 2003; Stocker et al., 2013). Intended and unintended biomass burning is another source of atmospheric aerosols in Southern Africa via the release of organic compounds, soot and BC that act as CCN. These aerosols also scatter and absorb light, depending on their properties, and in the high troposphere and stratosphere, they can also act as ICN (Myhre et al., 2013; Ross et al., 2003; Stocker et al., 2013). Dust is another large CCN that occurs over the Highveld. These particles originate from the central and semi-arid regions of SA (Piketh, Formenti, Annegarn and Tyson, 1999). According to Ross et al. (2003), the transport of CCN from other regions, north and east of the Highveld, could account for high CCN concentrations over the northern Highveld. Industrial emissions accounted for most of the CCN particles over the central Highveld area.

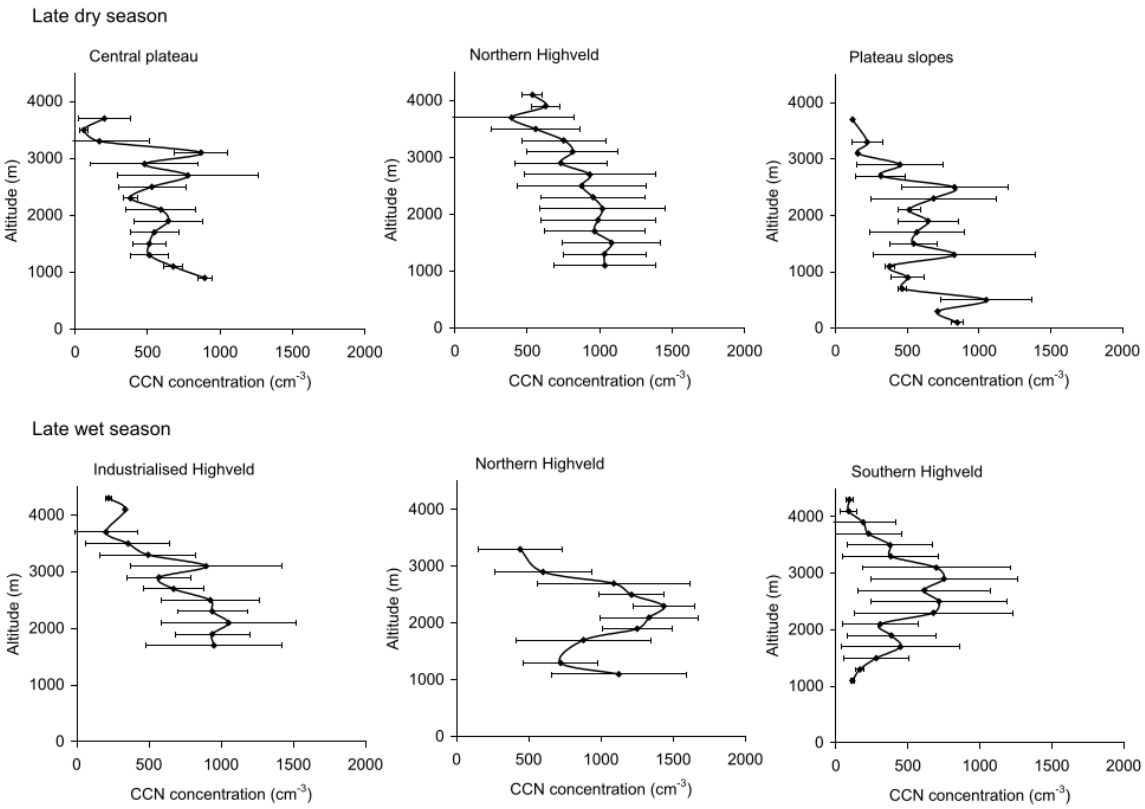

Figure 1.13: *CCN concentrations after the SAFARI-2000 and ARREX flights conducted by Ross et al. (2003) shows the number concentration of CCN during the late wet and dry season of the Highveld. It is also important to note the decrease of aerosols from the surface to the top of the flight. High surface concentrations decrease with an increase in altitude, however, in this Figure, we can see this is not always the case (see Northern and Southern Highveld).*

The N_c of aerosols/CCN is influenced by seasonal rainfall patterns, as precipitation leads to the savaging of aerosols (Balashov et al., 2014; Ross et al., 2003). It was found that CCN N_c was low during the Southern Hemisphere summer, during the rainy season. This would imply that over the Highveld, the main form of precipitation that leads to the deposition of CCN is convective weather events. In August and September, a high CCN concentration was observed during the late winter (early dry season) in August and September, when anticyclonic and stable conditions are prevalent over central SA (Balashov et al., 2014; Ross et al., 2003).

This section provided a general overview of aerosols, CCN and ICN characteristics in the atmosphere, implications in cloud formation, ice and precipitation processes, and the radiation budget. Two main rainfall processes are impacted by aerosol concentration and properties. This includes warm cloud and cold cloud precipitation. Both processes play an integral part in the hydrological cycle, and their radiative properties are, directly and indirectly, a function of aerosols. Globally, the IPCC report shows that the relative importance of aerosols on global cooling is considerable. However, heating by aerosols is also essential, and depending on the aerosol composition, it can directly absorb and warm the atmosphere. The importance of aerosols is stated in the above sections, and this underlines the need to study aerosols over the Highveld and their impact. The following section examines the use of NWP in cloud aerosol

studies and serves as a technical background for using NWP models in this research.

Numerical weather prediction in cloud-aerosol research

NWP models are employed by a variety of organisations throughout the world to understand the impact of aerosols on cloud microphysics, the radiation budget, and other atmospheric phenomena on spatial scales ranging from global to local-scale, and temporal scales predicting future climate scenarios decades ahead, to CPM trying to resolve aerosol impacts on small scale events, within minutes. These interactions are complex, as illustrated in Figure 1.14, representing the various cloud-aerosol interactions that have to be accounted for (Dudhia, 2014). Due to this complexity, processes are parameterised to improve model usability. However, parameterisation creates a large amount of uncertainty in NWP.

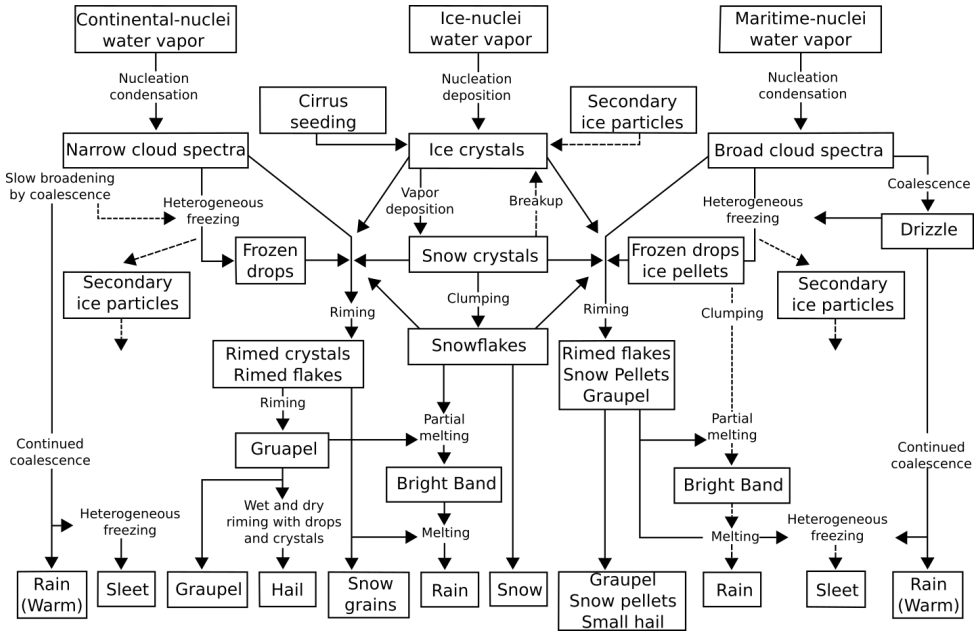

Figure 1.14: *The parameterisation of cloud-aerosol interactions needs to account for various complex interactions, as seen here. NWP resolves these processes through various parameterisations schemes (Dudhia, 2014).*

During model runtime, several assumptions are made on the initial N_c, size distribution, and position of aerosols in the atmosphere/cloud (Thompson et al., 2016). The coupling between the radiative parameterisation and aerosol microphysics parameterisation is important, and the physics applied in the parameterisation scheme has a major effect on the model output. Because it is a complex process to incorporate into NWP during runtime, necessary simplifications are made on radiation and aerosol properties. This meant that until recently, accurate, location-specific aerosols concentrations were not incorporated into various models, causing major uncertainty.

To overcome this, traditional NWP models required some form of alteration to the model physics to account for the specific impacts of aerosols, but this is not always viable in operational settings. A user could choose to use a specific NWP model, such as The Weather Research and Forecasting Model coupled with Chemistry (WRF-Chem), explicitly developed to simulate atmospheric processes involving chemistry (Thompson et al., 2016). Nevertheless, these models

were much more computationally expensive and designed for pollution case studies and not necessarily operational weather forecasting. New *aerosol aware* parameterisation schemes have been developed in response to these limitations. WRF's new *Thompson aerosol-aware* scheme (Powers et al., 2017; Thompson and Eidhammer, 2014) allows standard operational meteorological models to incorporate N_c of CCN and ICN during model runtime instead of the traditional fixed droplet N_c used in the past (Thompson and Eidhammer, 2014). This enhances an NWP model used by weather forecasters to capture aerosol impacts on the expected weather.

Thompson and Eidhammer (2014)'s new scheme yielded exciting results, which will be focused on here. Thompson and Eidhammer (2014) examined the effects of aerosols on a winter cyclone over the central USA. Building on his previous parameterisation scheme in WRF (Thompson et al., 2008), the paper incorporated an aerosol climatology derived from the 7 year Goddard Chemistry Aerosol Radiation and Transport (GOCART) global aerosols simulation to include a realistic aerosol N_c during model runtime instead of assuming an initial droplet N_c, as mentioned in the previous paragraph. The study relied on some consolidations of aerosols based on their known characteristics to create ICN and CCN classes for the model runtime. Aerosols with a mass $\geq 0.5\mu$m accumulated into ICN are called ice friendly aerosols or N_{ifa}, and other aerosol species apart from BC accumulated into CCN, referred to as N_{wfa} or water-friendly aerosols. The explicit definition of the aerosol count made the model computationally efficient for high resolution runs. From here, the study used WRF to simulate a control, clean, and polluted environment using the storm as a case study. The study found a marked difference in the median volume diameter (MVD) and liquid water content (LWC) of hydrometeors across the simulated environments with varying CCN concentrations as shown in Figure 1.15. Thompson and Eidhammer (2014) also allows users to specify an explicit N_c for CCN and ICN, and has some advantages over the use of a satellite-derived climatology of CCN and ICN concentration. First, if observational data is available for the region of interest and during the time of interest, an exact concentration can be specified. The CCN concentration is specified for the surface, and this value decreases exponentially up to 2000m, i.e. the top of the boundary layer. A second value is then specified, and this value remains constant up to the model top. The disadvantage of this is that the model assumes a simple value for the whole domain. If the domain is small, for instance, directly over a city, this method makes sense. However, for a large region with varying CCN and ICN concentrations, care has to be taken to ensure a representative value is accurate.

The three simulations were set up as follows. The GOCART aerosol climatology was set up and run for the control simulation with no user changes to the aerosol N_c. The control simulations explicitly changed the modeled aerosol concentration to represent a clean and polluted environment. The aerosol N_c was reduced to $\frac{1}{10}$th of the *control simulation* N_c in the clean simulation, while a factor of 10 increase in the N_c of aerosols from the *control simulation* was applied to examine a polluted environment. By examining the cloud MVD and LWC, Thompson and Eidhammer (2014) found that the N_c changed between the three environments as expected. The clean environment showed a large droplet MVD, while the droplet concentration was lower.

In contrast, the polluted environment showed a smaller MVD, but higher droplet number concentration. The LWC between the environments was also different. The clean environment had

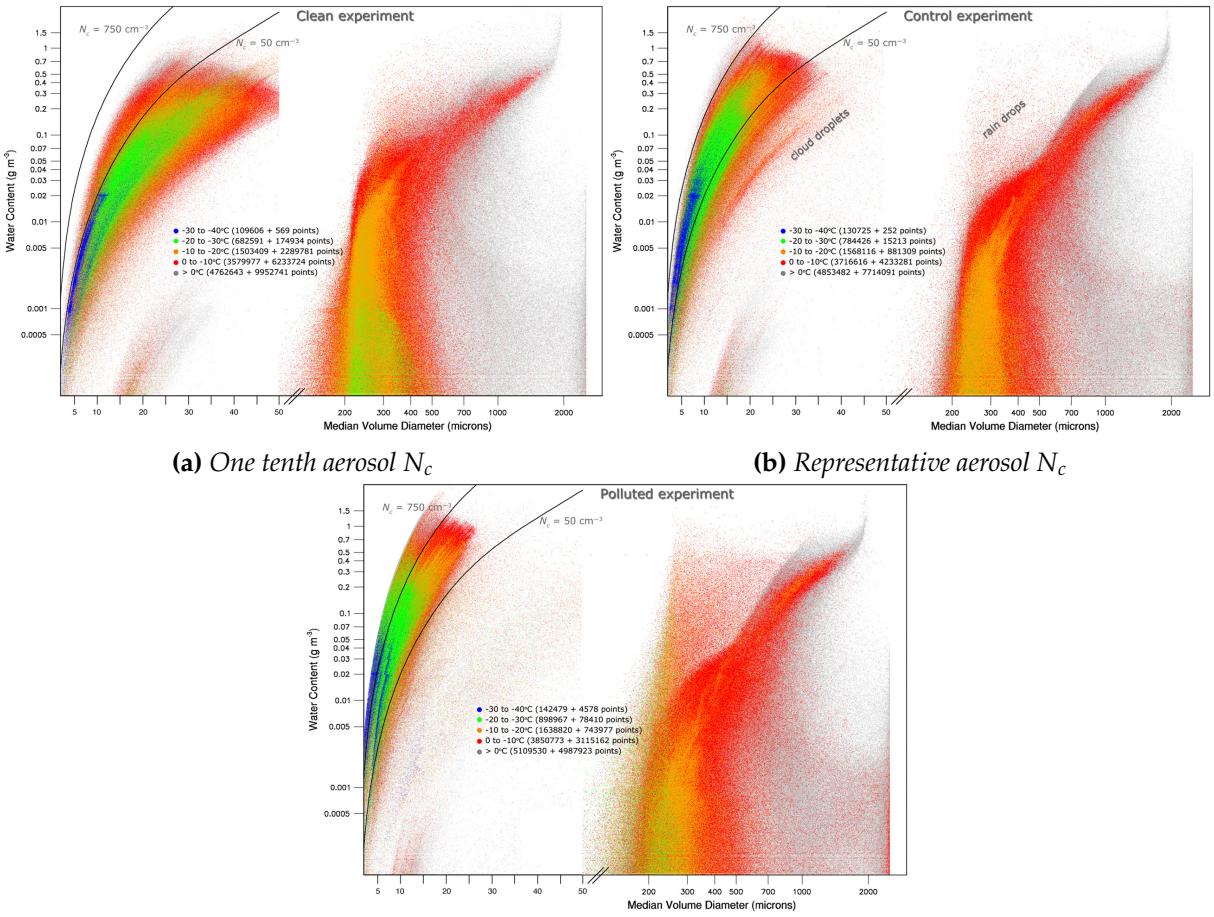

(a) *One tenth aerosol N_c* **(b)** *Representative aerosol N_c*

(c) *10x increase in aerosol N_c*

Figure 1.15: *Droplet number concentration in modelled clean and polluted environments after Thompson and Eidhammer (2014)'s study on aerosol impacts on a winter cyclone over central USA. The results indicate the difference between modelled clean (**a**), control (**b**), and polluted (**c**) environments. What is noticeable are the changes in the MVD and LWC of hydrometeors in the cloud.*

a lower LWC due to the lower number of droplets. Thompson and Eidhammer (2014) theorised that polluted environments with the higher number of droplets had an increased LWC, and the number of droplets reaching the freezing levels is higher in the polluted clouds as contact nucliation might be increased. Building on this study, Prein et al. (2017) used WRF with Thompsons new *aerosol-aware* scheme to highlight the possibility that there might be an increase in thunderstorm events over the continental USA, as seen in Figure 1.16, highlighting the possible increase in precipitation of future thunderstorms over New York City. This is supported by previous urban-convective-aerosol research by Van Den Heever and Cotton (2007), who found that urban derived background aerosols play a significant role in precipitation after convective initiation occurs. Although Prein et al. (2017) did not make any explicit link to aerosol concentrations, it shows that the use of new types of schemes can assist in understanding the nature of the atmosphere in a changing environment, possibly favouring convection.

NWP is consistently improving, from the early days of Lewis Fry Richardson's forecast factory where he dreamed of a large human calculator, forecasting the weather by hand(!) (Charlton-Perez and Dacre, 2011), to modern times when meteorologists can accurately predict the weather at the scale of a city. The implementation of a *real-world* aerosol budget in NWP is an exciting

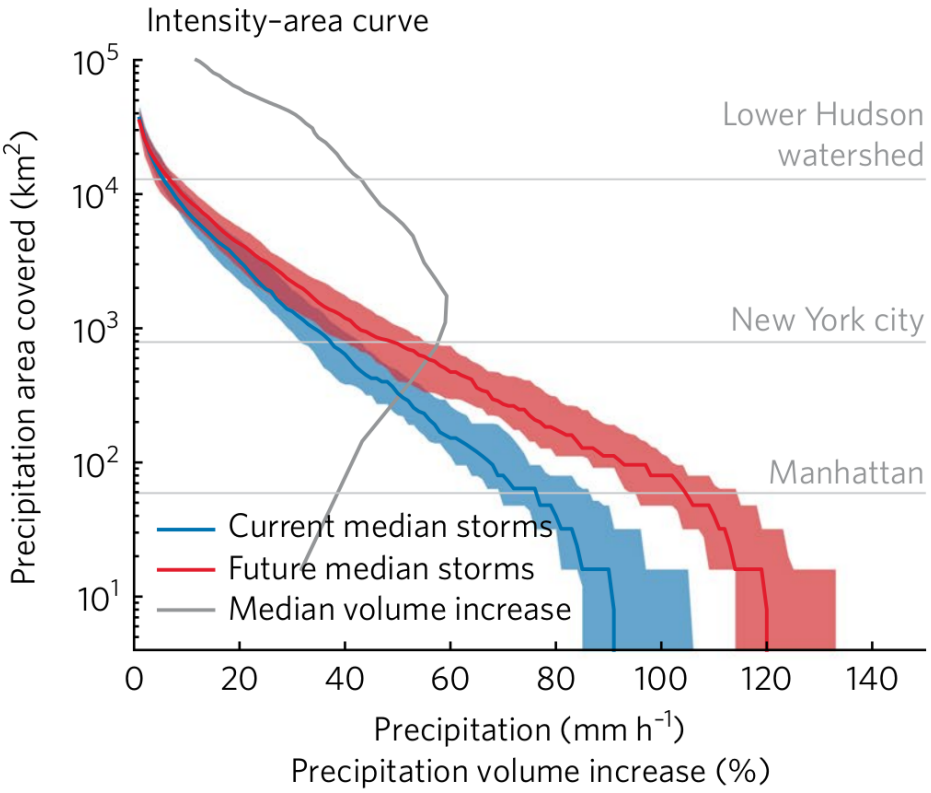

Figure 1.16: *Prein et al. (2017) used the new aerosol-aware scheme in research showing that future convective environments might be getting more severe, possibly leading to higher precipitation and flash floods. The above graph shows a possible future scenario for New York City, one of the world's largest and most famous metropolitan areas.*

development. With advances in computing power and model resolution, we can better understand anthropogenic impacts on various scales, which was difficult in the past. The application of aerosol aware schemes in the meso-γ scale range is already used in studies to examine changes in future convective environments, such as the paper by Prein et al. (2017) revealing that there might be an increase in future thunderstorms and flash floods in urban areas in the USA. This work is essential in South Africa too. Although past aerosol measurement campaigns have contributed significantly to our understanding of SA's aerosol profile, few CPM explicitly examine aerosol impacts on thunderstorms, which we aim to address in this study.

Cloud-aerosol applications in weather modification

Our understanding of the cloud-aerosol life cycle has led to the development of various cloud seeding programs worldwide to enhance or suppress rainfall, hail, and snow processes. This section will discuss the methods of intended cloud-aerosol modification. A mention is made of pyroconvection, the formation of clouds from fires that enhance convection and alter the aerosol profile. Fires are natural events in most cases, and pyroconvection is an exciting phenomenon due to the alteration of the cloud-aerosol profile and the high frequency of fires in South(ern)-Africa.

A natural weather modification phenomenon

"In March 1998, the Naval Research Laboratory (NRL) launched a satellite instrument named Polar Ozone and Aerosol Measurement (POAM) III. Just a few months after launch, POAM III started detecting mysterious clouds in the stratosphere in the sub-Arctic Northern Hemisphere. It was obvious that an unusual phenomenon was being recorded. We now know that these mysterious aerosol-cloud layers were smoke from forest fires that erupted like a volcano..." (Fromm et al., 2007)

Large scale burning events, such as a veld fires[7], can create an interesting phenomenon where convection and rapid aerosol loading occurs in a localised environment, leading to the formation of clouds. This is known as pyroconvection[8]. Pyroconvection can lead to the formation of pyrocumulus and pyrocumulonimbus clouds. In rare cases, this phenomenon can lead to the development of thunderstorms (Fromm et al., 2007; Keywood et al., 2013; Peterson et al., 2017, 2015). According to Peterson et al. (2017), cumulus clouds arising from fires have a distinctively different aerosol profile than traditional convective thunderstorms. Typically, the large aerosol N_c released during a burning event leads to the release of small hydrometeors that enhance cloud lifetime but seldom lead to heavy precipitation. The impact reaches beyond the troposphere, and Peterson et al. (2017) found that aerosol loading might impact ice crystal formation, and concentrations in the upper troposphere/lower stratosphere. Fires, especially in the high latitudes, deposit soot on snowpacks altering the albedo of snow surfaces increasing melting processes as was discussed earlier (Keywood et al., 2013). A similar phenomenon occurs during the eruption of volcanoes, which results in the release of large amounts of dust, ash, and sulphur into the atmosphere. Rose et al. (1995) calculated an ice mass of over 2 million tonnes in the clouds above volcanic eruptions using the Advanced Very High RadiometeR (AVHRR). These unintended modifications to the atmospheric aerosol profile show that various phenomena impact the cloud formation process.

Intended cloud-aerosol modification

Cloud aerosol research over the last decades has focused a lot on rainfall enhancement, or suppression, methods by altering the microphysical properties of clouds. Tessendorf et al. (2012) describes cloud seeding as the *enhancement of collision and coalescence* to improve the *precipitation efficiency of a cloud*. Cloud seeding methods are broadly defined into two groups, hygroscopic seeding and glaciogenic seeding (Bruintjes, 1999; Cotton, 1982). Hygroscopic seeding is applied on warm phase ($\geq 0°$) clouds, where water-attracting particles (e.g. salts/ammonium sulphates) are released into a cloud to enhance the N_c of the CCN (Bruintjes, 1999; Cotton, 1982). Glaciogenic seeding involves the release of silver iodide (AgI) in mixed-phase clouds. AgI is used as it has a characteristic structure that is able to mimic that of natural ICN, and promote ice growth in clouds (Bruintjes, 1999; Cotton, 1982; Vonnegut, 1947).

Intentionally altering cloud aerosol N_c through hygroscopic and/or glaciogenic seeding pro-

[7]South-African colloquialism for a wildfire
[8]*Pyro*; the Greek word for fire

grams has been a major subject of study over the last 40 years[9]. Active programs to enhance precipitation of rainfall and snowpacks exist worldwide and draw a great deal of attention. Our understanding of cloud-aerosol interactions has played a significant role in trying to alter the precipitation process intentionally. Nevertheless, we might unintentionally alter these processes through similar methods by increasing CCN and ICN in the atmosphere. If we include our changes to the land-surface area, we might increase and enhance local scale convection, much like the process of pyroconvection.

Local-scale urban heat island effects

Theories around the UHI effect have been well documented. Not only do the aerosol changes, as discussed in the previous section, impact precipitation processes, but intended modifications of the land surface area also change convective characteristics in and around urban areas. Not only will this change the thermodynamic profile as we discussed, but it has important implications for flooding management in urban areas (Liu and Niyogi, 2019). One of the first papers dealing with the unintended modification of precipitation processes over urban areas and land cover by Huff and Changnon Jr (1973) during METROMEX, indicated that large urban areas in the US change local precipitation processes dramatically, with a 4% – 25% increase in the mean precipitation downwind of urban areas. The increase in precipitation is possibly due to changes in the convective characteristics of the surface area over cities and CCN modification. Huff and Changnon Jr (1973); Kingfield et al. (2018)'s METROMEX work formed part of the first major experiment examining urban-industrial impacts on local clouds and precipitation in and around the St. Louis area (Changnon, 1992a; Changnon et al., 1977; Huff and Changnon Jr, 1973). During the same time, Garstang et al. (1975); Tyson et al. (1972) pioneered work to better understand temperature gradients around South African cities in what was known as the *Johannesburg Urban Heat Island Project* (Tyson et al., 1972). To achieve this Tyson et al. (1972) had a helicopter taking temperature measurements, while a motor vehicle simultaneously took similar measurements below the aircraft. Figure 1.17 shows an adaption of Garstang et al. (1975); Tyson et al. (1972)'s temperature profile over Johannesburg and the impact the city has on the downwind temperature profile. In the same Figure 1.17b, we can also observe a warm and cold bias in urban and rural areas during different times of the day – again showing how changes in the surface characteristics and roughness change the minor scale meteorology. In 1977, Held (1977) noted an interesting severe hail event during a prefrontal squall line over the central Highveld. In the paper Held (1977) makes particular reference to a group of cells within the storm system that showed more severe characteristics than the surrounding cells, these severe cells only occurred over urban areas of Pretoria, and Held (1977) speculated that this might have been enhanced by urban induced convection.

More recently, through the use of high-resolution NWP and land cover datasets, Chapman et al. (2017); Dimitrova et al. (2019) found that the effects of land surface changes may lead to an increase of up to 5°C in urban areas. However, these urban areas are not always well represented in GCM due to the small scale of these features. Krayenhoff et al. (2018); Ortiz et al. (2019)

[9]in the South-African context, if we take Mather (1991) as the first intended hygroscopic seeding publication, and Garstang et al. (1981); Mather et al. (1997) seeding experiments using dry ice a decade before that

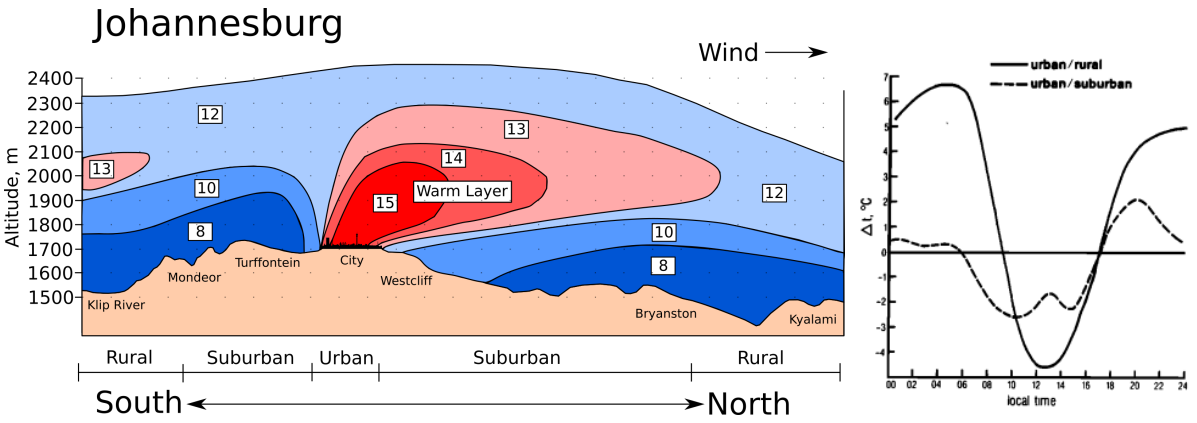

(a) *Idealized UHI profile* **(b)** *Excess Temperature*

Figure 1.17: *An adaption of Garstang et al. (1975); Tyson et al. (1972)'s urban heat island model for Johannesburg shows the effect of a southerly wind on the temperature gradient in and around the city. The changes in surface albedo and roughness will impact meteorology around the city and downwind, as seen in previous studies such as METROMEX. We refer to this Figure again in Chapter 6.*

speculate that cities and urban areas will have different local scale impacts under global climate change scenarios, most notably, the increase of extreme heat afternoons (when most convective activity occurs) over the cities in the USA. Moreover, because of the link between heat and thunderstorm formation, we can assume that Prein et al. (2017)'s (Figure 1.16) results showing an increase in convective events over cities is directly linked to warmer, more polluted environments.

The various factors that impact cloud dynamics and physics are broad. From the large scale synoptic circulation, the effects of land use on a local scale, to CCN on a micro-scale. The current thesis aims to understand these topics as it specifically relates to the occurrence of convective weather events over the SA Highveld, a region prone to convective storms, and also an economically important region for the continent. The study examines the problem holistically, from understanding the significance of these events in the region, the dynamics of the environment they occur in and then anthropogenic impacts on a very local scale. In the next section, we state the aims and objectives of this study and the rationale behind each objective.

Aims and objectives

Convective weather events occur under a variety of synoptic and thermodynamic conditions. There are however anthropogenic impacts that changes the characteristics of convective storms, and these are not yet well understood over major urban areas. The aim of the study is to build on the current convective storm literature of South-Africa by examining the following overarching theme:

What are the impacts of CCN and land-use modifications on convective weather events over the Highveld?

To achieve this, the study's main objectives are to:

- Characterise the nature of convective weather events over the Highveld using radar data
- Characterise the significance of convective weather events over the Highveld using national reports
- Characterise the synoptic and thermodynamic environment of significant convective events over the Highveld
- Evaluate local scale anthropogenic and non-anthropogenic impacts on convective events
- Examine changes in significant storm event characteristics under different CCN and land-use scenarios

In this broad introduction, we discussed several key aspects which form the main components of this study. The impact of convective weather on society. The importance of space and time in understanding weather phenomena. The climatology of convective weather over SA. Cloud-aerosol interactions. The effects of aerosols on droplet growth. The aerosol direct and indirect effects. The complexities of including aerosols in NWP. Several studies have stated that the projected increase in temperature may lead to an atmosphere favouring convection (Allen, 2017; Brimelow et al., 2017). However, these statements have some uncertainties as these events occur on a sub-grid spatio-temporal scale, which means storms are not well resolved in climate prediction models. Observations, crucial to initiate models, also seem to be decreasing, making model verification difficult (Reason and Keibel, 2004). By examining the spatio-temporal variability of convective weather events using radar and observational data, this study aims to build a detailed, and integrated dataset of these events for the region. This integrated dataset will guide the use of a novel CPM to simulate CCN and land-use impacts on convective weather. The importance of this study, and other research with a similar focus, helps us address some challenges still faced in the atmospheric sciences, as discussed in Gimeno (2013)'s *Grand challenges in atmospheric science* publication. This specifically relates to small scale processes (challenge 2), aerosol-cloud interactions (challenge 4), weather prediction (challenge 5), interactions between scales (challenge 8), extreme events (challenge 9), and urban weather and climate (challenge 11). These challenges share a common theme; *factors driving unpredictable weather that impact society is not yet fully understood*.

SA is in a unique situation. The country has a well-developed economy, insurance sector, and infrastructure. Numerous people live in poverty with an increased vulnerability to natural disasters, such as the weather events discussed here. Through this study, we might better understand our impact on convective events and the vulnerability faced by different communities in the context of a changing climate and changing urban landscape, where extreme events might increase in intensity, frequency, severity, and our contribution to this change. This, and similar studies, provide a pathway to better understand, plan, and mitigate future risk scenarios.

Chapter 2
Data and methods

The following chapter describes the study area, data sources, model setup, and statistical methods used in this study. The first part of this chapter provides an overview of the Highveld region pertaining to this study, followed by a description of the various weather and climate data sources used to characterise and quantify convective storms over the study area. We build a novel climatology that integrates surface radiosonde, radar data, and media reports of convective weather events within the region. Data from the SAWS Irene weather station is used extensively due to its long-term availability and proximity to SA's major industrial complexes and cities. We provide an overview of WRF's physics and dynamics used to simulate the convective weather case under different CCN and urbanisation scenarios.

The Highveld region

Located in the between 21°S – 35°S and 15°E – 35°E (see Figure 2.1), SA's weather is affected by both tropical and mid-latitude weather systems throughout the year. The location also means that most of the country is dry due to its location beneath the descending leg of the Hadley cell, with an average rainfall of 450 mm per year (Dyson et al., 2015). The Highveld, which forms the central area of this study, is located in the central, interior plateau of SA at a mean altitude of 1500m – 1700m above sea level and covers an area of 30000km^2 (Freiman and Piketh, 2003). The area is home to SA's major industrial complexes and 75% of all industrial activities. The region contains some of the world's largest gold and platinum mines in Johannesburg and Rustenburg. Agriculture activities in the Free-state, North-West, Mpumalanga and Gauteng covers 70% of the total area and contributes to the economy and food security of SA (Collett et al., 2010; Scheifinger and Held, 1997). The Gauteng region is SA's most densely populated province and home to 20% of the population (±12 million people) (Dyson, 2009) – many of them in informal housing structures.

In this study, the Irene weather station managed by SAWS is considered the best representative of the Highveld weather in terms of data availability. We will extensively use data from the daily radiosonde launches and the radar located in the area. Figure 2.2 and Figure 2.3, indicates a 200km radius around the main radiosonde and radar site. The 200km radius was conceived after research on proximity soundings, showing that the selected radius can accurately represent the thermodynamic environment (Craven et al., 2004; Dyson, 2015). Convective events occur on a space and timescale not always covered by the radiosondes, which is spatially and temporally isolated. However, the radar's 200km radius covers the majority of the industrialised Highveld, providing a high spatio-temporal source of data for precipitation characterisation. The selected area also regularly releases radiosondes and has a long-term data record from 1974 to the present.

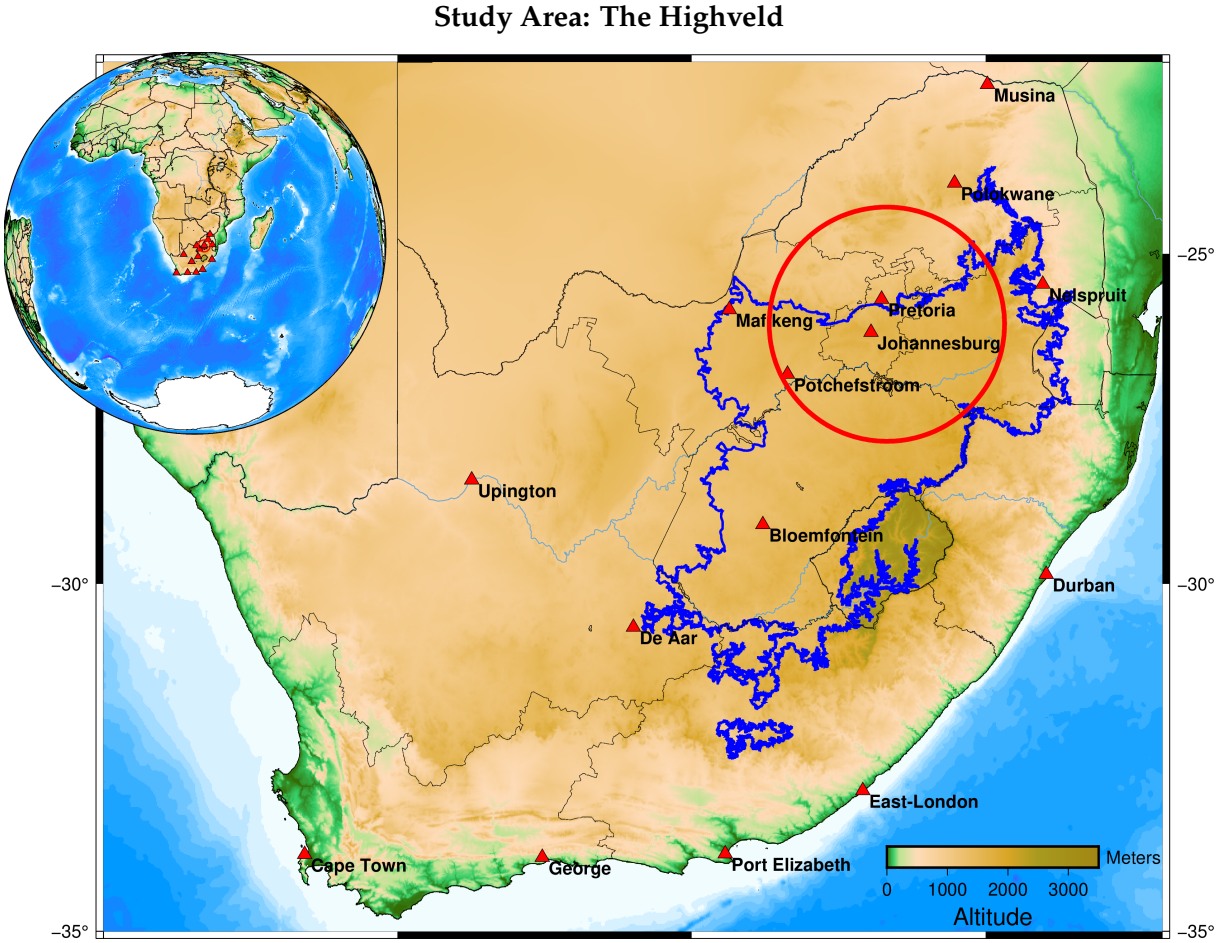

Figure 2.1: *The above map indicates SA and some major cities in it. The primary study area is the Highveld of SA, located in the central interior. The Highveld, demarcated in blue, consists of some major cities, including Johannesburg, Pretoria and Bloemfontein. As seen on the above map, the area of interest is indicated in a 200km zone around Irene, Gauteng.*

Weather and climate data

SAWS is the national weather and meteorological service and are the custodian of all SA weather-related data. SAWS has a well-developed observational network, as seen in Figure 2.2. According to SAWS (2018), the network consists of the following: 231 AWS, 12 climate stations, 1180 rainfall stations, 153 automatic rainfall stations, 23 sea surface temperature (SST) stations, 12 voluntary observational ships, 47 weather buoys, 14 radar sites, one global atmosphere watch station, 24 lightning detection sensors and 11 upper-air sounding stations. In recent times, data availability has drastically decreased, partly due to structural challenges and the SAWS policy change that limits data availability on easily and freely accessible platforms.

Surface observations

Some data collected by SAWS is available through NOAA; this includes the Integrated global radiosonde Archive (IGRA), Global Surface Summary of the Day (GSOD), and Global Historical Climate Network Daily (GHCN) as part of international mandates. Figure 2.4 shows the number of stations with data available online for public use. This study will make use of SAWS

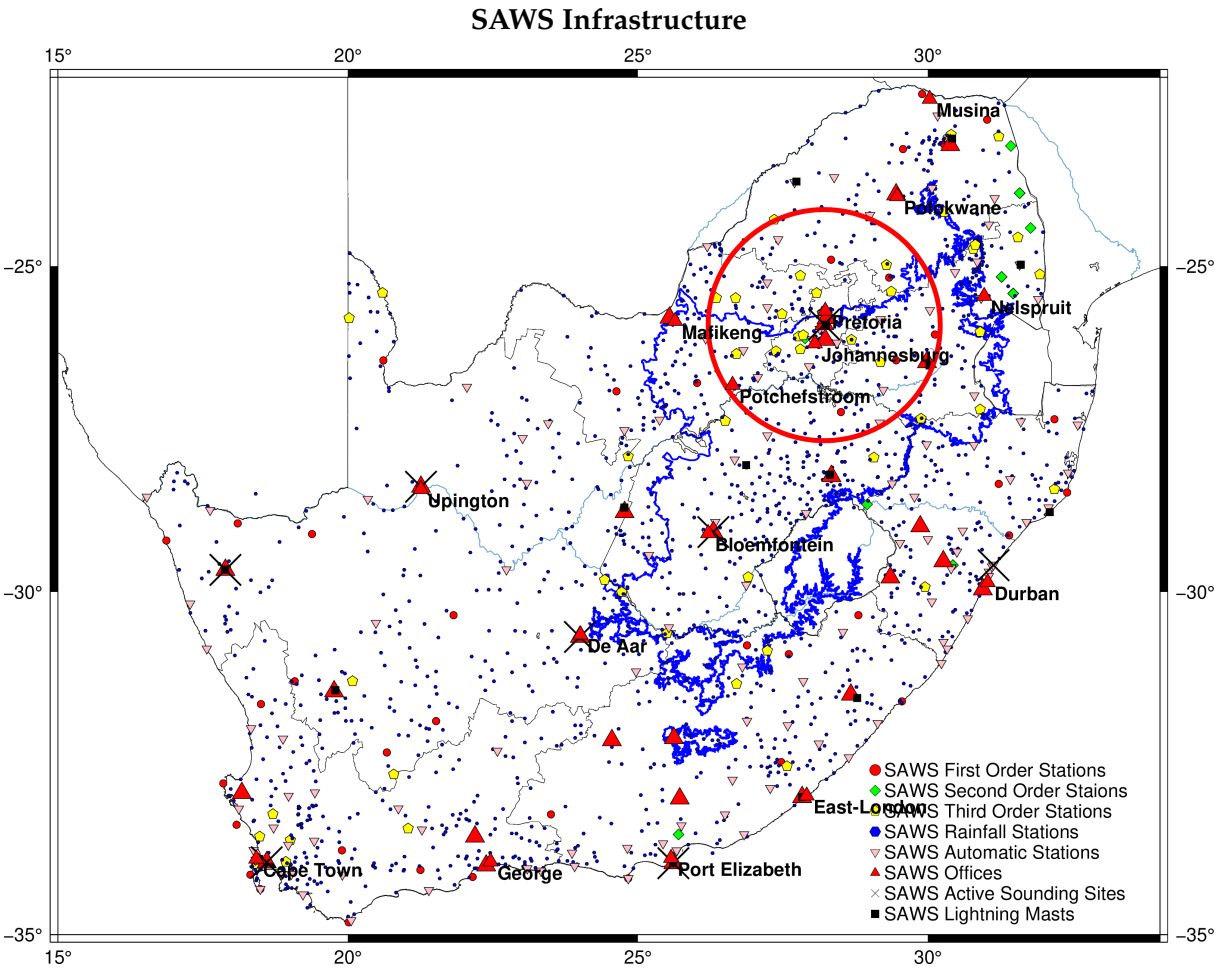

Figure 2.2: *The above map indicates the location of SAWS' various observational platforms. This study will mainly focus on events that occur over the Highveld of SA. The demarcated area indicates a 200km area around Irene. Not all the stations seen here has readily accessible data. However, as indicated in Figures 2.4 and 2.5, there are some sites which the public can access data through various partnerships SAWS has globally.*

and publicly available data from the IGRA. SAWS, GSOD, and GHCN data will be used to analyse surface variables for stations in the 200km radius around the selected radiosonde sites. For this study SAWS provided hourly temperature and rainfall data for the following weather stations within the area of interest: Wepener, Bloemfontein, Bloemfontein Weather Office (WO), Fauresmith, Glen College, Ficksburg, Bethlehem – WO, Taung, Bloemhof, Welkom, Kroonstad, Frankfort, Vrede, Vryburg, Klerksdorp, Potchefstroom, Vereeniging, Lichtenburg, Ventersdorp, Johannesburg Botanical Gardens, Springs, Tosca, Mafikeng – WO, Rustenburg, Grand Central, Pretoria Eendracht, Pretoria UNISA, Wonderboom Airport, Irene – WO, Bolepi House, & Pilanesberg. The GSOD archive contains 18 variables for over 9000 stations worldwide. The database includes minimum, maximum and mean temperature, dew point temperature, wind speed, mean sea level pressure (MSLP) and rain, hail, snow, tornadoes, and thunder indicators. The GHCN contains data from various stations worldwide, and the dataset is available as a daily and monthly mean product. In this study, only the daily products will be used if SAWS data does not cover a time period or region for the analysis. As seen in Figure 2.4, the GHCN contains more detailed and complete data products than the GSOD. The long-term validated

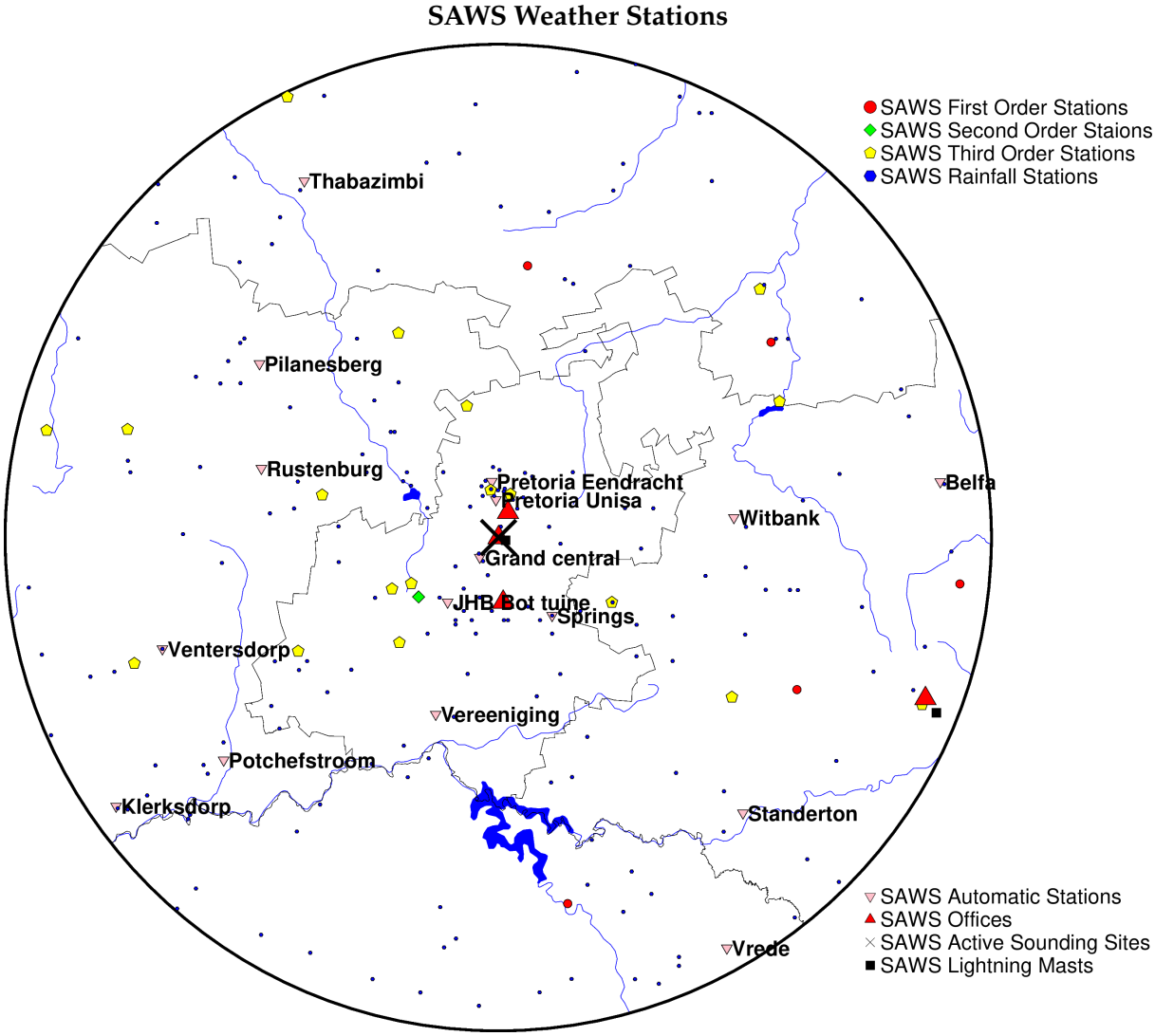

Figure 2.3: *The area above indicates a 200km radius around the Irene weather station where SAWS manages weather stations. Here radar observations, upper air sounding, and various surface measurements take place. The radar located at the site is a state of the art S-band radar managed by the SAWS. The area above contains major metropolitan areas such as Johannesburg and the surrounding suburbs, as well as rural towns, informal settlements, agricultural areas, and major mining complexes. Not all data seen in the Figure is publicly available.*

dataset, seen in Figure 2.4, refers to data used by National Aeronautics and Space Administration (NASA) GISS Surface Temperature Analysis (GISTEMP) research (Hansen et al., 2010). The GHCN undergoes a quality control procedure, documented by Menne et al. (2012). Figure 2.5 shows the same stations as the previous Figure 2.4, but only indicates the number that falls within the Irene radar range. Unless otherwise indicated in the subsequent chapters, publicly available data and data provided by SAWS are used in this study.

Radiosonde data

Data gathered from the IGRA database (Durre et al., 2006, 2008) for Irene is used in this study. The site has been launching radiosondes for over three decades, and this provides adequate data points to conduct a climatology of the region. Durre et al. (2006, 2008) conducts a quality

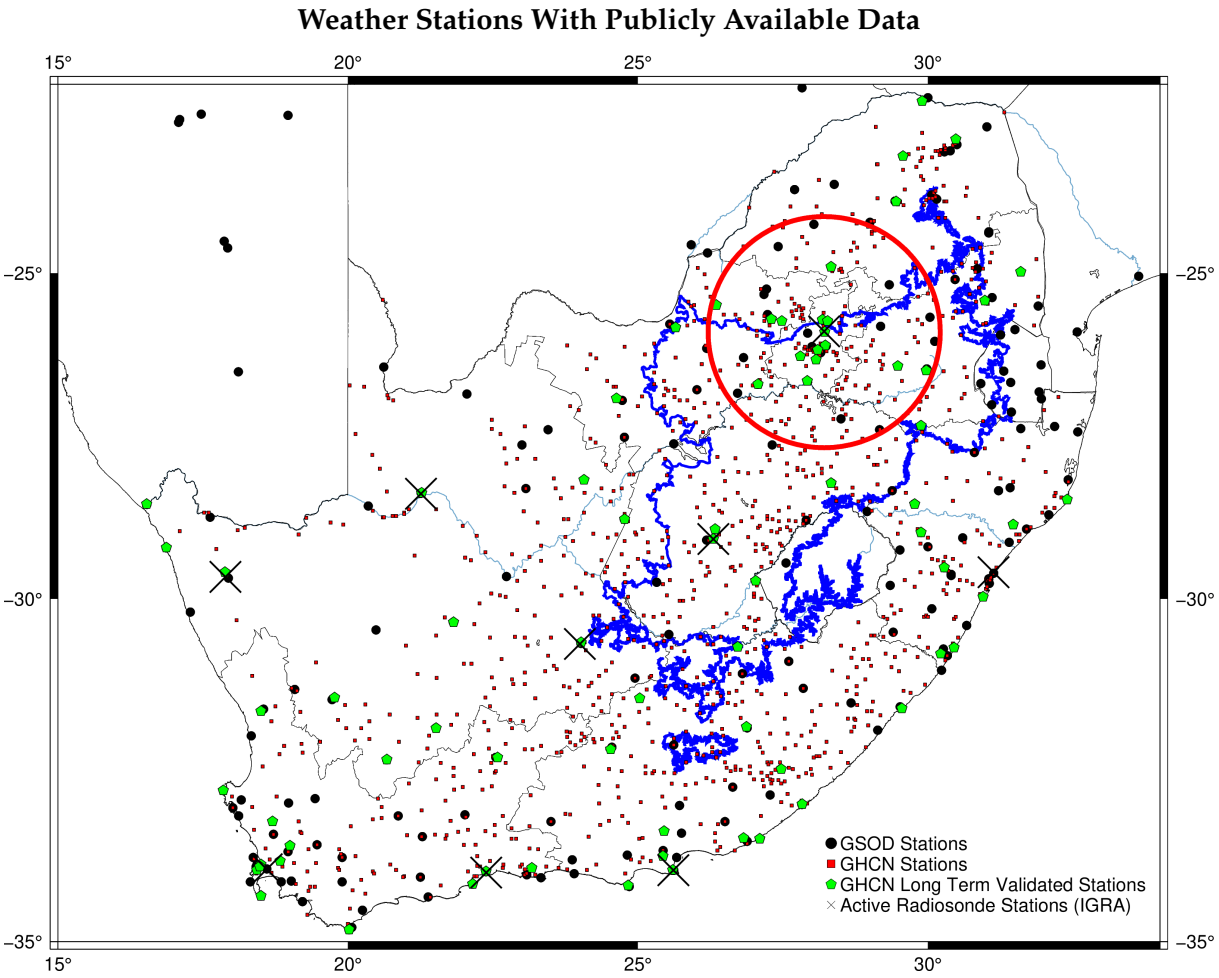

Figure 2.4: *The above map indicates the number of weather stations that have data available in the public sphere. The GSOD, GHCN and IGRA data is made available through NOAA. As mentioned, the demarcated area indicates a 200km area around Irene. Some of this data is used in this study, along with data provided by SAWS.*

control procedure before making the data publicly available. Similarly, Craven et al. (2004) states that contaminated soundings would be minimal in an extensive database of soundings and not have a statistically significant impact on the data analysis. Figure 2.6 shows the availability of radiosonde data for South-Africa from the IGRA database. In this study, the radiosonde analysis is similar to that of Dyson et al. (2015). However, Dyson et al. (2015) examined the thermodynamic environment and the relationship to rainfall events. No direct link is made to specific types of convective events. This study, in contrast, examines the convective environment using an integrated storm climatology of actual events; based on storm reports and radar data. Convective storms are directly dependent on diurnal heating and cooling of the Earth's surface, mainly in the afternoon, in this regard the 1200 Coordinated Universal Time (UTC) sounding represents the pre-convective environment before convective initiation occurs most accurately. This method has been utilised in various studies examining convective weather environments as described by Blamey et al. (2016); Dyson (2013); Dyson et al. (2015); Merino et al. (2013); Mohr and Kunz (2013). Research by Gettelman et al. (2002) tested the use of combined vs single 0000 UTC and 1200 UTC soundings in a trend assessment and found no effect in the overall trends when combining both soundings. Derived values that will be used from the radiosonde data

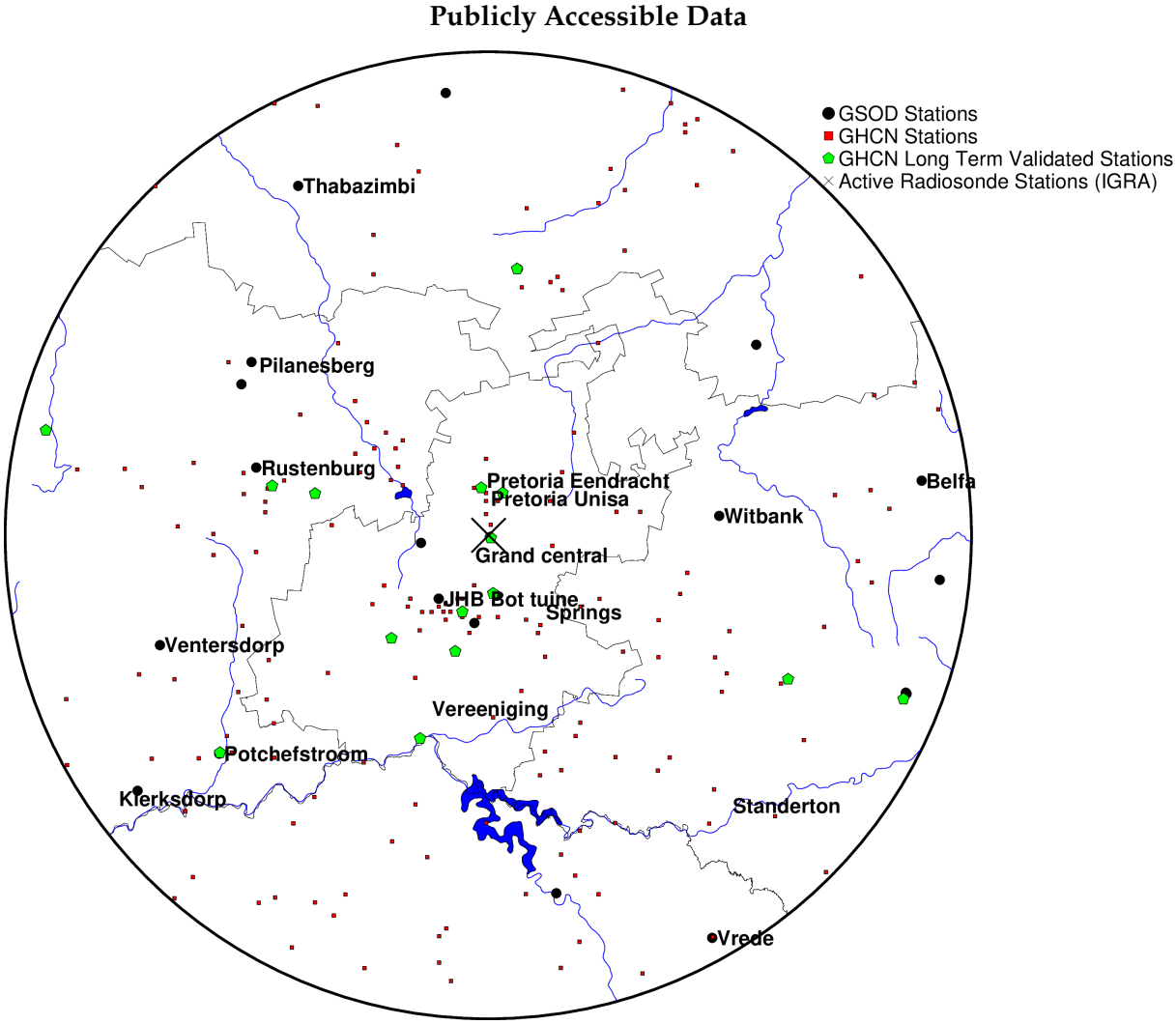

Figure 2.5: *A closer examination of stations that have publicly accessible data within the Irene radar range. Public accessible data provides a significant benefit to society in various ways. The data allows low-cost data analysis for various sectors that cannot necessarily compete with significant institutions that collect or pay for the state of the art data.*

include temperature, wind, and convective parameters (CP). CP are a theoretical measure of stability (instability) derived from the changing temperature, dew-point, relative and specific humidity, and wind fields as the sounding rises through the atmosphere. CP provide a good understanding of convective weather potential and the changing thermodynamic properties of the atmosphere, *in the mean*, when examining data over long periods (Mohr and Kunz, 2013).

Durre et al. (2006)'s IGRA dataset undergoes quality control (QC) before publication and additional QC procedures were applied to eliminate erroneous soundings. First, on the raw soundings, Dyson (2015)'s QC is applied, and the following criteria are used to remove soundings:

- Lat/Lon falls outside Gauteng and Highveld
- Tmin < -120°C & Tmax 45°C
- Relative Humidity > 100%

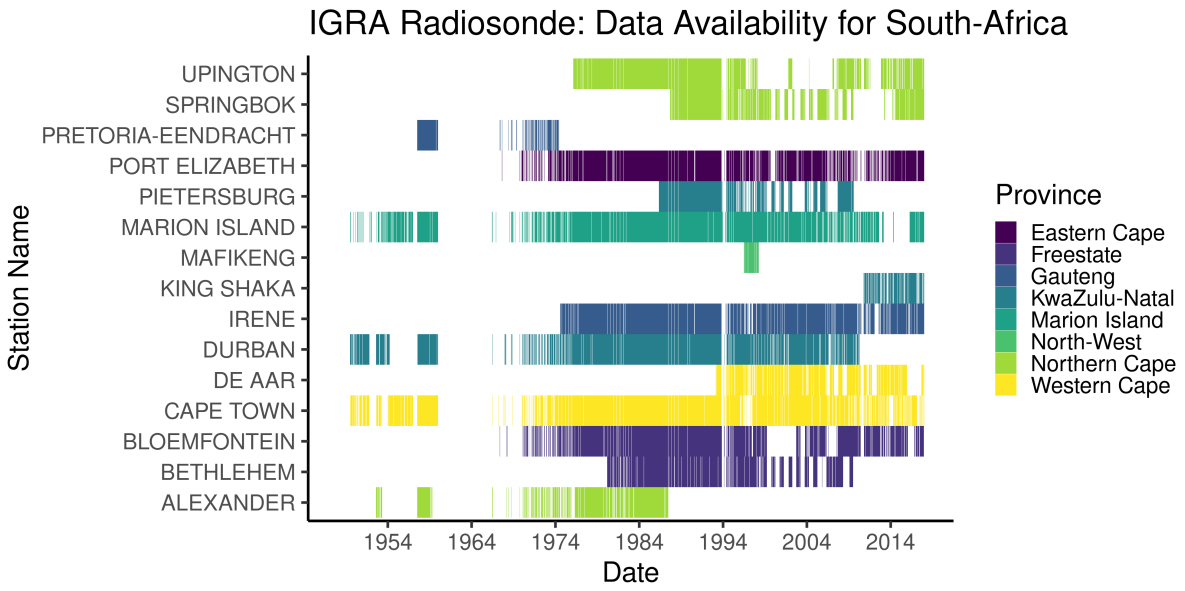

Figure 2.6: *Radiosonde data availability from the IGRA shows that SA has a well maintained historical archive of radiosonde data. In this study, Irene radiosonde data will be used to understand the occurrence of convective environments better.*

- WSmax > 150 m/s
- Tmin > 0°C > 500 hPa

All events where there was not a radiosonde launch on the day of the report is removed. Following Craven et al. (2004), all soundings with CAPE ≤ 150 J/kg are removed. Sounding are omitted if two consecutive soundings were duplicates. All 0000 UTC soundings were included after Groenemeijer and Van Delden (2007)'s work, which showed the 0000 UTC sounding not to significantly effect on the data. The inclusion of the 0000 UTC sounding means there are more soundings than reports in some cases.

Further quality control is implemented based Otte et al. (2017)'s multi-decadal analysis of various weather stations trends around Kilimanjaro, Tanzania, where a *Grubbs test* is employed removes significant outliers ($p < 0.05$) in all the datasets. Any other outliers were manually removed. This included one sounding with a LFC of 6000m and another with a LCL over 4000m. Any other erroneous sounding is assumed not to have a statistically significant impact on the dataset as analysed here due to the dataset size (Craven et al., 2004). After the above analysis, we extract the instability indices of event day, including "heavy rainfall and flooding" here. Lightning reports have more valid soundings than actual reports, and this occurred when there were two soundings (0000 UTC and 1200 UTC for the respective day). After the non-valid values are removed, there are approximately 227 soundings associated with convective weather during November, December, January, February, and March (NDJFM) over the Highveld (see table 2.1 and Figure 2.7). The QC procedures on the radiosonde data address issues that could represent unrealistic convective environments. Dyson et al. (2015) QC criteria has been developed for local conditions and was successful in creating baseline climatology of soundings for heavy rainfall events.

Table 2.1: *Number of weather reports across the Highveld collected in the Caelum reports, with valid radiosonde soundings from 1979-2018.*

Event type	Number of reports	Number of valid soundings	Completeness
All events (incl. non-convective events)	599	350	58%
Convective events (NDJFM in brackets)	443	278 (227)	62% (51%)
Hail	95	42 (28)	44% (29%)
Thunderstorm	14	10 (5)	71% (35%)
Lightning	48	54 (46)	100% (99%)
Tornado	36	11 (6)	30% (16%)
Heavy rain/flooding	250	161 (142)	64% (57%)

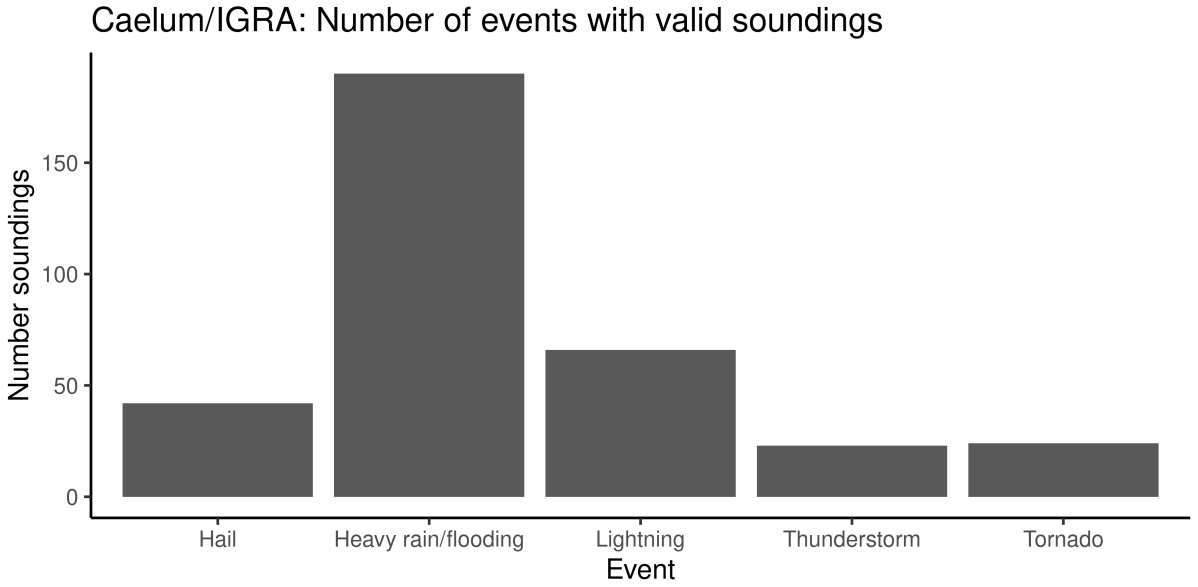

Figure 2.7: *Number of weather reports across the Highveld and Gauteng with valid radiosonde soundings from 1979-2018.*

The data, space and time conundrum in NWP

The greatest challenge of NWP is ensuring consistently accurate forecasts. Hindcasts, such as what the analysis in the above section, offers researchers an opportunity to evaluate model performance on a daily basis. However, the validation is only as good as the quality-controlled observational data and reanalysis data used. Ensuring these datasets underwent scrutiny and quality control will ensure accurate evaluation of the model outputs. Real-time forecasts are more challenging than hindcasts. The initial condition problem of NWP means accurate observations across space and time are essential to ensure forecasts that add value, and are trusted consistently. Over the last 40 odd years, the number of surfaces and upper-air observations in SA has decreased, as seen in Figure 2.8. Not only does radiosonde data, as we showed in the previous sections, provide us with valuable observations to evaluate the current state of the atmosphere, it is also a significant component of the global forecasting system, ensuring accurate initiation conditions. Having fewer soundings to initiate models will lead to more significant errors and difficulty to validate the model due to the lack of actual observational data. Satellite data has been groundbreaking in improving our NWP understanding by providing initiation data in remote areas but it comes with its own set of assumptions and errors. To address this,

there is a need to improve local measurement campaigns, ensure reliable radiosonde launches across the country, improve instrument capabilities, ensure calibrations and improve quality control measures. Not only will these improvements make a difference to the South African NWP landscape, but it will ensure global models, on all space and time scales, provides more realistic forecasts.

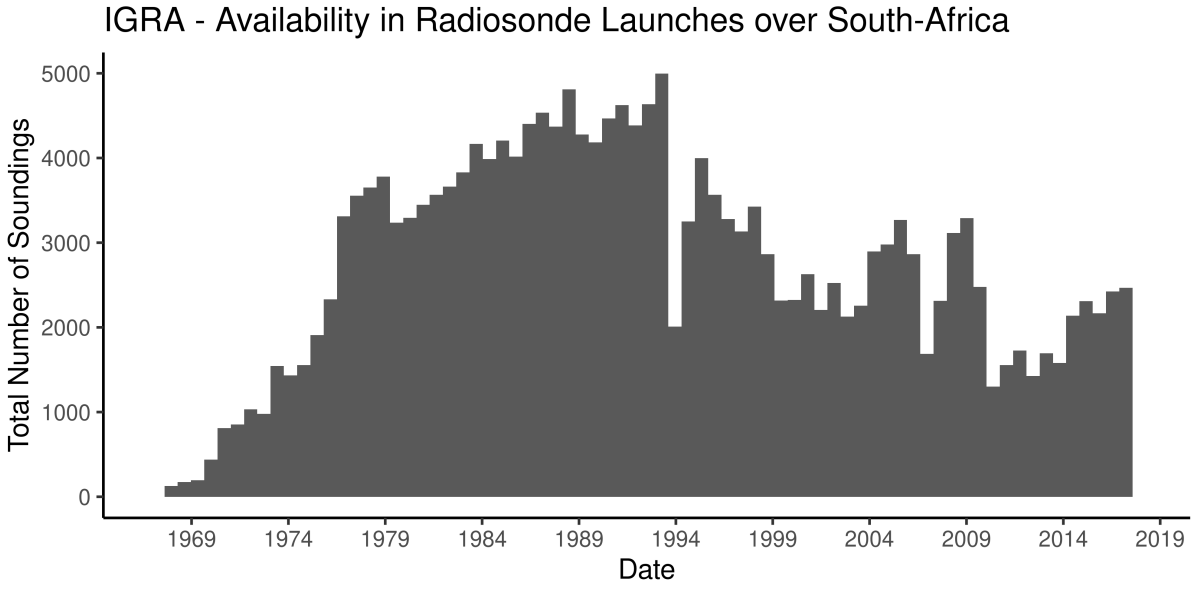

Figure 2.8: *IGRA sounding availability in South Africa show how the number of soundings and sounding locations, have decreased over time.*

Radar data

A weather radar is one of the most valuable tools to map and measure weather (specifically precipitating clouds). The high spatial and temporal resolution of radar data makes it exceptionally valuable in real-time weather monitoring and warnings. The advantages of radar stretch beyond its traditional use of a now-casting warning system. In data sparse regions, radar data can derive rainfall values where no other instruments exist. The most basic measure used in the radar meteorological community to understand the observed weather is radar reflectivity or dBZ. dBZ is a function of an electromagnetic wave power return from a target. The power function is determined by the concentration and scattering coefficient of the target. Uncertainties in radar data include ground clutter, and even biological targets, as the radar is agnostic towards the *type* target and returns all backscattering (Starzec et al., 2018). Understanding the characteristics of the clutter, the speed it changes between subsequent radar scans, and the direction of movement, allows forecasters to predict observable storms within a short time accurately. SAWS manages a state-of-the-art radar network across SA. In 2010 the organisation bought 10 S-Band radars, each with effective coverage of 200km covering most of the country. The network is often down due to power outages, and capacity shortage, making it difficult to provide operation products (Du Preez, 2017; Stein et al., 2019).

The network uses open-source radar software, Thunderstorm Identification Tracking Analysis and Now Casting (TITAN), developed by Dixon and Wiener (1993). TITAN tracks, forecasts

and extracts storm characteristics as a function of the power return. According to Stein et al. (2019), the SAWS radar network follows the following scan strategy, 12 elevation steps from 0.5°to 30°with a beam-width of 1°and 500 m range gates, and a full volume scan derived every 6min (Stein et al., 2019). Cluttering is a common problem around radar sites, and SAWS applies TITAN's default clutter removal algorithm to remove and disturbances in the data. Clutter is defined by using the mean dBZ point during a *dry* day where no weather occurs. If the point exceeds ten dBZ during these clean air scans, it is considered an unrealistic feature and removed in the subsequent scans (Stein et al., 2019). Figure 2.3 indicates the effective radius of the Irene Radar and area covered by the radar volume scan. Like Starzec et al. (2018), we remove all values below 35dBZ, assume this is not representative of convective weather events, and limit the data to NDJFM. During NDJFM, rainfall is mainly convective, and non-convective rainfall typically has a low dBZ return. The TITAN module *Tracks2ascii* is used to convert the original radar volume scans, after de-cluttering, into ascii table files suitable for spatio-temporal analysis. The de-clutter algorithm can result in the loss of some data points, but it is assumed these are negligible on the scale of convection.

There are three seminal papers by Carte and Held (1978); Kelbe (1984); Mader et al. (1986) respectively that propose a radar climatology in SA. This chapter builds on this original work and expands the data analysis to 5 years of radar data. During this time there are no known changes to the radar's scan strategy. The original papers mentioned above examined small subsets of data and, in some cases, only data collected during specific research cases, i.e. Kelbe (1984) during cloud seeding campaigns in the Lowveld.

Lightning Data

Lightning is a good proximity measurement for convective storm activity (Cecil et al., 2014, 2015; Chronis and Koshak, 2017; Takayabu, 2006). We incorporate 18 years (1998–2020) of Lightning Imaging Sensor (LIS) data from the Tropical Rainfall Measurement Mission (TRMM) (1998–2015) and International Space Station (ISS) (2017–2020) missions to validate the radar derived results on the spatio-temporal scale of convective storms. Both missions were conducted onboard polar-orbiting satellites, and some temporal inhomogeneity exists, but we extract over 190000 lightning flashes in the coverage of the Irene radar for analysis. We do not attempt to build a lightning climatology as it is beyond the scope of this study, but the data is a valuable addition to verify convective storm activity. Both TRMM and ISS mission's lightning data undergoes quality control before being released to the public (Blakeslee et al., 2014, 2020; Stolz et al., 2014).

Media reports

An updated version of Caelum (1991), provided by SAWS, is used in this study to understand the spatio-temporal distribution of documented severe weather events similar to that of Martins et al. (2017); Mohr and Kunz (2013); Paruk and Blackwell (1994). Caelum (1991) represents the most destructive and notable of events that had an impact on the South-African landscape and population. The first entry dates from 1647 and provides a comprehensive record of severe events. SAWS provides the data with a date, and spatial point, used to map the data. Data with incomplete spatial points, or spatial points not in the Highveld, was removed. Storms

containing keywords such as lightning, flash floods, hail, or tornadoes that represent convective events were extracted Events with no keywords were excluded as well. Using this keyword filter removes events other than those driven by convection. The subjectivity of this dataset is considered throughout the whole study, but it provides valuable information on storms that have impacted SA in some extreme sense. The small-scale nature of these events provides data where surface stations might not have been located to record events (Tippett et al., 2015).

The last printed version of Caelum (1991) from SAWS was in 1991. After that, SAWS has kept a digitised version of the database, as used here. The database provides details of the storm data, the closest city/town to the report, latitude and longitude, event type, and event details (usually only extreme events). Although the database is a treasure-trove of information, it has some issues that needed to be addressed before the analysis. We applied two significant changes in the database to ease classification and categorisation, as listed here:

- Storms were reclassified into discrete categories
  - As is, the digitised version of Caelum contains over 100 categories of weather-related events, many of them slight variations of the same type of event, for example, *"rain, cold conditions"* and *"rainy cold conditions"* occur in the database. To address this, all events based on keywords in the description were divided into the following categories:
    * Thunderstorms
    * Tornadoes
    * Heavy rain and floods
    * Lightning
    * Hail
    * Strong winds
    * Winter weather
    * Heatwave
    * Drought
    * Other (tropical cyclone, fog, high seas and fires)

- Classifications of storms into **severe** and **non-severe** categories
  - We build a severe and non-severe dataset by searching for keywords related to economic loss, mortality, livestock loss, etc., in the reports. Events with these keywords were classified as severe. Events without descriptions did not cause major damage or losses. Nevertheless, these events were severe enough to be included in the original dataset, and these events are classified as non-severe. In summary, the severe and non-severe database is built as follows:
    * **Severe:** storms that included a report with a description of extreme damage and/or loss of life
    * **Non-severe:** storms that were reported, but no official damage report is noted in the description

Several other changes are also made to the dataset regarding the date and time conventions. Some events occurred over two or more days, here only the first date of occurrence is used in the analysis; for instance an event that occurred on 2015/11/10 – 2015/11/14 is noted as 2015/11/10. The *"other"* category includes all secondary weather-related events, the most prominent of these being fire, fog and high seas. Using a broad category for "other" events is a subjective decision, which allows the study to focus on convective weather events. The QC brings about some interesting points of discussion. The most notable is that droughts are only recorded as a primary event from the early 2000s, an excellent example of the limitations and subjectivity prevalent in Caelum (1991).

Convective events explicitly reported in Caelum is analysed after following the QC discussed above. Here thunderstorms, lightning and hail events are combined for the analysis. There is some limitation: Heavy rain/flooding events could also be convective by origin; however, it is omitted as a convective event if this was not explicitly stated in the original description.

The last analysis attempts to quantify the losses suffered as a result of all events in the database. All events with descriptions in the dataset (i.e. severe events with damage report) is classified into three categories;

- events where human and livestock fatalities were reported,
- events with reported damage over ZAR 1million (not adjusted for inflation),
- and all other events with reported severe damage.

All events without a detailed report are omitted here. Again it has to be stated that this is not an objective database of all losses suffered. These reports are biased towards economically important and populated areas. We take careful steps to limit our analysis to better understand the seasonal and temporal variation in storm reports and frequency, and not to provide a trend of severe weather occurrence or possible effects of climate change as a function of reporting frequency. Not accounting for these constraints would be a fundamental misunderstanding of the data limitations. The data nevertheless provides a similar picture of weather events spatial distribution as that of Blamey et al. (2016); Schulze (1965); Taljaard (1981); Tyson (1986); Tyson and Preston-Whyte (2000). Following this QC we extract data for the Highveld region, and omit all data for the rest of SA.

Reanalysis data

The European Centre for Medium-Range Weather Forecasts (ECMWF)'s newly released ERA5 reanalysis is used in this chapter to build a high-resolution synoptic climatology of the atmospheric state as modelled during severe weather events based on Caelum reports. ERA5 has been shown to capture convective events such as MCC with accuracy (Mathias et al., 2019) and it has been used to validate climatologies in other regions with success (Somses et al., 2020; Taszarek, Kendzierski and Pilguj, 2020), indicating that it can be used with confidence to examine the synoptic environment associated with regional weather. We use the data here not to examine convective processes as modelled by ERA5, but to better understand the dynamic

environment over SA during actual reported weather events. Understanding the event-specific synoptic environment fills an important gap in the current research of severe weather synoptic climatology. Severe storm environments based on certain criteria (see Blamey et al. (2016)) are common to build a severe storm climatology. For example, these studies will consider that CAPE $\geq$ 2000J/kg has a likelihood of severe weather and derive severe weather likelihood from this proxy analysis. There is, however, evidence that two seemingly identical environments might have drastically different storms or none at all, especially in the case of extreme events such as tornadoes (Davies-Jones, 2015; Markowski and Richardson, 2014; Sisodiya et al., 2019; Taszarek, Allen, Groenemeijer, Edwards, Brooks, Chmielewski and Enno, 2020; Taszarek, Allen, Púčik, Hoogewind and Brooks, 2020; Taszarek, Kendzierski and Pilguj, 2020). That is why a severe storm climatology built on actual significant events might allow us to gain insight into the conditions under which a large number of actual events occurred.

Synoptic composite and clustering

Synoptic composite maps is constructed based on the mean synoptic conditions each respective convective type occurs in, during each respective month of the year Yarnal (1993). The maps are built using ERA5 Reanalysis data by visualising MSLP, geopotential height at 500 hPa (zg500) and CAPE. The method has has been applied in some severe storm studies by Goyette (2011); Morris and Simmonds (2000); Nastos and Matsangouras (2014). Using the average conditions under which rare events occur could mean small scale impacts can get lost within the dominant circulation patterns. To overcome this a principle component analysis (PCA) is used along with the composite classification.

A PCA is used to objectively derive synoptic patterns associated with significant convective environments that occur in NDJFM. Significant convective environments refers to days when a convective event was reported. To drive the PCA, MSLP and geopotential height at 500hPa (zg500) from the event day is forced into the PCA analysis. Each PCA run, for each convective type, was automated. First, an initial number of clusters is defined in the PCA analysis, i.e. 20 possible clusters, after the PCA is completed a Scree Test (Cattell, 1966) is used to identify the number of clusters that can explain at least 80% of the variance of weather leading to the respective convective type. These clusters are then plotted as synoptic weather patterns Lemus-Canovas, Lopez-Bustins, Martin-Vide and Royé (2019); Lemus-Canovas, Lopez-Bustins, Trapero and Martin-Vide (2019); Li, Zhang and Zhang (2016).

Land-Use Data

For Johannesburg, Garstang et al. (1975); Tyson et al. (1972) describe a UHI model (refer back to Figure 1.17), indicating the urban impact on suburban and rural locations relative to the city's central business district (CBD). In this schematic, we can see the possible temperature gradient caused by the changes in land surface and roughness of Johannesburg. Garstang et al. (1975); Tyson et al. (1972) did not explicitly measured rainfall as a function of the UHI, such as the METROMEX experiments in the USA. This chapter attempts to fill this gap by characterising radar-derived storms over specific land-use areas using the South African National Land-Cover (SANLC) (Department of Environment Forestry & Fisheries, 2019; Schoeman et al., 2013)

dataset. The SANLC contains 73 categories of land-use data for SA, and which is reclassified into five categories, i.e. rural, urban, suburban, informal and industrial. In comparison to MODIS, which is discussed in later section, the SANLC contains more classes of land-use (21 compared to 73). We used the following rationale in our reclassification:

- **Urban**: Mixed land-use areas, typical of the CBD with major artificial changes to albedo and surface roughness.
- **Suburban**: Formal residential areas with minor artificial changes to albedo and surface roughness, typically households and areas with parks and minor mixed use spaces.
- **Informal**: Informal residential areas with major artificial changes to albedo and surface roughness, uncovered surfaces and little artificial/historical vegetation.
- **Industrial**: Areas where large factories, mines, and power stations are located. Major, but localised, changes to land-use, high concentration of emissions and structures that might impact on cloud processes.
- **Rural**: No major disturbance of land surface albedo. Varied vegetation, including crops and natural vegetation.

The full SANLC (see Figure 2.9) and corresponding reclassification is listed in table 2.2 and table 2.3. The inclusion of industrial and informal settlements as separate categories is motivated by the fact that these land-use areas change the surface properties in distinct ways. For instance, Hardy and Nel (2015) found that areas in Johannesburg with dense vegetation and tree cover, i.e. traditional suburban areas such as the northern suburbs, have cooler temperatures than densely populated and built-up areas with little or no shading. Most industrial areas include mines and mine tailings. These areas are often uncovered and assumed to have a small local scale effect on storm characteristics. Informal areas have a complex land-use. These areas are sparsely vegetated, but the non-traditional building material such as "dwellings with corrugated metal sheet roof" (Mathee et al., 2021), means that the surface characteristics are different from a traditional city. In an informal settlement, materials are often highly reflective (i.e. high albedo) and do not retain any heat (Mathee et al., 2021), and can make up 80% of an settlement total building types (Mathee et al., 2021).

A significant limitation is the number of data points classified as rural (see Figure 2.9a) and 2.9b. Because the area is so large a wider variety of dynamically different storms will naturally be observed over rural areas. To address this, the dataset is normalised after Duong et al. (2007) on a scale of 0-1, allowing us to analyze the spatial and temporal characteristics of storm events in better detail, and remove any bias towards high frequency events. Refer back to Figure 3.1 to see the total number of events within the radar range without showing the spatial aspects of these event's occurrence, the spatial analysis is done in the following sections. Secondly, to limit the effect of topography, climatology, and radar attenuation at far distances and in the cone of silence around the radar, the analysis specifically focuses on the areas where these limitations can be reasonably managed. This includes using limited areas around the regions of interest that are reasonably close to the radar. Apart from reducing the number of rural points,

Table 2.2: *SANLC dataset categories 1-38*

No.	SANLC Categories	New Category
1	Contiguous (indigenous) Forest (very high, high, medium)	Rural
2	Contiguous Low Forest & Thicket (combined classes)	Rural
3	Dense Forest & Woodland (35–75% cc)	Rural
4	Open Woodland (10–35% cc)	Rural
5	Contiguous & Dense Planted Forest (combined classes)	Rural
6	Open & Sparse Planted Forest	Rural
7	Temporary Unplanted Forest	Rural
8	Low Shrubland (other regions)	Rural
9	Low Shrubland (Fynbos)	Rural
10	Low Shrubland (Succulent Karoo)	Rural
11	Low Shrubland (Nama Karoo)	Rural
12	Sparsely Wooded Grassland (5–10% cc)	Rural
13	Natural Grassland	Rural
14	Natural Rivers	Rural
15	Natural Estuaries & Lagoons	Rural
16	Natural Ocean, Coastal	Rural
17	Natural Lakes	Rural
18	Natural Pans (flooded @ obsv time)	Rural
19	Artificial Dams (incl. canals)	Industrial
20	Artificial Sewage Ponds	Industrial
21	Artificial Flooded Mine Pits	Industrial
22	Herbaceous Wetlands (currently mapped)	Rural
23	Herbaceous Wetlands (previous mapped extent)	Rural
24	Mangrove Wetlands	Rural
25	Natural Rock Surfaces	Rural
26	Dry Pans	Rural
27	Eroded Lands	Rural
28	Sand Dunes (terrestrial)	Rural
29	Coastal Sand Dunes & Beach Sand	Rural
30	Bare Riverbed Material	Rural
31	Other Bare	Rural
32	Cultivated Commercial Permanent Orchards	Rural
33	Cultivated Commercial Permanent Vines	Rural
34	Cultivated Commercial Sugarcane Pivot Irrigated	Rural
35	Commercial Permanent Pineapples	Rural
36	Cultivated Commercial Sugarcane Non-Pivot (all other)	Rural
37	Cultivated Emerging Farmer Sugarcane Non-Pivot (all other)	Rural

especially noticeable in the North-West, Free-State, Mpumalanga and Limpopo, and reducing other artefacts as mentioned, limiting the area allows us to examine characteristics of storms around Johannesburg, regions of different topography, over townships and power stations to better understand how these factors impact storm dynamics on a small scale.

Topography

The effect of topography plays an essential part in rainfall and convective storm processes over SA (De Coning et al., 1998; Schulze, 1965). It drives the initial uplift of parcels which enhances

Table 2.3: *SANLC dataset categories 38-73*

No.	SANLC Categories	New Category
38	Commercial Annuals Pivot Irrigated	Rural
39	Commercial Annuals Non-Pivot Irrigated	Rural
40	Commercial Annuals Crops Rain-Fed/Dryland/Non-Irrigated	Rural
41	Subsistence / Small-Scale Annual Crops	Rural
42	Fallow Land & Old Fields (Trees)	Rural
43	Fallow Land & Old Fields (Bush)	Rural
44	Fallow Land & Old Fields (Grass)	Rural
45	Fallow Land & Old Fields (Bare)	Rural
46	Fallow Land & Old Fields (Low Shrub)	Rural
47	Residential Formal (Tree)	Suburban
48	Residential Formal (Bush)	Suburban
49	Residential Formal (low veg / grass)	Suburban
50	Residential Formal (Bare)	Suburban
51	Residential Informal (Tree)	Informal
52	Residential Informal (Bush)	Informal
53	Residential Informal (low veg / grass)	Informal
54	Residential Informal (Bare)	Informal
55	Village Scattered (bare only)	Informal
56	Village Dense (bare only)	Informal
57	Smallholdings (Tree)	Rural
58	Smallholdings (Bush)	Rural
59	Smallholdings (low veg / grass)	Rural
60	Smallholdings (Bare)	Rural
61	Urban Recreational Fields (Tree)	Urban
62	Urban Recreational Fields (Bush)	Urban
63	Urban Recreational Fields (Grass)	Urban
64	Urban Recreational Fields (Bare)	Urban
65	Commercial	Urban
66	Industrial	Industrial
67	Roads & Rail (Major Linear)	Urban
68	Mines: Surface Infrastructure	Industrial
69	Mines: Extraction Sites: Open Cast & Quarries combined	Industrial
70	Mines: Extraction Sites: Salt Mines	Industrial
71	Mines: Waste (Tailings) & Resource Dumps	Industrial
72	Land-fills	Industrial
73	Fallow Land & Old Fields (wetlands)	Rural

convection and storm development (Betts, 2003). In the following analysis we use the aggregated 30-meter SRTM, coarser GMTED, and ETOPO1 data made available the by Amazon Web Services S3 public dataset to match elevation data with radar data points. The surface elevation of the study area is shown in Figure 2.10, and here we can see the surface elevation differs substantially between the northern and southern extent of the radar range. As we can see, elevation varies between 700 m up to over 2000 m in some areas. The Magaliesberg mountain range in the eastern part of North-West and the Waterberg mountains in the southern parts of Limpopo are notable ranges in the area. The Free State and southern Gauteng are characteristically high elevation, but no major mountain range is visible in the area. The northern areas

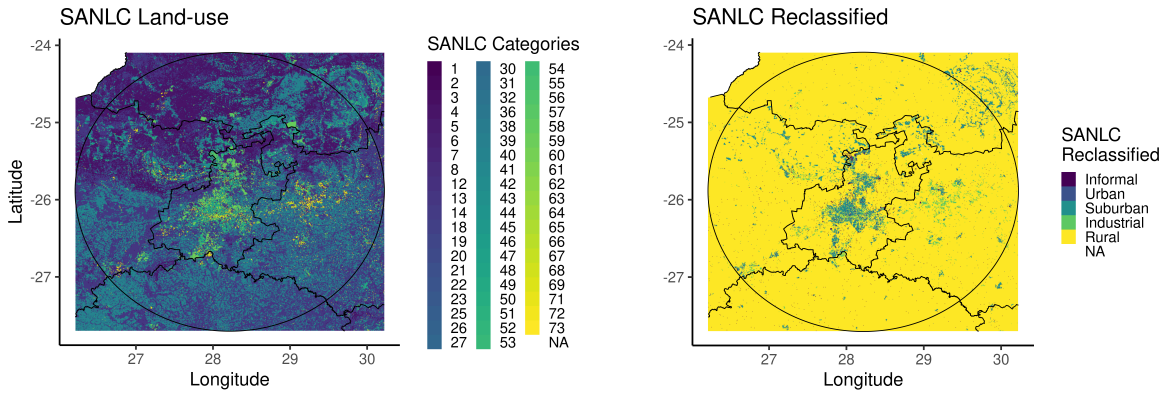

(a) *The SANLC Dataset* **(b)** *Reclassified SANLC*

Figure 2.9: *The SANLC dataset with the original land-use categories as described in table 2.2 and table 2.3 was reclassified in 5 simple categories to analyse storm occurrence within the radar radius.*

(western North-West and southern Limpopo) elevation is seldom above 1200 m, but the area is home to major mountain ranges, including Pilanesberg, Magalies and the Waterberg mountains. Towards the south (Free-state, Mpumalanga and Gauteng), the elevation is well above 1500 m, but no mountain range is visible. It is unlikely that the elevations reached by mountains in the Highveld (≤2000 m) will act as a major blocking feature in the region, but we examine this in detail later.

Figure 2.10 also shows the sites chosen for a detailed analysis on the effect of topography and orography on storms within the radar range. In the northern parts of the North-West, we examine the variation in storm characteristics as a function of simple and complex terrain profiles. This is indicated by the red circles inFigure 2.10. Due south of this, as highlighted by the yellow circles in Figure 2.10, the effect of the Magaliesberg mountain range on storm properties in two adjacent areas is examined. The topography of the rural, urban and suburban areas, and the area where an informal settlement and an industrial complex are present is also discussed in more detail in the later analysis. However, less emphasis is placed on the topography for the informal settlement and industrial complex.

WRF configuration and setup

WRF is a community-driven, open-source weather and forecasting model. WRF can be used on various scales, from large GCM studies to operational regional scale forecasting. The model has an extensive suite of physics and dynamical options and can be compiled using open-source compilers. Various parameterisation schemes have been developed and are freely available in WRF (Powers et al., 2017). The model has been successfully used in various idealised and operational cases (Kumar et al., 2008; Liang et al., 2012; Segele et al., 2013; Zhang et al., 2012). In Havenga (2018), WRF was used on a convective scale to simulate various hail events over the Highveld. The study was the first in SA to explicitly simulate convection using WRF, evaluate the selected cases' thermodynamic profile, and compare it to observed radiosonde soundings from the Irene weather station. Here WRF was able to accurately simulate the thermodynamic environment of these significant cases with reasonable accuracy. These convective permitting

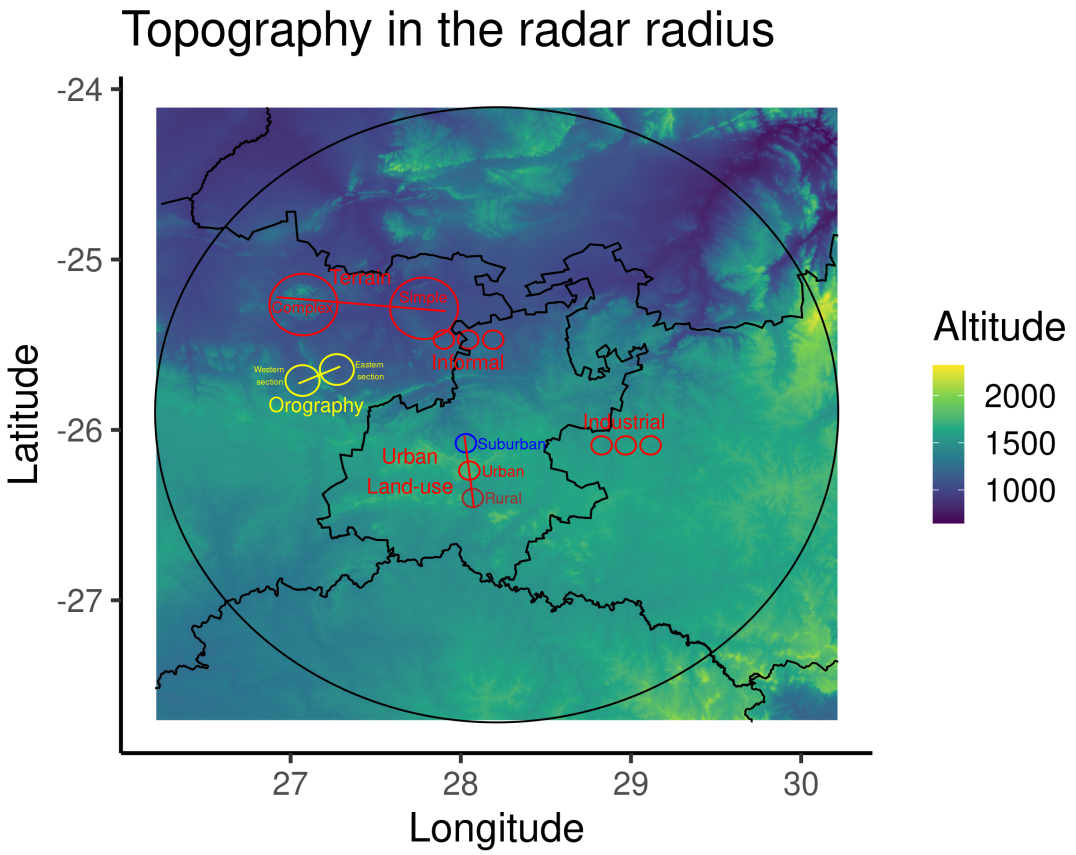

Figure 2.10: *The above figure indicates the surface elevation of the area encompassed by the Irene radar.*

models show that the model can provide insight into convective storm environments over the Highveld.

In this study, we aim to setup WRF so that it captures storm day dynamics reasonably well, and then from this control run we can analyse various idealised scenarios. The selection of parameterisation schemes is based on current literature (Crétat et al., 2012; De Lange et al., 2021a,b; Kuik et al., 2015; Maisha, 2014; Ratna et al., 2014) where various set-ups were evaluated, along with the current North-West University (NWU)-WRF setups that have been successfully used as an operational forecast model for the last two years. The latter has been run using convective parameterisation turned on, and a major difference in this thesis will be the exclusion of convective parameterisation, which has shown better forecasting skill (Pal et al., 2019; Prein et al., 2015, 2013).

WRFV4.1 based on the current NWU-WRF[1] that has been operational since 2019 and literature (see Crétat et al. (2012); De Lange et al. (2021a,b); Kuik et al. (2015); Maisha (2014); Ratna et al. (2014)) evaluating various parameterisation schemes over SA. The NWU-WRF setup is built on the National Center for Atmospheric Research (NCAR) regional climate model setup. Over two years of operations, the setup has proven reasonably accurate in capturing weather events over SA. The setup has also been accurate in capturing the local scale thermodynamics on CPM scale (Havenga, 2018). Changes to the PBL have been adapted based on De Lange et al. (2021a,b). We

[1]see www.lekwenaradar.co.za/wrf

detail the most important physics schemes in Table 2.4. New in this study is the inclusion of the New Thompson aerosol-aware parameterisation scheme.

We use ECMWF ERA5 reanalysis data to initialise our model[2]. ERA5 0.25°×0.25°resolution means a single grid is effectively 31 km. Because of the reasonably high-resolution, Varga and Breuer (2020); Wang et al. (2021) states that downscaling might not be necessary, as with previous generation reanalysis data types. However, both studies do show the added value of having a downscaled parent domain. We compromise and build the model domain as follows. A parent domain with 18 km resolution with cumulus parameterisation turned on, nest one at 6 km with convective parameterisation turned on and nest two at 2 km with parameterisation turned off. Convective parameterisation is still used at 18 km and 6 km to increase model runtime efficiency. The selected domains can be seen in Figure 2.11. A lower nest would be ideal, but this would require more computational power. Each simulation starts 15 hours before the event day to allow for model spin up and stabilization. For the severe storm that occurred on November 28, (1300 UTC – 1600 UTC), WRF is initialised on November 27, 2200 UTC, allowing for a spin-up of 15 hours before the first significant convection associated with the storm event occurs. The spin up time was decided after Zan et al. (2020), who examined convective initiation over complex terrain using WRF, the author used a similar setup and discarded the first 10 hours of the model run and produced accurate simulations. We identify the most intense period of the event from radar and or media reports and explicitly analyse the storms' dynamical (i.e. thermodynamics) and microphysical (i.e. ice number concentration) environment at this time step. It is helpful to analyse and compare the model thermodynamic profile with Irene's sounding of the storm day. Nevertheless, in the context of the study, we aim not to evaluate the model in detail but evaluate changes in the storm dynamics.

Table 2.4: *WRF configuration seen here indicates the setup used in this case study. The setup simulates the November 28, 2013, storm with reasonable accuracy. WRF allows the user to choose from a suite of setups. In the scope of this study, the goal was not to evaluate the use of various setups. Based on current operational WRF runs and literature on simulated events in SA, the current setup was selected.*

Numerics & Dynamics	**Configuration**
Initiation Data	ECMWF ERA5
Resolution	18 km, 6 km, 2 km
Integration time step	20 seconds
Map projection	Mercator
Geographical data	MODIS
Model spin up	15h
Microphysics scheme	New Thompsom, *et al.*
Longwave radiation	Rapid Radiative Transfer Model Global (RRTMG) Scheme
Shortwave radiation	RRTMG Scheme
Land Surface Model (LSM)	Noah LSM
Cumulus parameterisation	18 km – Tiedtke Scheme, 6 km/2 km - CPM
PBL Scheme	Mellor-Yamada-Janji (MYJ)

The current workflow for the simulation is as follows. The latest WRF pre-processing system (WPS) and WRF (V4.1) code was compiled on the NCAR Cheyenne supercomputer. WPS is the

[2]In Figure 5.2 to 5.6 we use ERA5 data to represent the synoptic conditions of different severe event's mean environments. The model as is captures severe convective environments with reasonable accuracy

preprocessing software where geographical and meteorological data are assimilated into files readable by the WRF program. In WPS, we first run a utility called *geogrid*. WPS interpolates MODIS land-use data for assimilation into the meteorological dataset that is used to initiate the model. WPS geographical output can be seen in the land-use categories illustrated in Figure 2.11. The WPS utility, *ungrib*, reads the selected meteorological data (in this case, ERA5 pressure level and surface level data) and creates intermediate files with the required WRF mandatory fields. After geogrid and ungrid was executed, the geographical and meteorological data can be assimilated into WRF readable files using the *metgrid* utility. If metgrid is completed, the output files will contain certain 3D meteorological data such as u-wind, v-wind and pressure at different levels. These files are then used to initialise WRF. In WRF, the selection of physics and dynamic suites is chosen as discussed previously. Best practice guidelines recommend that resource allocation be determined using the smallest domain size and resources based on the number of velocity points in west-east and south-north domains. In this case our smallest domain was west-east == 133 and south-north == 136. Using the following formula ((west-east)/25)×((south-north)/25), 28 processors is allocated to run WRF. WRF has two utilities that need to be initiated, first the *real* program, which creates initial files and then the WRF program can be initiated which generates the WRF simulation files.

The default WRF-MODIS land-use data accurately represents the urban areas in Gauteng, as seen in Figure 2.11. The Greater Johannesburg area is well defined, which is the most important area in the context of this study. WRF uses a lookup table to define various coefficients associated with land use type and the selected land-surface model, in this case, the Noah LSM. The following parameters are defined in the VEGPARAM.TBL lookup table for Noah LSM (as described in the Noah LSM physics suite):

- ALBBRD: Surface background snow-free albedo
- CMXTBL: Max canopy capacity
- Z0BRD: Background roughness length
- SHDFAC: Green vegetation fraction
- NROOT: Rooting depth
- RSMIN: Minimum stomatal resistance
- RSMAX: Maximum stomatal resistance
- RGL: Parameters used in radiation stress function
- HS: Parameters used in vapour pressure deficit function
- TOPT: Optimum transpiration air temperature
- CMCMAX: Maximum canopy water capacity
- CFACTR: Parameters used in the canopy interception calculation

- SNUP: Threshold snow depth (in water equivalent meters) that implies 100 percent snow cover
- LAI: Leaf area index

Each of the MODIS land-use categories has a defined coefficient for each variable (see Sequera et al. (2016) for an overview of coefficient values).

Before WRF is initiated the physics scheme has to be configured according the needs of the study. The control run used the old Thompson scheme (Thompson et al., 2008) and following this an modified Thompson aerosol aware scheme was applied. The Thompson aerosol microphysics scheme (Thompson and Eidhammer, 2014) has two methods of calculating the total CCN and ICN concentration during model runtime. The scheme can employ a global climatology from the GOCART climatology. Here a seven-year mean of sulfates, dust, BC, sea salts and organic carbon is used to derive local CCN concentration. The second method requires the user to modify the CCN and ICN during model runtime explicitly. Here a CCN concentration for the near-surface is given (nCCN0) and the final CCN concentration at 2000m (nCC1). (Thompson and Eidhammer, 2014) lets CCN decrease exponentially from nCCN0 to nCCN1 and hereafter it remains constant through the model levels. The second method will be employed in this study using Ross et al. (2003); Terblanche et al. (2000) to guide the CCN forcing for Highveld. The number concentration for CCN and ICN is explicitly expressed in the Thompson physics module. Here the (Thompson and Eidhammer, 2014) applies a simple number concentration for CCN near the surface between 200 – 1000m (i.e. the PBL) and then another number concentration for CCN above the PBL. By default, the nCCN0 concentration below 2000m is set to 300cm^3 and decreases exponentially to 50cm^3. Consider that the average CCN at 2000-3000m is 640cm^3 (Ross et al., 2003) and possibly higher than that at surface (Varghese et al., 2016). This might indicate that CCN concentrations is significantly underestimated in current model simulations and a higher concentration is needed for continental cases.

CCN only changes are examined first as follows; in the control run, all variables remain the same using a simple WRF setup (CNTR (control run)). In the increased CCN run, all land-use variables remain the same. However, we include an aerosol-aware scheme with a moderate CCN concentration of 300cm^3, decreasing exponentially to 50cm^3 above 2000m (AER1 (aerosol 1 run)). Subsequently, we force the model using a new CCN concentration based on observations from SAFARI-2000 and ARREX campaigns. The only observation studies of aerosols directly over the Highveld were done in SAFARI-2000 and ARREX campaigns. Using CCN data from Ross et al. (2003) (see Figure 1.13), we force the model using an average surface concentration of 1000cm^3, decreasing exponentially to 500cm^3 above 2000m and remaining constant aloft (AER2 run). Next, an increased pollution run with a CCN surface value of 2140cm^3, decreasing exponentially to the Ross et al. (2003) average of 680cm^3 above 2000m (AER3 run) is conducted.

Next, we include simulated changes in land-use by simulating a *polluted city*, (i.e. worst-case) and an improved *green city* (i.e. sustainable/greener city). In the polluted city-run, we propose two scenarios. First a polluted city (Polluted City Simulation Run (POLCITY)1) run is conducted with a high albedo and low vegetation cover. The high albedo is characteristic of current

townships in and around Johannesburg, which use highly reflective corrugated iron as building material (Mathee et al., 2021). The green fraction and Leaf Area Index (LAI) is decreased, i.e. fewer plants, and the vegetation characteristics are similar to that of barren and sparsely vegetated landscapes. In the second polluted city (POLCITY2), the albedo is decreased and surface roughness increased, i.e. more paved surfaces and buildings. The green fraction and LAI remains similar to POLCITY1. POLCITY2 is set to be similar to a traditional UHI. Finally, the study examines a "greener" urban area, the Green City Simulation Run (GRNCITY) (Green City) run. To simulate a greener urban area we create a moderate albedo scenario as plants have reflective characteristics (Kondo et al., 2001; Sailor, 1995; Yin et al., 2016), decrease surface roughness and increase the LAI and green fraction. The green city vegetation characteristics are similar to that of a mixed forest after this changes. In Table 2.5, the detailed changes made to the microphysics and the land-use parameters are described.

Table 2.5: *The table below shows the most important changes to each of the various runs conducted in this study. The control run uses the default Thompson microphysics scheme with no modification to the physics. In all other runs, the CCN concentration is altered. Each run is abbreviated as follows: CNTR (control run), AER1 (Aerosol 1: Moderate CCN concentration (300–50cm^3)), AER2 (Aerosol 2: SAFARI-2000 average CCN for the industrial Highveld (1000-500cm^3)), AER3 (Aerosol 3: SAFARI-2000 maximum CCN for the industrial Highveld (2140-680cm^3)). The CCN values in brackets indicate the exponential decay from the surface to the model top in the CCN concentration. In the next three runs CCN concentration remains as was seen in AER1 (300–50cm^3), the land-use is modified and WRF is forced with three scenarios as follows: POLCITY1 with increased surface roughness, increased albedo to mimic highly reflective corrugated roofing material, and decreased LAI to mimic a township. The second POLCITY2 run is similar to a traditional UHI and surface roughness is high, albedo decreased, and decreased LAI and green fraction like a barren landscape. A final GRNCITY simulation is conducted where with decreased surface roughness, a moderate albedo and increased LAI and green fraction*

	CNTR	**AER1**	**AER2**	**AER3**	**POLC1**	**POLC2**	**GRNC**
CCN (cm^3)	0	300/50	1000/500	2410/680	300/50	300/50	300/50
Surface Roughness	50	50	50	50	100	100	40
Albedo (%)	0.18	0.18	0.18	0.18	0.40	0.10	0.20
Leaf Area Index (min/max)	1	1	1	1	0.1/0.75	0.1/0.75	2.8/5.5

The above section details the setup used to simulate a severe storm event under different scenarios. By refining WRF's land-use and CCN representation and refining them specifically to represent South African conditions with greater accuracy, we hope to add value to the future forecasts of severe events. The benefit can extend further than severe storm representation. Urban planners can use high-resolution models to examine buildings impact on weather, how green spaces or greening of urban spaces can alter storms and temperature profiles and heat stress (Arghavani et al., 2020). The research allows various sectors to quantify risk and exposure under various future scenarios better and will benefit informed decision making. The following section briefly provides an overview of the selected severe weather event simulated under the scenarios mentioned above.

Limitations of the study

Due to the complex nature of convective events, there are major limitations in any analysis that tries to examine the dynamical environment of a fairly chaotic system. The section will briefly

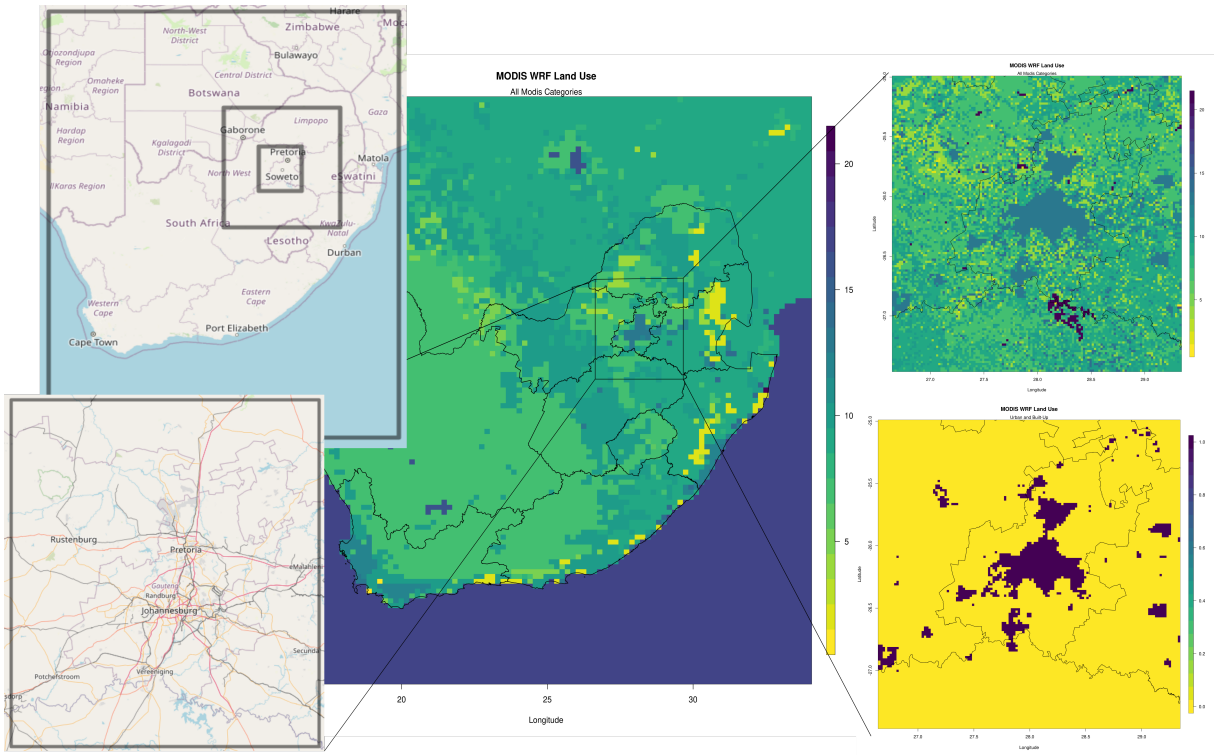

Figure 2.11: *The WRF domains above indicate the chosen setup based on the downscaling of the ERA5-reanalysis data. We use an 18km parent domain, with a parent to nest ratio of 3. Subsequently, the nests are as follows, 18 km, 6 km and 2 km. The 2km domain will explicitly simulate convection, with the feedback turned on between the parent and nest domains. The default MODIS land use data used in this study represents urban areas reasonably well. Here, we can see that the Greater Johannesburg area, Pretoria and smaller regions such as Rustenburg, Potchefstroom, Secunda and Emalaheni are well defined. The land use categories can be seen in Table 2.6.*

outline the major limitations of each chapter.

Chapter 4: Characterising the nature of convective events using radar data

The radar data does not cover the whole of the Highveld. There are several structural considerations that has to be taken into account as well. Beam propagation occurs as distance from the radar increases, i.e. the height of the base beam increases. Storms that are on the edge of the radar scan are distorted, and where there is topographical features the radar beam can be blocked. A second limitation is that the study uses a threshold dBZ to identify convective storms, as defined by Keat et al. (2019), there are however various assumptions associated with using a *threshold dBZ*, but this provides a reasonable separation of convective events from other weather events.

Chapter 5: Characterising convective weather events from media reports

In this chapter, the analysis makes use of media reports to examine the impact of storm events. Media reports are biased towards heavy populated areas and should not be used to assume the unique dynamic environment of an event. The reports are valuable to identify events and

Table 2.6: *MODIS 21 class land-use categories represent the urban areas in and around Gauteng with a reasonable degree of accuracy (compared with the SANLC dataset as seen in Figure 2.9). To simulate anthropogenic impacts, we change the albedo and green fraction values of the urban regions.*

Nr	Description
1	'Evergreen Needleleaf Forest'
2	'Evergreen Broadleaf Forest'
3	'Deciduous Needleleaf Forest'
4	'Deciduous Broadleaf Forest'
5	'Mixed Forests'
6	'Closed Shrublands'
7	'Open Shrublands'
8	'Woody Savannas'
9	'Savannas'
10	'Grasslands'
11	'Permanent wetlands'
12	'Croplands'
13	'Urban and Built-Up'
14	'Cropland/natural vegetation mosaic'
15	'Snow and Ice'
16	'Barren or Sparsely Vegetated'
17	'Water'
18	'Wooded Tundra'
19	'Mixed Tundra'
20	'Barren Tundra'
21	'Lakes'

quantify the risk and losses that the event cause, and also when these significant events occur. Unreported events, or events that occurred where there was no observations, will be lost in an analysis such as this. A second limitation is the grouping of some convective events as separate events, this is mainly related to thunderstorms and lightning. A thunderstorm is broad term for a convective event, and within a thunderstorm there can be hail, lightning, rainfall or tornadoes. Lightning is also typically associated with all types convective events, however, due to its impact is examined separately.

Chapter 6: Examining the synoptic and thermodynamic conditions under which convective events occur in

This chapter assumes an economically significant event was also dynamically significant, which is not necessarily true. Furthermore, the study builds a synoptic composite of severe events, however, the synoptic composite makes broads assumptions on the dynamic environment these events occur in. The method is however recognised by Yarnal (1993) and has been applied in some severe storm studies by Goyette (2011); Morris and Simmonds (2000); Nastos and Matsangouras (2014). However, due to local scale nature of convective events and the variety of conditions they occur under, building a composite of the synoptic conditions will average out unique conditions that events can occur in. This is a major limitations, and to overcome this an objective clustering method is also conducted, this method shows the frequency of synoptic

types associated with each respective event. The radiosonde limitations have been discussed, but a major consideration is that the sounding might not be representative of a storm that occurred far away from the launch site due to the local scale nature of convective events.

Chapter 7:Using radar to characterise storms over different areas

In this chapter we analyse small subsections of radar data, however, similar to chapter 4, there are limitations due to beam depletion, distance from the radar, topography, and beam blocking. The chapter tries to address this by using sites that are relatively close to the radar and not on the limits of the radar range. The second limitation is that the subsections we use is fairly subjective, and does not consider all the effects on the storms over the selected areas such as downwind effects. We try and support our results by including the LIS data which counts lightning strikes in a region.

Chapter 8: The limitations of using NWP to characterise a storm event

In chapter 8, the use of WRF on a single case event is the major limitation due to the chaotic nature of convective storm development. It would be preferable to run dozens of cases under different initial conditions, however, due to the high resolution of the case these 6 scenario's provide a starting point for further analysis as we showed a significant difference in convective characteristics under these different conditions. A second limitation is the selection of variables to represent different urbanisation scenario's in Johannesburg. The assumptions made on land cover characteristics, albedo and vegetation was not based on any in-situ measurements over the region, however, we limited the changes to the model parameters to these variables to keep the model as simple as possible initially. Future simulations should be driven by in-situ measurements which will mean that local urban areas will be represented by their own unique characteristics.

Conclusion

To understand the anthropogenic effects on convective storms over the Highveld, a suite of data sources are used. The study uses radar data, media reports, new generation ERA5 reanalysis data, radiosonde data, weather station data, LIS and high resolution NWP models to understand the nature of convective events over the Highveld in greater detail. The results build up to chapter 8 where the high resolution NWP is employed to simulate an significant event to examine the effects of local scale changes on the CCN and land-use on the convective storm. The significance of this study allows us to understand how small scale changes, change the nature of convective events.

Chapter 3
The nature of convective weather events over the Highveld

Data from the Irene S-band radar is used to characterise convective storms for a 200 km radius around the radar, that includes Gauteng and a large portion of the industrialised Highveld. The radar data provides a high spatial and temporal dataset of weather events by measuring reflectivity of rain or ice particles in the atmosphere. From this data, we can derive storm severity and extract various storm characteristics to better understand the nature of convective events over the region.

Introduction

In this study, a localised climatology, based on actual severe events as reported in media, the Irene soundings and radar, is constructed. Radar data offers high resolution spatial and temporal data as a function of hydrometer reflectivity in the atmosphere. We can derive the size, speed, direction, height above ground, and distances from the radar of various types of storms by using electromagnetic waves (Marshall et al., 1955; Voormansik et al., 2021). Typically, a radar scan will provide a full 360°*view* of the immediate lower atmosphere, at various elevations every 5 minutes, but radar data also has various uncertainties that must be accounted for. The reflection, refraction, and attenuation of the electromagnetic pulse can lead to data loss. Radars have a limited range; this includes a 20 km radius close to a radar, known as the cone of silence (Burgess et al., 2002). Furthermore, at distances over 150–200 km, to limit the effect of the Earth's curvature the base elevation scan observes the mid-cloud features, which is why radar ranges are limited (Marshall et al., 1955). In South Africa, climatologies that specifically examined radar data are rare as the radar data is typically only used to understand severe case studies. Three papers by Carte and Held (1978); Kelbe (1984); Mader et al. (1986) form the basis of South African weather radar research, but these papers were limited by the size of their datasets and the processing power used at the time. A more detailed overview of the research by Carte and Held (1978); Kelbe (1984); Mader et al. (1986) is provided in the next chapter. With the introduction of software such as TITAN, processing radar data has become a much easier task, and large datasets can quickly be interrogated and examined.

Radar derived convective storm characteristics

This section aims to incorporate radar data into already existing methods of building climatologies. Radar allows us to capture events on a high spatio-temporal resolution and in areas where in-situ measurements are scarce. Radar also captures valuable data related to severe storm parameters, including cloud composition, mass, storm direction, and hydrometeor concentration and characteristics. This chapter focuses exclusively on the temporal characteristics

of all the radar data from 2013 - 2017 to characterise the seasonal and hourly occurrence of thunderstorms over the Highveld. There are three seminal papers by Carte and Held (1978); Kelbe (1984); Mader et al. (1986) respectively that propose a radar climatology in SA. This chapter builds on this original work and expands the data analysis to 5 years of S-band radar data. The original papers mentioned above examined small subsets of data and, in some cases, only data collected during specific research cases, i.e. Kelbe (1984) during cloud seeding campaigns in the Lowveld.

The climatology of severe convective events over South Africa is well detailed and discussed in the introductory chapter. During the summer months, thunderstorms from October to March are the predominant rain-bearing system for the Highveld, but severe rainfall and hail events can cause damage when such storms occur. The severe damage these events cause highlights the importance to better understand these events. This chapter builds on the current body of knowledge by improving our understanding of the temporal variations of thunderstorms in the region. First, using the Irene S-band Radar, we derive the seasonal statistics of convective events. Keat et al. (2019); Stein et al. (2019)'s threshold value used in their study to separate convective storms from stratiform events of 35 dBZ is applied to identify convective storms within the radar's 200 km radius, and all data below this value is removed. This selective quality control is applied to remove all reasonably unrealistic radar signals while maintaining a large sample size. We include LIS data from the TRMM and ISS missions here to validate the radar-derived dataset. The LIS dataset has proven beneficial to build climatology of convective thunderstorms (Cecil et al., 2014, 2015; Chronis and Koshak, 2017; Takayabu, 2006). Lightning data has been successfully used to characterise various aspects of convective storm climatology in SA (Bhavika, 2007; Gijben, 2012; Gijben and De Coning, 2017). The diurnal and monthly characteristics of lightning data are used as a proximity variable to identify convective storm activity. Lightning mostly occurs during thunderstorms when deep convection is present and is a good proxy measurement for thunderstorm presence. Data from these sensors originates from polar-orbiting missions, causing temporal uncertainty, but provides valuable data to better understand storm characteristics in the study area.

As seen in Figure 3.1a, all events with a dBZ over 35 is aggregated into one year. Aggregating the data has the advantage of filling data gaps that may have occurred in previous years if the radar was out of operation and to quantify thunderstorms in space and time on high resolutions. A long-term climatology here is not build in this chapter, but a seasonal, monthly, and hourly characterisation. The occurrence of thunderstorms is similar to the general summer climatology of convective weather events as described in the introduction (Figure 1.6b). From October to March, the number of convective events increases in frequency. In January, the number of events peak (without assuming the lifetime and severity of the events, as detailed later in this section). The number of events decrease from February, and from the end of March, the occurrence of thunderstorms over the Highveld is low until the start of October. The data accurately captures all convective cells in the area of interest and not just those over a weather station. The hour of maximum thunderstorm activity, when dBZ are the highest, peak rain rate occurs and when the highest cloud top are observed, is examined. This has not been done in detail over Gauteng and parts of the Highveld before. In addition, the high resolution lightning dataset from the

TRMM and ISS missions is to validate the radar data analysis.

The TRMM and ISS lightning dataset (Figure 3.1b) shows a similar trend of thunderstorm occurrence in the study area. The number of lightning events does not directly correlate with the number of storms; however, the lightning dataset indicates that we already see high lightning activity as early as October, with a peak in December. However, the TRMM and ISS missions may not pick up shallow cumulus where no lightning necessarily occurs during some time of the year, particularly mid-summer when shallow cumulus in the form of isolated thunderstorms prevail, whereas the radar does capture these events. The TRMM and ISS early summer bias could also be explained by the prevalence of deep convection and possibly supercells, during early summer, because ice processes are dominant during storms that occur in this time, there would be an expected increase in lightning. Lightning is directly linked to ice presence in the cloud and a good indicator of hail probability (Changnon, 1992b).

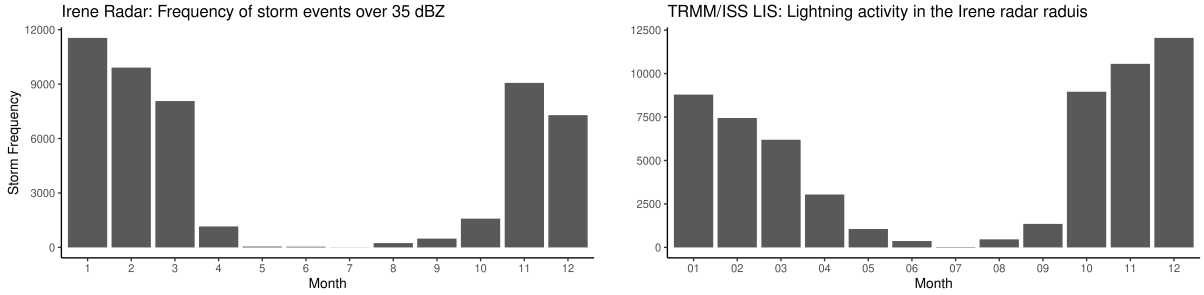

(a) *Radar* **(b)** *LIS*

Figure 3.1: *November to March is the period with the highest frequency of convective events as derived from the Irene S-band radar. Although not directly correlated to the radar data, the lightning data indicates that October - March has high lightning activity (which we assume is a good proxy for deep convection). Lightning data is, however, from polar-orbiting satellites, which have temporal inhomogeneities.*

In the subsequent analysis, radar dataset is classified into the following risk levels, after Stull (2018), as used by the USA Air Traffic Control (ATC); **moderate** storm risk (35-40dBZ), **heavy** storm risk (40-50dBZ), and **extreme** storm risk (> 50dBZ). After reclassifying of the data into risk categories, the subsequent analysis allows us to better understand storms based on their risk profile. The term risk is complex and dynamically severe storms might not result in severe damage. In this section risk refers to the possibility that a storm with certain characteristics could be harmful when a vulnerable population is exposed to it. As seen in Figure 3.2a, the storm events' total contribution and relative occurrence based on the new classification. As expected, moderate storms (35-40dBZ) were most prevalent throughout the year, and can be any form of minor convection such as isolated thunderstorms, which is typical over the region. The relative occurrence of moderate and severe storms is illustrated in Figure 3.2b. Most storms within the Irene radar radius per annum are moderate; on average 20000 moderate events occur, 12000 heavy events and only 70 extreme events. The number of events declines as the dBZ increases. Figure 3.2b also illustrates that extreme events are rare and make up the smallest number of storms. Nevertheless, extreme events relative occurrence is most frequent in November. The importance of studying these events, which seemingly occur less than 70 times a year, lies in the fact that they cause excessive damage in a unpredictable manner.

Reflecting on Figure 1.6b by Carte and Held (1978), as discussed in the introduction, shows a similar distribution of events as seen in our analysis of the mean dBZ over the Highveld. High reflectivity correlates with hail size, which is typically associated with severe storms, the analyses shows that extreme events are most common during November when, according to Carte and Held (1978)'s original research, the largest hailstones are also observed. However, January and February show the highest frequency of events observed, probably because isolated thunderstorms occur more frequently than severe supercells.

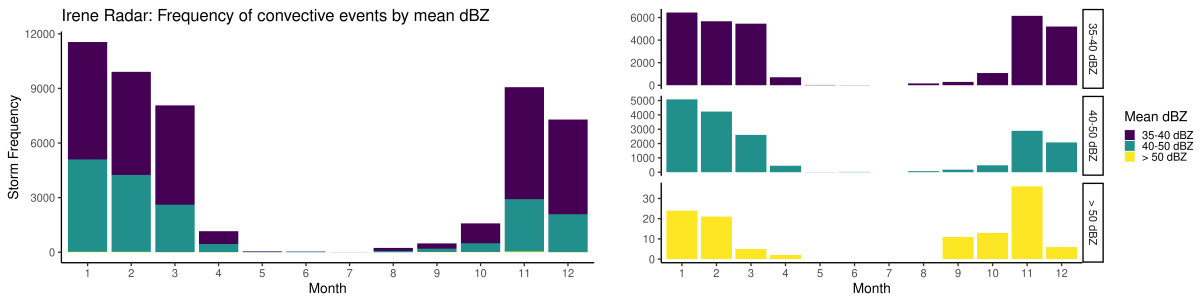

(a) *Detailed frequency of mean dBZ* **(b)** *Events separated by their total relative contribution*

Figure 3.2: *The Figure shows the relative occurrence of characteristic storm types and the mean dBZ for all events are analysed. Most events have a low reflectivity signal. Figure b indicates a more detailed breakdown of the mean dBZ storm characteristics; take note of the y-axis; here, we observe that November is the month with the highest occurrence of storms with a mean dBZ of over 50. This reflectivity is typically observed in storms classified as extreme and associated with large hail and flash floods.*

The current analysis examines the maximum reflectivity recorded during all events that fall in the Irene radar radius; this has the advantage of understanding the nature of events in better detail. Using the Pearson correlation coefficient, we can see that the maximum and mean dBZ are directly related to each other and with a coefficient of 0.956. Storms with a high maxima typically also have a longer lifetime and higher mean reflectivity. Non severe storms typically remain non severe throughout their whole lifetime.High maximum reflectivity moments in a storm often result in the most damage, and this signal can get lost when just analysing the mean. It is thus important examine storms highest instantaneous reflectivity. In Figure 3.3, the accumulated number of storms is examined as a function of the storms instantaneous maximum dBZ. The distribution of storms in this analysis is similar to the previously discussed mean climatology. However, here we see that storms over the Highveld often pose a heavy to extreme storm risk during some part of their life cycle.

On average, the occurrence of storms that could be considered to be associated with a heavy risk occurs 20000 times per year. In comparison, reflectivity values associated with extreme risk only occur 7000 times per year. Consider that this could be an instantaneous measurement. It does not indicate that over 7000 extreme events occur in a year, just that in any given event's lifetime, there is a moment when extreme dBZ characteristics are recorded. This is where analysing the mean, as done at the beginning of this section, is valuable to understand the storm characteristics on average.

This section described the seasonal characteristics of cloud reflectivity measured within the Irene S-Band radar radius. The number of events categorised as moderate convection numbers

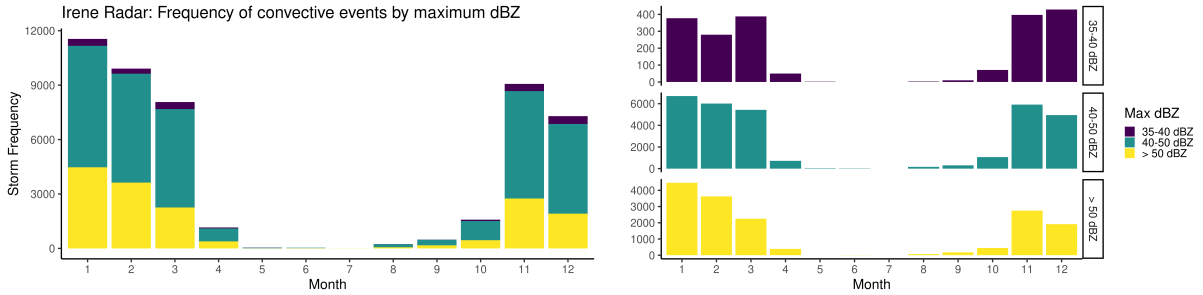

(a) *Detailed frequency of maximum observed dBZ* **(b)** *Events separated by their total relative contribution*

Figure 3.3: *The maximum observed reflective during a storm's life cycle is shown here. The Highveld is often exposed to storms that could pose a heavy or extreme risk during some time of their life cycle.*

around 20000 per year; this could be shallow cumulus clouds where only slight precipitation occurs. In later sections, more details about the relationship between precipitation and reflectivity will be examined. Most storms over the region have a high dBZ value during their lifetime, although the events can have a low mean dBZ. When examining the maximum dBZ, we can see, on average, that a large number of events have a maximum dBZ between 40-50. Events with a mean dBZ over 50 are most common during November; however, the maximum instantaneous reflectivity of all events indicates that January is the month with the most extreme convective activity. In the next section the diurnal characteristics of convective events as measured by the radar is discussed.

Diurnal characteristics of radar observed convective events

Convection is driven by surface heating and temperature gradients in the atmosphere, and while the formation of severe thunderstorms is more complex than this, there has been little research on the radar-derived characteristics of convection on an hourly scale. Using radar data can add to the current knowledge on convective initiation, as the data covers a large spatial area and records data in areas where radiosondes are not launched. The temporal limitation of radiosondes are also well documented, and SAWS only releases two weather balloons daily; although this is valuable, the radar's 6 minute volume scan provides better now-casting products, detailing storm characteristics in much more detail. Examining the radar data in conjunction with radiosonde will provide valuable, high temporal data on convective environments over the Highveld, as done later in this chapter.

This section builds on the seasonal/monthly analyses by characterising convective event's diurnal properties; this adds value in understanding convective storm occurrence during different months of the year. The Irene Radar does a volume scan every 6 minutes of the 200 km area it covers; here, we only consider events with reflectivity over 35dBZ. We first consider the general characteristics of all radar-derived reflectivity on a 24-hour scale, similar to the previous section. Figure 3.4a indicates the frequency of events with a signature over 35dBZ. Here we see that convective activity is at a maximum between 1300 – 1500 UTC, or 1500 – 1700 South African Standard Time (SAST). Lightning data from the TRMM and ISS missions (Figure 3.4b), show a similar trend, with peak convective activity starting at 1300 UTC.

Figure 3.5 shows the monthly and hourly patterns of the mean observed dBZ. The number of

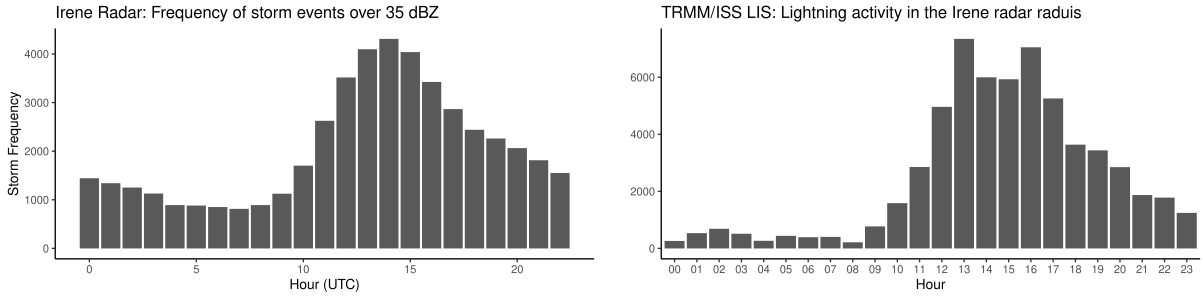

(a) *Radar* **(b)** *LIS*

Figure 3.4: *Convection mainly occurs during the summer months when surface heating is at a maximum. Here we indicate the diurnal pattern associated with convective activity. Maximum convective activity is observed between 1300 and 1500 UTC, or 1500 and 1700 SAST. Similarly, the lightning data from the TRMM and ISS missions show most lightning activity occurring early afternoon. The dataset is not in direct agreement, but this is expected as the missions are from polar orbiting satellites, which causes temporal inhomogeneities.*

events increases at the start of November, and peaks in January when the number of storms with dBZ over 50, that can be classified as an extreme events, occur most frequently. After analysing Figures 3.2, 3.3, and 3.5, the next analysis on the radar data for NDJFM, when there is the maximum number of summer convective events.

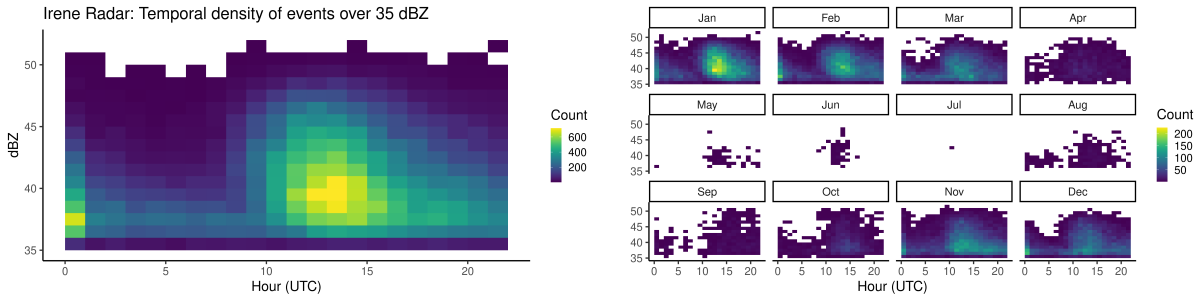

(a) *Aggregated hourly radar reflectivity* **(b)** *Monthly and hourly radar reflectivity*

Figure 3.5: *NDJFM months showed the most radar-derived convective activity in the Irene radar range.*

This section confirms that convective activity peaks during the summer months and afternoons over the Highveld. January has the most convective activity between 1400 and 1700 local time, while November has the highest mean dBZ activity. By focusing the rest of this subsection on NDJFM convective events, we discard any winter rainfall events. To understand the diurnal variation of convective thunderstorms, we still use the full 24-hour dataset for this period, but only data for the afternoon events will be analysed in certain sections. There is a distinct signal between early summer convection (November) middle summer convection (January - February) and late summer convection (March) that has to be considered. The next part of the chapter builds on the convective storm characterisation by delving into specific storm properties such as cloud top, rain rate, volume and area as observed by radar, later an analysis is conducted to examine any differences between areas with varying land use.

Cumulus characteristics during the summer

Assuming that most Highveld convective activities are associated with Cumulus clouds (Cumulus Congestus to large Cumulonimbus clouds), the subsequent analysis aims to better understand the general structure of these clouds over the Highveld. Volume scans conducted by radar produce a vertical profile of the atmosphere. The drawbacks are that the base of the beam increases with an increase in the distance; this is one of the main reasons any radar scan strategy is limited to a certain distance (200 km in the case of SAWS radars); otherwise, the radar will start to observe mid-level structures as the base of the cloud if the feature is far away. By focusing on the period when convection is most prominent (NDJFM, 1400 – 1900 UTC), the Pearson coefficient shows no significant correlation between the observed reflectivity and the cloud base, whereas cloud top and mean and maximum dBZ are highly correlated (0.7); this is expected as supercells and their associated Cumulonimbus clouds tower high into the troposphere.

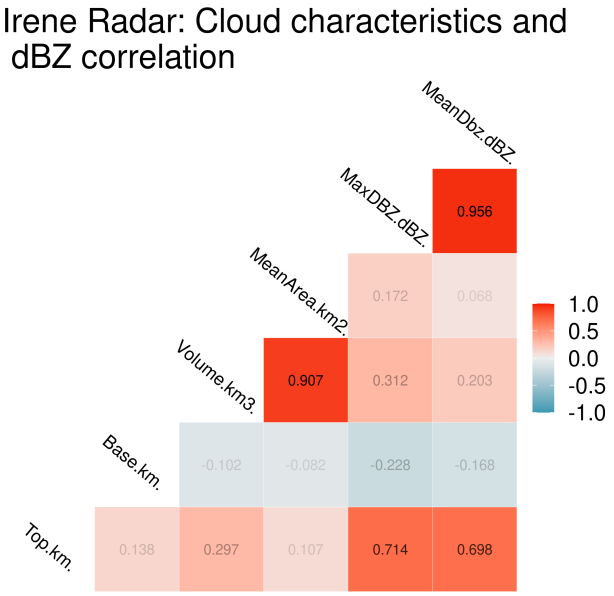

Figure 3.6: *The top of the cloud and the observed reflectivity is highly correlated. Cumulonimbus clouds stretching up to the tropopause are typically associated with severe storms.*

Although there is no significant correlation between reflectivity and cloud base, the section briefly examines this part of the cloud to better understand cloud structure during the summer months, as seen in Figure 3.7. Cloud base is derived from the lowest beam reflectivity, the radar observes cloud base to increases further away from the radar as a function of the earth's curvature, creating uncertainty in the cloud base climatology. With these uncertainties considered, this section just serves as an overview of cloud base characteristics. In all months analysed here, there is a higher than average cloud base with the onset of convection. A plausible explanation for this is the strength of the updrafts causes the cloud base to be higher during the early afternoon hours. Similarly, the base reaches saturation at higher levels initially. As an event dissipates or precipitates, the updrafts are no longer dominant. The cloud base decrease slightly with the onset of precipitation (Alber et al., 2021; Tomsett and Toumi, 2000). However, the cloud base is not related to the mean, or maximum dBZ, and a Pearson coefficient of -0.2 confirms this.

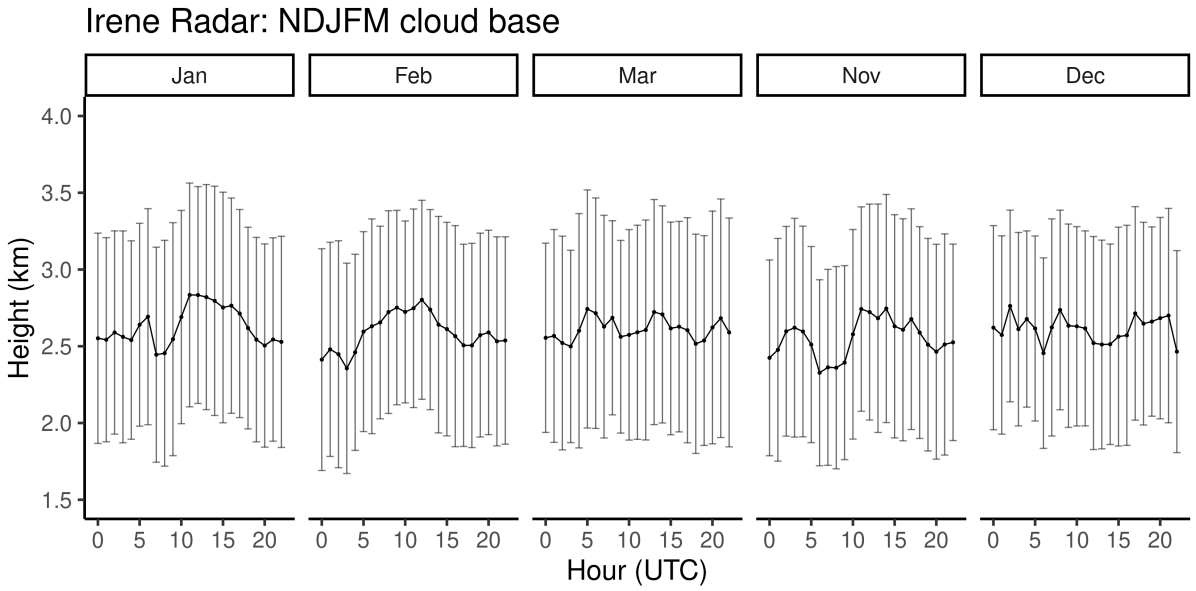

Figure 3.7: *The diurnal characteristics of the convective cloud base vary between the early and late summer months. January has the highest cloud base on average during the afternoons when convective activity is at a peak. Local noon is at 1400 UTC*

There is a good correlation between the cloud top and the observed dBZ for NDJFM months, as indicated by the Pearson coefficient of 0.6 (Figure 3.6). Here we do not distinguish between squall lines and ordinary thunderstorms yet but focus on the general structure of clouds as a function of reflectivity. The high correlation is expected as summer convective storms are mainly associated with tall Cumulus Congestus and Cumulonimbus, or supercell, clouds which can extend to the top of the tropopause. Particles such as ice with high reflectivity are abundant at these heights, creating mixed-phase clouds, where ice coexists with supercooled liquid particles. Considering the radar scanning limitations, which means that maximum cloud tops might not be observed, we focus on the mean and third quantile cloud top measurements to understand the varying convective characterise between early, mid and late summer months. On average, these structures are at a maximum during January in the afternoon between 1400 – 1500 UTC; the mean cloud top height during this time is 8.3 km (+-2 km), while the 3rd quantile height is 9.8 km.

The mean and third quantile for November and February is similar at heights of 7.9 km and 9.1 km (+-2 km), respectively, while December and March have the lowest mean cloud top observed overall at 7.5 km (+-1.9 m). Figure 3.8 indicates this diurnal and monthly variation of the observed dBZ value. The mean size area of events over the Highveld is generally between 10 km^2 to 25 km^2, as indicated in the probable size distribution in Figure 3.9; the Pearson coefficient indicates no direct correlation between cloud top and observed dBZ (coefficient of 0.1); however, there is a difference in the distribution of events based on the observed reflectivity. The radar-derived convective cloud volume and cloud top relationship (Pearson coefficient of 0.3) show a similar distribution to the mean area relationship. The largest storms occur infrequently and are associated with extreme dBZ values.

As seen in Figure 3.10, the mean direction of radar-derived storm motion shows a characteristic

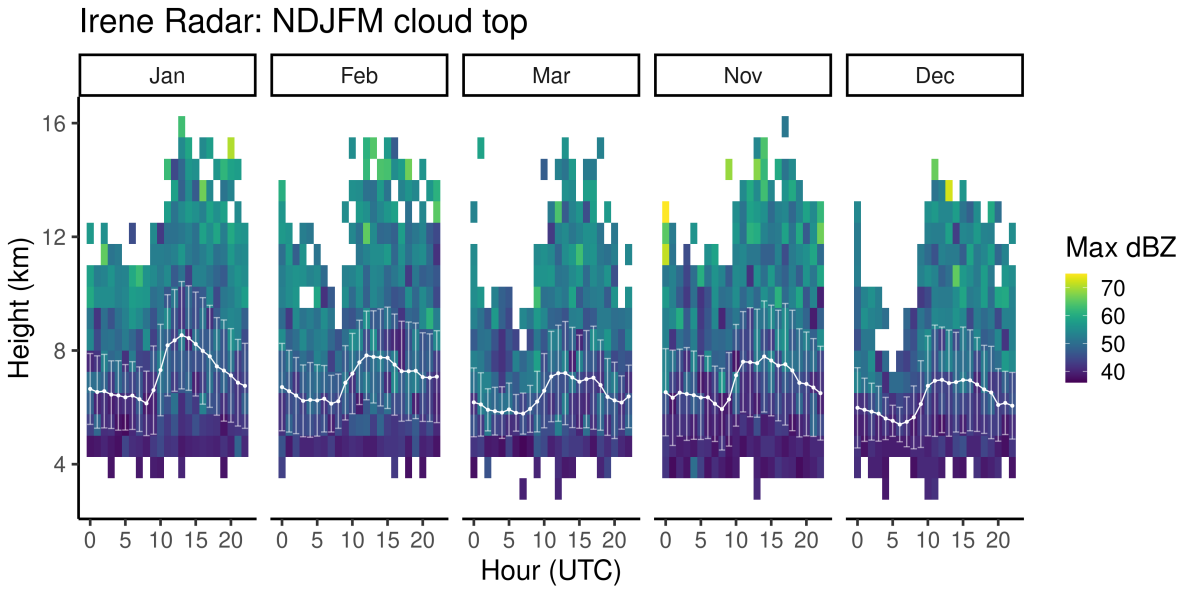

Figure 3.8: *The relationship between the observed reflectivity and cloud top is pronounced. The Pearson coefficient of 0.6 indicates that most cloud structures top is related to the mean and maximum dBZ observed.*

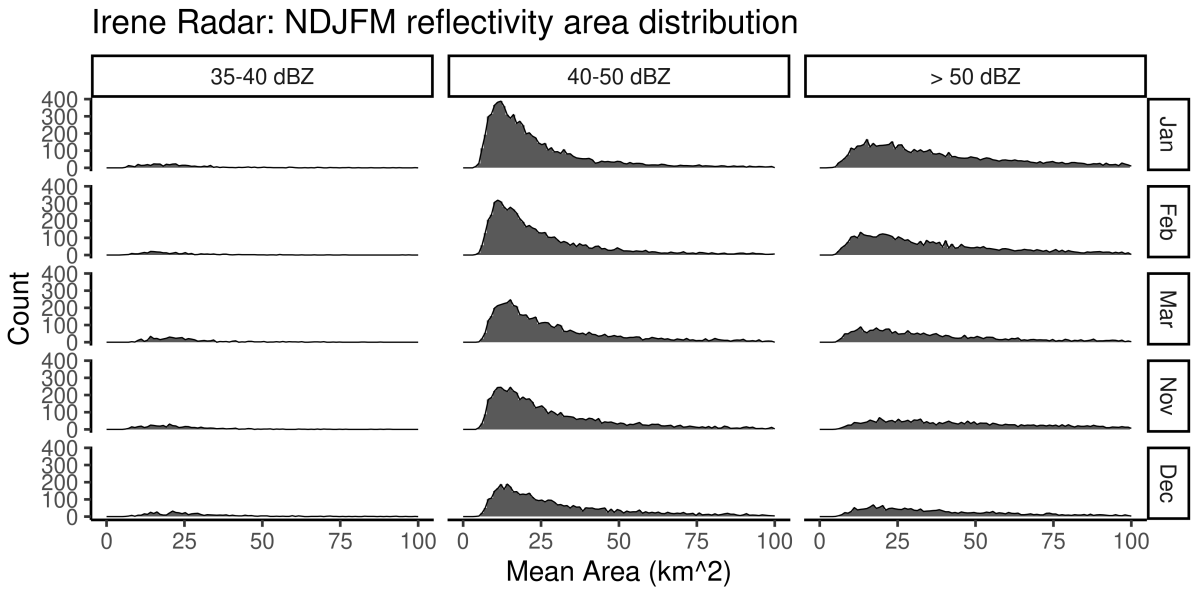

Figure 3.9: *The mean area of radar-derived storms indicates that storms range, from small isolated thunderstorms with an area of < 5 km^2 and less frequently, large supercells and squall lines over > 100 km^2.*

pattern directly linked to the mid-latitude westerlies and tropical tropical wave forcing dominant during early to late summer, respectively. Dyson (2015) classifies this as extra-tropical and tropical circulation types. The presence of less pronounced mid-latitude/westerly waves during November months impacts the mean direction of storm motion; during this time, storm movement is predominantly westerly. The mean direction the storms are steered during this time is 254°in November, and for December (241°). Storm steering occurs mainly through upper-level winds in the troposphere up to the tropopause. This movement is noticeably different during January, which is considered mid-summer, where mean storm direction is in January(200°),

February (212°), and March (215°). During this period, tropical low dominate the circulation, which impacts the mean storm direction.

Storm motion, calculated as the as the mean distance of the storm movement between successive scans, also varies during early and mid summer months. In Figure 3.10 the mean storm motion, from the radar derived cloud base to cloud top is indicated. Most storms during November and December have a high mean speed of 8.5 m/s and 6.8 m/s, respectively, while storms in January (4.2 m/s), February (4.6 m/s) and March (4.6 m/s) are considerably slower than that of early summer events and associated with more stationary and shallow cumulus convection. With the onset of autumn in March, the storm speed increases as a function of the extra-tropical westerly wave again. This changes the nature of dominating storm processes from tropical to extra-tropical (Dyson, 2015).

In this section, the basic structure of Summer thunderstorms is discussed. Convective initiation typically occurs at 1000UTC and cloud severity is at a maximum at 1500UTC. As convective updrafts decrease and precipitation occurs, the clouds dissipate during the late afternoon after 1500UTC, and the mean storm area, rain rate, and cloud top decreases. On closer inspection of Figure 3.8, is seen that the maximum cloud top height peaks at different times during the NDJFM period due to the prevailing forcing of the mid-latitude and tropical low in the early to late summer months, respectively. In November, the maximum cloud top is observed in the late afternoon at 1600 UTC (1800 SAST), while January peaks are generally observed much earlier during the day at 1300 UTC (1500 SAST). Assuming that surface heating is not yet at a maximum, and surface water is not yet as abundant, in November, it could explain the cloud top's delayed development compared to January where surface heating reaches a maximum, and if there is surface moisture available from the more rapid cloud development can occur. The mean storm direction (Figure 3.10) indicates that there is a noticeable difference in the steering direction of the storms during November and January, and this is a function of the prevailing upper-level winds impacted by the westerlies and tropical circulation during these months, respectively. We also see more slow-moving storms in January as the upper levels winds are not that strong in steering storms west. This helps explain why we observe events with a higher mean dBZ during November; large supercells and MCC need strong upper-level winds to steer them over surface large distances but it also allows increased moisture influx and enhances shear and rotation.

In conclusion, the radar-derived wind fields show that conditional instability and differential advection result in fast-moving supercell formation in November. In contrast, convective instability and surface heating dominate the formation of slow moving convective storms in January. Further investigation on the effect of differential advection would be fascinating in the South African Highveld context, as little research around this is currently available.

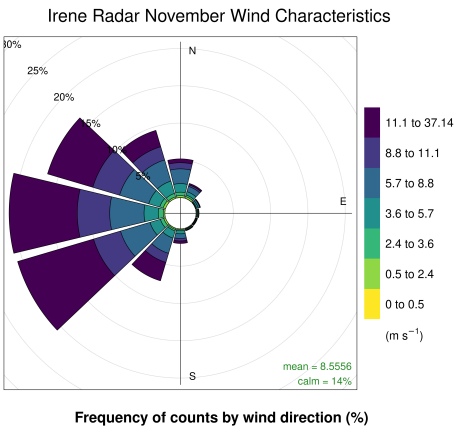

(a) *November*

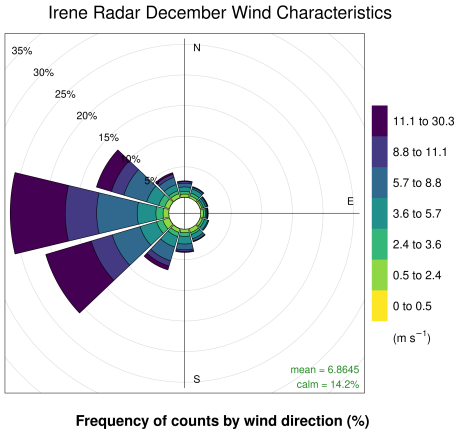

(b) *December*

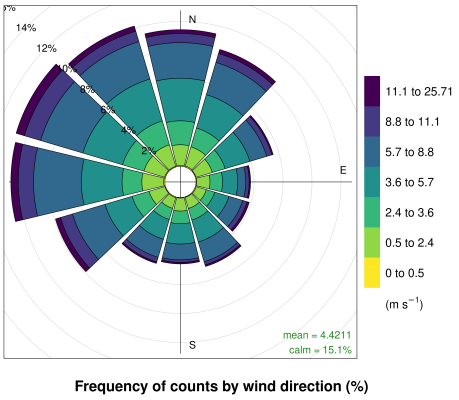

(c) *January*

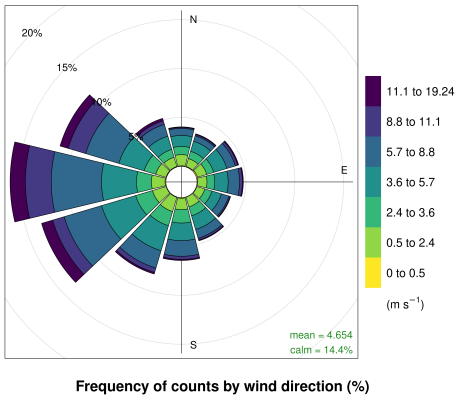

(d) *February*

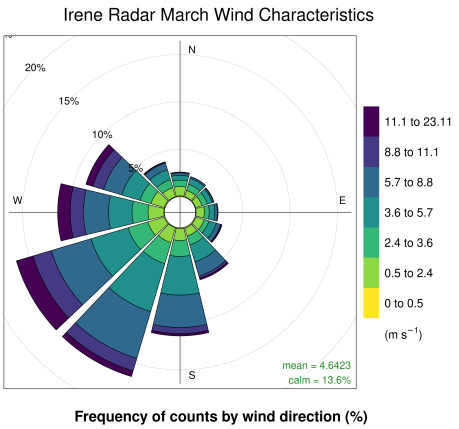

(e) *March*

Figure 3.10: *Mean storm motion shows the impact of westerly and tropical forcing present during early and mid-summer months, respectively. Upper-level winds mainly influence storms motion. The westerly waves dominate these winds, and the difference in storm direction and speed between mid-summer and January is significant. Storm motion is noticeably slower in January with a mean speed of 4.5 m/s compared to early summer months when storms are fast-moving with speeds up to 8.6 m/s. However, surface easterlies generally provide an influx of moisture. During January the wind direction is more varied, and slower than early summer months when the westerlies are less dominant.*

Radar derived precipitation characteristics

It is important to understand the relationship between the reflectivity, cloud structure, and the radar estimated rainfall rate to better understand the characteristics of moderate, heavy and extreme convective events during the afternoon summer months. By applying the Pearson correlation on radar reflectivity and structure, as detailed previously, we now add radar-derived precipitation to the equation. We can see that the estimated precipitation rate, based on the standard Marshall-Palmer drop size distribution of $200R^{1.4}$ (Keat et al., 2019), is highly correlated to the cloud top (0.6) and reflectivity characteristics (0.9) of NDJFM events (Figure 3.11). We can use this knowledge to better understand radar-derived rainfall estimates and precipitation characteristics during extreme events, i.e. characterising the rain rate maximums during the storm life cycle.

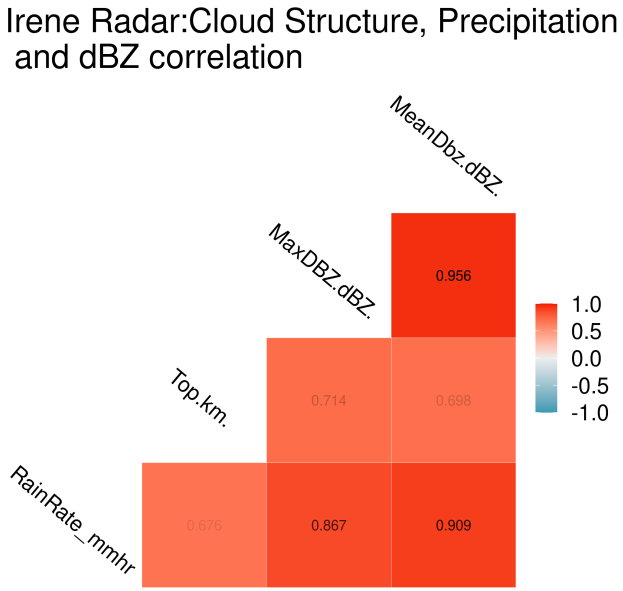

Figure 3.11: *There is a high correlation between cloud structure, reflectivity and radar estimated precipitation. We excluded the cloud base as the previous section showed that the cloud base is not correlated to reflectivity or precipitation. The diurnal relationship between radar reflectivity and precipitation maxima during NDJFM months can be understood in finer detail.*

During the convective storm season, radar-derived estimates indicate November is the month when the precipitation rate is the maximum; here, a maximum rain rate of 162 mm/hr is estimated with a mean of 14.7mm/hr (+-10 mm/hr). January and February have similar maximum estimated rain rates (130 mm/hr), but these two months have the highest mean rain rates at 16.2 mm/hr (+-9 mm/hr) and 15.7 mm/hr (+-8 mm/hr), respectively. December and March have the lowest observed maximum rain rate (90 mm/hr) and also the lowest mean rain rates 13.3 mm/hr (+-8 mm/hr) and 13.5 mm/hr (+-7 mm/hr), respectively. As seen in Figure 3.12, the highest radar estimated maximum rain rate is associated with cells larger than 50 dBZ, however, events between 40-50 dBZ are on average, more common than these extreme events. It has to be noted that the rain rate observed in the cloud is not necessarily reflected in the surface station. The cloud can move fairly quickly over an individual station. In summary, although we expect the most severe storms to also have the highest rain-rate, because they are less common, smaller

sized cells might pose a greater risk as a function of relative occurrence.

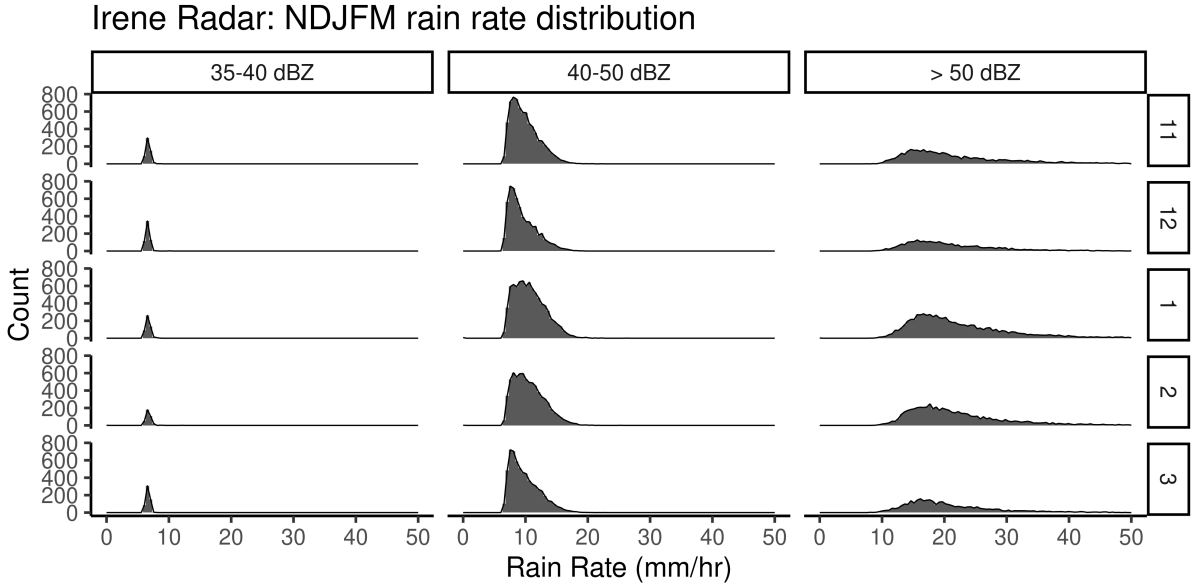

Figure 3.12: *The probability distribution of radar-derived rain rates indicates that events between 40-50dBZ occur more frequently than extreme events. Smaller sized cells might pose a greater risk as a function of relative occurrence.*

Due to the high correlation between observed reflectivity and rain rate, we expect that late afternoon will be when the highest rain rate is recorded for each month and hour. This is confirmed in this analysis. The highest average rain rate for all months combined is at 1200 UTC, or 1400 SAST, with a mean rain rate of 17 mm/hr (+- 10 mm/hr). From 1100 to 1400 UTC, 1300 to 1600 SAST, the rain rate is similar at over 17 mm/hr across all months. From 1800 UTC, 2100 SAST, the rain rates decrease substantially (<15 mm p/hr). In November, the maximum instantaneous rain rate is at 1600 UTC, but care has to be taken when examining the maximum rain rate as this is an instantaneous measurement. Figure 3.13 shows the monthly and diurnal variation in the rain rate; when radar recorded reflectivity is over 50dBZ, the chance of severe flash flooding due to high rainfall is significantly higher than events characterised by a low dBZ and Figure 3.14 supports this findings. Both Figures show that November has the highest maximum observed rain rate, while January has the highest mean rain rates. The nature of the early and late summer convection is discussed later on in detain, but the changes observed here is possibly due to the convective storm types that dominate the during the respective times of the year. In November fast moving convective storms, driven by conditional instability will dominate, while convective driven, tropical circulation will increase the development of isolated thunderstorms during mid-summer.

Using the Pearson Coefficient as a guideline, this section described the seasonal and diurnal characteristics of radar-derived cloud structure, area and volume characteristics, and rain rate. In agreement with past literature on the climatology of SA and SA thunderstorms, we can see that during the Highveld summer month's convection plays a prominent role in the atmospheric dynamics of the area. By extracting only NDJFM months data for reflectivity measurements over 35dBZ and categorising them into moderate, heavy and severe events, we can see that cloud

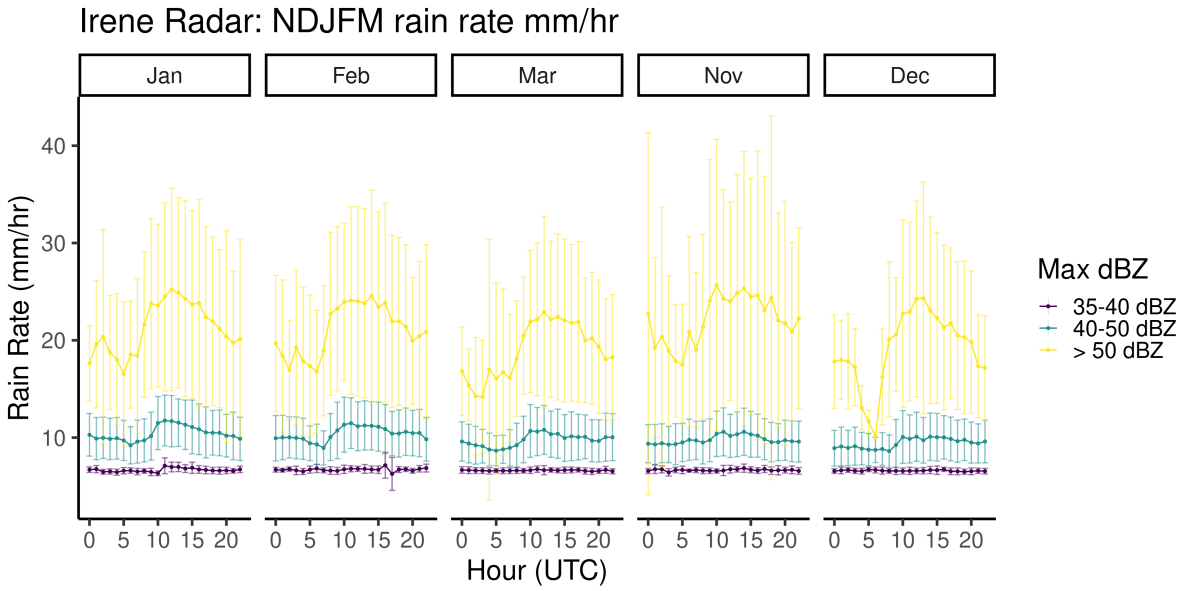

Figure 3.13: *There is a direct correlation between precipitation rate, the diurnal cycle of convection, and the dBZ observed. What is interesting to note in this Figure is that the highest precipitation rate (162 mm/hr) is observed during November. Afternoon precipitation peaks during extreme convective activity (> 50dBZ) across all months.*

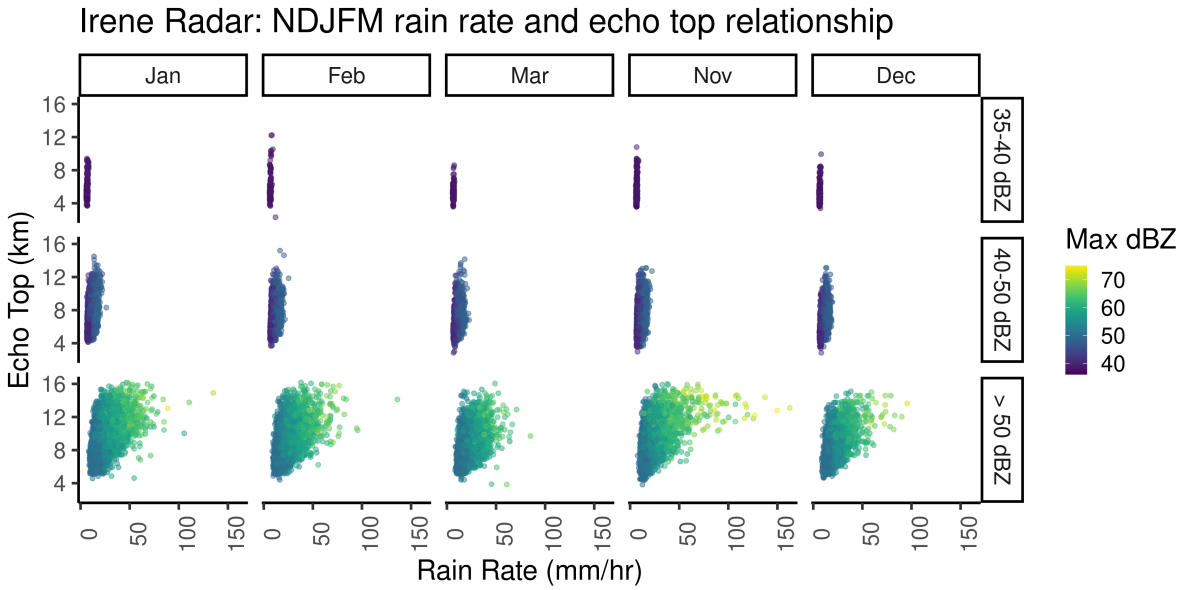

Figure 3.14: *Radar derived rain rate is correlated to the radar cloud top. During November the maximum rain rate is the highest with frequent observations of rain rates > 100 mm/hr. However, during January the mean rain rate is higher. Higher mean and maximum reflectivity will increase radar derived rain rate as a function of the Marshall-Palmer distribution. This does not relate to actual surface rainfall.*

top has a direct correlation between the rain rate and reflectivity. Most events can be classified as moderate, and the normal distribution of data indicates that the rain rate rarely exceeds 30 mm/hr, even during convective events. The mean area of a storm is not a good indicator of maximum rain rate, and we expected this as a thunderstorm can have a minimal spatio-temporal distribution. In the following section, we examine extreme radar-derived events in more detail–

specifically, the occurrence of hail and flash flooding in the study area.

Extreme convective event characteristics

The last section of the radar analysis will focus on the occurrence of radar-derived variables associated with the most extreme convective events as defined below. The relationship between severe storms and reflectivity is not a directly linear relationship as hydrometer concentration, diameter and scattering properties are not uniformly distributed in a cloud (Warren et al., 2020). There is, however, some derived methods developed to deduce hail probability, this includes Foote Kraus Index (FOKR) (Foote et al., 2005), Waldvogel probability index (Waldvogel et al., 1979), hail mass aloft and vertically integrated hail mass and the locally developed Storm-Structure-Severity (SSS) index (Visser, 2001). The FOKR and Waldvogel index is based on the height of reflection above the surface, assuming an arbitrary altitude equals a freezing level within the atmosphere where ice processes start to form hail. The freezing level occurs at temperatures lower than (0°C), however, supercooled liquid can remain in the atmosphere at temperatures as low as (-38°C). Due to hail size and scattering characteristics, the algorithms assume that dBZ values over 45 and above a certain level (i.e. 3km) is directly related to the presence of hail in the cloud. Based on these assumptions, the FOKR index attempts to derive hail size in four categories (where ΔH_{45} is the height of the 45dBZ echo), i.e.

1. Z_{max} > 40dBZ above 3km MSL – first hail signature, potentially dangerous
2. Z_{max} > 45dBZ above 3km MSL – dangerous at later stage, possible hailstorms
3. Z_{max} between 45dBZ and 55dBZ, ΔH_{45} > 3km – hailstorms
4. Z_{max} > 55dBZ and ΔH_{45} > 4km – severe hailstorms associated with supercells

We use the FOKR scale and we extract category 3 and 4 data from the Irene radar dataset to examine events with an extreme probability of hail occurrence. Thus, the hail threshold for the analysis is Z_{max} > 45 dBZ and ΔH_{45} > 3 km. Sindhu and Bhat (2019) provide a detailed overview of similar thresholds used to separate extreme events, and in all cases, a reflectivity over 40dBZ at varying altitudes forms the basis of the selection. Most extreme events correlate with high dBZ, high cloud tops and high rain rate (all variables have a coefficient > 0.5 where at least one hail specific variable is the dependent variable).

The most significant limitation is the amount of data for severe storms such as this; even considering the high spatio-temporal measurement of radar technology, few storms turn out to be severe (but it only takes one event to wreak havoc (Barry, 2014)). Figure 3.15 shows the frequency distribution of severe events for one year, events that have fallen within the FOKR category three often occur, but events with a maximum dBZ over 55 are infrequent during all months of the year. November has the most extensive distribution of extreme events, while January has the highest frequency of extreme events (FOKR category four). From here, we examine the derived hail mass aloft, precipitation rate, mean radial velocity, storm speed and vertically integrated hail mass of extreme events. The selected criteria are not exact to extract all hail events; the

relationship between hailstorms and reflectivity is complex. It can occur under various conditions, but this serves as a good measure of the extracted events with an high probability of hail occurring.

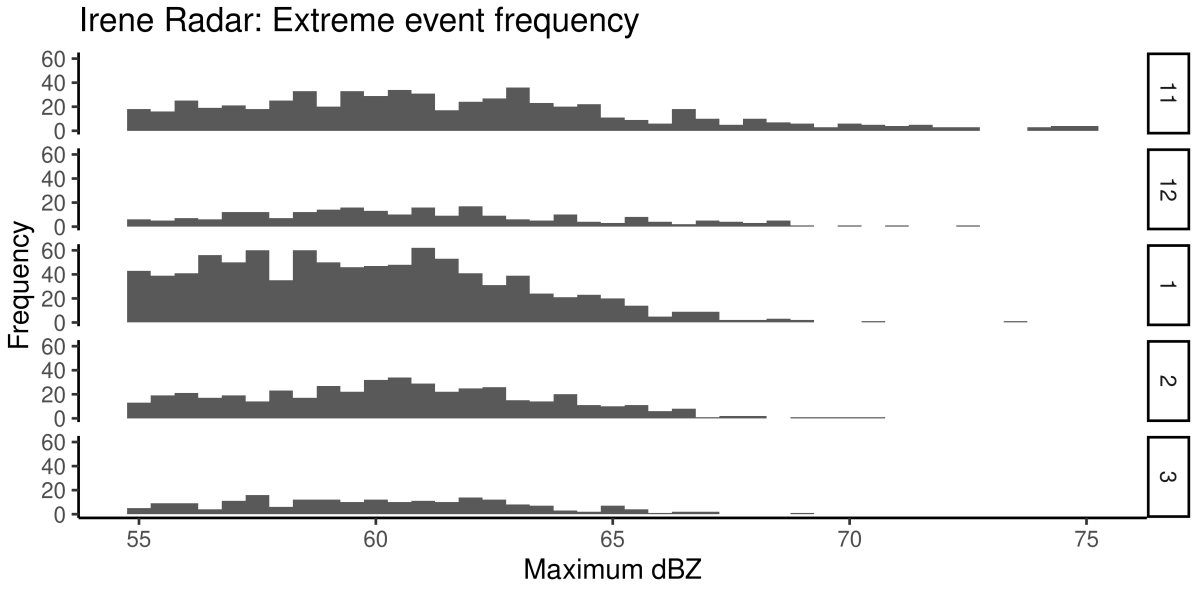

Figure 3.15: *Using the FOKR classification as a guideline, the above Figure indicates the frequency of events where $Z_{max} > 45dBZ$ and $\Delta H_{45} > 3$ km. November has the most extensive distribution of extreme events, while January has the highest frequency of the total number of events. Considering the previous section, we know that speed and direction between these months are different, and stationary, isolated, storms characterise January, while November has fast moving, rotational convective cells.*

In Figure 3.16 it is observed that the mean area of severe events over 50 dBZ with rain rates over 25 mm/hr is on average 105 km^2 in all months. Most events with the highest rain rates have a characteristically small mean area; for instance we can observe a storm in November with rain rate over 120 mm/hr, and less than 100 km^2 in size. For comparison, the City of Johannesburg Metropolitan Municipality is 1645 km^2.

Due to the rare nature of these events, we aggregate the data for NDJFM in this analysis. Figure 3.17 indicates the relationship between cloud top, a vertical extent function, and the hail mass aloft for the aggregated data. Tall clouds, typically associated with deep convection and possibly supercells, have the highest hail mass concentration. The radar is agnostic towards hail reaching the surface, but clouds with radar estimated tops over 10 km show signs of ice processes present and a high chance of hail occurring. Similarly, the highest mean precipitation during extreme events is directly correlated to the cloud top (Figure 3.18). However, when the cloud top is at 13-14 km, the highest maximum rain rate is observed.

These extreme events associated with the FOKR category ≥ 3, are rare over the Highveld, relative to convective events that have a low mean and max dBZ, however, understanding some of the spatio-temporal characteristics, such as the typical size, rain rate, month of occurrence, assist in better understanding the impacts and possible mitigation methods we can use, and plan for, during a storm season. The section showed that radar derived precipitation can exceed over 120 mm/hr for areas less than 12km^3, and that during January we have the highest occurrence

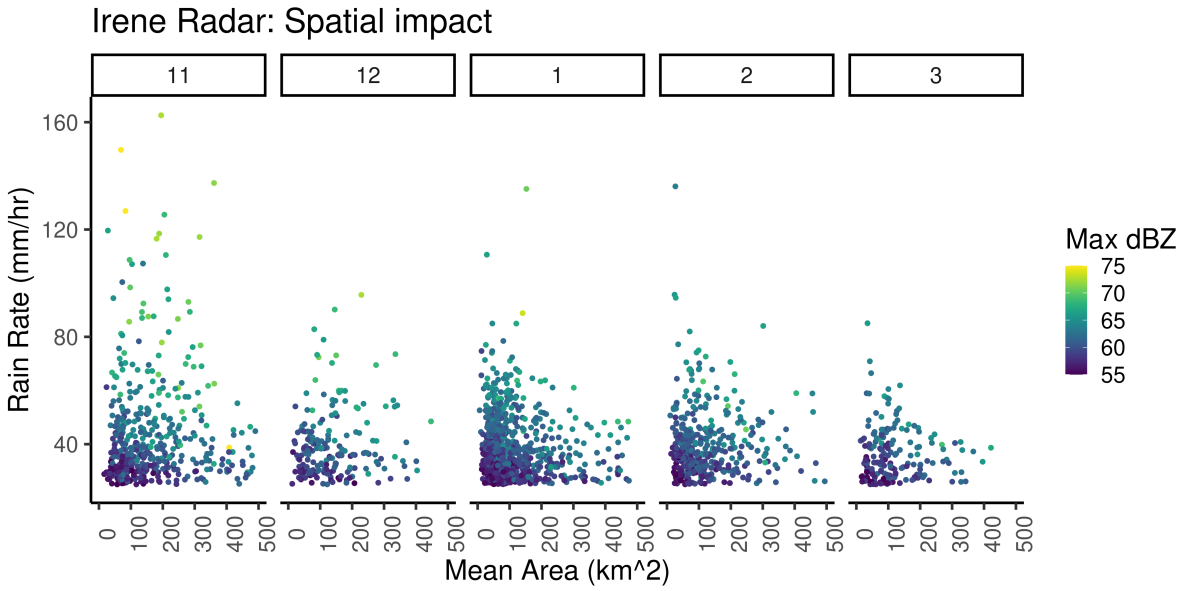

Figure 3.16: *Extreme convective events with $Z_{max} > 45dBZ$ and $\Delta H_{45} > 3$ km are characteristically small, and most events with the highest rain rate have the smallest mean area, i.e. November events with $Z_{max} > 65dBZ$ are less than 250 km^2 in size, and this becomes even more apparent when we consider that Johannesburg is 1645 km^2.*

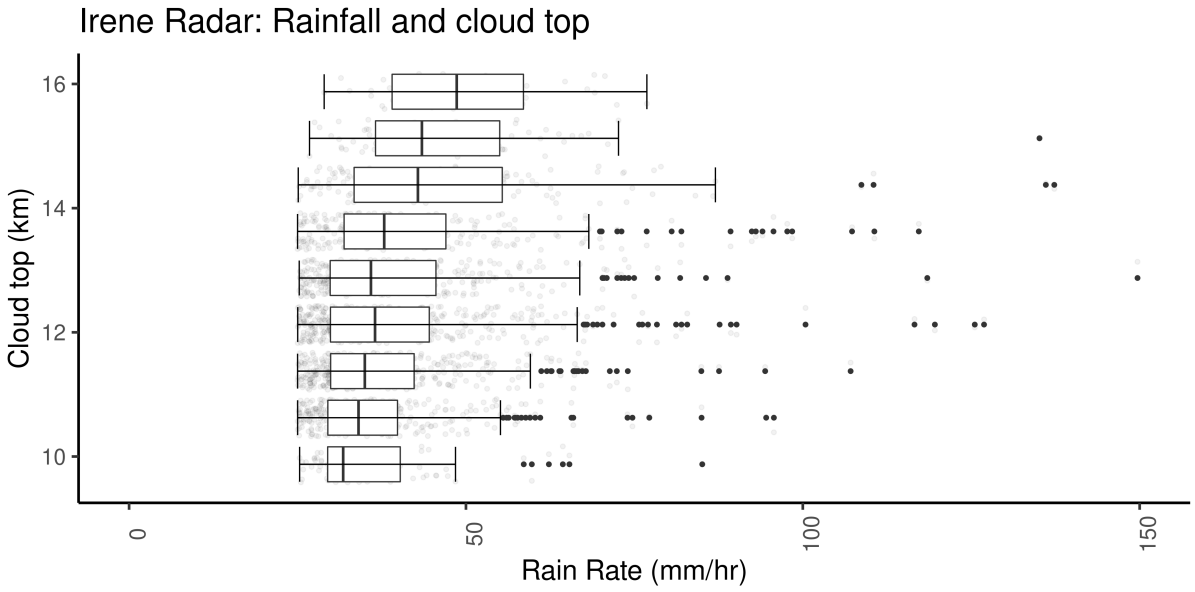

Figure 3.17: *Radar derived cloud top observations show that the hail mass aloft is strongly dependent on the cloud extent. Ice processes start to dominate in the upper atmosphere and hail/ice formation is accelerated when the freezing level is reached. Clouds with a height of over 10 km have a high probability of hail occurrence.*

of these events, but the most severe events occur in November. These events remain rare, but is life threatening and unpredictable.

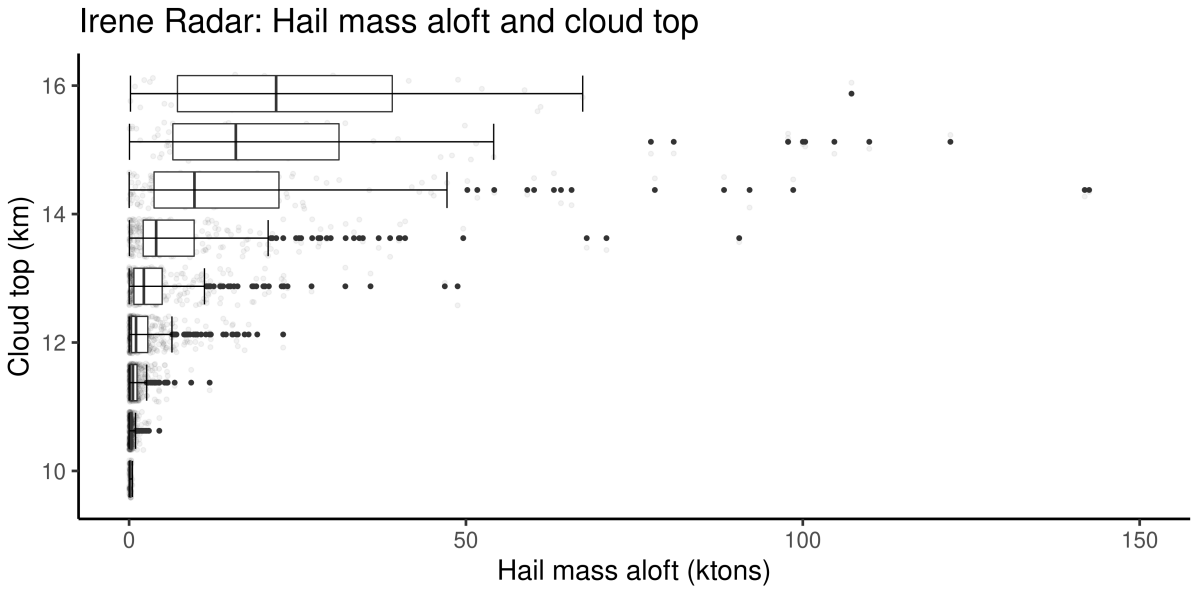

Figure 3.18: *The hight of the radar derived cloud top is directly correlated to the mean an maximum precipitation. Clouds at 13-14 km have the highest maximum rain rate, while clouds at 16km (highest observed tops) have the highest mean value.*

Conclusion

The radar data showed that most convective storms initiate at 1300 UTC and peaked at 1500 UTC before dissipating. On average most storms were not severe, but during the lifetime of the event, instantaneous measurements of the maximum dBZ indicate that storms exceed 40dBZ during their lifetime at some stage. Most storms with a mean dBZ over 50 occurred in November. November storms were characterised by strong winds aloft and the mean speed of winds of convective events were the highest in November. If we examine the mean direction of storms during this time, we can see that the extra-tropical, westerly wave nature of the atmosphere was dominant, which enhances conditional instability. In contrast, isolated convective storms dominate in January and February. These storms were slow-moving. They were mainly present during strong easterly/tropical circulation and surface convection as discussed later. Similarly the nature of precipitation during these convective events shows us that the most intense precipitation is often short lived and over a small aera, this is particularly life threatening. During January there is a high frequency of severe convective events that show severe characteristics (FOKR ≥ 3), but the most severe of these events occur in November.

The study provided an overview on the nature of convective storms over the Highveld. This included characterising the timing of convective storms, cloud characteristics such as cloud top, speed and direction of movement, and severity. The next section builds on this by examining the significance of convective weather events to the population of the Highveld. Subsequently, this study attempts to characterise the synoptic and thermodynamic conditions convective events occur under. By understanding the characteristics of convective events across scales, the study can better identify conditions that drive convective storms and the possible impacts, intended or unintended, on convective weather events.

Chapter 4
The significance of convective weather events

"Yet not all meteorologically significant events would strongly affect society; conversely, not all outbreaks of large societal impact would be unusual meteorologically".
This statement by Ćwik et al. (2021) is thought-provoking. Why do we choose the events we do for scientific analysis? Similarly, we can think about the thought experiment, *"If a tree falls in a forest and no one is around to hear it, does it make a sound?"*

In this chapter, we analyse media reports from Caelum (1991) and its subsequent updates until December 2017 to examine the significance of convective events for the Highveld region. There is specific focus on convective weather, the extent of damage caused by these events, and which events are the most impactful for the region during summer months.

Introduction

The first reported event in Caelum that documented a fatality occurred on Christmas Eve, 1705, in Stellenbosch when floods *killed five people and destroyed* $^1/_3$ *of wheat crops*. There was no significant increase in the number of reported events until the late 1800s; this could be due to various factors related to population density, means of communication, etc. From the early 1900s, there is an exponential increase in the number of reports. The introduction of television, printing press, population increases, economic growth and most recently, the introduction of the internet and social media has resulted in an exponential number of storm reports in comparison to the previous century. A similar statement is made by Ćwik et al. (2021), where they noted that the increase in tornado reports in the USA are due to a variety of factors such as new reporting techniques, public participation, interest in the weather[1], increased surface observations (not only meteorological instruments, but general surveillance such as closed circuit television, motor vehicle dash cams, drones, and social media), and the availability of fast internet. It is noted and emphasised here that Caelum (1991) is a highly subjective account of convective weather, as it relies on human reported data. However, no other meteorological source in South Africa dates back to the 1640s, which justifies the use of the Caelum (1991) publication in this chapter. Although the publication has proven an invaluable and interesting data source, it has yet to be thoroughly analysed, even considering its limitations and biases. We build on these reports and include a detailed analysis of various thermodynamic and synoptic conditions under which these events occurred using radiosonde and ERA5 reanalysis data, respectively.

Media reports are heavily biased towards populated areas and cannot be used as objective analyses of storm occurrence. However, it is valuable to use this dataset to choose specific events for analysis that resulted in damage or loss of life. From the first reports in the mid-1600s to the mid-1800s, we can see that the number of reports were relatively low, as illustrated in Figure

[1]storm chasing has become a commercial activity in the USA

4.1. From the late 1800s, there is an increase in the number of events reported, possibly due to a growing population, increased access to printing material, increased media sources, and the increased movement of people. Because the dataset has such long-term inhomogeneities, it is necessary to break the data down into monthly datasets. This allows for the last 100 years of data to be viewed on a seasonal scale.

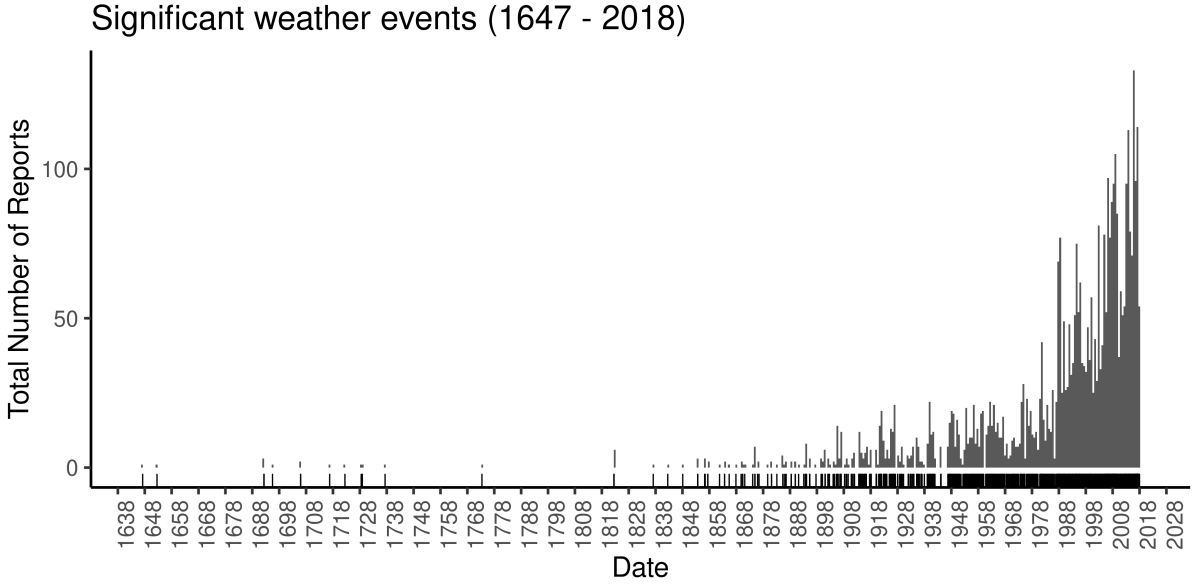

Figure 4.1: *The number of reports over the previous century were relatively low. There is an increase in the number of reports around the late 1800s, possibly coinciding with the subsequent migration of people inland in previously sparsely populated areas. The increase in the population of SA, economic growth, and the printing press's impact played a part in this increase of reports. Since the mid-2000s, the internet and social media have increased public participation in storm reporting and awareness, leading to even more reports.*

Overview of significant weather in Highveld

As seen in Figure 4.1, the first weather reports detailed in the SAWS digitised version of Caelum starts in the mid-1600s. However, this is for the whole of SA. By extracting the significant storm reports for the Highveld as seen in Figures 4.2a and b, we can see storm reports for the Highveld region only became more frequent in the early 1900s (more likely as a function of reporting frequency than the actual increase of convective events). In the first analysis of severe and non-severe events, as seen in Figure 4.2a, we can see how all events increased with time in the Highveld. Some events classified as severe (or non-severe) could be physically and dynamically similar to current events. However, population dynamics and reporting frequency has changed throughout the datasets evolution. This means that all reports are not standardised. It is not feasible to do long-term analysis on the trends of convective weather events based on these reports. As seen in Figure 4.2b, the number of "non-severe" events dominate the total number of reports as expected. This is because extreme events, i.e. severe events, are infrequent compared to moderate events.

A monthly and seasonal breakdown of significant events provides a valuable picture of convective weather event frequency for the Highveld region. The temporal analysis allows us to

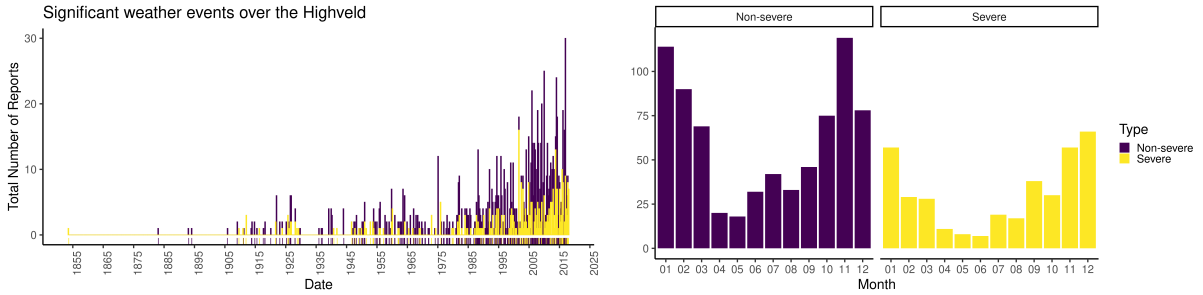

(a) *Highveld weather reports* **(b)** *Monthly distribution of severe events*

Figure 4.2: *Figure a, above, shows all severe and non-severe weather reports extracted for the Highveld region. The frequency of media reports related to weather events only became more prominent in the early 1900s, while the general Caelum dataset (Figure 4.1) first reports date back to 1647. However valuable the dataset is, it is not objective towards populated and economically important events or areas. In Figure b, we can see that the total relative contribution of non-severe events is much more than severe weather events, which we expected due to the rare nature of extreme events.*

examine specific storm types and their seasonal distribution without the bias towards reporting years. In Figure 4.2b and in Figure 4.3a, severe weather reports are mostly a summer occurrence for the Highveld region and are dominated by convective events. Convective events in this case include general thunderstorms, hail, lightning and flash floods (Figure 4.3b). The result is not surprising as the continental high-pressure system dominates the winter months over South Africa, which results in mostly fine and dry conditions with an absolute stable layer preventing any form of convection.

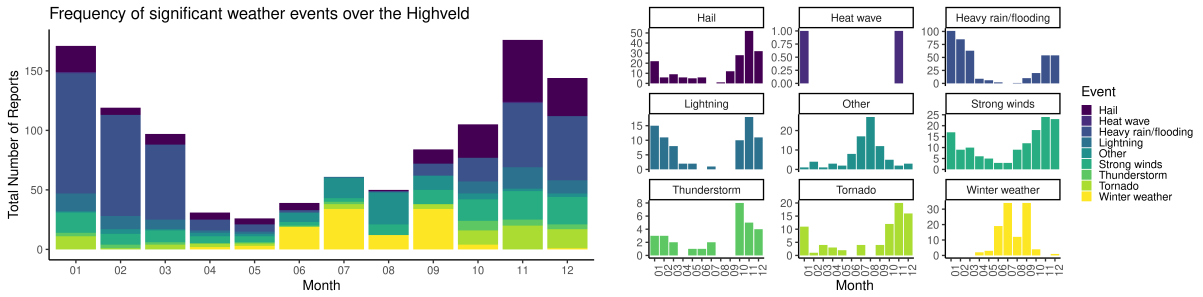

(a) *Frequency of severe weather reports* **(b)** *Events separated by their total relative contribution*

Figure 4.3: *In Figure a, above, we can see that the most severe weather over the Highveld occurs during the summer months. As expected, this is mainly in the form of convective weather events, including hail, lightning, flash floods and general thunderstorms as seen in Figure b.*

The actual economic damage for all these events is hard to quantify when examining the media reports. Some reports contained detailed economic and mortality details, and others have more vague mentions of damage without specific details. With this in consideration, all the reported damage from severe weather over the Highveld is summed up in Figure 4.4. For this analysis, we simplify the media reported damage into three categories, human and or livestock death, over ZAR 1 million in reported damages, and other significant events where damage was reported without any of the other losses explicitly mentioned. The results show that severe weather has resulted in over 20 events with ZAR 1 million or more losses, while the number of events leading to deaths is three times that. The likelihood that events go unreported in some areas

is high. This under-reporting means that the damage from severe reports could be even more. As discussed in the introduction, the definition of damage is relative. Various events result in the loss of historical sites, lost workdays, repair days–costs that are not directly reported in the immediate aftermath of an event.

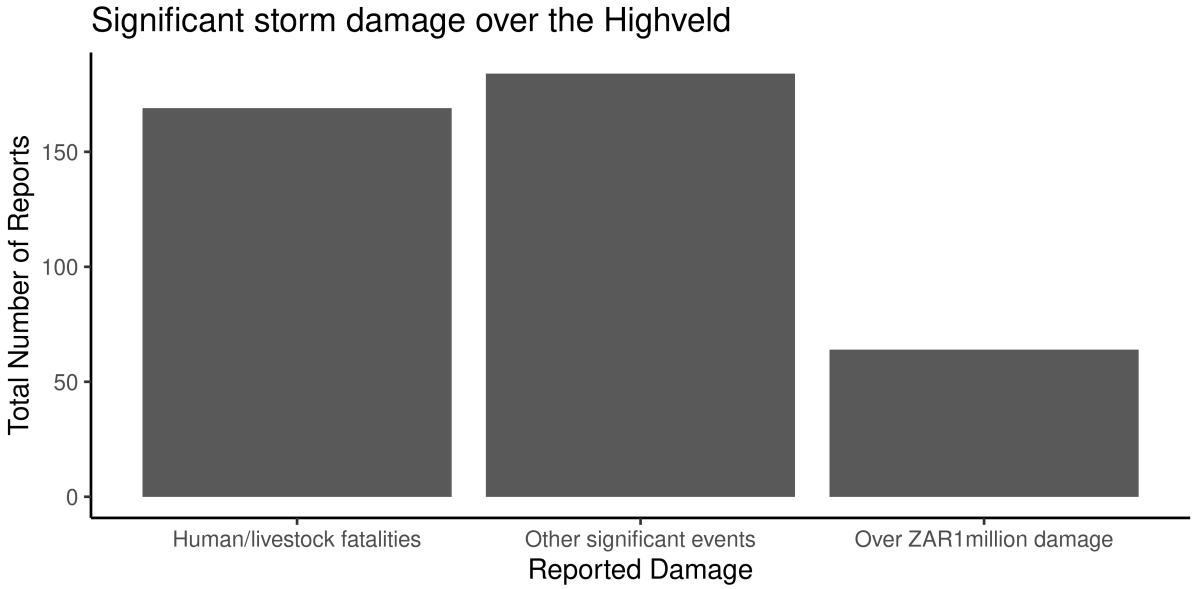

Figure 4.4: *By classifying reports into three major categories based on the damage reported, we can see that over 20 events have caused more than ZAR 1million in damages. Over 80 events have resulted in the death of humans and livestock. A majority of events caused damage without any explicit mention of the economic loss or mortality. We can speculate that this number is far higher as many events go unreported, and media reports are biased towards populated areas.*

The relatively frequent occurrence of severe weather events and the subsequent damage recorded necessitates the research to better understand the conditions under which these events form, what specific time stakeholders need to be in a state of alertness, and what possible future mitigation methods we can use to minimise our risk. In the rest of this section, the media reports will be used as a foundation to better understand convective events over the Highveld by building simple climatologies of the media reports to examine the atmosphere's synoptic and thermodynamic state during the days these events occurred.

An analysis of convective storm reports

The previous section examined all severe weather reports, irrespective of the type of event. The following section will only examine convective events over the Highveld in more detail by extracting the reanalysis data and upper-air soundings for a coinciding report and building a climatology of conditions these events occurred in. As mentioned in the introduction of this section, we only examine events that are classified as thunderstorms, hail, and lightning. Heavy rains and flash floods are also included here, but these events are not explicitly categorised into well known convective types. However, these events have a strong signal during summer, and it is interesting to compare the convection types during early and late summer and hail compared to heavy rainfall. First, the results examines the occurrence of severe compared non-severe convective events over the Highveld, as seen in Figure 4.5. The results are surprising.

Looking back at Figure 4.2 we can see that non-severe weather events dominate the region's total number of storm reports. However, Figure 4.5 shows that convective events classified as severe are disproportionately represented in comparison. We see more severe reports than non-severe reports in December, February and March, while November and January have a relatively similar number of either report. In agreement with the literature is the seasonal distribution of these events, where most severe events are observed in early summer (refer back to Figure 1.6b in the introduction).

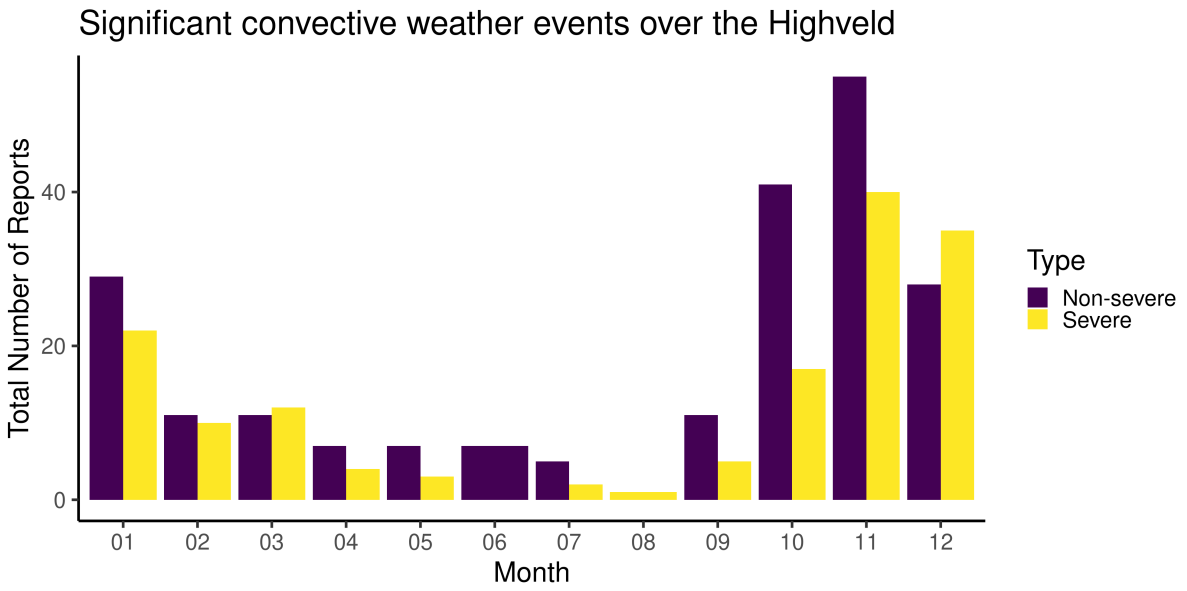

Figure 4.5: *Severe convective events occur almost as frequently as non-severe convective events over the Highveld during the summer months. This contrasts with the overall representation of severe and non-severe events, where we see that across all seasons, non-severe events dominate. The monthly distribution of events is similar to the climatologies of past studies.*

By aggregating all the reports into the month of occurrence reports (Figure 4.6), we see that most events have a strong summer presence as expected. Hail reports dominate early summer, and because hail is also associated with thunderstorms and lightning, we can assume that these events are also grouped under the banner of "hail damage" during reports. Tornadoes are rare, and in this dataset, there are 34 reported tornadoes for the Highveld from 1979 to 2018 and 67 total with the inclusion of pre-1979 reports. This can be an exciting topic for further research, where we examine tornadic vs non-tornadic supercells over the Highveld. What is also worthy of further investigation is the occurrence of winter tornadoes. In the whole dataset, there are 12 winter tornadoes and three reports over the Highveld; 10 May 1949 in Bronkhorstspruit, 21 May 1954 in Benoni and the most recent one on 25 July 2016 over Thembisa (ENCA, 2016).

The study excluded reports classified as "Heavy Rainfall/ Flooding" in the section above, but subsequently, we explicitly compare hail events and heavy rainfall. It is expected that early summer will see more hail reports (relative to the total number of hail reports) and late summer more heavy rainfall reports (again relative to the total number of heavy rainfall reports) due to the extra tropical and tropical properties of convection types during these months respectively. In Figure 4.7, hail reports are most frequent during early summer as expected, and heavy rainfall is most common during mid-summer, but also occurs throughout the year. As seen in the

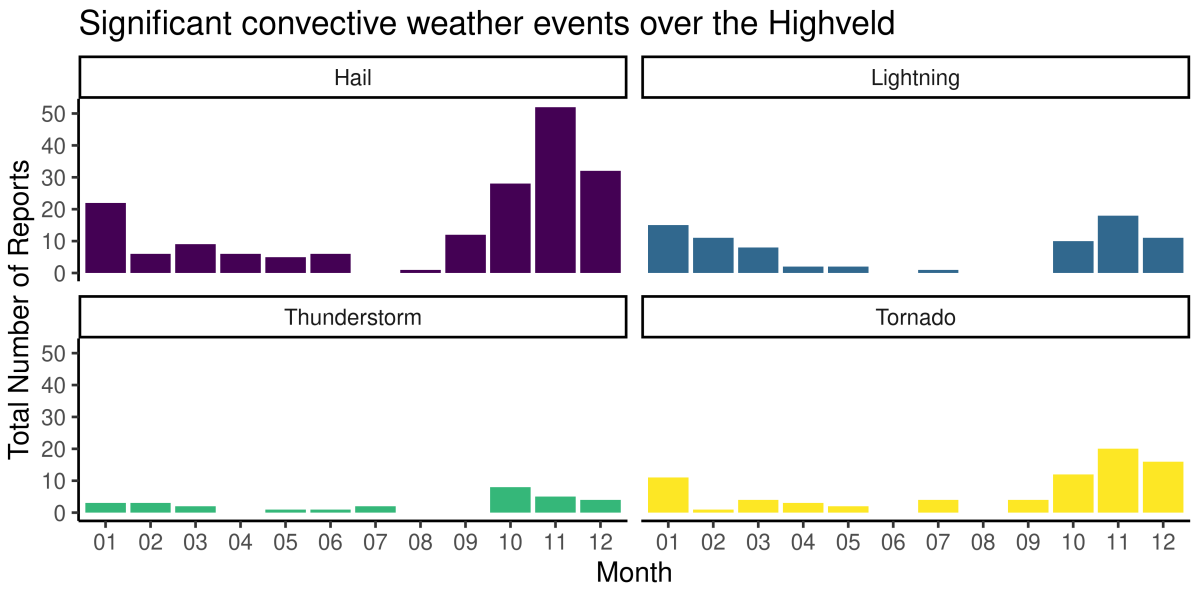

Figure 4.6: *Convective weather event reports dominate the summer months. Hail storms gather the most media attention; however, because these events are a function of thunderstorms, we can assume that thunderstorms and lightning may also fall under the banner of hail events. Tornado's, however rare, do occur over the Highveld and in this study, we see 34 reported cases of tornadoes in the study region (there are 67 tornado reports for the Highveld if we include pre-1979 reports).*

radar data, differential advection and storm speed are much higher during the early summer months, sustaining supercell storms, enhancing rotation and leading to long-lived storms over the Highveld.

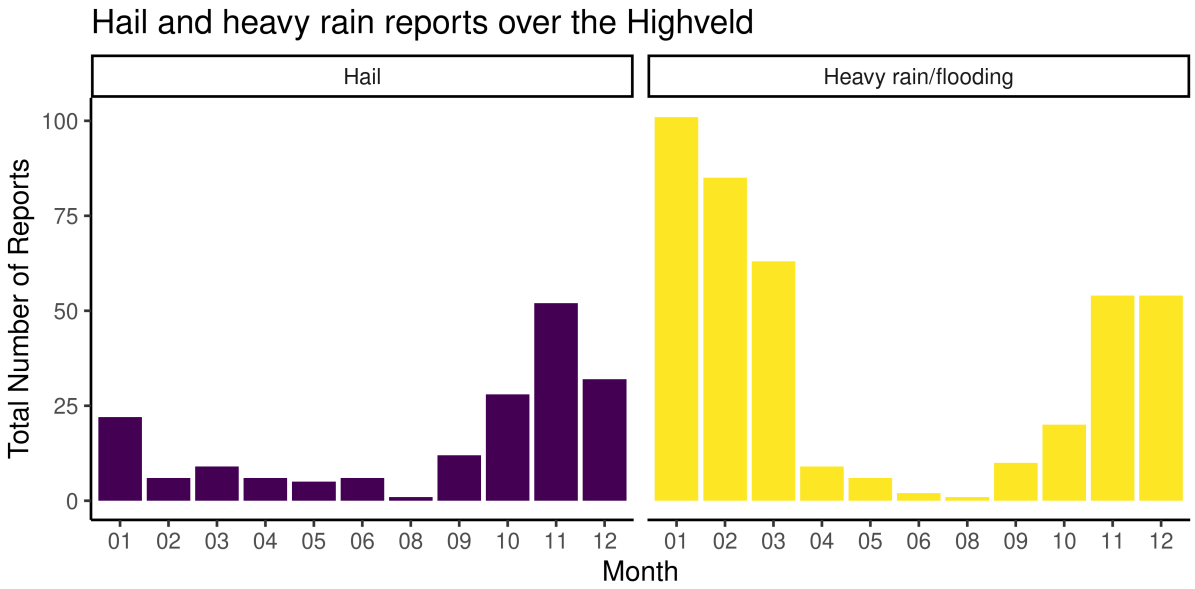

Figure 4.7: *Relative to the total number of reports for hail and heavy rainfall/flooding, respectively, it can be seen that hail is predominantly an early summer (November - December) threat. While heavy rainfall can occur throughout the year, it is more noticeable during mid-summer (January to March).*

Over the last four decades (from 1980), the number of weather reports have been fairly consistent. Figure 4.8 shows that on average the number of hail reports have remained fairly consis-

tent, with the Highveld experiencing between 25 to 50 significant hail events per decade, while rainfall reports have increased from 50 in 1980 to over 100 in the 2010's. More significantly, Figure 4.9 shows that while hail reports have remained fairly constant, with a couple of significant years in 1995, 1996 (De Coning et al., 1998) and 2016 (Simpson and Dyson, 2018), there is a pronounced increase in the number of rainfall events in the region. In the later sections the trend of the atmosphere above the Highveld becoming tropical in nautre and favoring rainfall, is examined, and this is supports the results seen here.

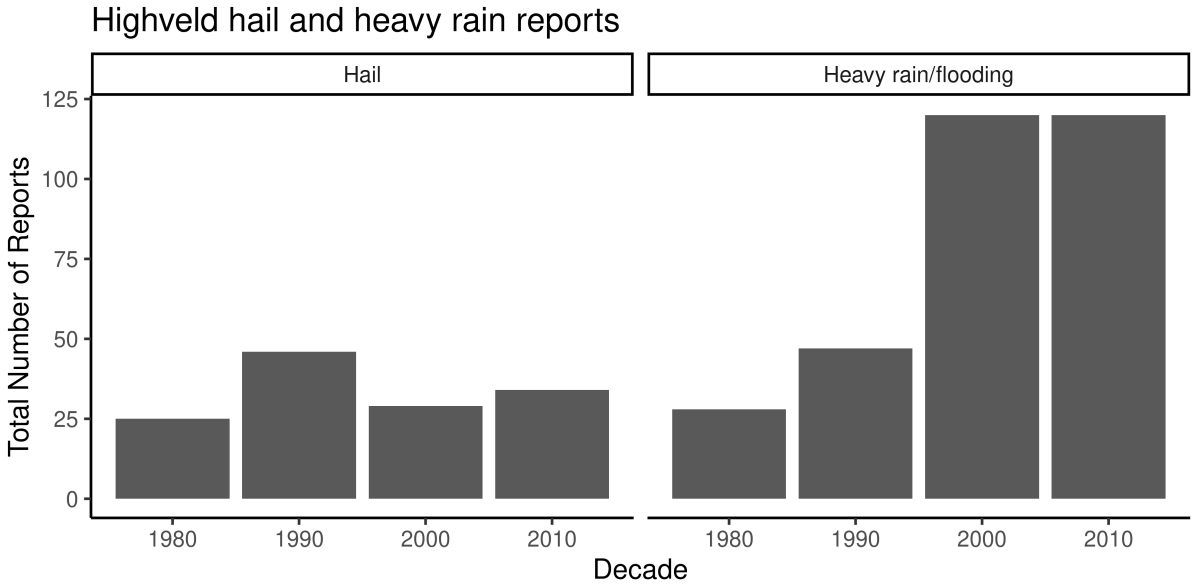

Figure 4.8: *Number of hail and rainfall reports per decade shows that the number of hail events have remained fairly consistent, however, there is a major increase in rainfall events over the region.*

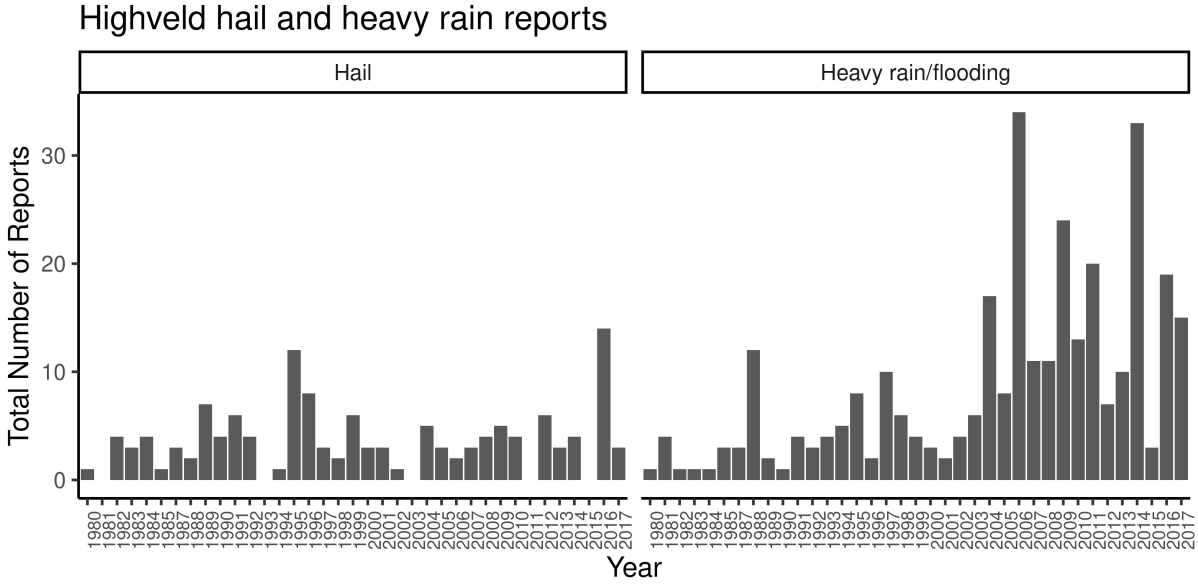

Figure 4.9: *Number of hail and rainfall reports per year indicate that rainfall have been a major impact on the region, and is increasing in frequency. Hail events have remained fairly consistent, even with the rise of digital media.*

Conclusion

Weather reports provide valuable insight into the effects, economical, and societal, that weather can cause to a community. The reports not only highlight the losses, but by analysing these events in detail there emerges a clear pattern of the spatio-temporal impacts of different events in a region. Along with understanding the dynamical environments these events occur in, understanding the typical damage caused can help stakeholders to better prepare for the risks associated with different events, during different months.

This section focussed specifically on significant convective weather events over the Highveld, and in this analysis the results show that heavy rainfall and flooding, on average, caused more severe damage over the Highveld than any other event in all months. Hail events in SA have been some of the costliest and deadliest for the people of the region, and these hail events occur most often in November. However, convective storms during all months can lead to the loss of lives and livelihoods. The environments these events occur in, and improving our understanding of it on different scales, can assist us to improve forecasts, reduce exposure and improve planning for future mitigation. The impact of significant events could be even more pronounced as the results show that the atmosphere over the Highveld is increasingly favouring convective conditions as discussed later in chapter 7. And in this section, it is interesting to see that over the last four decades the number of hail reports have remained fairly consistent, while heavy rainfall reports have increased substantially, supporting the trend of an environment favoring heavy rainfall over the region while extra-tropical forcing become less prominent.

In the first chapter the thesis examined the nature of convective events over the Highveld. The study found that convective storms occur frequently in all NDJFM months, however, during November there is a large number of significant events associated with hail, and this is supported by the findings in this section that showed that hail is the most significant event in November. The previous section also showed that January has the highest frequency of convective events, but these events are slower, and have less severe mean characteristics. Similarly, the media reports show that heavy rainfall and flooding is most common in January, indicating that rainfall, possibly from isolated thundershowers, is the dominant convective event during this time. The next chapter examines the specific synoptic and thermodynamic environment that the categories of convective events occurred in. By understanding the interaction between the large scale circulation, local scale thermodynamics, and the resulting surface weather, our understanding of riks and exposure under future conditions can be improved.

Chapter 5
The synoptic and thermodynamic environment of significant convective weather events

By building on the previous chapter where reported events were characterised, this chapter examines these events in more detail, and defines them as *significant convective* events throughout the rest of the chapter. This chapter examines the synoptic environments of significant convective events documented from 1979 to 2017 using new generation ERA5 reanalysis and IGRA data. The IGRA radiosonde dataset (1979-2017) is subsequently used to better understand the thermodynamic characteristics associated with the significant events over the region.

Introduction

Understanding convective weather has been an important theme in South-African research. Blamey et al. (2016); Dyson (2015); Mason and Jury (1997); Schulze (1965); Taljaard (1981), has detailed this through various research methodologies, from building radiosonde climatologies to using new generation reanalysis data to examine environments favouring convection. These studies, and many more, have, over time, allowed us to form a reasonably complete picture of the South African storm landscape on a large scale. Nevertheless, on any scale, uncertainties come into play. Here is a brief overview of some problems that have to be accounted for when using a specific instrument. Radiosonde climatologies, as detailed by Dyson (2015), is limited by the number of weather balloons released daily. Blamey et al. (2016)'s climatology using reanalysis data provides a accurate view of the general storm environment. However, the products fail to characterise individual cumulus cells accurately, which could easily initiate, precipitate and decompose without being captured in an RCM scale run. Weather station data as assimilated by Schulze (1965) also suffers from a spatial limitation, and an isolated thunderstorm can easily be missed by a single station in a large area with few observational platforms. Using radar, radiosonde and reanalysis data, the thesis builds an accurate overview of the spatio-temporal characteristics of convective weather over the Highveld area for the months when most severe convective events occur in NDJFM. A theoretical representation of this integration and the benefit is seen in Figure 5.1. Here we can see how the limitations of individual observational platforms can be addressed using an integrated approach, as done in this chapter, to better understand conditions conducive to convective storm formation. These individual climatologies might seem trivial, but no study in South-Africa has integrated these sources to build an integrated convective event climatology.

Severe storm environments

The following results builds on the reports of convective events and examines the specific synoptic and thermodynamic conditions these reported events occurred in. The synoptic-scale

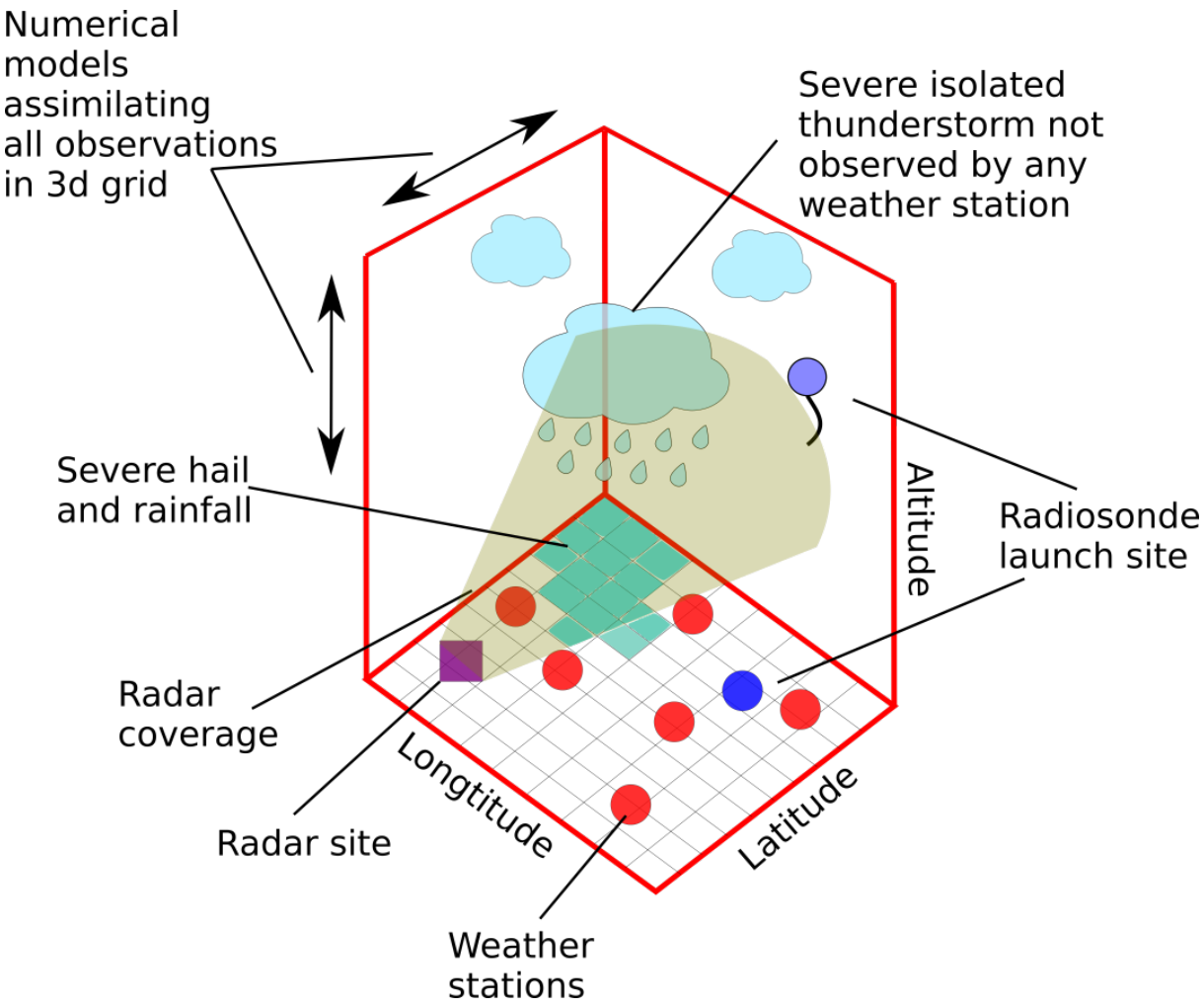

Figure 5.1: *The theoretical representation of various in- and ex-situ measurement methods highlights the importance of using an integrated approach when analyzing convective thunderstorms that are rare in space and time. This Figure shows how randomly spaced weather stations fail to capture a severe thunderstorm over a region. The radar does, however, capture the 3D profile of the atmosphere but fails to capture accurate surface estimations as the measurements a function of reflectivity characterisitcs. The radiosonde provides valuable vertical profile information but is only launched once a day and at a single position. NWP assimilates all this information to provide a simulated picture of the atmosphere, which is helpful for understanding events' physical and dynamical evolution, but is also limited by parameterisation assumptions and computing limitations.*

analysis makes use of the new generation ERA5 reanalysis data. The synoptic-scale allows us to examine the general conditions these events occurred in. This includes large-scale circulation systems, such as tropical temperate trough (TTT) or ridging anti-cyclones, and the differential pressure between various model levels, typically the surface and 500 hPa. ERA5 data also includes various fields such as CAPE and CIN, which provide an opportunity to examine severe storm environments in greater detail, on a large scale Hersbach et al. (2018); Li et al. (2020); Taszarek, Allen, Púčik, Hoogewind and Brooks (2020); Taszarek, Kendzierski and Pilguj (2020).

The thermodynamic scale is much smaller than the above synoptic-scale and valid for a small area. To understand the thermodynamic state of the atmosphere, we use radiosonde data. Radiosondes record variables such as pressure, environmental and dew point temperature, hu-

midity, wind speed and direction. In South Africa, Dyson (2015) completed an analysis of soundings related to heavy precipitation events, and building on this, Blamey et al. (2016) used simulated soundings to better understand severe weather environments across SA. We build on this by examining soundings for media reported severe events.

Synoptic environments favouring significant events

"it is the waves, stupid"
Harry von Loon during a 2004 interview (Von Storch et al., 2004)

In this section ERA5 reanalysis data is used to examine the synoptic circulation associated with severe weather reports from 1979, the start date for the ERA5 dataset, over the Highveld as defined in Figure 2.1, along with Gauteng. First, we extract reanalysis data for all the dates on which severe and non-severe reports occurred, as listed in Caleum. Following this, the mean synoptic conditions per month/per event is examined. Two important issues arise with this method. First, storm environments can vary drastically, i.e. two *seemingly* identical environments can yield somewhat different storms. Secondly, the scale of convective storms is small, ranging from the upper micro-α to the lower meso-γ range. The resolution of the reanalysis data is 0.25°by 0.25°, which means individual convective events like isolated thunderstorms can be smaller than the model grid size. ERA5 data has shown improvement in capturing small scale features, which in the context of this analysis proves helpful to understand the larger conditions driving these storms. (Li et al., 2020; Mathias et al., 2019; Rodríguez and Bech, 2020; Sisodiya et al., 2019; Taszarek, Allen, Groenemeijer, Edwards, Brooks, Chmielewski and Enno, 2020; Taszarek, Allen, Púčik, Hoogewind and Brooks, 2020; Taszarek, Kendzierski and Pilguj, 2020).

According to Tyson and Preston-Whyte (2000), all heavy rainfall and or severe convective weather requires two basic processes, i.e. low-level convergence and high-level divergence; however, the interaction is slightly more complex than this. In Southern Africa, the daily weather is heavily impacted by Rossby waves and smaller-scale baroclinic instability patterns, the interaction between tropical and mid-latitude disturbances, moisture transport from the tropics and warm Indian oceans, the movement of the ITCZ, and teleconnections such as Southern Oscillation Index (SOI) and El Niño-Southern Oscillation (ENSO). Along with this, smaller-scale effects associated with diurnal heating and cooling, inversions, urban boundary layers and heat islands, topography and aerosols have to be accounted for. In this discussion, we highlight the general NDJFM circulation, associated with each event's synoptic conditions and only highlight the explicit role of that MSLP, 500 hPa and convective instability (i.e. CAPE) in the various months that the selected weather events occur. An analysis of the thermodynamic environment follows this to examine the smaller scale variances associated with severe events.

There are however limitations to using synoptic composite maps. Synoptic composite maps do not represent the full variation of synoptic types that severe events can occur under. To this end the next section addresses this limitation by using an objective clustering method, PCA, to explain the number of possible synoptic patterns giving rise to a particular event.

The composite synoptic maps for hail events (Figure 5.2) indicate the strong extra tropical influence in the upper levels, while a strong pressure gradient at the surface and high CAPE is generally present. Onshore advection of warm moist air from the Indian Ocean through the ridging anti-cyclone, and an tropical low and/or trough, transports lower level moisture to central parts of SA. Mid-latitude westerly waves at 500 hPa in the upper air is prominent throughout all months, particularly during early and late summer. As a result of this, substantial upper-level divergence occurs, while conditional instability is enhanced due to cold air aloft. Shear as a function of differential surface and 500 hPa circulation will also enhance severe storm potential (examined in later sections), the ridging anti-cyclone and tropical low will generally have strong tropical (predominantly easterly) surface winds, while strong westerlies at 500 hPa will enhance rotation and increase storm severity. Localised instability, as a function of CAPE, is prominent during all months when hail events occur. It is interesting that less CAPE is observed when the most extreme hail events are reported (November), while January and February have the highest observed CAPE but low frequency of hail reports. The dry line over the Northern Cape province is also apparent in all hail cases. Although much research has been conducted on dry line and convective initiation in the USA, not much research exists in SA apart from De Coning and Adam (2000), where a dry line was observed during tornado events in SA, and Washington and Howard (2019)'s paper on the structure and characteristics of the dry line feature over Southern Africa. This feature can also possibly enhance thunderstorm occurrence as seen in the Sahelian region (Taylor et al., 2017). If we consider that mid-level moisture associated with tropical circulation remains consistent, with increased surface heating due to drought and desertification, convective initiation along the dry line might occur more frequently. However, more research needs to be conducted in the South African context.

Heavy rainfall (Figure 5.3) events might not be exclusively convective in their dynamics during the summer months. Similar to hail conditions, we see a strong mid-latitude forcing during early and late summer. However, as we saw in the analysis of Caelum, heavy rainfall occurs most frequently in mid-summer months - January and February. During these months, rainfall events are associated with less localised instability (CAPE) and a weaker pressure gradient over the central interior than hail events. Moist air advection is of tropical origin and tropical cyclones with rainfall reaching Gauteng would be included here. Subtropical high-pressure systems over North-Eastern parts of SA aid in transporting moist air from the South-Indian ocean and tropical zones, while subtropical cyclones (see low-pressure over Northern Cape) can aid in large scale rainfall and uplift. East of the tropical continental-low, we could expect surface convergence and upper-level divergence, particularly in early (November) and late summer (March).

The synoptic conditions of severe thunderstorm events (Figure 5.4) also indicate strong upper-level meridional flow and divergence at 500 hPa during the early summer months (November - December. Thunderstorm conditions are not impacted by strong upper-level divergence during mid-summer, as seen in January and February. However, it seems like localised instability is a more prominent driver of thunderstorm formation during this time. We will examine the local scale conditions later to derive the general wind speed at various levels for different months of the year. Apparent in all months is the ridging anti-cyclone over the eastern escarpment resulting in the advection of moist air from the eastern escarpment, aided by the tropical advection,

also apparent during mid-summer months.

The average synoptic conditions observed during severe lightning reports (Figure 5.5) are similar to hail conditions. We expect this as lightning processes are enhanced by the presence of ice particles in clouds. At 500 hPa, westerly waves are observed over the subcontinent, most notably during November and December, enhancing conditional instability. The 500 hPa isobars are south of the central interior during January and February, possibly decreasing shear during these months. Localised, convective instability, as indicated by the high CAPE, is the primary driver of storms at this time. Surface circulation indicates tropical moist air advection from tropical disturbances. TTT features become visible later in summer when mid-latitude disturbances become apparent south of the subcontinent, linking with the tropical low.

The synoptic circulation and localised instability associated with tornado (Figure 5.6) events are relatively unique compared to the other event categories. First, we see strong upper-level flow at 500 hPa in all cases, while surface flow shows a strong pressure gradient (i.e. strong surface winds) and tropical moist air advection in early summer. The well-pronounced surface pressure gradient and strong upper-level westerly flow enhance the rotational components associated with rotating supercells and smaller, deadly mesocyclone features, i.e. tornadoes. Localised instability is well-defined with CAPE $\geq$ 2000 J/kg over some parts of the country on days when tornadoes were observed. It should be noted that the February tornado here was on 18 February 2008 over Cradock (News24, 2008); although the region is far from Gauteng, it borders on the furthest reaches of the Eastern Cape Highveld (Figure 2.1). It was, however, excluded from the thermodynamic analysis later, which centred around Gauteng. Tornadoes from these circulation types around KwaZulu-Natal and Eastern Cape are common. The ridging anticyclone creates a strong pressure gradient at the surface. The strong localised instability and topography around the escarpment enhances lift, and strong westerly flow at 500 hPa aids in strong wind shear and rotation. It is worth investigating the dry line impact on convective initiation and tornado genesis over the central areas of SA (De Coning and Adam, 2000).

The synoptic analysis reveals several key characteristics associated with convective storms in NDJFM months. Most of these have been well documented but is worth mentioning again here. First, early summer convection is coupled with strong upper-level westerly flow in all cases, as represented by the 500 hPa levels in all maps. Strong upper-level westerly flow enhances conditional instability, cold air advection, and in the case of hail, ice formation. We can also see in severe tornado cases that these upper-level winds enhance the rotational component of these storms. As summer progresses, these upper-level westerlies are less pronounced, and local-scale effects start to dominate, especially in during heavy rainfall and thunderstorms. During this time, locally isolated thunderstorms, driven by convective instability, will be more apparent over central SA (this is also realised when we examine storm movement in the thermodynamic and radar analysis). Here surface heating will play a dominant role in the initiation of convection. During hail and tornado events, upper-level winds and strong localised instability (high CAPE) is apparent at all times. It is expected that a similar analysis with cloud band structures will reveal TTT, when coupled meridional flow and tropical circulation forms large cloud bands over SA, as a dominant feature during severe rainfall and other events. An important feature of this is the presence of heat lows over Namibia and the Northern Cape, where the dry line

(Washington and Howard, 2019) feature could enhance convective initiation, as is especially apparent in early summer hail and tornado events (De Coning and Adam, 2000).

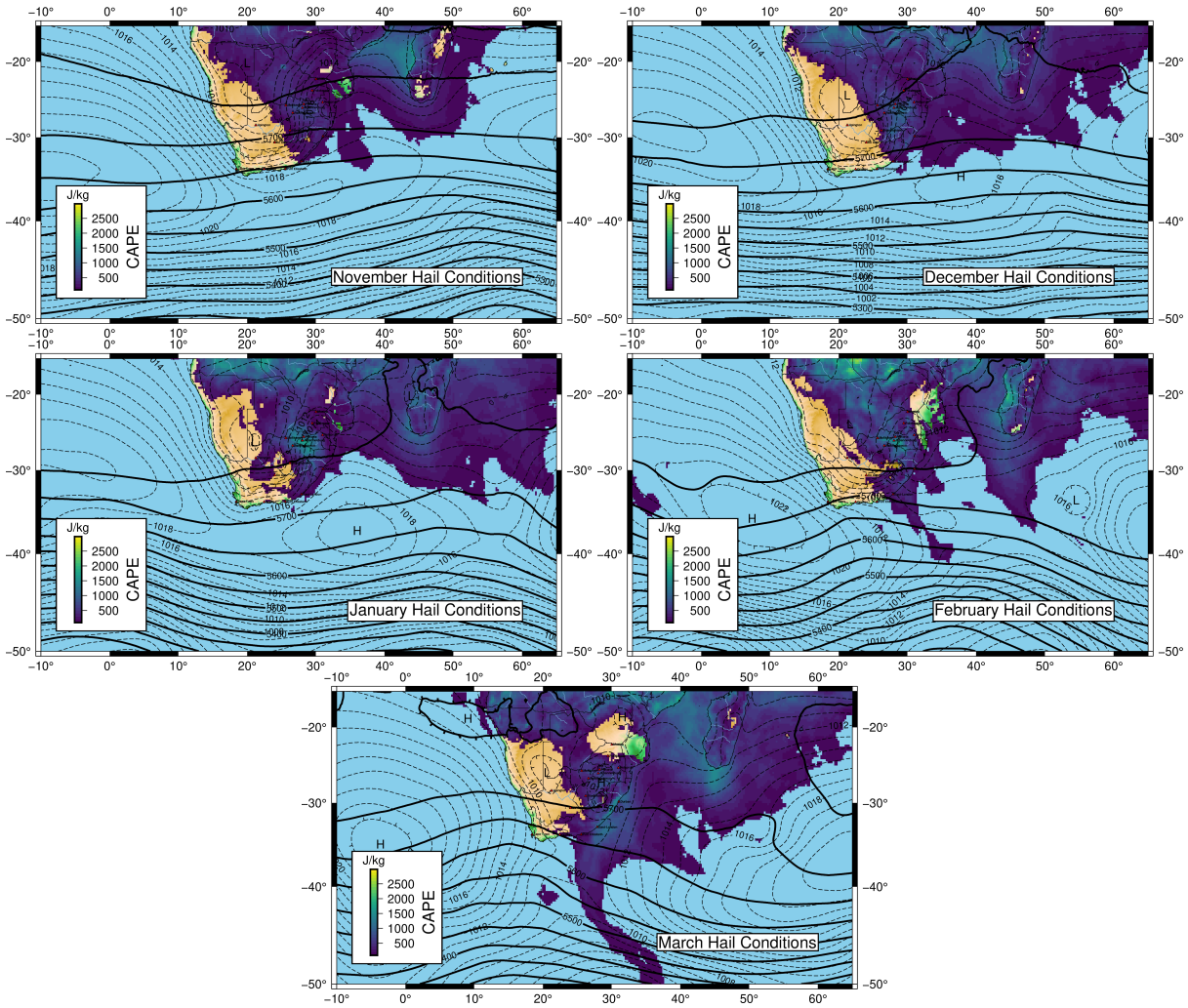

Figure 5.2: *ERA5 synoptic conditions associated with severe hail reports show several critical characteristics associated with hail events. First, during early summer, we see the westerly wave prominent at 500 hPa driving conditional instability, second warm air advection at the surface is driven by the ridging anticyclone over the eastern escarpment, and tropical continental waves, finally CAPE indicates localised instability possibly aided by the intense pressure gradient over the interior of SA.*

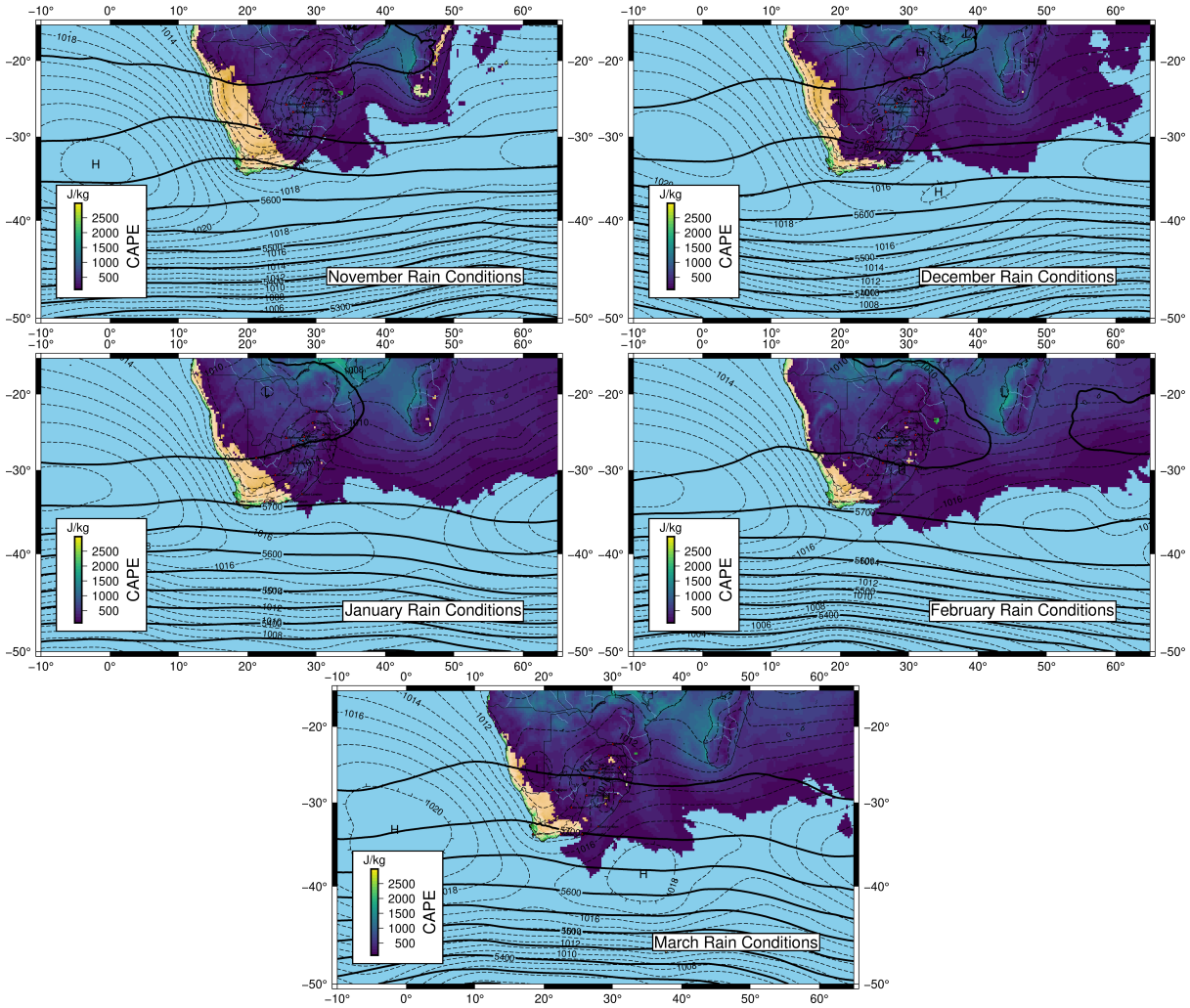

Figure 5.3: *ERA5 synoptic conditions associated with severe rain reports indicate an environment where instability is less pronounced than other convective events. CAPE indicates widespread unstable conditions, and as expected, the strong pressure gradient seen in other convective categories is less apparent. Moist air advection is mainly tropical, and 500 hPa indicates less upper-air divergence during mid-summer when most severe rainfall events occur. However, we see subtropical cyclones over central SA during mid-summer as well.*

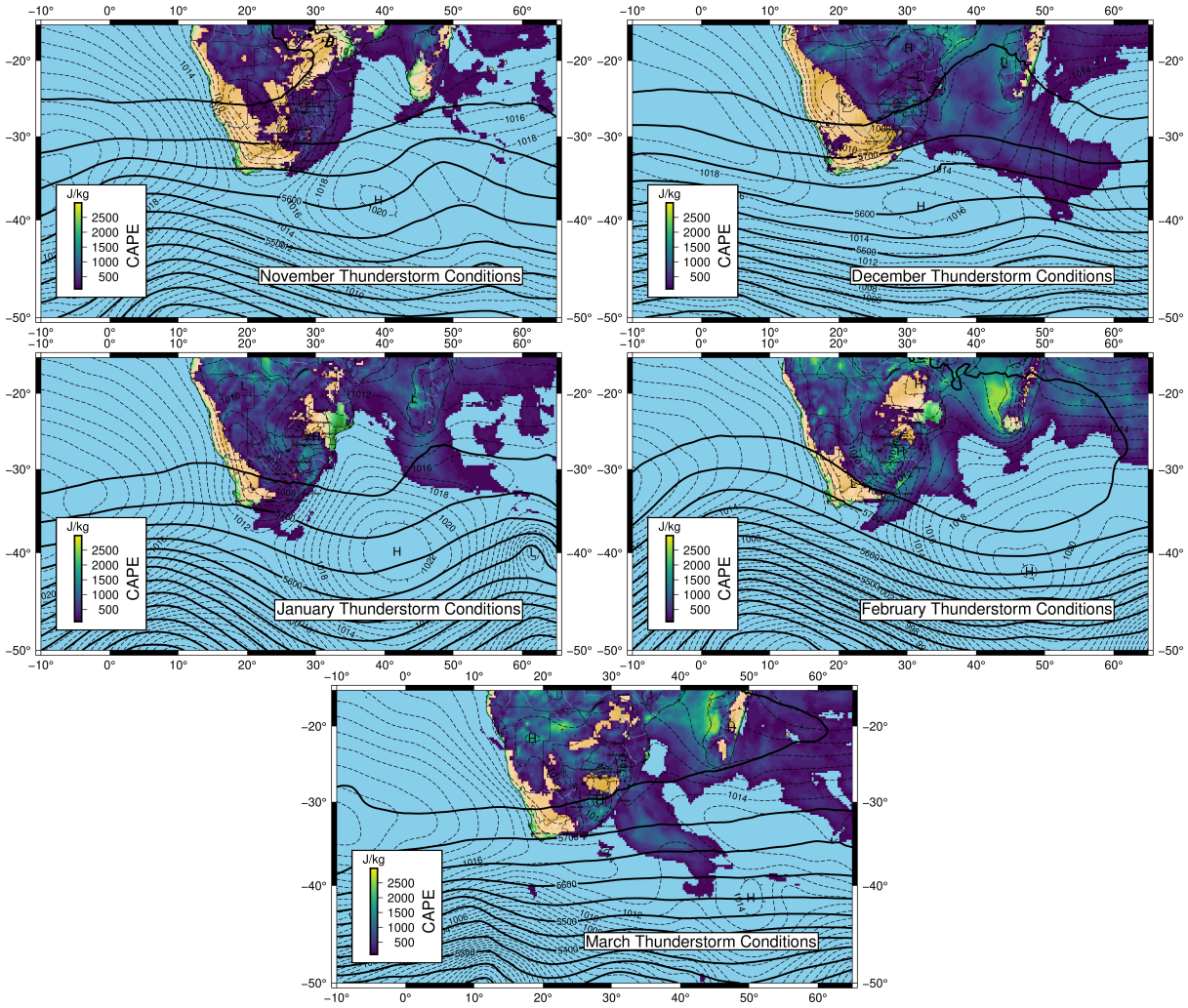

Figure 5.4: *ERA5 synoptic conditions associated with severe thunderstorm reports show upper-level divergence is a prominent feature during early summer events. However, these upper-level winds are marginal during mid-summer, and localised instability drives these events over central SA. A ridging anticyclone and tropical through results in warm moist air advection from the east, and CAPE indicates localised instability plays a vital role in thunderstorms during all months.*

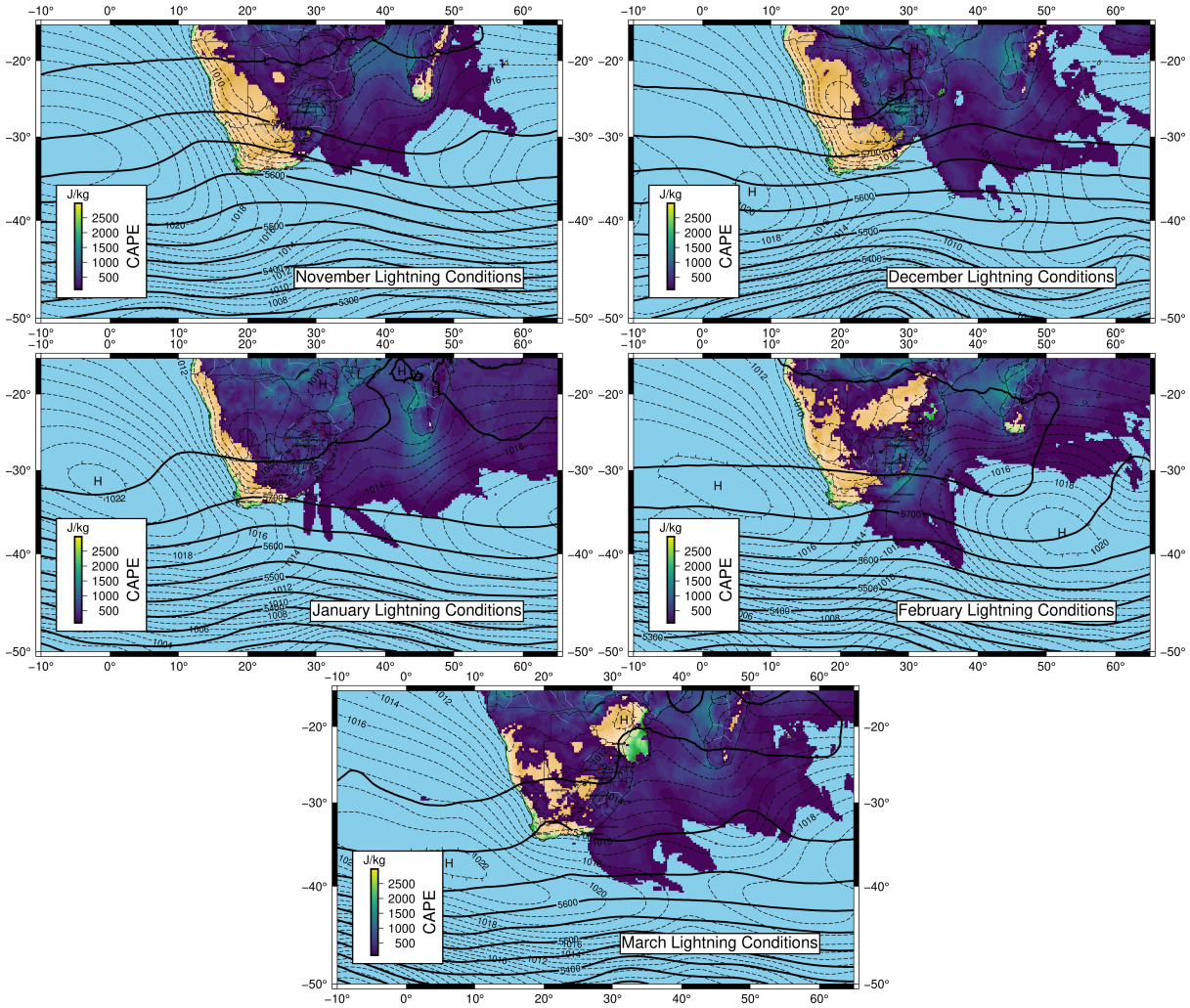

Figure 5.5: *ERA5 synoptic conditions associated with severe lightning reports indicate strong westerly flow at 500 hPa during early summer months and to a lesser degree during later months. High CAPE indicates localised instability is prominent during early summer, however, less so during mid and late summer. January conditions of severe lightning are associated with widespread instability, possibly TTT circulation. Late summer (March) conditions do not show as severe an environment as other months, but isolated instances of lightning might result in fatalities during this time*

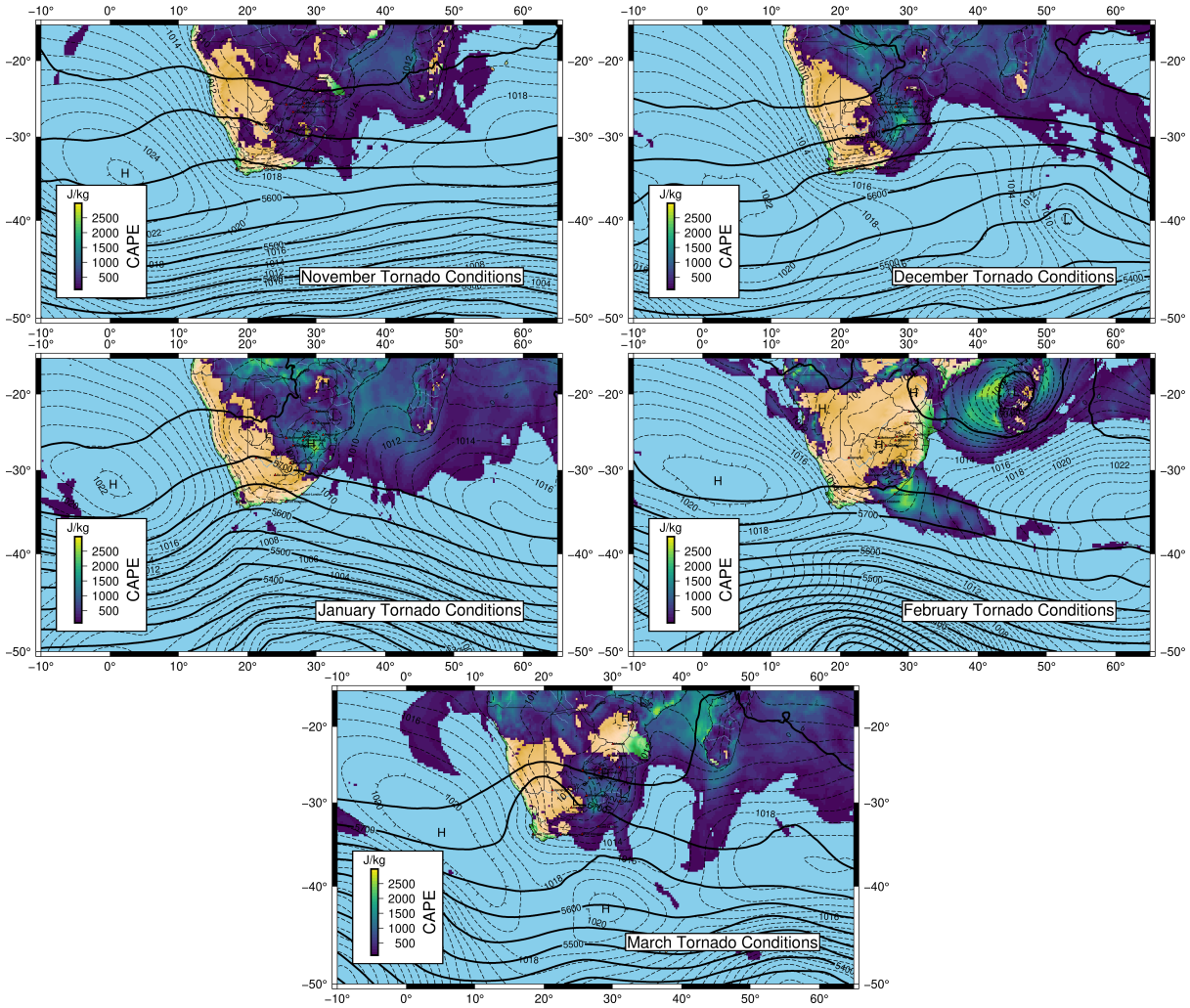

Figure 5.6: *ERA5 synoptic conditions associated with severe tornado reports show strong westerly flow at 500 hPa during all months. A strong surface pressure gradient and localised instability indicate ideal conditions for rotation updrafts and tornado formation. Moist air advection is primarily tropical in origin, and a ridging high-pressure system is also observed in February when a tornado occurred. During November, the ridging high-pressure system resulted in a single tornado observed over Cradock in the Eastern Cape and was included here as the town is in the far south portion of the Highveld.*

Objective clustering of synoptic patterns associated with significant events

The previous section examined the mean conditions under which significant convective events occurred in, known as synoptic compositing. Due to the small-scale nature of convective events, synoptic compositing will not capture the individual synoptic patterns that these events can occur under. To address this, a better method of identifying synoptic patterns associated with the respective convective events is used, i.e. objective clustering. The following section makes use of a PCA to derive synoptic patterns associated with significant events. MSLP and geopotential at 500 is used in this section to drive the analysis. Several severe storm indicators such as CAPE could be included, however, due to the local scale nature of such a variable it could result in unrealistic clusters on the synoptic scale. Wolski et al. (2018) also found that CAPE was not a good predictor of heavy rainfall events in their SOM based analysis. In Figure 5.8 to 5.12, the results of the PCA analysis is shown. In all cases only synoptic types that represent 80% of the variance is shown and discussed for each case respectively. The appendix contains the geopotential at 500 and mslp maps to support the analysis below.

In the first PCA all the significant events are combined. The events are combined because in many cases these events do not occur in isolation of each other and the distinction between the events in media reports was subjective. In Figure 5.7, 16 synoptic types explain 80% of the synoptic types that can lead to significant weather over the Highveld region. This section will just discuss the main features of all the synoptic types as the analysis hereafter examines specific synoptic conditions associated with the specific convective event. In all cases the westerly wave at 500 hPa is visible over the subcontinent. The westerly wave, as discussed previously, is an important system in sustained supercell development. This is especially evident during early summer when the westerly waves have not yet been displaced south of SA. The influx of moisture from the ITCZ in the form of TTT or continental tropical low-pressure systems, plays a cardinal role to advect moist air over the region. The ridging high pressure which is typically associated with transition months between winter and summer, and formed by the passing of mid-latitude cyclones, is an important system in November for hail formation. As discussed by Ndarana et al. (2021), two types of ridging anticyclone, are dominant over the region, and heavy rainfall is typicall associated with meridional flow and strong tempreature gradients. Wind shear, and differential advection, between the surface and 500 hPa is important to enhance rotation and storm movement, where the surface isobars and westerlies overlap strong directional shear can be expected. Surface winds can enhance low-level turbulence and convection, and this can be derived from the pressure gradient which, as seen in all clusters, is prominent over the Highveld.

80% of significant hail events over the Highveld is explained by 13 clusters as seen in as seen in Figure 5.8. The most frequent weather type across associated with hail is the synoptic pattern seen in cluster 1. Under these conditions strong zonal flow is observed at 500 hPa over the Highveld, and at the surface tropical flow associated with the ITCZ is visible. The cluster that is most prominent in November, when the most severe hail events are observed, is cluster 3, 7 and 8, with cluster 8 occurring most frequently during November. Cluster 4 occurs exclusively

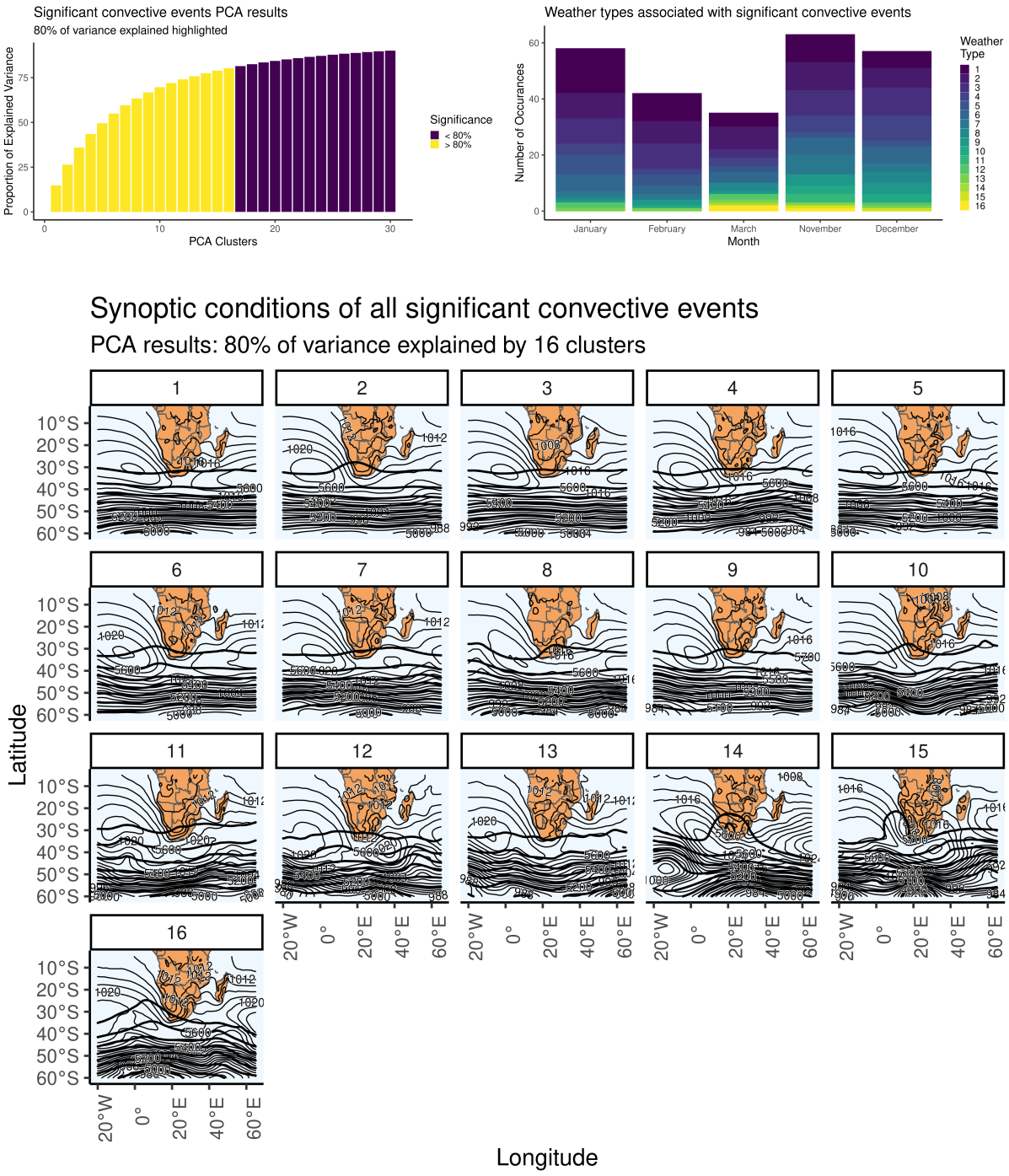

Figure 5.7: *16 Synoptic types (or clusters) explain 80% of significant convective events over the Highveld. Several important features stand out, i.e. a westerly wave present over the subcontinent, TTT or continental tropical low that enhances moisture advection from the ITCZ, and strong pressure gradients at the surface. The combination of these variables; heat, differential winds between the surface and 500 hPa, conditional instability and adequate moisture, means the environment is ideal for convective storm development during the SA summer.*

in November. All of the above mentioned clusters have a prominent ridging anticyclone at the surface with strong zonal flow at 500 hPa. The most expensive hailstorm to date that occurred on 28 November 2013, and caused over ZAR 1 billion in damages is associated with cluster 2.

Here the ridging anticyclone extends far over the eastern seaboard, while there is a pronounced disturbance in the upper air above the Highveld which would have enhanced rotation and potential instability. Also associated with this cluster is an hail event on 15 December 1994 which killed 5 people, and injured 70 people over Johannesburg, and a hail event that resulted in the loss of over 350 livestock in the eastern Highveld. December hail events primarily fall under cluster 8, with equal percentage of variance explained by cluster 1, 2, 7, 9 and 13 repetitively. In the case of cluster 1 and 9, the ridging anticyclone is absent over the eastern seaboard, but there is strong tropical flow from the ITCZ. Cluster 2 and 7 both have a strong ridging anticyclone. Cluster 13 is the only weather type that is only associated with December, and does not occur during other months. In cluster 13 the south-Indian high ridges over the east coast, with strong tropical continental low present over north-western SA along the dry line. At 500 hPa the westerlies are south of SA, and this circulation type would typically be associated with long lived and slow moving supercells. Cluster 10 and cluster 2 explain most of the variance for hail events in January, in cluster 10 the ridging anticyclone is located due south of the country, and at 500 hPa there is little influence on storm development by the westerlies. This circulation is expected when the ITCZ moves south and results the westerly waves displacement. These storm would be slow moving and isolated over the Highveld. February and March is dominated by cluster 1 where zonal flow are observed at 500 hPa over the Highveld, and the TTT over the central interior would bring an influx of moisture. The impact of the ridging anticyclone is not significant during this time according to the PCA.

80% of significant rainfall events fall into 16 clusters. The high number of clusters is evident due to the nature of rainfall being associated with more than one type of weather system, and typically all convective events have rainfall occurring. In Figure 5.9, it is immediately clear that rainfall occurs under significantly different synoptic conditions when compared to hail events in Figure 5.8. In all cases, except cluster 12 (a cut off low system), the westerlies at 500 hPa are south of the Highveld. The cluster that is most frequently associated with heavy rainfall across all months is cluster 7, this cluster is characteristic of a TTT, which is a major rain-bearing system in SA. Significant rainfall events in November is explained by cluster 3 and 4. Cluster 3 has shows a weak ridging high over the eastern sea board, but there is indications of localised low-pressure system over the Highveld with some influx of moisture from the tropical through. Cluster 4 shows a disturbance at 500 hPa that would enhance conditional instability (common during November), and also a well defined tropical low for influx of moisture at the surface. In December, cluster 7, followed by cluster 4, 6 and 8, is the most prominent during significant rainfall. As indicated, cluster 7 can be associated with a TTT. Cluster 4 and 6 show a similar tropical low over the surface which could also be associated with TTT patterns during this time. Cluster 8 is associated with ridging anticyclone. Cluster 1, 2 and 3 explain most of the rainfall observed in January. In cluster 1 there is a visible disturbance in at 500 hPa over SA, while cluster 2 and 3 have strong zonal flow at 500 hPa. In all three clusters, the influx of moisture is mostly tropical in origin. Cluster 16 occurs exclusively in January and here a continental tropical low over the Highveld is visible, while the westerlies are well south of the region. In February and March cluster 7 is again the main rain-bearing system over the region.

The next two convective synoptic types, thunderstorms and lightning, typically do not occur

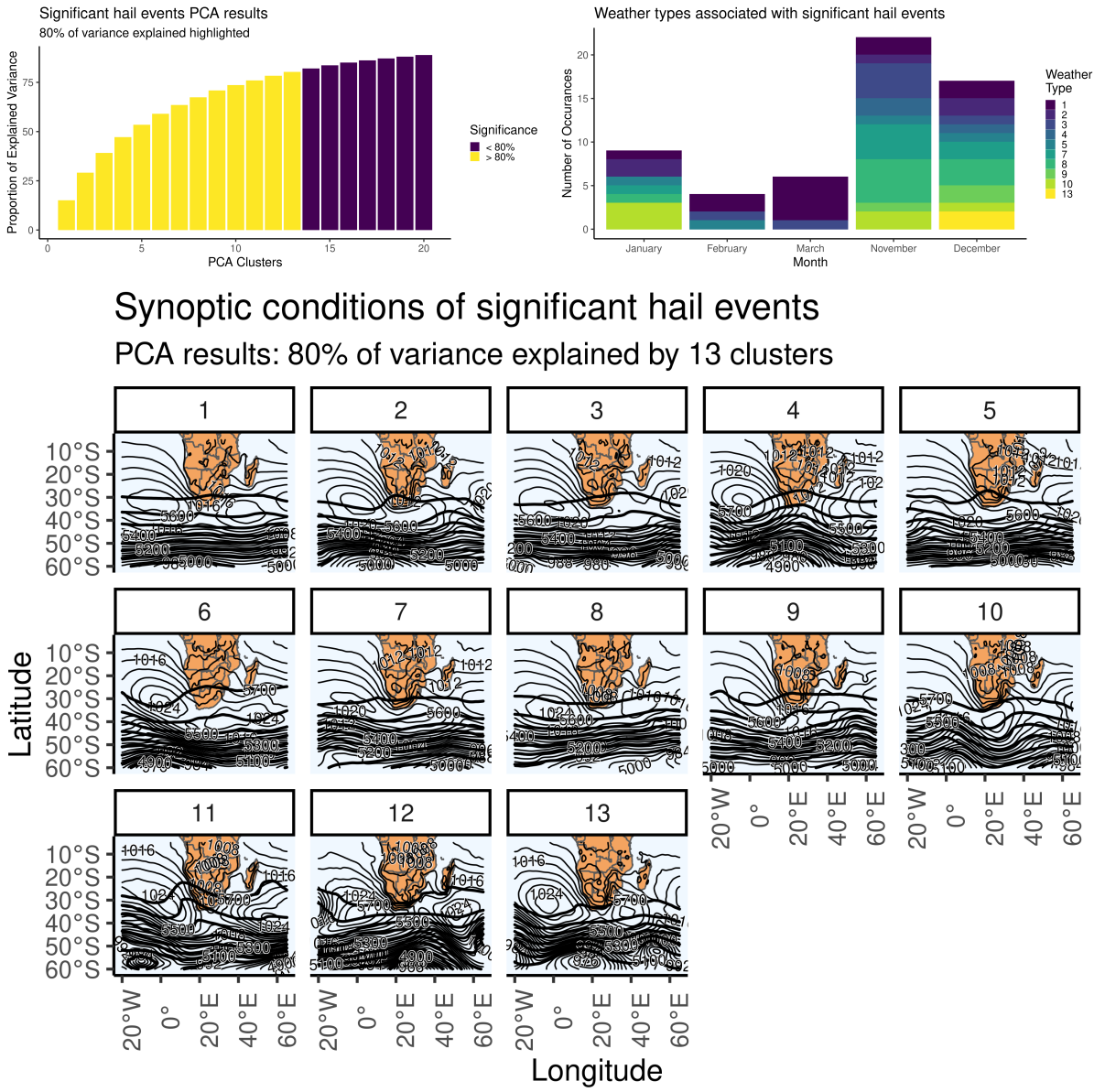

Figure 5.8: *13 Synoptic types (or clusters) explain 80% of significant hail events over the Highveld. Clusters that explain most of the significant hail is associated with westerly wave over SA at 500 hPa and ridging anticyclone.*

in isolation, but was separated here based on the reported cases. 80% of thunderstorm cases is explained by 8 clusters as seen in Figure 5.10. Cluster 1 occurs in mid-summer (January to February), while cluster 3, 4, and 5 only occurs in early summer (November, and December). In November, cluster 2, 3, 4 and 5 can result in significant rainfall. In cluster 2 - 4 the westerly wave at 500 hPa is well defined over the central interior, and a strong pressure gradient is visible. Along the pressure gradient storm initiation will occur, and this could be associated with "thunderstorms" instead of heavy rainfall and hailstorms, as storms will still be in the initial stages of development. Only cluster 5 is associated with a ridging anticyclone, similar to that seen in hail clusters. December thunderstorm occurrence is explained by cluster 3, 4, 5 and 7. Cluster 3 - 5 have been discussed. Cluster 7 shows a well defined TTT over the western interior, and this could also be associated with a weak TTT. Three Clusters explain most of the occur-

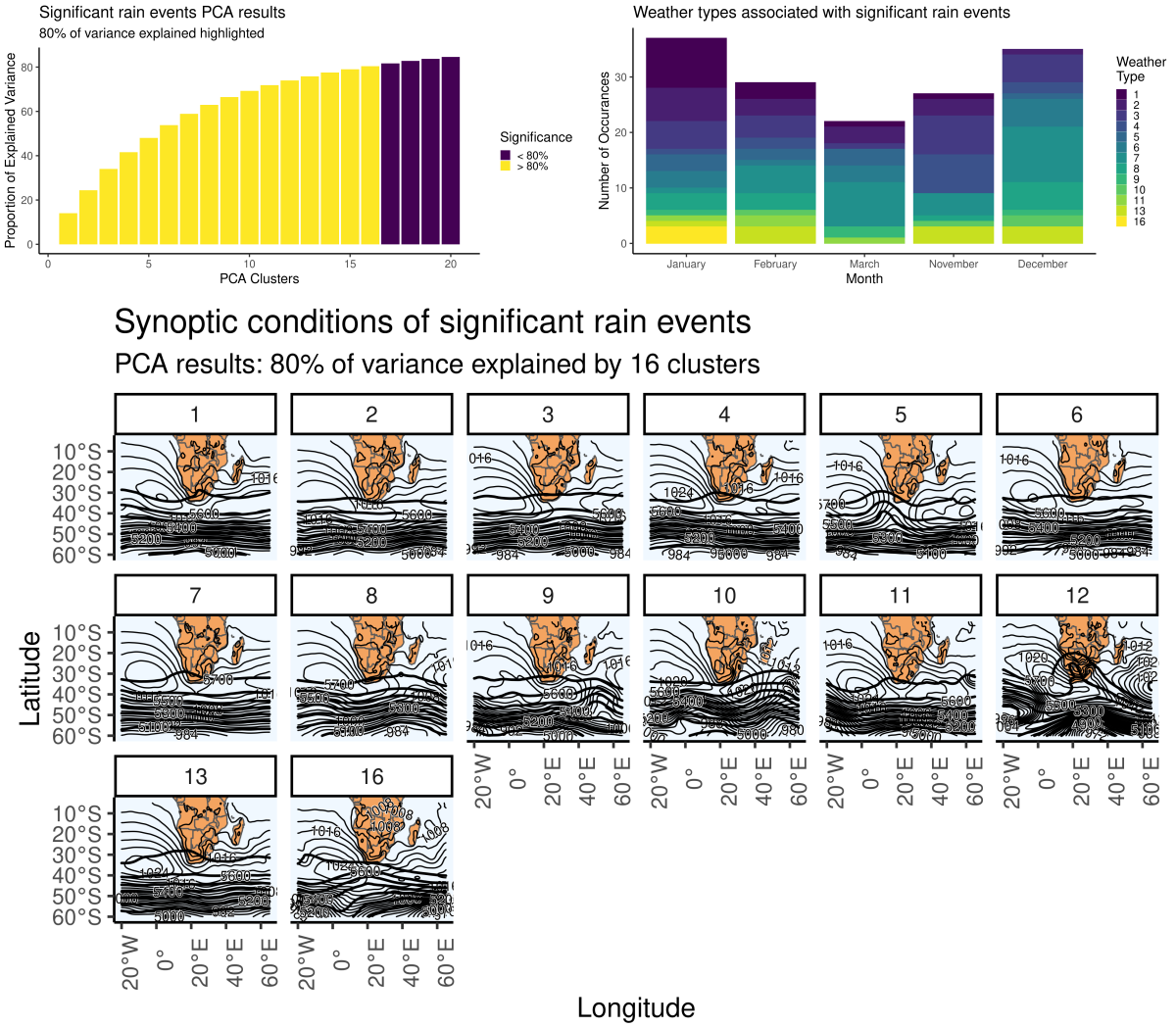

Figure 5.9: *13 Synoptic types (or clusters) explain 80% of significant rain events over the Highveld. In most cases cluster 7, possibly associated with a TTT, explains most of the variance in rainfall for the Highveld.*

rence of thunderstorms during January. That is cluster 1, 2 and 8 (cluster 8 occurs exclusively in January). Cluster 1 shows characteristics of a west coast trough, but this could also enhance TTT over the region, as a clear mid-latitude cyclone is also visible during this time. To the east in cluster 1, there is ridging high from the south Indian ocean which would also enhance surface moisture and a strong pressure gradient is visible on the surface. Cluster 2 similarly shows a well defined tropical low, with a strong pressure gradient over the Highveld, along which storms could initiate. Cluster 8 is a important rain-bearing system for SA, and at 500 hPa a cut off low can be seen, with a TTT extending across SA. March is associated with cluster 1 and 6. Cluster 6 has a weak ridging anticyclone that follows the passing mid-latitude cyclone due south. At 500 hPa, the westerlies are still due south of the continent, indicating an environment favouring convective, tropical storms.

Lightning events do not occur in isolation from thunderstorm, hail or heavy rainfall events, but due to their significance these events are examined explicitly. 80% of lightning events occur in 11 clusters, as seen in Figure 5.11. The most prominent cluster during all months is cluster

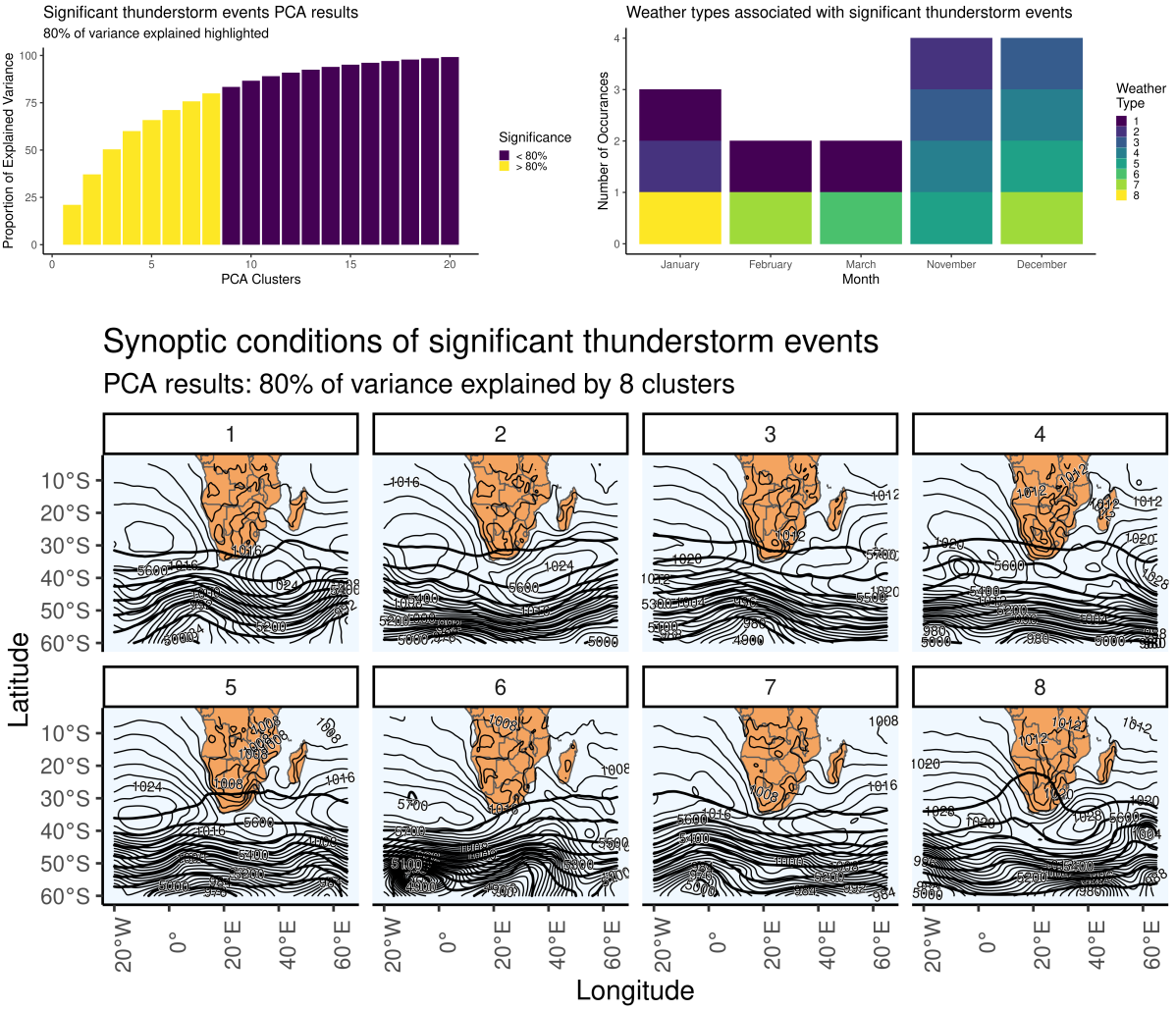

Figure 5.10: *8 Synoptic types (or clusters) explain 80% of significant thunderstorm events over the Highveld. Conditions under which thunderstorms develop are varied, but in most cases a strong surface pressure gradient is visible over central SA, along with an influx of moisture associated with the TTT.*

1. Cluster 1 shows a disturbance over the central interior at 500 hPa, which is ideal for storm development, at the surface there is fairly insignificant ridging high along the east coast. This ridging high would enhance convective storm development along the escarpment, but it does not seem to rise above this topographical feature. A well defined TTT over the interior will result in moisture at the surface. A localised low over central South-Africa is also visible, which could indicate strong local scale instability in this cluster. During November, cluster 1 (as discussed above) and cluster 3 explains most lightning events. Cluster 3 shows a disturbance in at 500 hPa, and the westerlies is located above the subcontinent, and this would enhance conditional instability. A strong pressure gradient is visible along the region of interest, and along this pressure gradient storm development will be favoured. In cluster 6, the position of the high-pressure system below SA is unique compared to the other clusters and is associated with the passing mid-latitude cyclone. The position of the westerly at 500 hPa is also typical of other November storms observed in the previous clusters. December lightning events are explained by cluster 4 and cluster 11 (cluster 11 occurs exclusively in December). There is strong meridional flow at

500 hPa in cluster 4 and the influx of moisture along the Highveld is almost exclusively from the tropical systems. The deep penetration of the westerly wave during in this cluster will enhance conditional instability, wind shear and storm development. Cluster 11 shows a deep tropical low at the surface and a weak ridging anticyclone. One would expect storm development mainly along the eastern seaboard, but the synoptic maps show a well defined localised low over the Highveld which could lead to localised storm development. A TTT could also develop over the region along the deep trough. Lightning events during January can be explained by three clusters, that is cluster 1 (already discussed), 2 and 3. Cluster 2 does not have the same characteristic tropical low as seen in other clusters, but instead the data indicates localised low pressure systems over the Highveld, and strong zonal flow at 500 hPa. Cluster 3 is associated with a well defined tropical low and strong pressure gradient over the Highveld. Along the pressure gradient storm development would be favoured. In cluster 3, the westerlies at 500 hPa are deep enough over SA to enhance instability and favour thunderstorm development associated with hail and lightning. Cluster 1 and 2, which was already been discussed, is most associated with February lightning events. Most march storms occur in cluster 1 and cluster 10. Cluster 10 is associated with a deep continental tropical low, and ridging anticyclone. The pressure gradient lines indicate that storm development will mostly be favoured along the south-western Highveld.

Tornado events are a rare occurrence over SA, nevertheless these events do result in considerable impact over the Highveld region. According to the PCA results, as seen in Figure 5.12, 9 clusters are dominant when tornado are present. In 5 clusters (1, 6, 7, 8 and 9), there is a pronounced disturbance at 500 hPa over the subcontinent. The disturbance of the westerlies at this level, will enhance conditional instability. Strong zonal flow will enhance shear and rotation from the surface to the upper levels. Cluster 4 is the most dominant cluster across all months. In cluster 4 the flow across the Highveld at 500 hPa is fairly zonal, and at the surface there is a weak ridging anticyclone, but well defined continental tropical low-pressure over Botswana. Along the tropical low and the ridging high, there is a strong pressure gradient. This pressure gradient will enhance surface convergence, and favour storm formation along this region. November tornado conditions are dominated by cluster 4, followed by cluster 3. Both clusters are typical of November storm events, with a tropical low at the surface, strong westerly flow at 500 hPa over the Highveld. Cluster 3 also has a weak ridging high, which is commonly observed during this month in other convective events. December events are observed under three clusters, i.e. 4, 5 and 6. Cluster 4 was already discussed above, in cluster 5 the localised low over the Highveld would enhance local instability, there is also strong flow at 500 hPa on the south edge of the Highveld, along with a strong pressure gradient at the surface where rotation could be enhanced between the surface and 500 hPa. Cluster 6, similarly, has a localised low over central SA, and the north-eastern part of Lesotho. However, the upper level low-pressure system in cluster 6, at 500 hPa, can increase moisture and rainfall in the western Highveld by favouring large scale uplift. The pressure gradient observed along the western Highveld would be the most likely area of tornado development where there is a strong surface pressure gradient, and westerly flow at 500 hPa. January tornado conditions are observed in three clusters, i.e. 1, 2 and 6. In all three cases there is a strong pressure gradient situated over the western part of SA, and also along the central Highveld. The tropical low is apparent in cluster 1, at the sur-

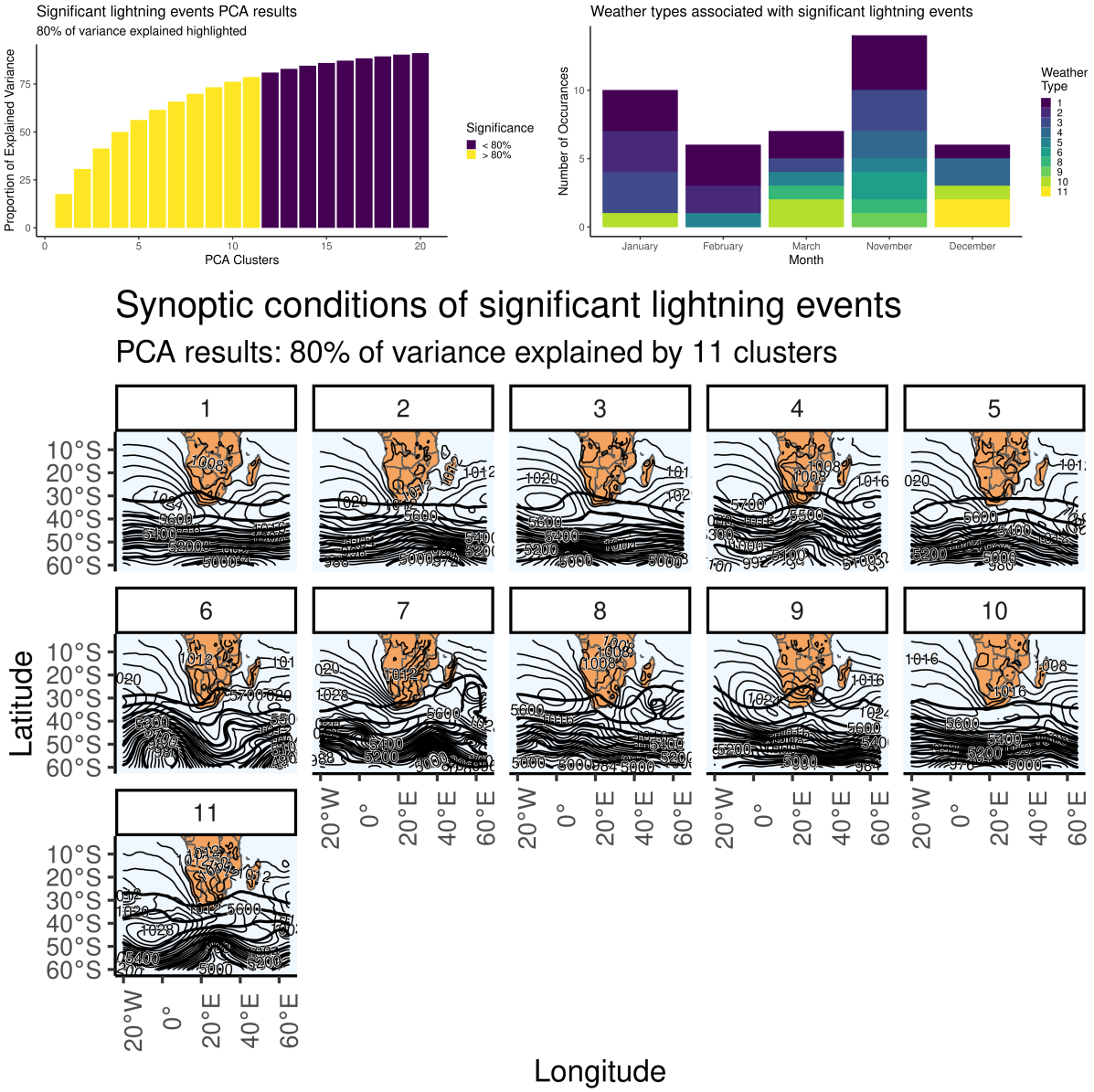

Figure 5.11: *11 Synoptic types (or clusters) explain 80% of significant lightning events over the Highveld. Lightning events mainly occur under conditions where there is strong westerly flow at 500 hPa, a strong pressure gradient along the Highveld and an influx of moisture from the tropical regions along the tropical low.*

face. In cluster 2 and 6, there are localized low-pressure systems over the region of interest, and along these pressure lines, strong winds and rotation could be expected. Only cluster 1 is associated with February tornado events. In cluster 1 there is a strong westerly disturbance at 500 hPa, with a localised low-pressure in the Highveld region, and a weak ridging high-pressure, mainly over the south eastern seaboard. Tornado development is mainly expected along this surface low-pressure at the leading edge of the 500 hPa flow. In March, cluster 4, 5 and 6 are the dominant clusters during significant tornado events. Clusters 4 and 6 have been discussed. Cluster 5 occurs exclusively in March, and in this cluster flow at 500 hPa is observed over the most of the central Highveld. On the surface there is localised low-pressure system on the eastern Highveld, with a deep west coast trough along the western Highveld. In this cluster, as in

the other clusters, tornado development can be expected where the pressure gradient is well pronounced, and along the 500 hPa westerlies, as this would enhance conditional instability and wind shear, ideal for tornado development.

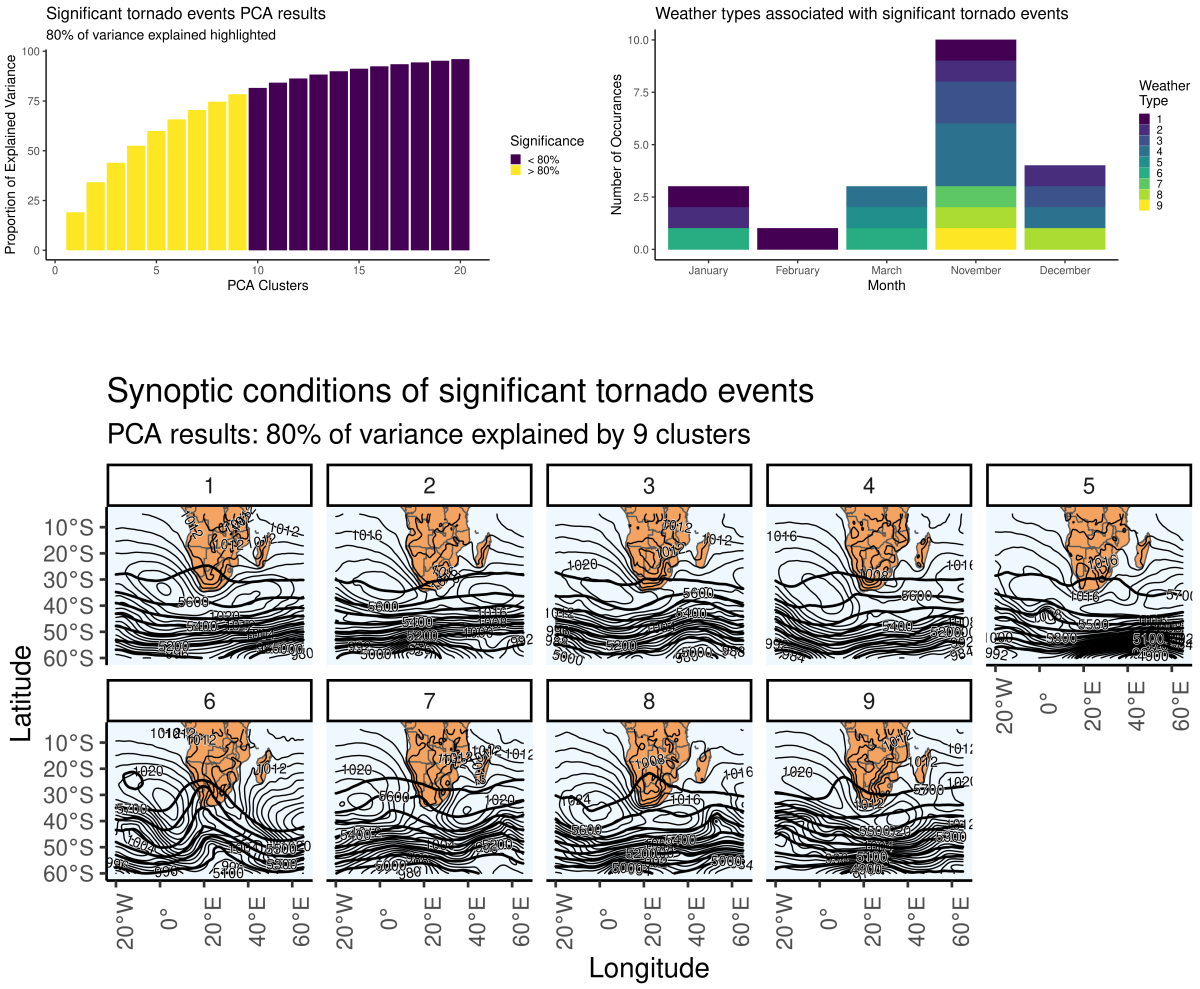

Figure 5.12: *9 Synoptic types (or clusters) explain 80% of significant tornado events over the Highveld. Tornado events mainly occur under conditions where there is strong westerly flow at 500 hPa above the Highveld. As with the other clusters a strong pressure gradient along the Highveld would enhance the chance of convective storms and tornado development. The tropical low is also present in all cases, and important in moisture advection from the tropics.*

The objective cluster analysis was able to show the variety of synoptic conditions convective events can occur in. The main limitations of the PCA (and the previous synoptic composite map) is the lack of local scale meteorological features in the analysis. Events are not only dependent on the interactions we described above, but also the local scale features such as topography, small scale land-use, local instability, urban areas, and favourable local scale thermodynamic conditions.

Thermodynamic conditions associated with significant events

Examining the thermodynamic environment by looking at selected CP is valuable to better understand the interplay between moisture, temperature and enhanced lifting through functions such as CAPE, the LCL and LFC. The first part of the analysis, as seen in Figure 5.13 and table 5.1, shows the derived CP as a function of the month in which all the categories of convective events collectively take place. CAPE (Figure 5.13a) is equally distributed throughout NDJFM months. However, the median CAPE values tell us that we see more extreme events during November and December, and we can see that December has the highest median and mean CAPE. During mid-summer, the median CAPE of reported events is considerably lower, indicating less favourable conditions for severe events.

The LCL (Figure 5.13b) is a good indicator of the level of saturation, i.e. cloud base, while the LFC (Figure 5.13c) indicates the level at which a parcel rises freely until it cools down to the environmental temperature. If the LCL and LFC show slight variance, i.e. they are similar in height, we can expect severe storm development according to past studies by Craven et al. (2004); Ganeshan et al. (2013); Groenemeijer and Van Delden (2007). LCL values vary quite significantly from early to late summer months. Saturation is generally reached at higher levels during November, while mid-summer has the lowest LCL. In November, the high LCL could be due to a reasonably stable atmosphere still dominant, inhibiting cloud formation. During this time the moisture from the ITCZ is still limited, in contrast to January where it is at its most southern position. In early summer, more convection is needed to lift a parcel through the atmospheric CIN or cap (not plotted here) before a parcel can reach the LFC and start to rise freely. This is also why we have more severe thunderstorms during November. As the energy needed to overcome the cap builds up, it becomes explosive, i.e. the parcel can rise quicker and higher as the environmental temperature above the cap is significantly colder than the rising parcel that is suppressed by the stable layer. In contrast, the low LCL and LFC values support the formation of less severe convective cells. According to Groenemeijer and Van Delden (2007) a low LFC and LCL have limited forecasting values but indicate likely tornado development, as we discuss later on. In November and December, the mean freezing level is 3000m (+-100m), 200 m higher than January and February. The maximum freezing level for early summer is almost 1000 m lower than mid-summer. During early summer, the low freezing level favours ice formation and hail storms, while the higher freezing level during mid-summer allows for hail to melt before it reaches the surface. This also supports the extra-tropical vs tropical nature of the atmosphere during these respective months when we see colder mid-levels and enhanced conditional instability during early summer, while mid-summer is dominated by surface convection.

Table 5.1: *In addition to the above Figure, we detail the mean (the Figure above shows the median values) observed convective parameters during severe reports by month.*

Month	CAPE (J/Kg)	LCL (m)	LFC (m)	FRZL (m)
November	1818	1116	1795	2945
December	1951	935	1640	3078
January	1866	892	1634	3231
February	1782	900	1534	3244
March	1634	995	1526	3059

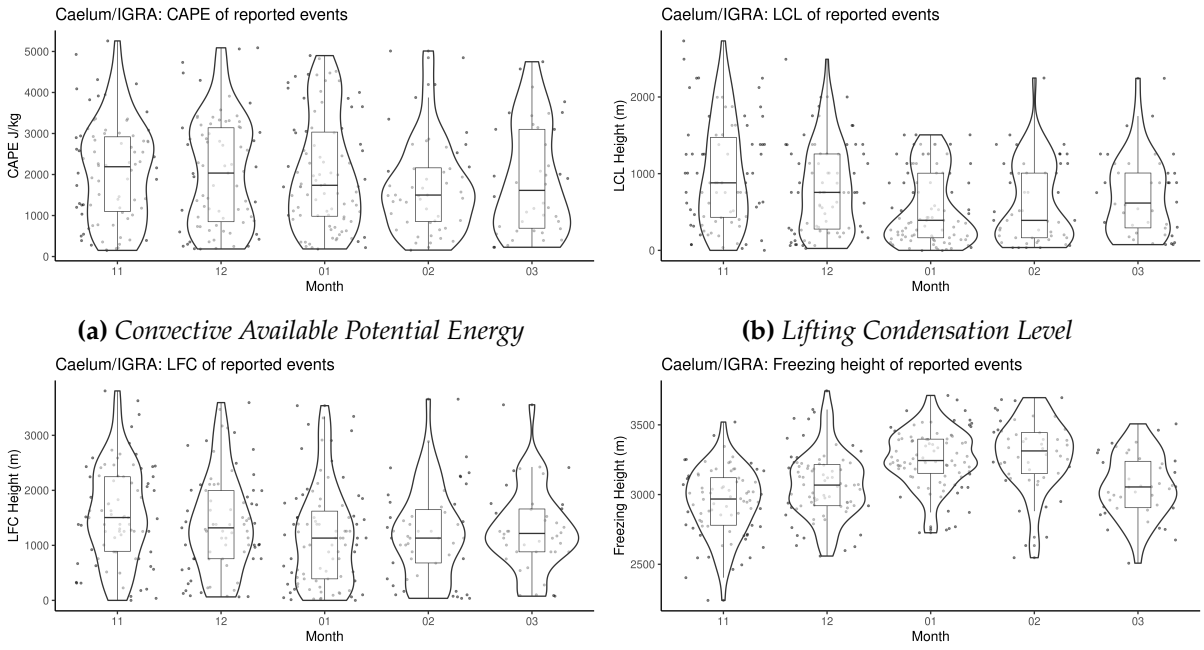

(a) *Convective Available Potential Energy*

(b) *Lifting Condensation Level*

(c) *Level of Free Convection*

(d) *Freezing Level*

Figure 5.13: *The Figure shows the environment in which all categories of convective events take place. CAPE (a) is equally distributed throughout NDJFM. Mean CAPE is lower on average during January, and as we have stated, this is when convective instability dominates. The LCL (b) and LFC (c) relationship shows a correlation to severe storms occurrence. The freezing level (d) is also crucial for ice processes. The low freezing level in early summer favours hail formation and shows how the extra-tropical nature of the atmosphere during this time impacts instability type, i.e. conditional instability as opposed to convective instability.*

In the following analysis, we examine the relationship of the individual reported events and derived CP's such as CAPE, LFC, LCL after Groenemeijer and Van Delden (2007), and we include the freezing height as seen in Figure 5.14. The mean CAPE (Figure 5.14a) for all events indicates strong instability during the days when severe storms were reported, which is expected as CAPE is generally high in the summer months. Hail reports had significantly higher mean and median CAPE values. Assuming heavy rainfall, flooding, and thunderstorms are reports of non-hail producing thunderstorms, we can see that these events had the lowest mean CAPE; however, keep in mind that heavy rainfall and flooding reports could be due to non-convective rain-bearing systems (i.e. stratiform rain). Groenemeijer and Van Delden (2007) were able to distinguish large and small hail in their 2007 study, but this is not possible in this analysis as extracted hail size measurements are not always noted and/or validated, therefor we can assume hail reports classified as severe (Figure 4.5) are mainly associated with large hail.

The LCL and LFC Figures 5.14b and c of the various events are slightly different than expected. In Figure 5.13, the LCL and LFC during November indicates an environment favourable for convection, and it is expected that events such as tornadoes and hail would show a similar relationship as observed. However, the conditions under which they occur do not reflect the same environment as seen in November. We can conclude that the LFC and LCL can indicate an overall environment that is suitable for storm formation, but individual events can occur under conditions that do not reflect the mean monthly storm environment. The LCL for tornadoes is

similar to what Craven et al. (2004) found favourable for tornado development in the USA: an LCL ≤ than 1000 m. Excluding heavy rainfall, we can see that the LCL of all events is 1000 m (+- 100 m). A low freezing level, observed in Figure 5.14d, is however a good measure of hail probability. The current data can assist to better define the thermodynamic conditions under which hail forms.

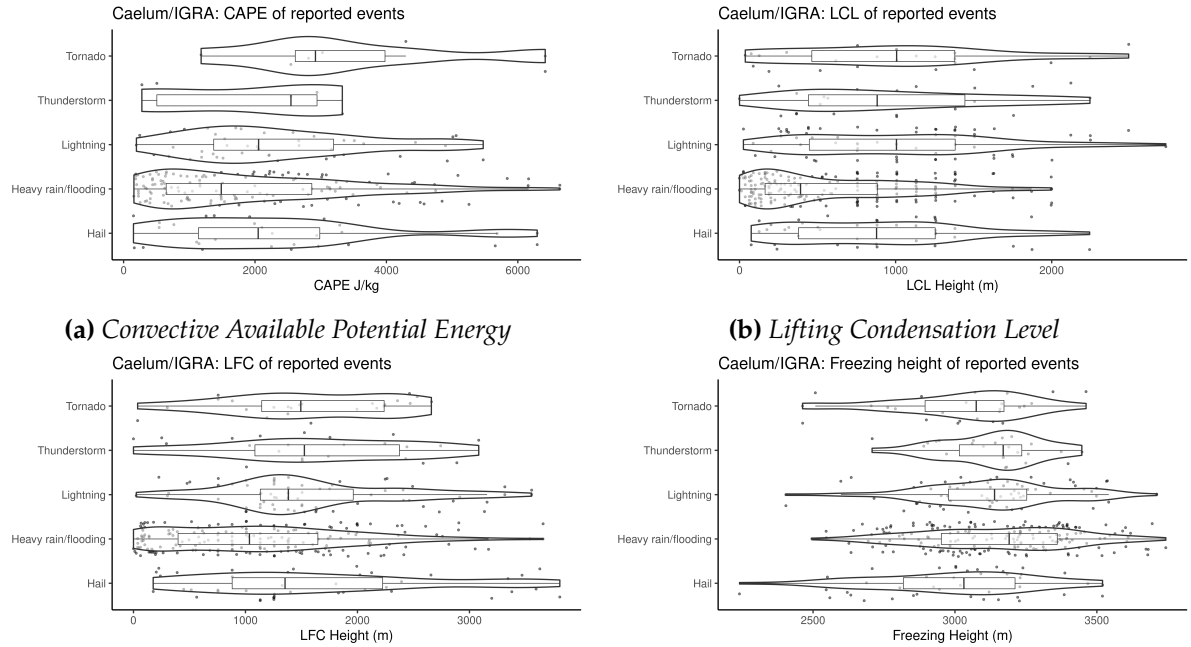

(a) *Convective Available Potential Energy*

(b) *Lifting Condensation Level*

(c) *Level of Free Convection*

(d) *Freezing Level*

Figure 5.14: *Similar to Figure 5.13, we examine the CP for the different reported convective events from the Caelum dataset to better understand the conditions under which these events form. As expected, CAPE varies significantly among days when individual events occurred. High maximum CAPE values (>3000 J/Kg) are observed in all events types. The median CAPE for lightning and tornado reports are the highest. The LCL and LFC of events show considerable variation based on the time of year that events occur. The LCL and LFC favouring convection is a function of the time of year, rather than the specific event. Severe hail reports are associated with low freezing levels, as observed in November months.*

Table 5.2: *In addition to the previous Figure we detail the mean observed convective parameters during severe reports by event.*

Event	CAPE (J/Kg)	LCL (m)	LFC (m)	FRZL (m)
Hail	2526	1023	1675	3024
Thunderstorm	2129	1171	1642	3127
Lightning	2249	1029	1503	3154
Tornado	2255	830	1627	3058
Heavy rain/flooding	1937	781	1290	3148

The freezing level height has value in understanding the occurrence of hail events, and in Figure 5.15a, we observe the average temperature occurrence at 500 hPa during NDJFM months, and in Figure 5.15b, temperatures at 500 hPa, per event category. The frequency diagram of freezing level at 500 hPa shows the coldest temperature occurs most frequently in November and during hail and tornado events. However, because the low freezing level is associated with strong westerlies at 500 hPa, this is also the period when shear and differential advection will be the strongest, favouring rotating storms.

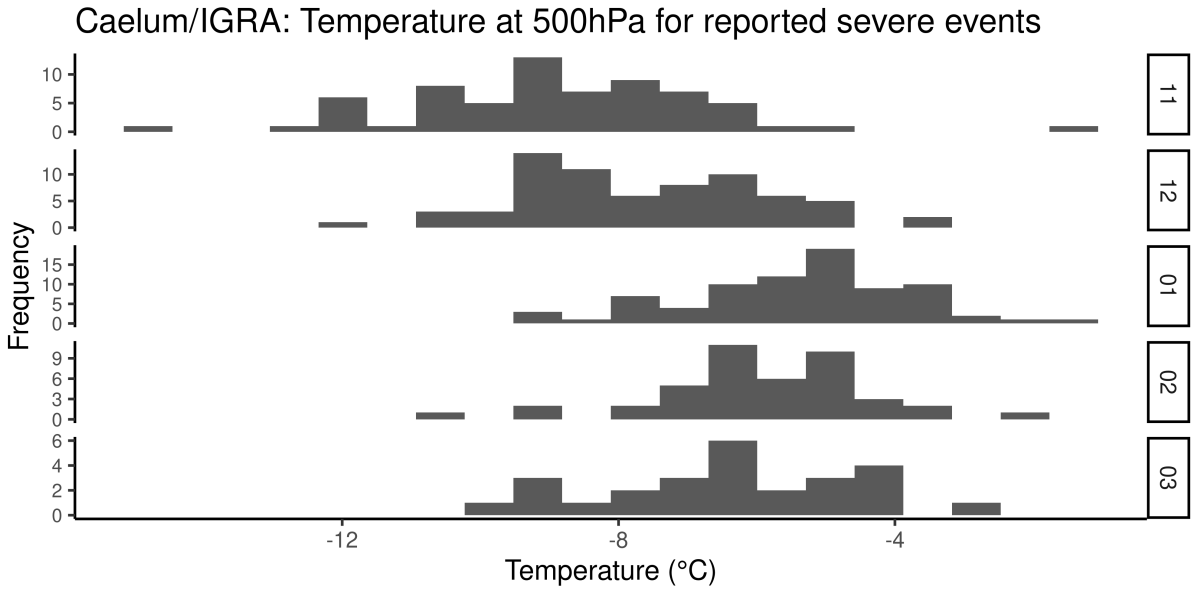

(a) *500 hPa temperature, event*

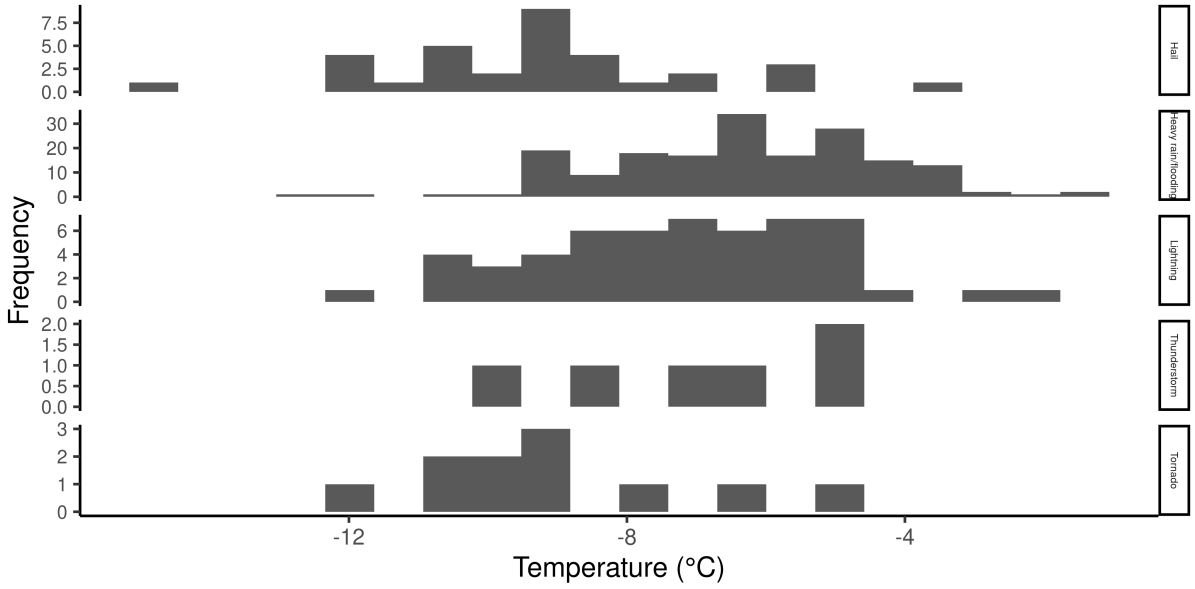

(b) *500 hPa temperature, monthly*

Figure 5.15: *The temperature at 500 hPa for reported severe events is considerably different between NDJFM months and between event categories. Hail and tornado events are more prevalent during occurrences where strong westerly flow at 500 hPa is present. Westerly flow at 500 hPa enhances wind shear and ice formation and favours rotational supercells, while other events occur in more varied conditions.*

The above section examined some CP associated with severe storm reports from 1979-2018 based on previous work by Craven et al. (2004); Dyson (2015); Groenemeijer and Van Delden (2007). A resonably complete database of soundings for coinciding severe weather reports provided valuable information about the thermodynamic state of the atmosphere associated with these events. The selection of CP was arbitrary but provides basic information about the state of the atmosphere during different times of the year and events. The environment under which these events occur is variable, but instability, moisture (represented by CAPE) and a low freezing level plays a major role in the type of weather experienced. The importance of differential

surface and upper level winds was highlighted in the clustering section, and in the next section we examine the wind profile as recorded by radiosonde data.

Wind profile of significant events

The wind speed (wspd) and wind direction (wdir), from surface to 500 hPa, as seen in Figure 5.16 for the combined NDJFM events is examined in the next section. At the surface winds, during all months, are predominantly north north-east. As was seen in the previous section on the synoptic environments, these winds are tropical in origin and result in an influx of moisture over the Highveld, a key ingredient for convection. At 500 hPa, winds are westerly during all months, and during significant events. Westerlies not only enhance conditional instability, but due to the directional shift from the surface to 500 hPa, favourable wind shear conditions increase convective potential, and favour rotation and fast moving convective structures. Wind speed at 500 hPa does decrease from early to mid-summer as the extra tropical cyclones and westerly waves shift south and tropical systems dominate the circulation. The data shows that mean wind direction from the surface to the upper levels for the whole sounding are westerly during all months. November is characterised by higher average wind speeds than other months. The increased wind speed supports the synoptic data analysis where strong westerlies at 500 hPa is observed, which would steer storms west. November's mean wind speed is 12.5 m/s (max 52 m/s), January 10.75 m/s (max 57 m/s), February 10 m/s (max 58 m/s) and March 11.68 (max 42 m/s). The wind direction during NDJFM months is 215°, 208°, 185°, 180°and 206°, respectively.

November Surface Winds

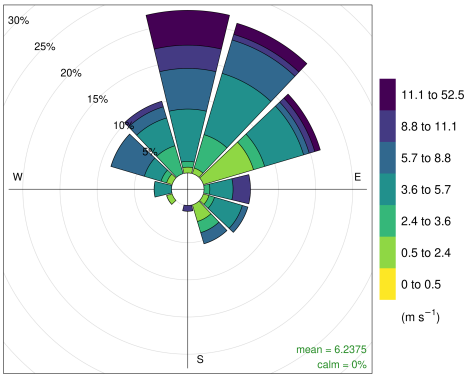

Frequency of counts by wind direction (%)

November Mid-Level Winds

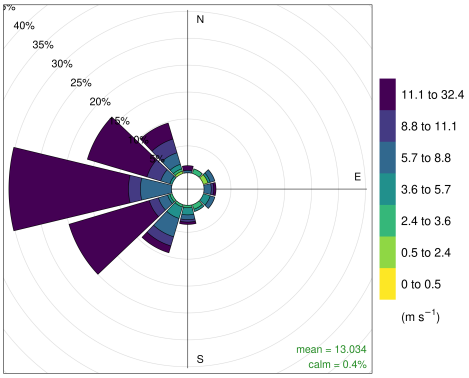

Frequency of counts by wind direction (%)

December Surface Winds

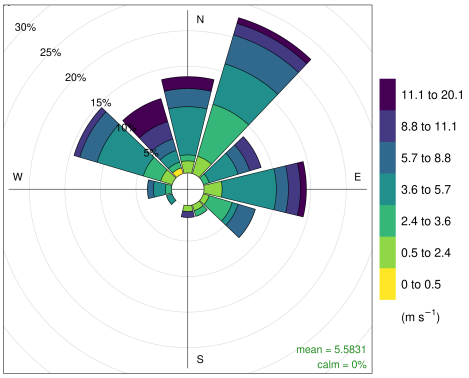

Frequency of counts by wind direction (%)

December Mid-Level Winds

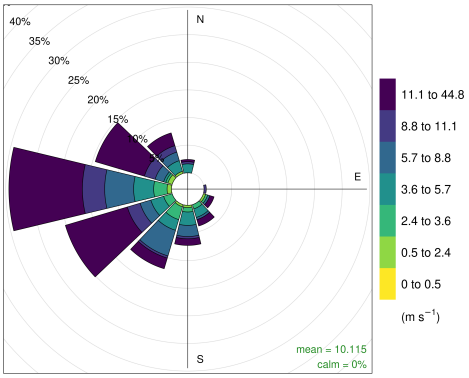

Frequency of counts by wind direction (%)

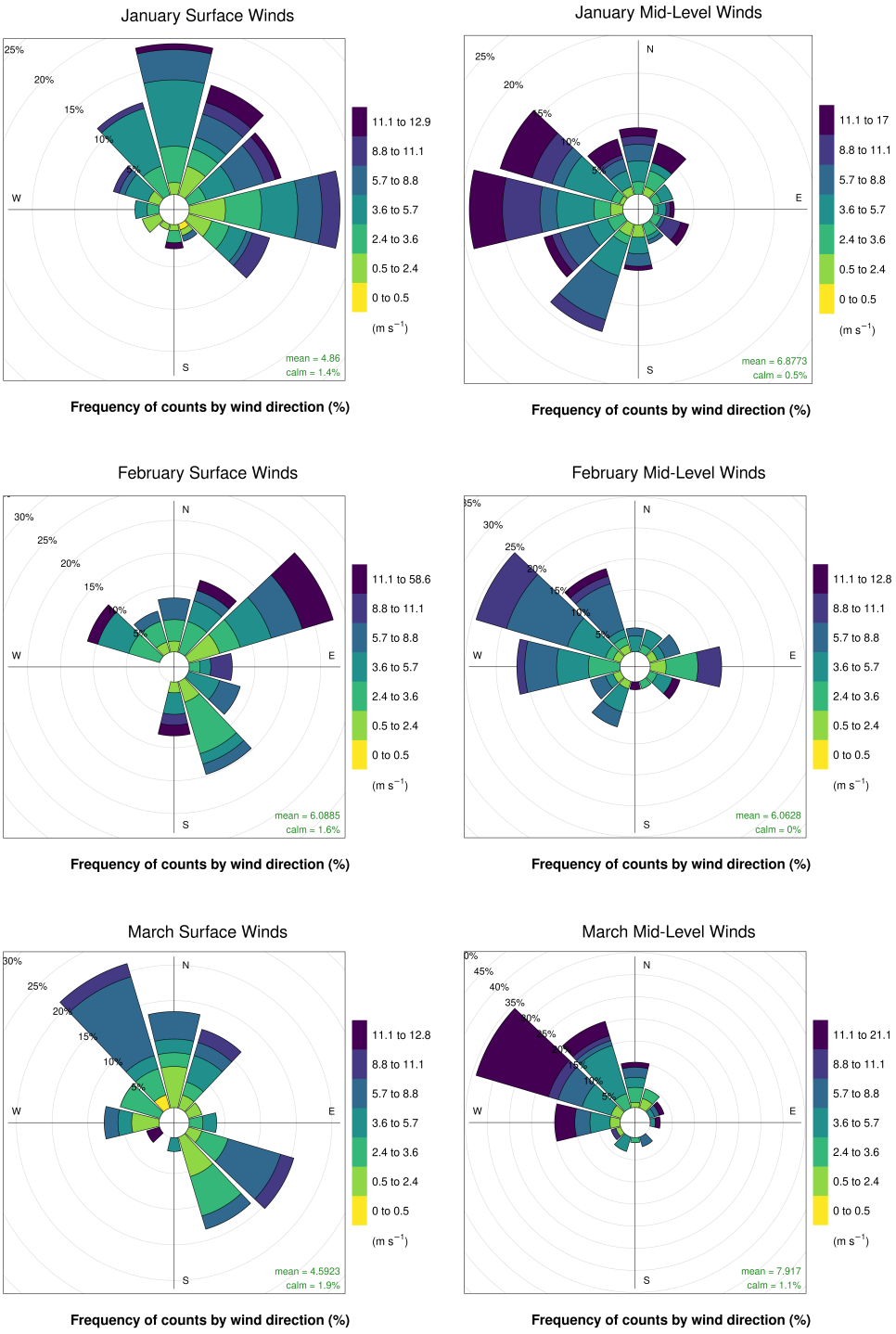

Figure 5.16: *The dominant wind direction at the surface during all months is north north-east. These winds arise from the tropical low, or continental tropical lows, and are responsible for moisture influx from the ITCZ. At 500 hPa, winds are westerly, and driven by the westerly waves. This directional shift is important in storm formation, enhances rotation and conditional instability.*

In the next section, the wind speed and direction for the event-specific sounding data is examined. The wind speed and direction for the individual events as shown in Figure 5.17 supports the previously discussed findings where the mean wind direction is predominantly westerly for NDJFM convective events (i.e. west to east). Similar to the monthly analysis, surface winds associated with convective events are predominantly north-east and tropical in origin. At 500 hPa, westerly winds dominate, enhancing wind shear between the surface and 500 hPa, and this also favours rotation. Conditional instability is enhanced if the upper level winds at 500 hPa is remains colder than the environmental lapse rate (Dupilka and Reuter, 2006; Matwitz, 1972; Simpson and Dyson, 2018; Tyson and Preston-Whyte, 2000). The maximum wind speeds in the whole sounding up are observed during tornado days at 64 m/s, followed by hail events with maximum wind speeds of 61 m/s. These two events also have the highest mean wind speeds recorded at 13.11 m/s and 13.31 m/s, respectively. Due to the variety of events associated with heavy rainfall, this category has the lowest mean wind speeds at 11 m/s, and thunderstorm events have the lowest maximum wind speeds at 38 m/s. The mean direction for all events is reasonably similar, i.e. for hail (152°), tornado (148°), and lightning (150°) events. Heavy rainfall and thunderstorm events mean wind direction is slightly more south at 157°and 165°. Assuming a gradual change of wind direction from fast moving westerly-winds in early summer to slow, tropical circulation, November will match the conditions for severe hail events, while January and February will be most conducive to heavy rainfall and isolated thundershowers, respectively.

Hail Surface Winds

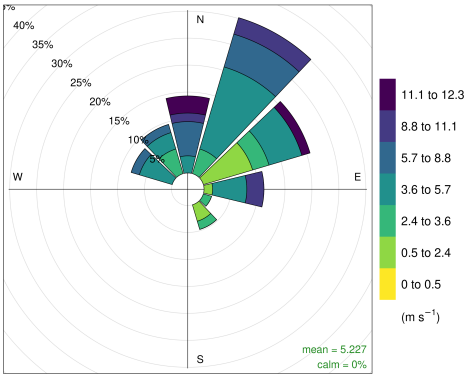

Frequency of counts by wind direction (%)

Hail Mid-Level Winds

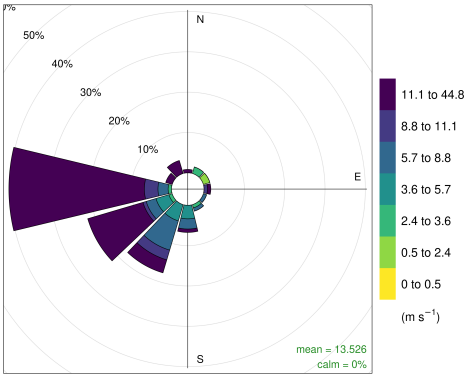

Frequency of counts by wind direction (%)

Lightning Surface Winds

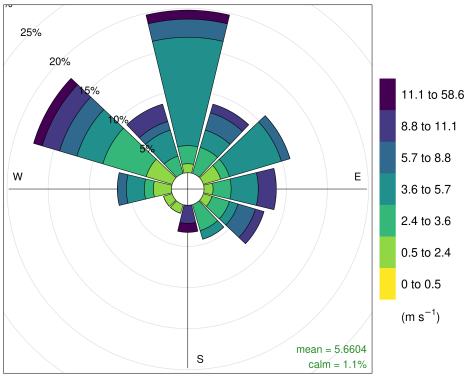

Frequency of counts by wind direction (%)

Lightning Mid-Level Winds

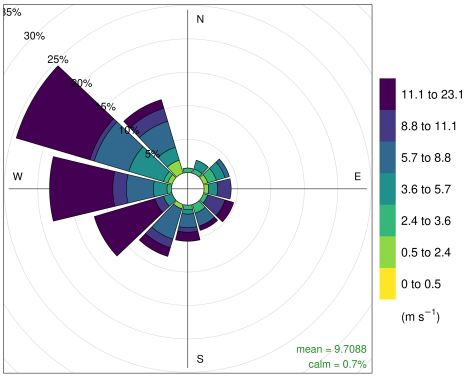

Frequency of counts by wind direction (%)

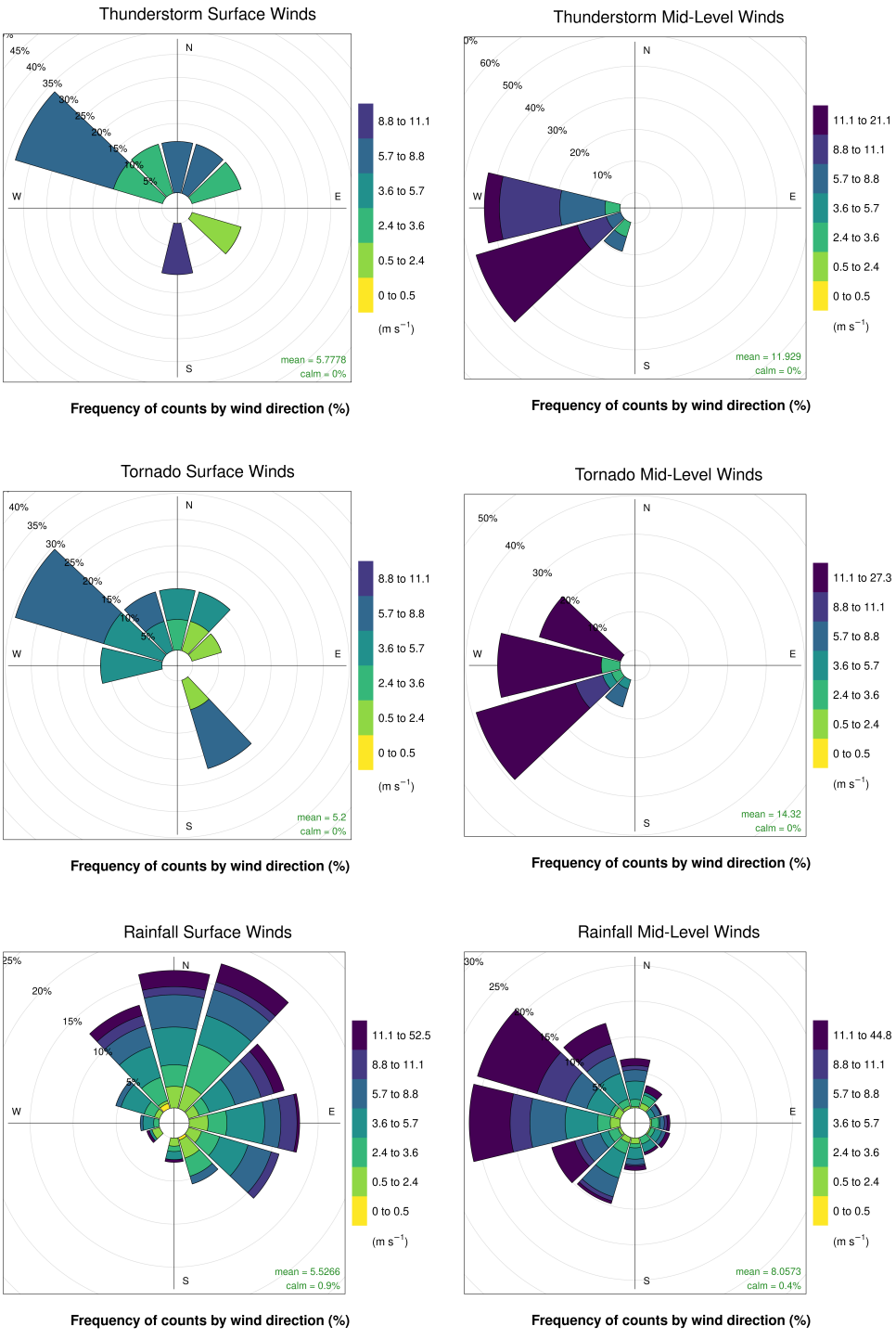

Figure 5.17: *At the surface winds during convective events are predominantly tropical (easterly) as was shown in the monthly analysis and the synoptic analysis. Similarly strong westerly winds at 500 hPa are characteristic during all convective events. During rainfall the influence of the westerlies are least pronounced, indicating that rainfall events occur under a wider variety of conditions.*

Wind Shear and CAPE of significant events

To understand the differential winds and the impact on the reported severe events, we derive bulk wind shear between surface, 850hPa, and 500 hPa levels using the following formula from Dupilka and Reuter (2006),

$$\text{SHR} = \sqrt{\frac{(u_2 - u_1)^2 + (v_2 - v_1)^2}{|z_2 - z_1|}} \tag{5.1}$$

u is the u-wind component at a given level, v the v-wind component at a given level, and z is the corresponding pressure level. The bulk shear indicates the vertical difference in winds between two levels in the atmosphere. Vertical wind differences could enhance rotation and increase the lifetime of storms, but can also lead to early dissipation of storms if it is too strong or too weak (Doswell, 1991; Dupilka and Reuter, 2006; Matwitz, 1972; Thompson et al., 2007). (Dupilka and Reuter, 2006, Pp.326) summarises current literature as follows; *weak wind shear is associated with short-lived thunderstorms, while squall lines develop in unidirectional sheared environments, and supercells have strong directional shear in the lowest 2 km*. We see that events occur under variable conditions that increase the difficulty of discriminating between definite severe storm environments and non-severe storm environments. Figure 5.18 indicates that tornado events have the highest mean bulk wind shear, 12 m/s, but the highest maximum shear was recorded during a hail event at 33 m/s. Mean hail wind shear is 11 m/s, similar to previous case studies in SA (Simpson and Dyson, 2018). Heavy rainfall, lightning and thunderstorm events have a mean shear value of 7 m/s (+-0.5 m/s). Median values for heavy rainfall reports are the lowest at 5 m/s for all the matching radiosondes. As previously mentioned, not all heavy rainfall events are necessary convective by nature. However, all the above results indicate that NDJFM convective weather occurs under high speed and directional sheering conditions. Wind speed, direction at the surface, and the 500 hPa flow impact the type of events observed.

Due to the prominent role of CAPE and shear in severe weather forecasting, it is valuable to understand the correlation between these two variables as seen in Figure 5.19. When combining all shear and CAPE values for all NDJFM events as seen in Figure 5.19a, it is observed that these events occur under a variety of conditions, even during low shear, and low CAPE environments (Brooks, 2013; Brooks et al., 1994, 2003; Craven et al., 2004; Sherburn and Parker, 2014). Typically, storm development will be hindered if the shear is too high, but the graphs discussed here match the actual days' that storm events occurred, allowing us to examine the shear that led to high impact surface weather in the past. If we examine each convective category individually as we do in Figure 5.19b, we can see that the correlation between CAPE and shear is not consistent across events. Hail events show a correlation between high CAPE and shear environments. However, there is a negative correlation between the tornado event's recorded shear and CAPE. It has to be noted that low CAPE environments can lead to the development of severe convective storms (Sherburn and Parker, 2014). The difference between the forecasted storm and the actual event occurrence could be due to various factors, including the timing and availability of the sounding, and the proximity of the sounding in relation to the event's location. It remains the forecasters' job to consider all the available information during a forecast. Relying on one

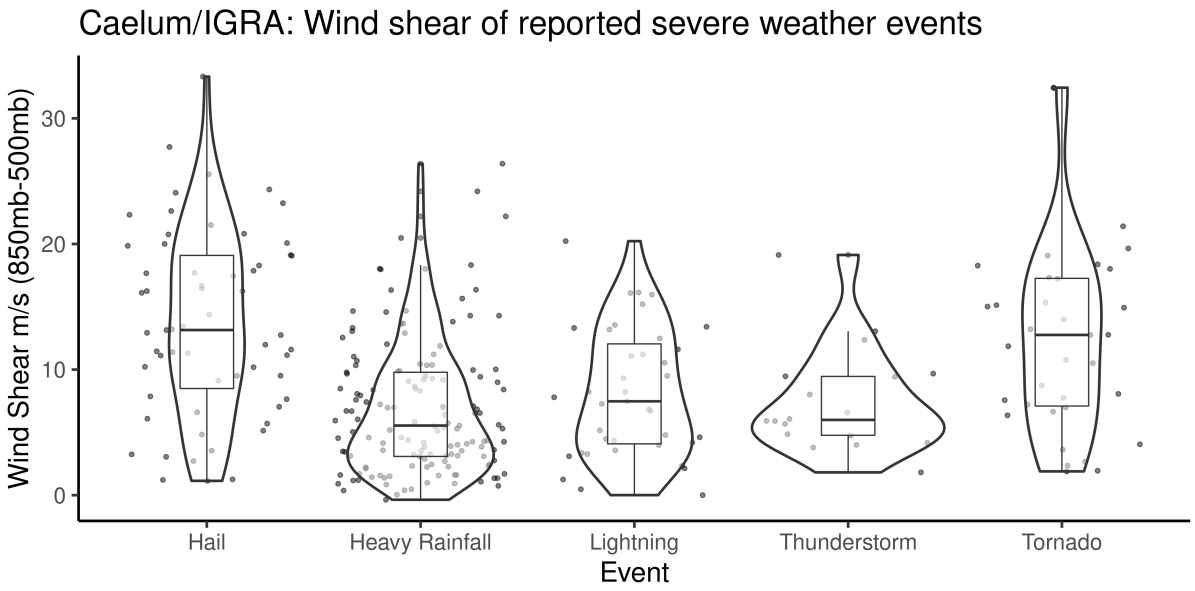

Figure 5.18: *Bulk wind shear between the surface and 500 hPa for reported severe convective events shows the wind shear conditions under which these events occur in, are variable. Tornado events have the highest mean wind shear (12 m/s), followed by hail events (11 m/s). However, the highest maximum wind shear was observed during an hail event at 33 m/s.*

data source such as a sounding, or one forecasting variable such as CAPE, can lead to a missed forecast.

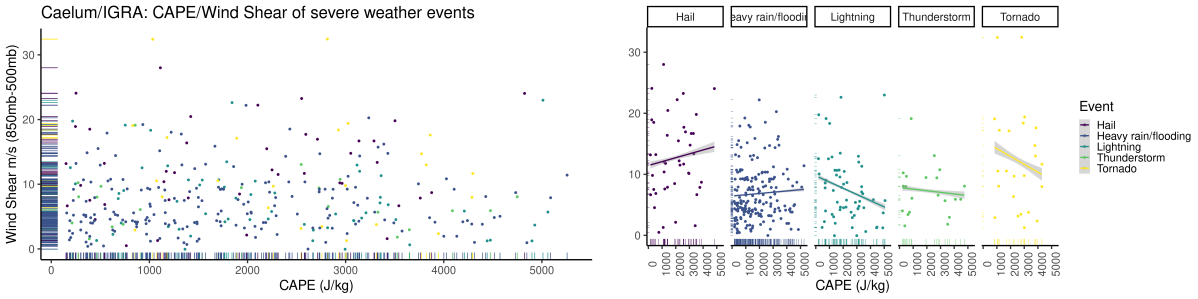

(a) *All convective events*

(b) *Events by type*

Figure 5.19: *CAPE/Wind shear relationship for reported severe convective events indicates no direct correlation between the severe weather type and wind shear. High shear and CAPE conditions are expected during severe storm development, but storms develop under a magnitude of conditions, even when common stability indexes indicate unfavourable conditions.*

Conclusion

The synoptic and thermodynamic environment under which significant convective storms occurred in was characterised using ERA5 reanalysis data and radiosonde soundings from the IGRA database. A composite map of the mean monthly conditions for each respective category of was analysed by averaging MSLP, geopotential at 500 hPa and CAPE. The composite maps showed that tropical lows are important to advect moisture over the region, while a strong westerly waves over the subcontinent enhances conditional instability and wind shear. The composite maps also show that a strong pressure gradient at the surface is typical during all types of

convective weather events. Less pronounced, is the impact of the ridging high-pressure system over the eastern escarpment, however, it does have a significant impact on enhancing low-level moisture during transition months between winter and summer (Ndarana et al., 2021). The composite maps do suffer from a major limitations, and that is that individual synoptic types that can lead to significant storms are hidden by averaging. To address this, an objective clustering method, PCA, was applied. The PCA was able to distinguish between the dominant types of synoptic patterns associated with convective events, and also the types of convective events. We examined synoptic types that explain 80% of the variance in experienced surface weather, and similar to the composite map the tropical low, strong westerlies at 500 hPa and a strong pressure gradient at the surface, is the most important features that are present during significant convective weather. The ridging high is also once again shown to enhance convective storm possibility particularly during early summer, but for Highveld weather the tropical systems are more prominent during all types of convective events.

The radisonde data provides an insightful role on the local meteorology, which is not captured by the large scale analysis. In the radisonde analysis, all convective events have dominant easterly, north easterly, winds on the surface. At 500 hPa there are strong westerly winds which enhance conditional instability and wind shear, and this supports the synoptic analysis. Thermodynamically, a low freezing level is associated with most significant hail storms, and November has the lowest freezing level. Hail and tornado events have the highest bulk wind shear and rainfall the lowest. High CAPE is associated with hail, while November is the month with the Highest mean CAPE. CAPE decreases significantly as summer progresses. Heavy rainfall occurs under a variety of conditions, and this is expected as rainfall typically occurs with all other convective events as well.

In the next chapter the impacts of land-use and topography on the radar derived convective events within the radar range is examined. This will allow us to better understand the unique characteristics of storms in the region, under different land-use scenarios.

Chapter 6
Small scale impacts on radar derived convective events

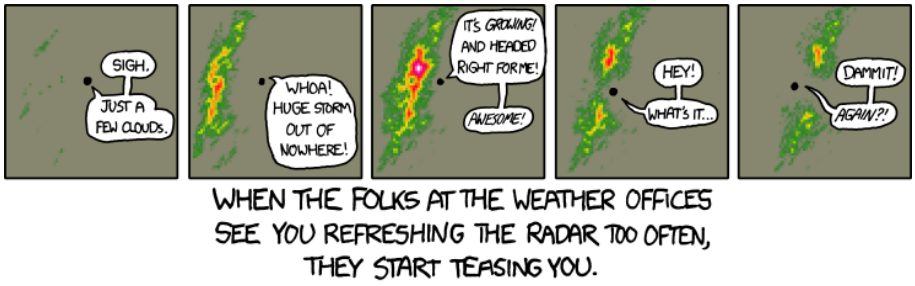

From xkcd.com, What If? 2: Additional Serious Scientific Answers to Absurd Hypothetical Questions

This chapter examines the spatial characteristics of storms over the Highveld to address the objective, i.e. *Evaluating local scale anthropogenic and non-anthropogenic impacts on convective events*. This chapter asks the main question, *what are the small scale impacts on radar derived convective events?*. However, the question has several nuances that is examined, as land-use characteristics across the region is complex and have to be taken into account along with the temporal variation of storms. This section attempts to understand topography, land-use and urban impacts on convective weather within the Irene radar range.

Introduction

This chapter examines the spatial characteristics of convective thunderstorms over the Highveld, and we differentiate between different land-use areas in our analysis. Carte and Held (1978) did an early examination of the characteristics of hail events using radar data, but this was done with no direct correlation to land-use and topography. In this paper, Carte and Held (1978) found that an echo over 40dBZ at 6 km is only 50% effective as a hail forecast measure. We make no effort to build a hail forecasting algorithm, but it highlights the difficulty in forecasting convective thunderstorms. The next crucial analysis was by Mader et al. (1986). Mader et al. (1986) built a climatology of storms over the Highveld by using a fairly small dataset in his analysis. Only storms with Z_{max} > 45dBZ and ΔH_{45} > 3km was considered in his research, and meant that he only examined 19 convective weather events during the campaign. Another study in SA by Kelbe (1984) is arguably the most detailed radar analysis of storms, specifically the characteristics of various cumulus type clouds in SA. However, this research was conducted for the low-veld region and was based on days when cloud seeding occurred. Due to structural, operational, and policy changes, SA's radar data is limited, but the high resolution of the data provides valuable insights into storm dynamics. Kelbe (1984) notes *discontinuities in the radar data may have resulted in some deep convective storms remaining unaccounted for...* A discrepancy we

wish to address in this study. Other research has mainly focused on case studies where event-specific radar data was analysed (see De Coning and Adam (2000); De Coning et al. (2000, 1998); Rae (2014); Simpson and Dyson (2018); Terblanche et al. (2001)).

Spatio-temporal characteristics of convective storms

The general spatial and temporal characteristics, without accounting for land-use and topography influences, is examined first. In Figure 6.2 we examine the normalised density of all storms for NDJFM within the radar range. The normalised data shows a high density of storms in the centre and southern parts of Gauteng, with a clear south-easterly band of high-density events. This high-density reflectivity band seems to follow a TTT pattern and highlights the phenomena's general contribution to summer rainfall over the area (Hart et al., 2010; Macron et al., 2014).

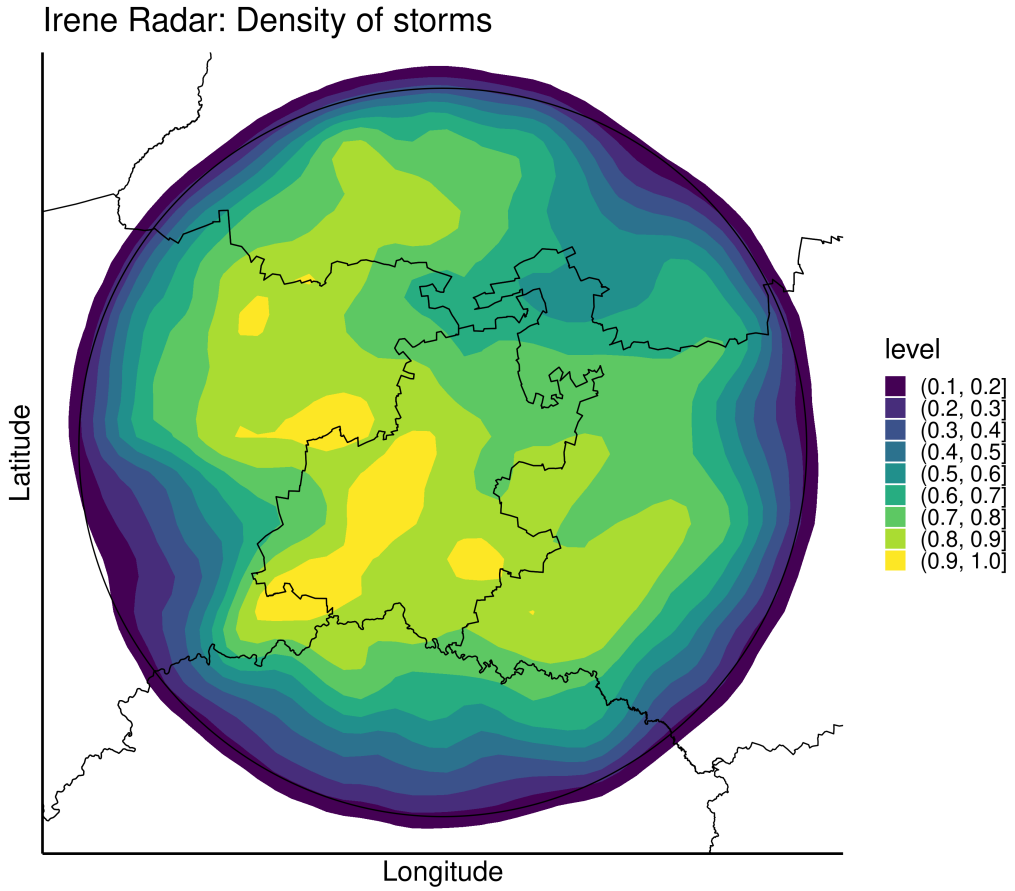

Figure 6.2: *The normalised density of all radar observed summer storms within the Irene radar range indicates areas of higher storm frequency. Various factors such as climatology, topography, and even smaller-scale effects such as land-use can play a role in the variations observed here.*

By examining the above storm densities at a higher temporal resolution, as seen in figure 6.3, it becomes clear there is an early, mid and late summer signal. In November, there is a high density of storms in the south-eastern range of the radar (i.e. south-western Mpumalanga), and with the progression of summer, the density of storms shifts north – northwest. In November, the highest density of events can be seen over the North-Eastern portion of the North-West province. In March convective weather over Gauteng is at minima and concentrated over the

southern parts of Limpopo. These shifts can be described by the annual movement of mid-latitude systems and the ITCZ, and their interaction with each other. Moisture transport from the tropical easterlies also becomes a dominant process during mid-summer, driving convective instability. The synoptic climatology for convective weather events as described in Figures 5.2 – 5.6 shows the mean circulation during severe convective events and strong upper-level flow at 500hPa and tropical (easterly) surface winds providing surface moisture is present during all types of convective events in the region. As we break down the data into smaller time frames, features such as the TTT become less apparent. The relative importance of the TTT for rainfall, but not necessarily severe localised convective events, has been stated in literature (see De Coning et al. (1998); Hart et al. (2010); Macron et al. (2014); Mason and Jury (1997)), and has to be considered throughout the examination of the area's weather.

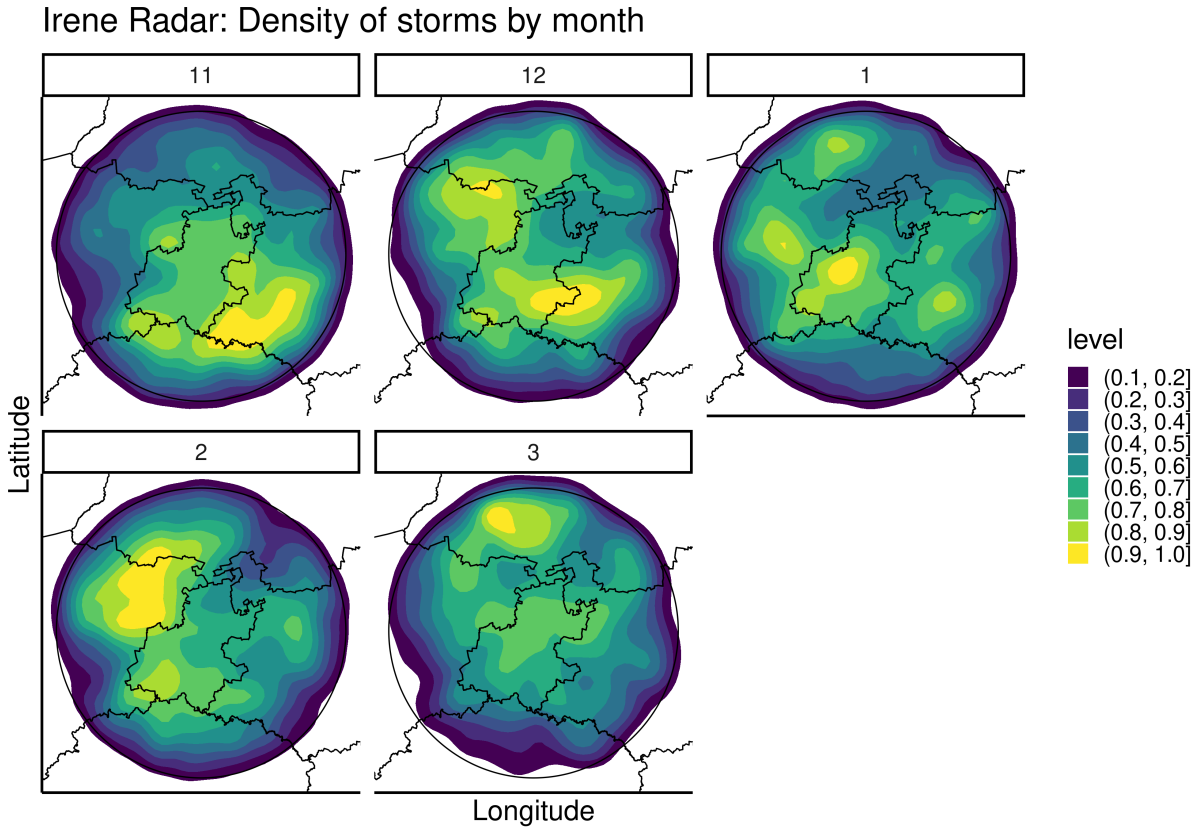

Figure 6.3: *In contrast to Figure 6.2, we can break down the radar observations into smaller time frames to observe the monthly normalised density of convective events over the Highveld. We can see an apparent variation between the areas of storm frequency during different times of the year. The mean climatology and movement of tropical and extratropical systems are the most obvious explanation for this.*

The two figures above serve as an introduction to discuss the general density of convective weather events within the Irene radar range. It is clear that there is a variation in the spatial characteristics of storms we experience during summer. At the time scales we used here, we can attribute it to synoptic circulation and climatological variations (e.g. between eastern Mpumalanga and southern Limpopo); however, as we start examining the data on an hourly basis, the effects of topography and land-use will be more apparent. On this scale, we start to see short-lived events driven by shallow convection, and we can analyse convective initiation

characteristics instead of seeing a mature storm bias.

Impacts of topography and land-use on convective storms

Next, we do a more detailed analysis on storms within the Highveld region and the effect of topography and land-use on convective events, their distribution and occurrence within the Irene radar range.

Topography

First, we plot the density of storms, as seen in Figure 6.4, to examine the general distribution of storms as a function of elevation (above sea level). Many storms between 40 and 50 dBZ are concentrated at an elevation of +-1600 m. However, this can be deceiving as a large portion of the Highveld is at a mean elevation above 1500 m. The local scale effect of complex topography is not visible, i.e. the impact of mountain ranges on local convection. This is addressed in the following sections by extracting data for various terrain types to quantify and understand their individual impact.

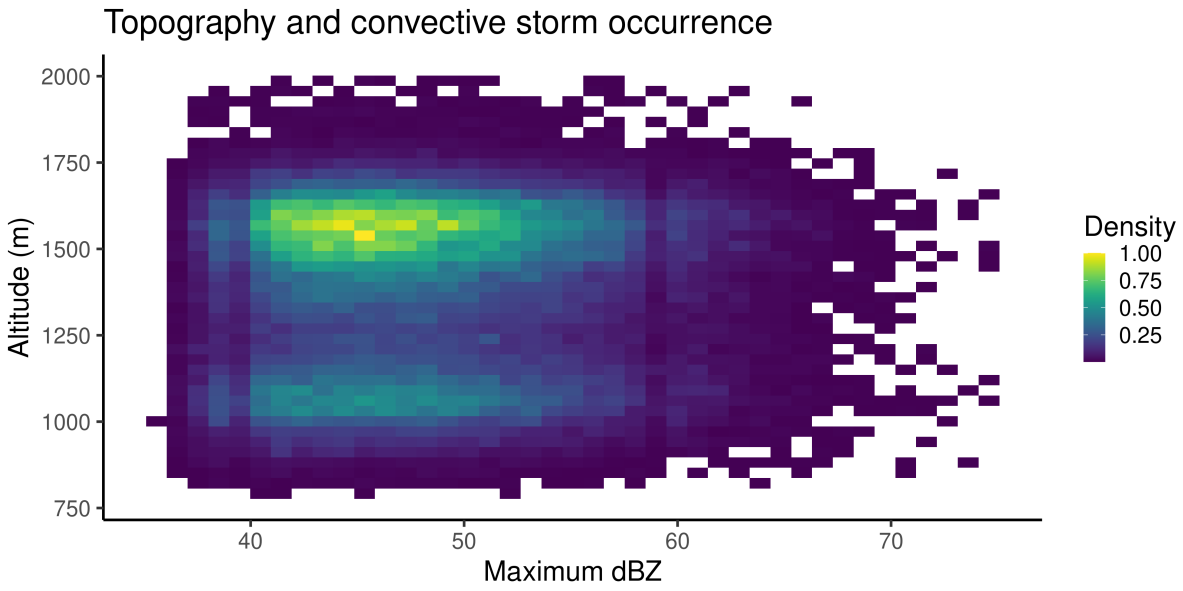

Figure 6.4: *The Figure shows the density of storms over specific topography within the Irene radar range. We can see that most of the storms occur at 1600 m elevation; however, a more detailed analysis is necessary to understand the local-scale effects of topography and orography better.*

Simple vs complex terrain

Using a smaller subset of the data over varied topography allows us to better examine the impact of terrain, orography, and elevation on storm occurrence, as seen in Figure 2.10. Radar data is extracted for two neighbouring regions, Pilanesberg (27.0752, -25.2643) and Legonyane (27.7838, -25.2861), in the North-West province. These two areas are reasonably close to each other, albeit one with a complex topography and one with simple topography. In Figure 6.5, elevation profile is drawn to show how the surface area differs between the two regions. The maximum elevation

is 1402m, mean elevation 1116m and lowest elevation 972m. Land-use impacts are still omitted in this analysis as both regions are predominantly rural, and it is assumed that the general synoptic forcing of the two regions will be similar due to the close proximity to each other allowing us to examine the explicit impact of topography.

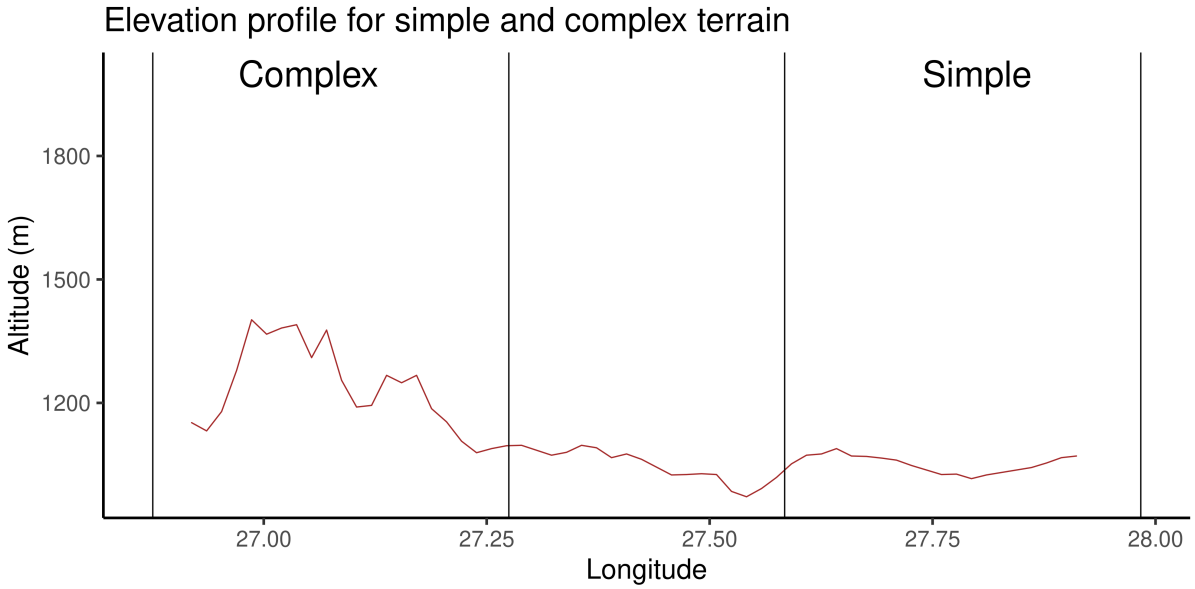

Figure 6.5: *The elevation profile seen here shows the differences in topography between areas in proximity to each other. As indicated in Figure 2.10, the complex terrain is centred around Pilanesberg (27.0752, -25.2643), while the simple terrain is centred around Legonyane (27.7838, -25.2861). Radar data is extracted for these regions and analysed to see if there are any significant effects between areas with simple and complex surfaces. Both areas are rural with informal settlements in the region, and the proximity to each other means a similar climate is expected.*

Figure 6.6 shows the maximum reflectivity derived from the radar data over the selected areas. The results show that the maximum observed dBZ over complex terrain is substantially higher (72dBZ) than simple terrain (66dBZ)[1]. The median, and the distribution of the data indicates that, on average, dynamically similar storms occur in both areas, but with higher cloud tops over the complex regions. The mechanism for this is most likely changes in the localised uplift over the mountains. Subsequently, the basic cloud structure of these terrains, i.e. cloud base and cloud top, is examined.

Complex terrains might favour convective storms' development when examining the cloud characteristics (cloud base and top, Figure 6.7). Higher than average cloud bases (Figure 6.7a) and tops (Figure 6.7b) occur more frequently over complex terrain, i.e. uplift in the area is enhanced on a local scale.

Using LIS data from the TRMM and ISS (Albrecht et al., 2016; Cecil et al., 2014, 2015; Chronis and Koshak, 2017; Kaltenböck et al., 2009; Molinari et al., 1999; Takayabu, 2006; Taszarek, Allen, Groenemeijer, Edwards, Brooks, Chmielewski and Enno, 2020) missions, the LIS data is aggregated into 18 years (1998-2020) of NDJFM lightning data. As seen in Figure 6.8a and 6.8b, the data validates the radar observations. The cumulative number of lightning counts over complex

[1]dBZ is measured on a log scale

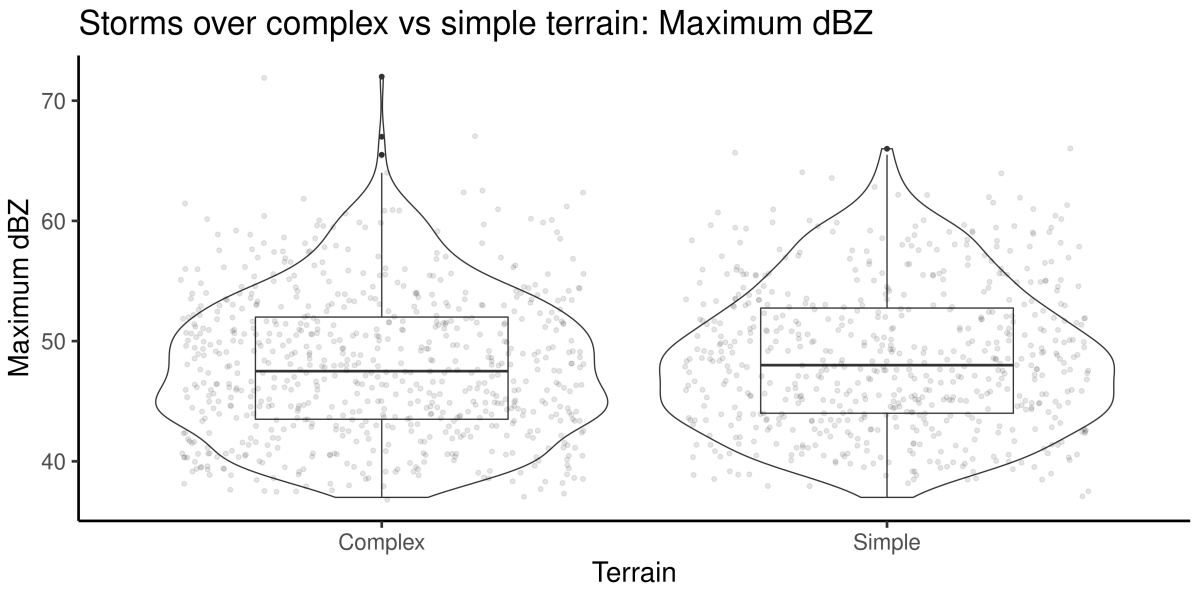

Figure 6.6: *The maximum observed dBZ over simple and complex terrain types indicates that over complex terrain, in this case, the Pilanesberg mountains, more convective storms are occurring. However, on average, a normal distribution of storms occur between two regions close to each other with different surface characteristics. The occurrence of higher maximum dBZ is speculated to be the result of enhanced localised lifting.*

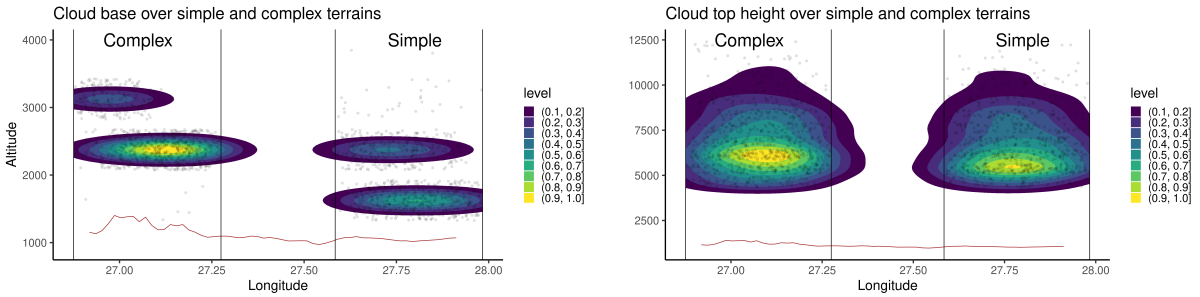

(a) *Cloud base height*

(b) *Cloud top height*

Figure 6.7: *The cloud characteristics over complex and simple terrains differ substantially. Although maximum cloud top is similar in both cases, clouds over complex terrain have a higher cloud base and top, and possibly more severe storms. Most likely due to enhanced lifting on a local scale in the region.*

terrains is higher than simple terrains, supporting our initial findings that, on average, complex terrains have more lightning activity during all summer months than simple terrains and that convection might be favoured over the complex topography around Pilanesberg (and possibly other areas) compared to flat areas, with few, if any, mountains. The relationship between elevation and lightning was also examined by Bhavika (2007); Gijben (2012); Gijben and De Coning (2017) who found similar results, showing that slope and elevation has a noticeable impact on lightning occurrence in SA.

An interesting case study in this regard is the severe hail storm that occurred over Sun-City on 15 December 2018 (TimesLive, 2018). Radar data from the storm day shows how a small convective cell developed south of Sun-City (at the foot of the Pilanesberg) at 1246 UTC. It moved over Sun-City and was elevated by the mountains within the space of an hour. By 1350 UTC,

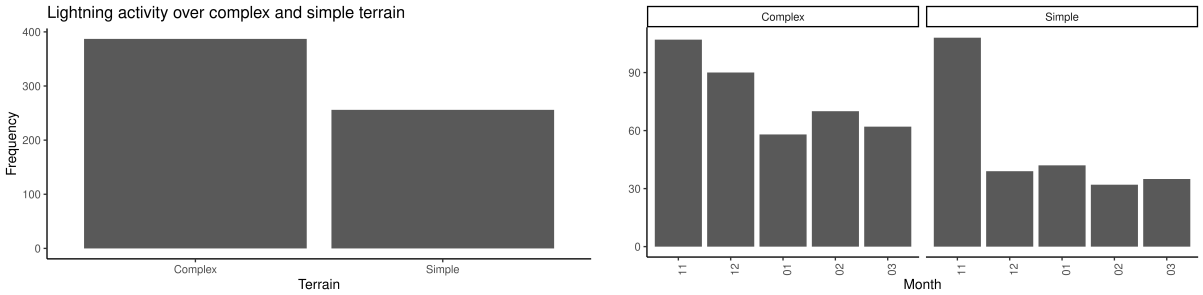

(a) *Cumulative Frequency* **(b)** *NDJFM Frequency*

Figure 6.8: *Higher convective storm activity over is observed complex terrains, both as a function of all months and across the individual months. The data used here is from the LIS data from the TRMM and ISS missions from 1998-2020. Spatial inhomogeneities exist because these are polar-orbiting satellites, but the data is valuable when aggregated over the whole period to derive the convective climatology.*

the storm, with a maximum dBZ over 40, was located directly above the resort. By 1430 UTC, the cell moved due east and seemed to be steered along the mountain edge. In this case, over 200-holiday homes was damaged. The damage was estimated to be in the millions (Kubheka, 2018).

Local scale orographic impacts

The previous analysis examined two topographically different areas and the variation in storm characteristics between these areas; however, the impact of mountains as a possible blocking feature of storms also invites further investigation. The region within the Irene radar range does not have large mountain ranges such as the Drakensberg. However, the Waterberg mountains in the far north section of the radar range (southern Limpopo) and the Magaliesberg Mountain range west of Gauteng in the North-West are useful landforms to investigate this effect. Because the Waterberg mountains are far from the Irene radar, we choose the Magaliesberg to investigate storm characteristics directly east and west of the mountain range in the Rustenburg area.

Although the Magaliesberg Mountain range is not SA biggest mountain range, there is still significant differences observed in the cloud base (Figure 6.10a) and top (Figure 6.10b) between the eastern and western section which also impacts precipitation. The maximum elevation is 1581m, mean elevation 1230m and lowest elevation 1109m. In the east, during summer, a number of events with a low cloud base is observed. It is worth further investigation to see if these are possibly rotor clouds. Rotor clouds form due to turbulence on the lee side of mountains (Doyle and Durran, 2002). Geldenhuys et al. (2020); Van Der Mescht (2012); Van Der Mescht and Eloff (2013)'s papers deal with mountain flow in the coastal regions of South Africa, there is little literature dealing with the possibility of this flow in the Highveld or the Magaliesberg. The phenomena indicates that there is possible enhancement of turbulence on the leeward side (i.e. the eastern section) of the mountain as seen in other countries (Labbouz et al., 2013).

In Figure 6.10b, observations show that the mountain affects the cloud top height between the two regions. While a higher than average cloud top is observed in the west (8.3 km +-100 m and maximum 14.3 km +-100 m) (where the dominant winds prevail from), on the lee side of the

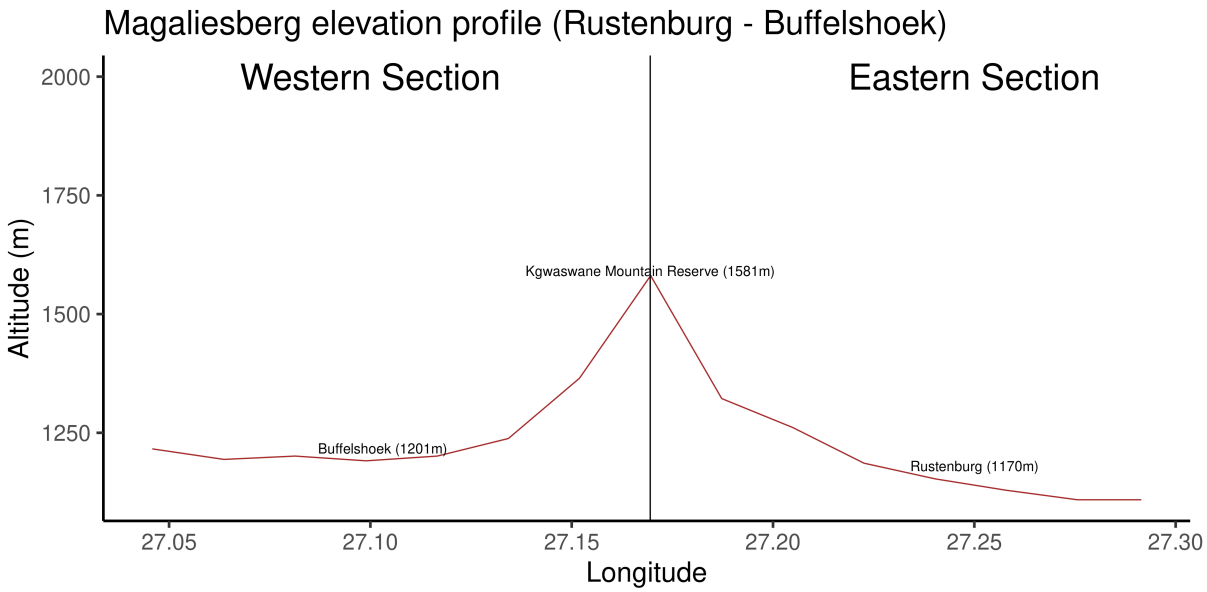

Figure 6.9: *The Magaliesberg elevation profile, as seen here, indicates the study area within the Irene radar range where the effects of orographic features on summer storm characteristics is analysed. Two 10 km radii on either side of the mountain as indicated by the yellow circles in Figure 2.10.*

mountain, there is a higher density of storms (i.e. the eastern side). It can be speculated that enhanced convective initiation occurs as a function of the wind's movement over the mountains. The lower cloud top (6.7 km +-100 m and maximum 13.6 km +-100 m) might be the result of the earlier onset of precipitation. As discussed above, the prevailing wind direction, seen in Figure 6.10c, plays an essential part in the cloud characteristics. We can see that the mountain also acts as a blocking feature. In the western section, a higher density of westerly winds is visible, while the eastern section has a lower density of these winds for the same period. The early onset of precipitation on the leeward side might have further downwind effects if examined in more detail (Barros and Lettenmaier, 1994).

The following results show the reflectivity characteristics of storms on either side of the mountain. Figure 6.11 indicates that western side storms are, on average, more severe, with a slightly higher, but not significant, mean reflectivity of 48dBZ compared to the lee-side (eastern) of the mountain (mean 47dBZ. Events on the eastern side have lower average reflectivity, but the radar observes more events. This difference in frequency suggests that shallow clouds with lower precipitation occur more frequently directly east of the mountain range.

Lightning derived data from the TRMM and ISS missions does not indicate a clear difference between western and eastern storm activity with the same level of confidence as the complex vs simple terrain analysis. In Figure 6.12a, the cumulative frequency of lightning events over both regions, the eastern side of the mountain, or the lee-side, shows a higher number of lightning counts than the western side, and this supports the radar-derived analysis that indicates the density of storms is higher on the lee-side of the mountain. Figure 6.12b shows that there is, however, randomness in the occurrence of lightning events. December has a high number of events on the mountain's lee side, however, there is no significant difference in the overall lightning activity between the regions.

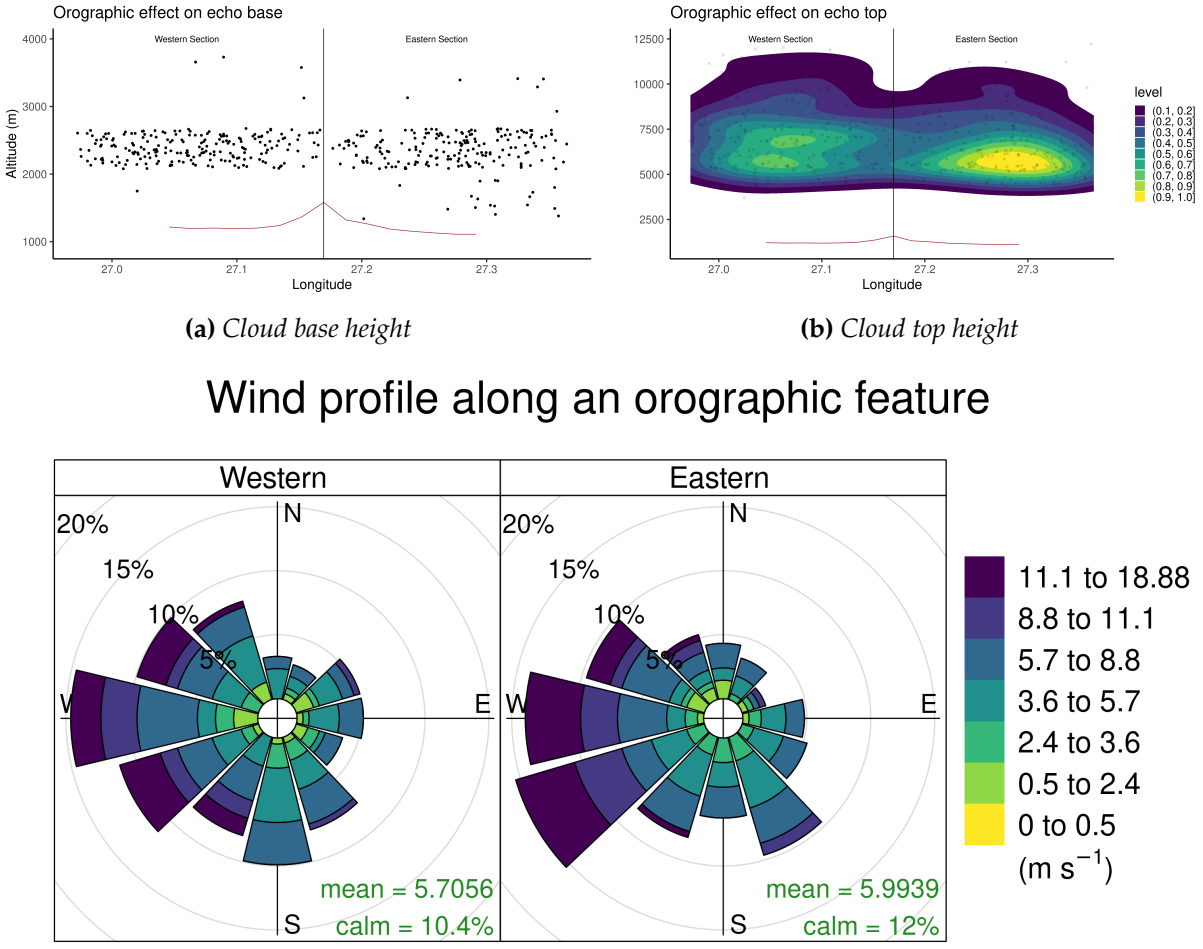

(a) *Cloud base height*

(b) *Cloud top height*

(c) *Mean wind direction and speed*

Figure 6.10: *Cloud characteristics between two regions separated by a mountain rage indicate that even a small orographic feature impacts the characteristics of storms and clouds in the vicinity. Low cloud base on the lee-side of the mountain, i.e. the eastern section, can be observed in subfigure a.*

The above section provides a simple but practical overview of topography and orography's effects on radar-derived storm data. Two areas close to each other but with differing topography affects the cloud composition. Complex terrain can enhance convection, and higher cloud base and top and maximum dBZ is observed over these regions in comparison to the simple terrain site. Subsequently, the effect of a mountain range on cloud characteristics between two neighbouring areas is explored, and the results show that even a small orographic feature such as the Magaliesberg Mountain has differing cloud characteristics on either side of the range. A higher number of events is seen directly east of the range, albeit with less severe characteristics (low cloud base, tops and low maximum dBZ) than western observed storms. The mean wind direction plays a crucial role here, and we theorise that shallow convection is enhanced on the lee side of the mountains.

This section proves it is challenging to separate topography and orography from any climatological study, especially one examining features on such a small scale. We omitted a seasonal

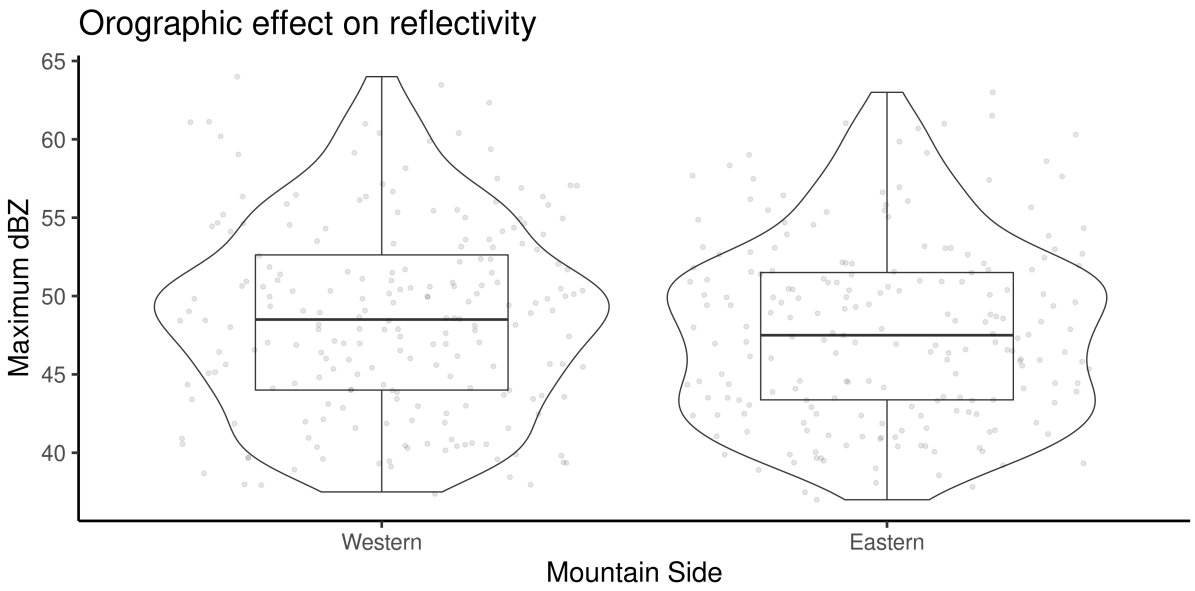

Figure 6.11: *The above figure indicates a difference between the radar observed reflectivity west and east of the mountain range. On the west side, storms have a higher median and maximum dBZ. The eastern side has a more significant number of storms with lower reflectivity, but this indicates that storms on the lee side of the mountain are less severe but more prominent (i.e. frequent shallow clouds compared to deeper clouds on the western side).*

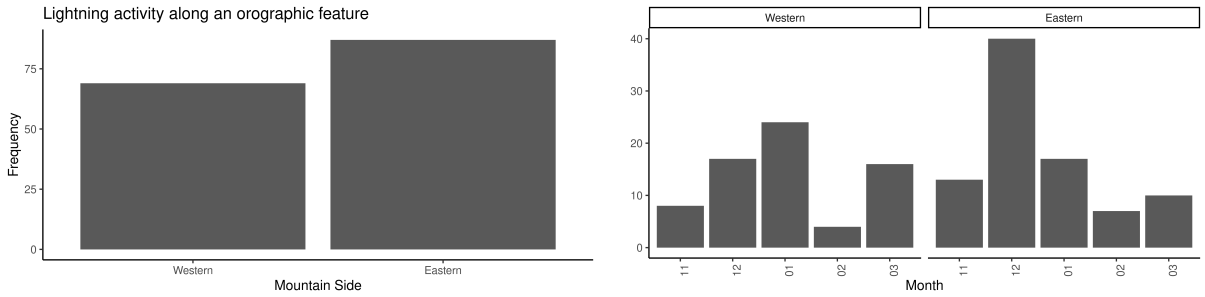

(a) *Cumulative Frequency* **(b)** *NDJFM Frequency*

Figure 6.12: *Lightning data supports the radar results indicating more convective activity along the eastern, lee side, of the Magaliesberg mountains.*

analysis of discussed topics here, as a detailed storm climatology is done in Chapter 4. Instead, this section shows that the complexities are observable across varying terrain. In the next section, we focus specifically on land-use. However, as seen here, and considering that Johannesburg and the surrounding area have a highly complex topography, we assume a possible cumulative and complex impact on the region's convective storm characteristics.

Land-use and urban impacts

As discussed in the introductory section of this chapter, we use the SANLC and reclassify the original 73 land-use categories into urban, suburban, rural, informal, and industrial categories for analysis in this chapter (table 2.2 and table 2.3). In Figure 6.13, we can observe the total number of data points per land-use category. As expected, rural areas dominate the area in the radar radius. As a result, we can expect many storms with varying characteristics in rural areas,

which will bias the distribution of storm characteristics. Limiting our study area to well defined boundaries close to each other and of equal size, assists to overcome these limitations.

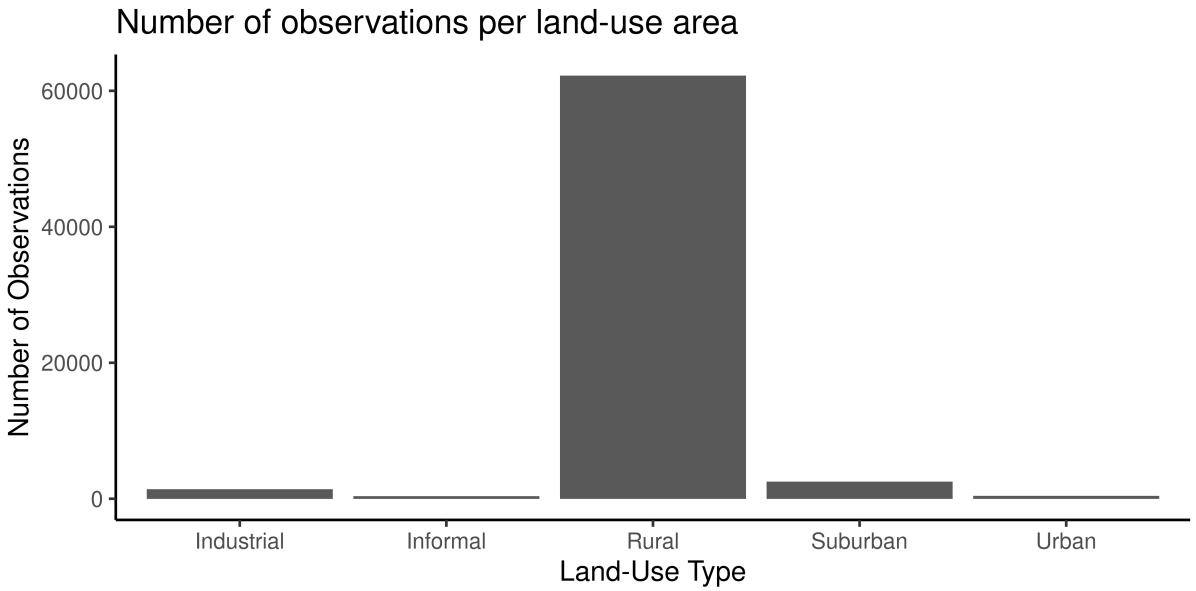

Figure 6.13: *Most land-use area is rural land, and subsequently, the number of observations (all months) over rural land dominates the dataset. This means that the sheer variety of physically and dynamically different storms experienced will be more extensive. To limit this, we extract a small subset of data in and around Johannesburg that captures all the reclassified areas, with an equal distribution of data points in each category.*

To overcome this rural bias, we limit the area to small subsets in and around Johannesburg, informal areas in northern Gauteng and industrial areas in Mpumalanga, as seen in Figure 6.14. For the urban land-use analysis, three areas are defined as suburban, urban and rural. Here we explicitly recreate[2] the original north-south cross-section of Johannesburg first researched by Garstang et al. (1975); Tyson et al. (1972) during the Johannesburg Heat Island Project. The area captures the three major land-use areas reasonably well, i.e. rural, urban and suburban areas. While a few informal and industrial areas are nearby, they do not cover significant areas within the selected urban area. To overcome this, we extract data over Ga-Rankuwa in northern Gauteng and the surrounding settlements. We analyse storm characteristics directly east, and west of this region as seen by the three circles marked 'informal'. To analyse industrial impacts, we examine a small area over the Kendall power station in Mpumalanga, and again we examine the storm properties directly east and west of this site.

Radar climatology in and around greater Johannesburg

Similar to the analysis of the topographical impacts on thunderstorm development, the region examined here has a complex topography, as seen in Figure 2.10. All three areas marked 'urban', 'rural', and 'suburban', are above 1500 m elevation, and in Figure 6.15, the north-south elevation profile indicates the complexity of the topography within the region. Johannesburg City, located in the urban defined area, lies well above the suburban and rural areas. This fact

[2]a tribute to the pioneering research done by Prof. P.D Tyson

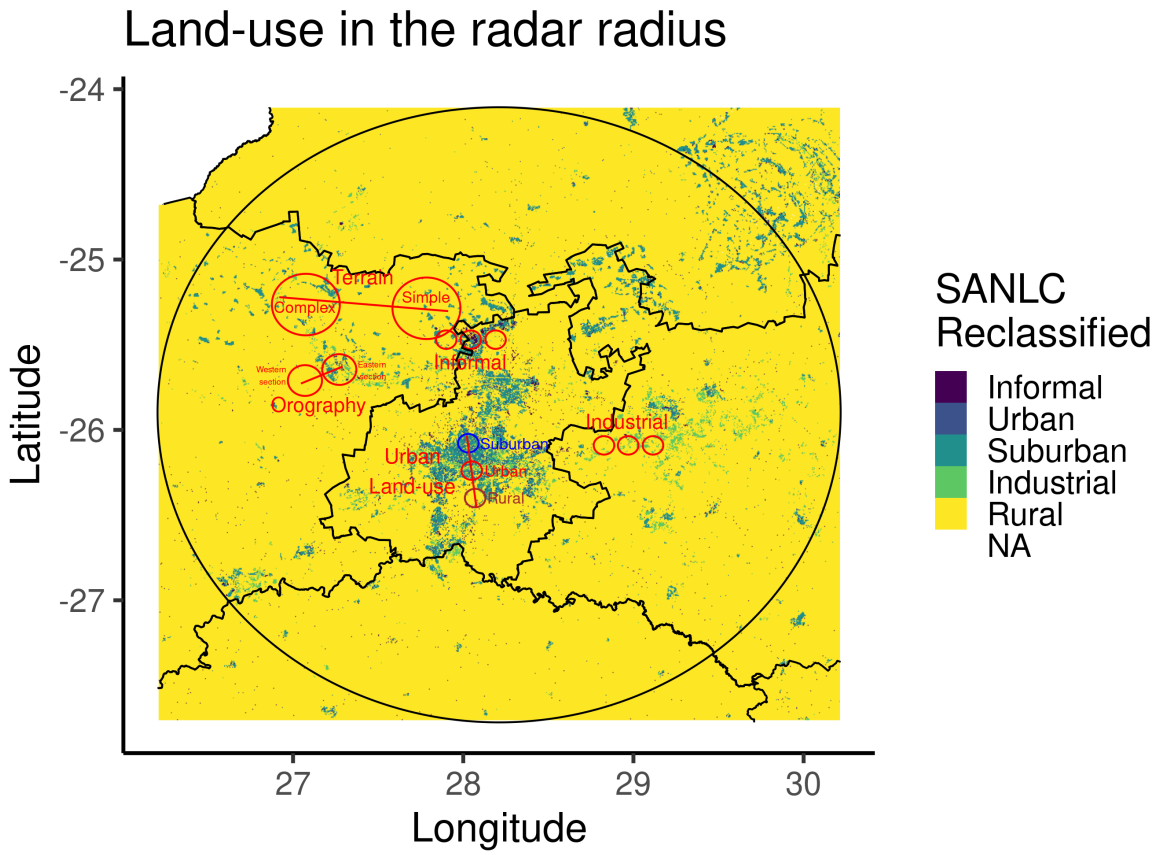

Figure 6.14: *Three areas in the centre of Gauteng are used to study the various characteristics of storms in and around urban areas. The selected areas are also similar to the sections studied in the original Johannesburg Urban Heat Island Project (Garstang et al., 1975; Tyson et al., 1972). north of this area, we examine the impact of informal settlements on storm characteristics. Ga-Rankuwa and the surrounding settlements fall within the central polygon, while we use the eastern and western polygons to examine the storm characteristics in neighbouring this settlement. In Mpumalanga, we apply a similar method where the Kendall power station falls in the centre polygon, and we analyse storm characteristics directly east and west of this site.*

alone has significant implications for cloud properties. The maximum elevation is 1756m, mean elevation 1592m and lowest elevation 1482m. Distinguishing between topographical and pure urban impacts is a difficult task in a region with the complexity of Johannesburg.

The number of data points that falls within the three urban *regions* (rural, urban, suburban) and the land-use categories within these areas is visualized in Figure 6.16. The areas are well-matched to the major region we defined, i.e. in the rural areas, most data points are observed are indeed rural. Figure 6.16a is the rural area, the suburban area is Figure 6.16b, and the urban area Figure 6.16c. The land-use within the city region is mixed-use and this is expected as Johannesburg city has industries, suburbs and parks in the urban area.

The basic NDJFM cloud structure associated with convective weather over the three areas is examined here. In various sections throughout this thesis, cloud top height has been discussed, referring back to the thermodynamic analysis where we saw low freezing levels associated with severe storms (Figure 5.14d), and high cloud tops and radar-derived precipitation rate (Figure 3.8). This emphasises that the height of the cloud top has important implications for precipita-

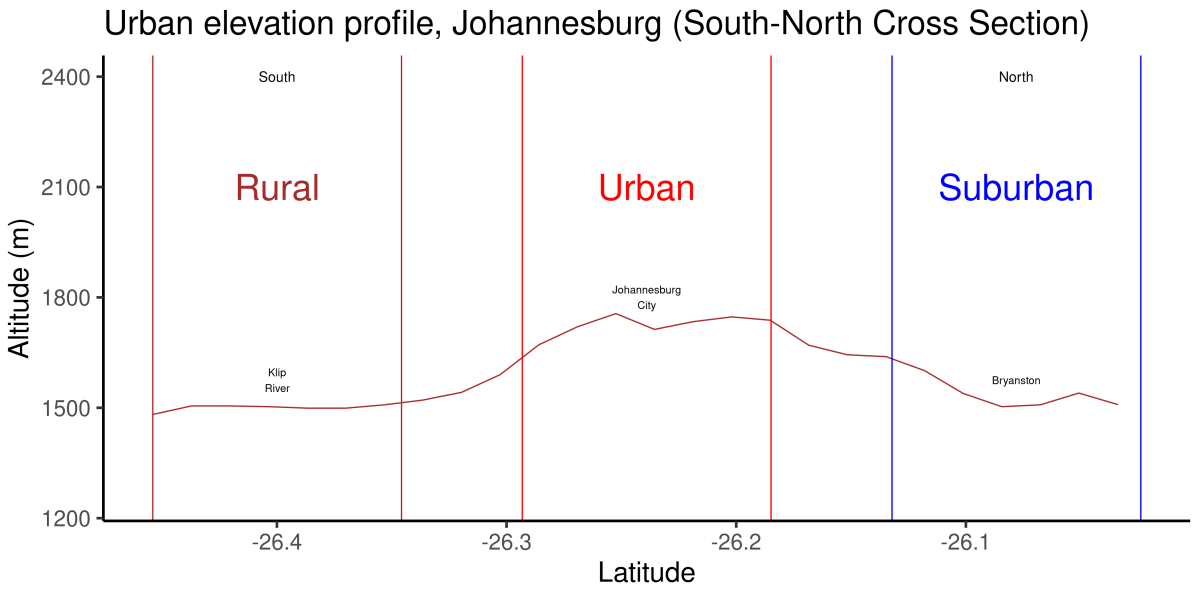

Figure 6.15: *Using the same cross-section as defined during the Johannesburg Heat Island Project, the topography of the region used in the following analysis is shown above. As seen in the previous analysis, complex topography will impact storm characteristics in the region.*

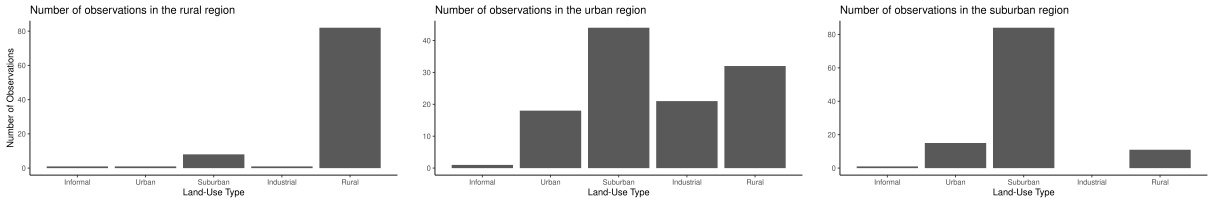

(a) *Rural* **(b)** *Urban* **(c)** *Suburban*

Figure 6.16: *The number of data points that falls into the SANLC for each major area in the urban analysis (rural, urban, and suburban) is shown above.*

tion development. The effect of topography and orography on cloud top is significant (Figure 6.9), and considering Johannesburg topography, we cannot ignore this. However, Figure 6.17 shows a higher density of convective events in urban areas (i.e. more observations). The specific cloud tops do show some degree of variation. The mean cloud top for all regions is 7 km (+-200 m), but the maximum cloud tops observed differs significantly. Over urban areas, we observe tops with a maximum of 15 km (+-100 m), while the suburban area maximum observed cloud tops are 13 km (+-100 m) and over rural areas 11.3 km (+-100 m). A better indication of actual cloud tops is to look at the upper quantile of clouds. In urban areas, the upper quantile is also significantly higher (9.1 km) than all other areas (7.6 km for rural areas and 8.3 km for suburban areas).

It is helpful to examine the reflectivity characteristics of storms over the regions as proximity of severity. In Figure 6.18, we can see changes in the mean of maximum observed dBZ between the different areas. Rural areas have the lowest mean dBZ (40 dBZ) and mean maximum dBZ (49 dBZ). Rural and suburban areas have a higher mean and maximum dBZ values, but these are insignificantly different between the two areas. The mean for urban and suburban areas is 41 dBZ, and the mean of the maximum for both is 56 dBZ. We can, however, see that the highest

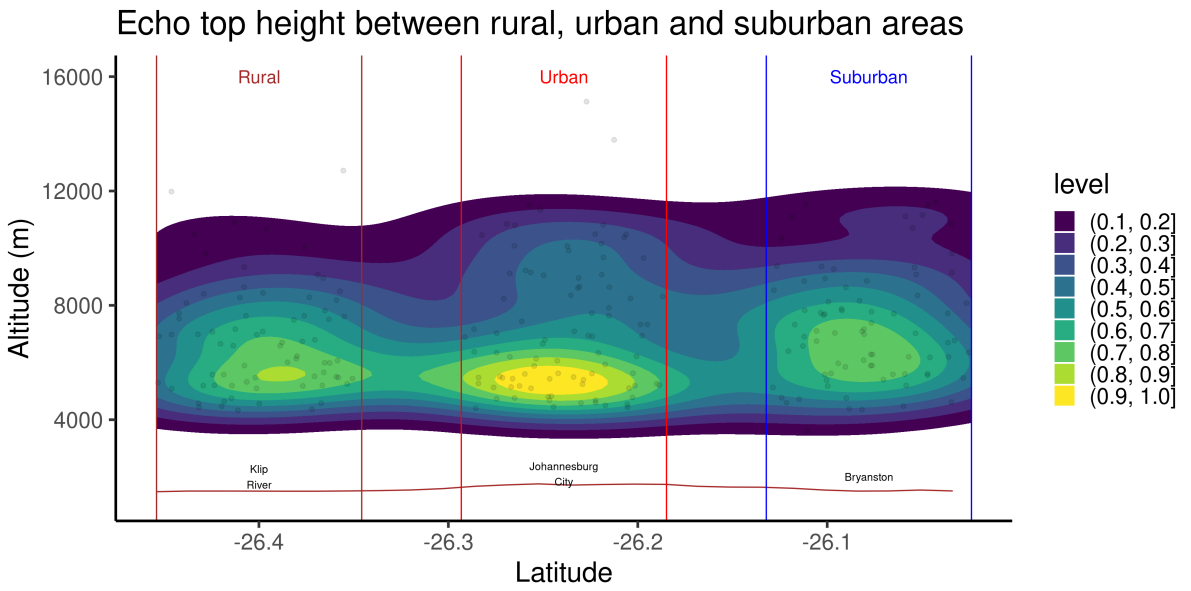

Figure 6.17: *On average the highest cloud tops occur over urban areas, while rural areas have the lowest cloud tops on average. There is also a higher density of events over urban areas. These factors suggest that areas over Johannesburg city might have a higher likelihood of severe weather occurrence.*

single measurement of dBZ is observed over a suburban area. However, we omit this from the discussion here as this section only aims to understand changes on average. Single events, although not necessary outliers, can be anomalies that can occur over any region at random. However, this analysis indicates that rural areas have lower cloud top and lower average mean and maximum dBZ observations than storms in urban and rural areas around Johannesburg.

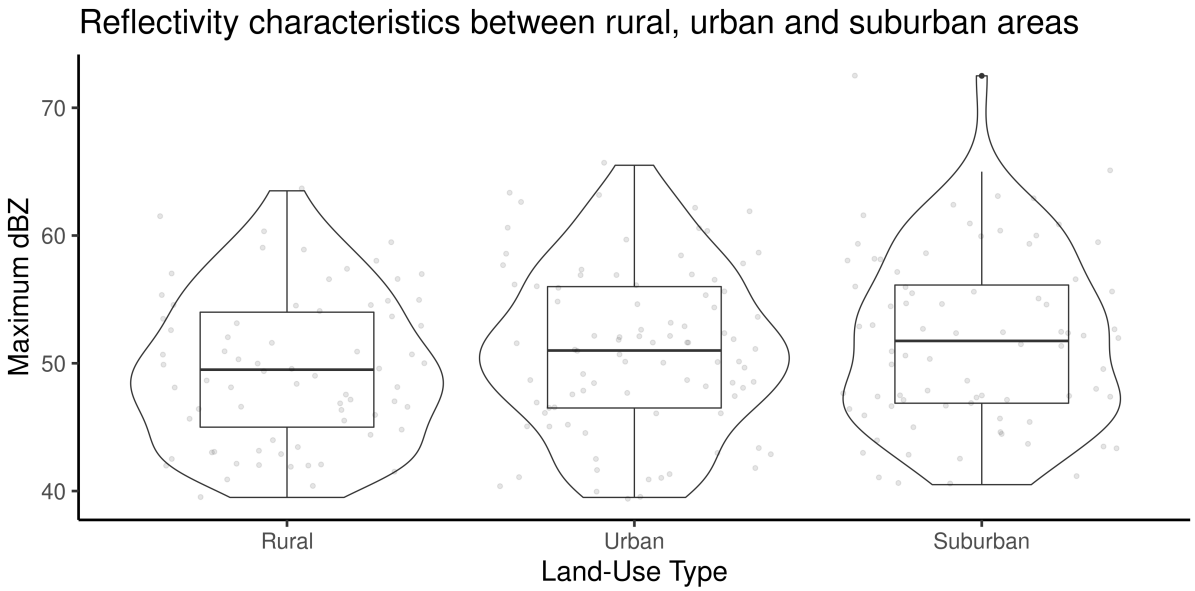

Figure 6.18: *Radar-derived reflectivity indicates that rural areas have less severe storms than urban and suburban areas in the same region if we use maximum reflectivity as proximity for severity. Urban and suburban areas in this study do not show significant differences in the mean of the maximum observed reflectivity and also the mean reflectivity, which is not shown here.*

The rain rate and the maximum observed dBZ show a direct correlation[3] (Figure 6.19). Over rural areas, there are significantly lower rain rates compared to urban and suburban areas which have higher rain rates, and might be more vulnerable to occurrences of flash floods. The impact is amplified as these regions are densely populated, and the amount of infrastructure susceptible to damage is significantly higher.

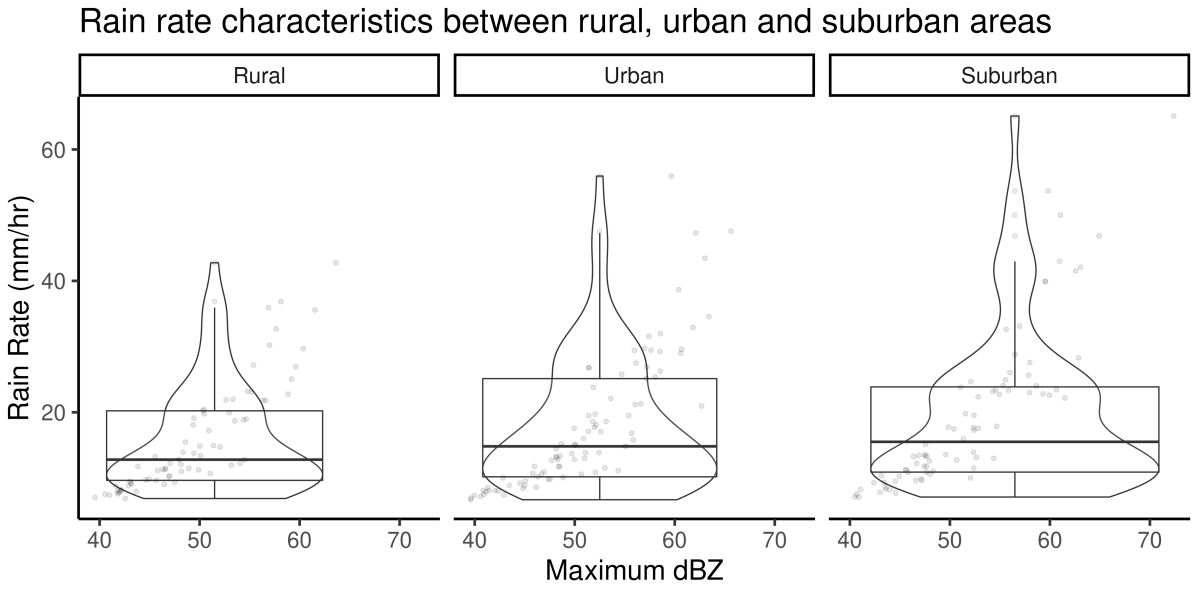

Figure 6.19: *Severe rainfall is, on average, the lowest over rural areas. In contrast, urban and suburban areas over and in the vicinity of Johannesburg have higher rainfall intensities. Considering the population and economic differences between the rural, urban and suburban areas, this increased risk of flash floods and high rainfall has important implications for disaster risk planning.*

The variability of lightning over the three defined areas allows us to validate the above findings, and in Figure 6.20a, our our findings are verified. Rural areas have characteristically lower lightning activity, while urban and suburban areas show a higher cumulative number of lightning events. Figure 6.20b shows that there is, however, natural variability in these events across different months. Over rural areas, there seems to be a higher number of lightning events in March compared to the urban and suburban areas. Storms could possibly initiate over the rural area and grow as it moves over the city and suburban areas. However, natural variably on the scale of convective thunderstorms might result in natural randomness, and it is difficult to make statistical assumptions on the actual impact of land-use on the storm frequency in this case. The cumulative number of events is a better indication that convection is favoured over urban and suburban areas.

In our first analysis of storm dynamics as a function of land-use areas, we examine the characteristics of storms from radar and lightning data in Johannesburg and the surrounding areas. We see that a rural area south of Johannesburg has a lower number of convective events than urban and suburban areas. The Johannesburg area has a complex topography, and as we have seen, this in itself affects storm occurrence. The results show that Johannesburg and the surrounding suburbs have more convective events than rural areas. The advantage of this knowledge can

[3]as a function the Marshall Palmer distribution

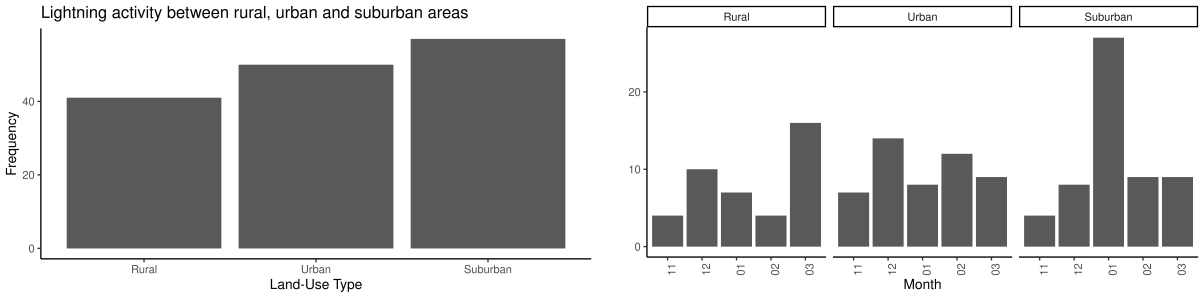

(a) *Cumulative Frequency* **(b)** *NDJFM Frequency*

Figure 6.20: *Lightning observations from the TRMM and ISS missions support radar observations that indicate a higher frequency of convective activity over urban and suburban areas than rural areas. However, the monthly data shows local scale variability means this is not always the case. Rural areas can also have periods with higher lightning activity, i.e. March. However, we assume some randomness on this scale of observation, and the cumulative number of events is a better indication of convective activity.*

help us to target resources into mitigation and risk management in this area differently than we would over the rural areas.

Radar climatology around major informal areas

Within the urban area there are pockets of informal settlements; however, we used a more well-defined (isolated) informal settlement for this analysis to reduce the effects of other land-use categories. If we choose a township close to a major urban area it would have been difficult to make statements about the township area as the urban area might have a significant impact. The selected area marked as informal in Figure 6.14 contains settlements around Ga-Rankuwa (centre circle, with a radius of 6 km) in northern Gauteng. Two circles directly due east and west examine the storm properties in the neighbouring regions for comparison, this is 'informal east' and 'informal west' in the rest of this discussion. The topography in this region is simple, and it is assumed that no significant impact will occur as a result of this, and therefor omit a detailed discussion of the topography here. Explicitly separating informal settlements from the urban areas is essential, not only from a meteorological point of view, but these communities face different challenges when exposed to natural disasters in comparison to the challenges more affluent urban and suburban communities face and less populated rural areas (Mathee et al., 2021; Musungu et al., 2012; Satterthwaite et al., 2020; Scovronick et al., 2015).

The three selected areas are mainly classified as rural (informal west and informal east), while the informal settlement, Ga-Rankuwa, has mixed-use characteristics according to the reclassified SANLC dataset. The west to east orientation of the selected sites around the informal settlement might influence observed storm because the dominant movement of summer storms observed to develop eastward. Other factors might also impact storm dynamics over the informal area. Studies have shown that informal areas have higher than average surface temperatures than suburban areas in a similar region (Hardy and Nel, 2015; Ngulani and Shackleton, 2020; Scott et al., 2017). There are differential local-scale air-pollution characteristics (Hersey et al., 2015; Naidoo et al., 2014) due to various activities, including increased domestic burning and uncovered surfaces in informal settlements. On the scale of convection, these factors may have

an impact on storm dynamics.

This analysis starts by examining the cloud top characteristics over the three regions, this is a good indicator of the general cumulus and storm severity. In Figure 6.21, we can see that storms over the area marked as informal have a lower mean cloud top (6.8km) than the western (7 km) and eastern regions (7.3 km). Interestingly, the western area maximum cloud top is over 2 km lower than both the informal (12.1 km) and informal eastern section (12.9 km). The dominant wind direction could impact observed differences in storm dynamics over the eastern area, assuming the informal area acts as a convective triggering mechanism.

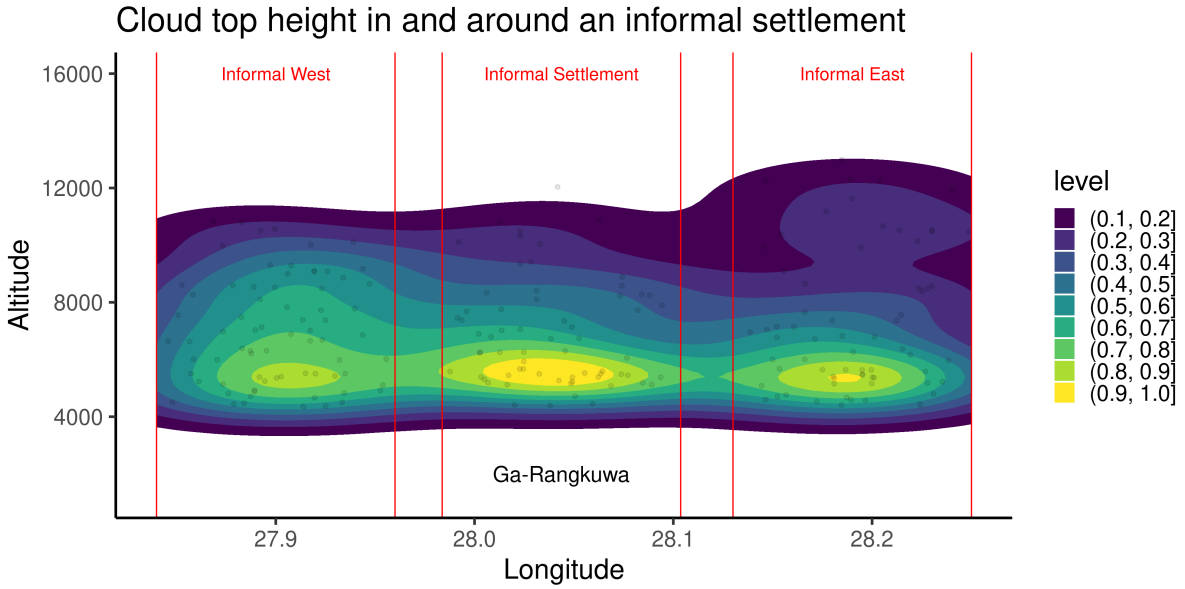

Figure 6.21: *Cloud tops over the informal areas indicate slight differences between the selected areas. Maximum cloud top shows the most significant variation with up to 2 km difference between the informal west (10 km), informal (12.1 km) and informal east (12.9 km) tops.*

The observed maximum dBZ do not indicate many variations between the areas (Figure 6.22). On average, all storms show reflectivity values of 50dBZ (+- .50dBZ). The highest maximum dBZ is, however, recorded over the informal area (70dBZ) in comparison to the western (64dBZ) and eastern (66dBZ) areas. This is surprising as we would expect the eastern area with a higher maximum cloud top and higher mean rain rate, discussed in the next paragraph, to also have higher observed dBZ. Nevertheless, as mentioned earlier, the nature of convection events means that convective events could still occur randomly over any area.

The radar-derived rain rates is examined for the three areas in Figure 6.23. The previous results indicate that the western edges of study sites have less severe storms if we use cloud top and maximum dBZ as a proxy analysis for severe weather, supported by the rain rate analysis. The western area shows 15.5 mm/hr rain rates, while the maximum rain rate is only 47 mm/hr. Over the informal settlement, we see higher rain rates in the mean (17.1 mm/hr), where the maximum rain rate (91 mm/hr) is derived. The eastern section has the highest mean rain rate (17.5 mm/hr), the 3rd quantile (23.2 mm/hr (eastern), 18.6 mm/hr (western) and 20.3 mm/hr (central)), rain rate. The maximum (56 mm/hr) is well below the high value observed over the settlement.

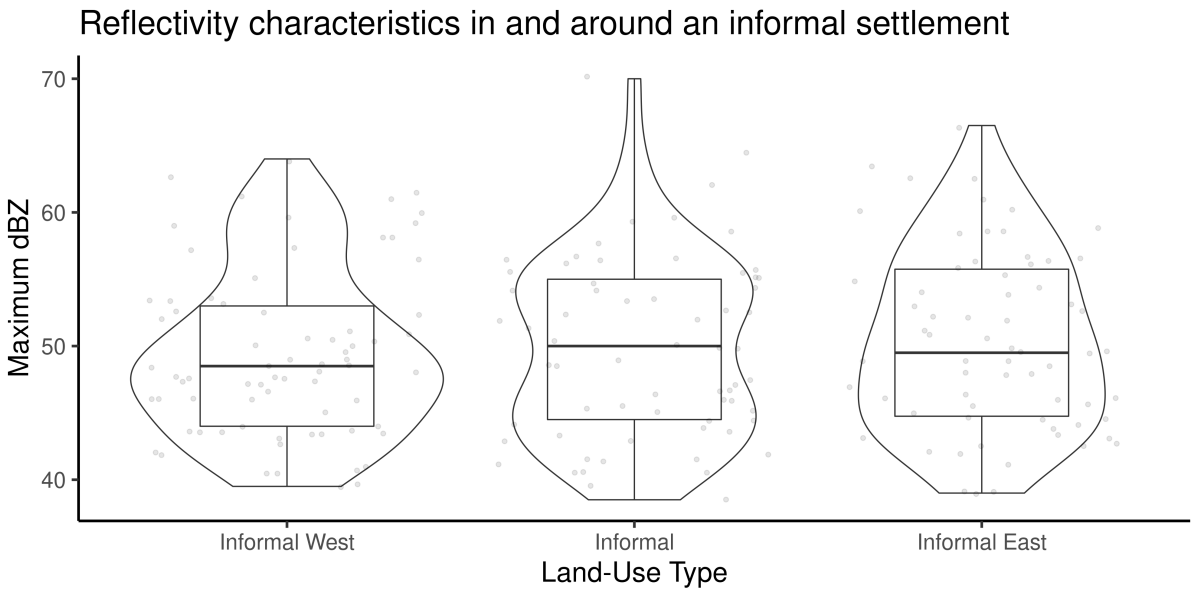

Figure 6.22: *The mean dBZ is similar to the western, central and eastern parts analysed. However, the highest maximum dBZ are observed over the central part, directly above the informal settlement.*

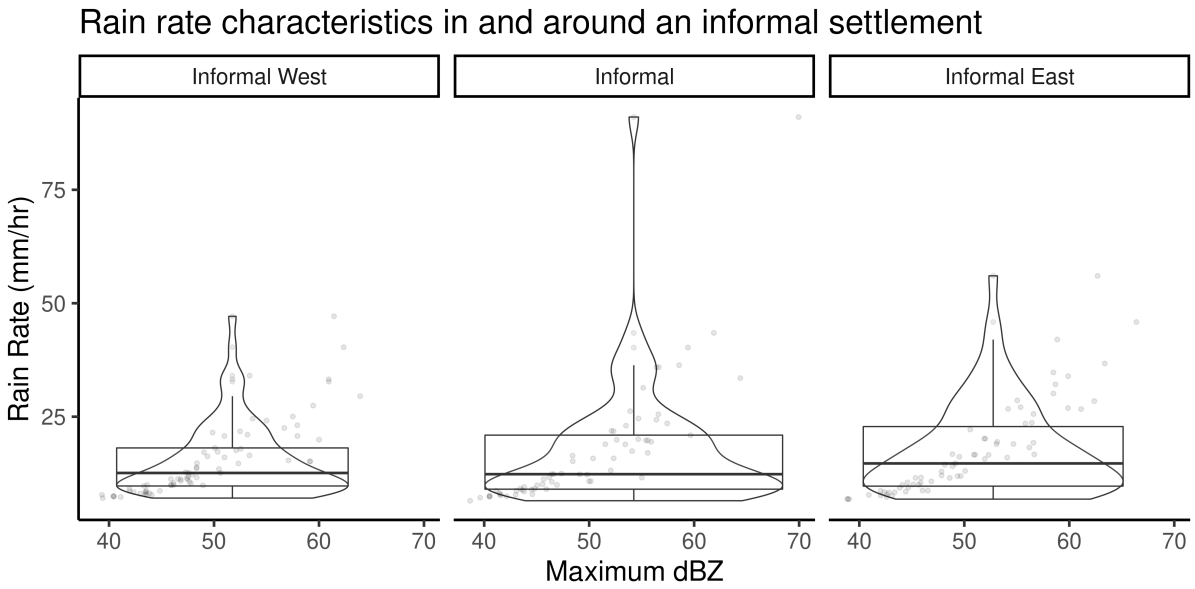

Figure 6.23: *The eastern section of the selected areas has higher rain rates than other sections and the highest observed rate is over Ga-Rankuwa (91 mm/hr). A closer examination reveals that a single event with a maximum dBZ of 70 caused this high derived rain rate, and removing it would show that the eastern section has more severe events in the mean. However, events with reflectivity values over 70 do occur and are not removed.*

Lightning data from the LIS onboard the TRMM and ISS missions show that convection, using lightning as proximity variable, is the highest over the Ga-Rankuwa. Not only is lightning observed here more cumulatively, but apart from November, there is higher lightning activity than in the neighbouring areas during all months. The western area has the second-highest cumulative lightning activity, but this is not significantly less than the eastern region. The monthly lightning activity between the western and eastern regions varies slightly and is also not signif-

icant.

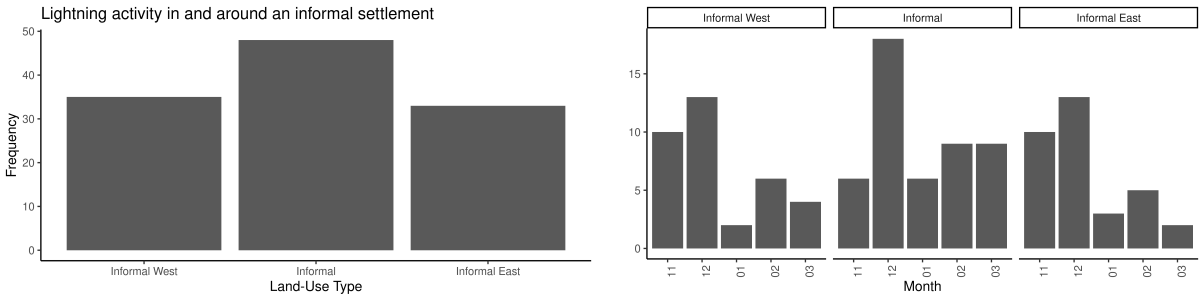

(a) *Cumulative Frequency* **(b)** *NDJFM Frequency*

Figure 6.24: *Data from the LIS aboard the TRMM and ISS missions show that lightning activity is highest directly over the informal settlement. Although the highest single event between the three regions occurred directly over the settlement, the eastern area had, on average, a higher rain rate and cloud top. Differences between the eastern and western sections are, however, marginal and considered insignificant.*

The effects of an informal settlement in the Irene radar range and the possible effects on storm characteristics over, and to the east and west, of the settlement was examined in the above section. Because the topography, as seen in Figure 2.10, is relatively simple across the neighbouring regions, the topographical impact is not examined here. Using several radar-derived variables indicative of storm severity, including cloud top, maximum reflectivity, and rain rate, we show a difference in the mean storm dynamics of each region. At the same time, the means of the variables show that east of the settlement has the highest cloud tops and mean rain rates. We see that the highest maximum values are observed directly over the settlement. We expand the analysis and see that lighting is the highest directly over the informal settlement, with insignificant differences between the eastern and western areas. While it is clear that interactions between storm dynamics and land-use is complex, we can see that even in close proximity, the mean variation of storm characteristics over informal and neighbouring areas is significant.

Radar climatology around major industrial complexes

Similar to the above section, a small area in Western Mpumalanga is isolated to examine the impacts of a major industrial area, in this case, Kendall Power Station, on the cloud properties in the area. The selected area is marked as 'industrial' in Figure 6.14, and the centre circle is located directly above the power station, with a radius of 6 km, while two circles directly east and west of the power station is used to examine the storm characteristics in the neighbouring regions, named 'industrial east' and 'industrial west' in the discussion. It is outside the scope of this study to do a detailed characterisation of the Kendall power station, and the study only provides an overview of the station with a detailed analysis of the local scale rainfall impacts.

Coal-fired power stations such as Kendall constitute a significant source of atmospheric aerosols, including highly hygroscopic particles such as sulfur dioxide (SO_2) (Chidhindi et al., 2019), acting as an important CCN particle (Lee et al., 2012). However, this might also affect the local scale tropospheric thermodynamics (e.g. Tosca et al. (2015) showed how local scale burning increased tropospheric heating therefore decreasing precipitation). The major difference between the current analysis, the urban-rural, and the informal settlement analysis is the concentrated

emissions as a function of the stack height directly over the power station, i.e. emissions released into the PBL. In the case of the Kendall power station, the stack height is 275 m. The general topography around the power station is relatively simple and not examined in further detail.

Figure 6.25 shows the cloud top height directly over the power station. Cloud top height is effectively lower over the power station site (max 12 km), and east (12.8 km) of the power station than west of the site (max 14.3 km). The eastern side has the highest density of events (i.e. the highest number of storms are east (downwind) of the power station).

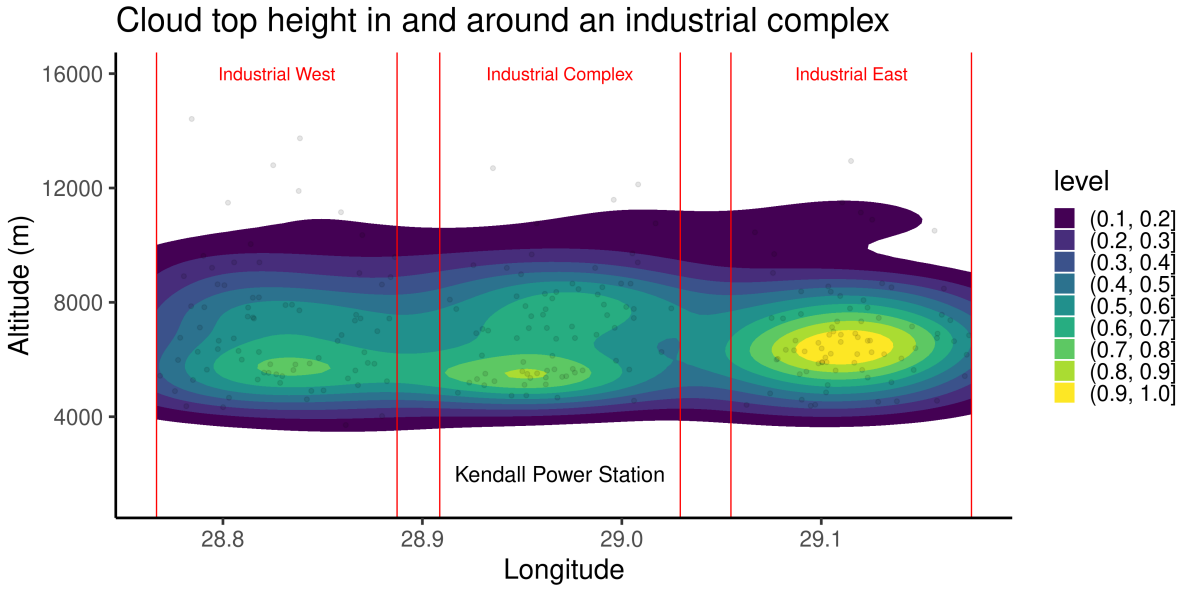

Figure 6.25: *Cloud top height over, east and west of a major industrial complex show different storm characteristics. Directly over the power station, radar-derived tops are the lowest between the selected sites. Due west, the highest tops are observed. East of the power station, we see the highest number of events although these events have lower cloud tops.*

Figure 6.26 indicates that there is storms with higher reflectivity and possibly more severe characteristics west of the industrial site. The maximum dBZ between the western and industrial sites are similar (+-50 dBZ), but the maximum dBZ are significantly higher east (65 dBZ) and west (69 dBZ) of the industrial site (61 dBZ). Mean reflectivity is the lowest east (48dBZ) of the industrial complex. In conclusion, more convective storms are observed west of the industrial site. Over the industrial complex, the least convective storms are observed, and east of the complex, there are more mildly convective storms than the other regions.

It is worth inspecting the mean wind direction over the selected industrial complex. Figure 6.27 shows the mean wind direction is due west (129°), as observed in Figure 3.10 and 6.10c. Interestingly, in Chidhindi et al. (2019)'s receptor modelling analysis around a power station near Kendall, there is not higher observed concentration of pollutants west of the power station. However, convective thunderstorms that are observed with the radar do not represent the mean conditions, but perturbations of the atmospheric mean. Although the exact mechanisms for rainfall enhancement by power stations are not discussed here, the radar data indicates industrial lee side modifications are present.

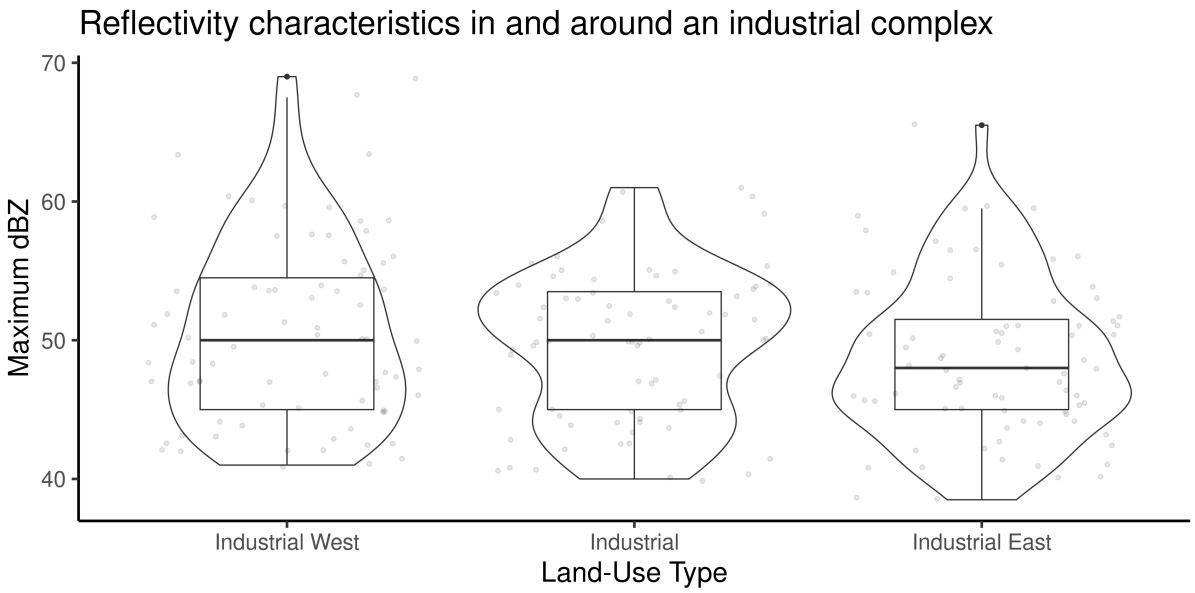

Figure 6.26: *East and west of the industrial site, we see higher maximum observed reflectivity. Although mean reflectivity is similar between the western and industrial sites, the mean reflectivity is the lowest east of the industrial site, but it has the highest number of radar observed storms.*

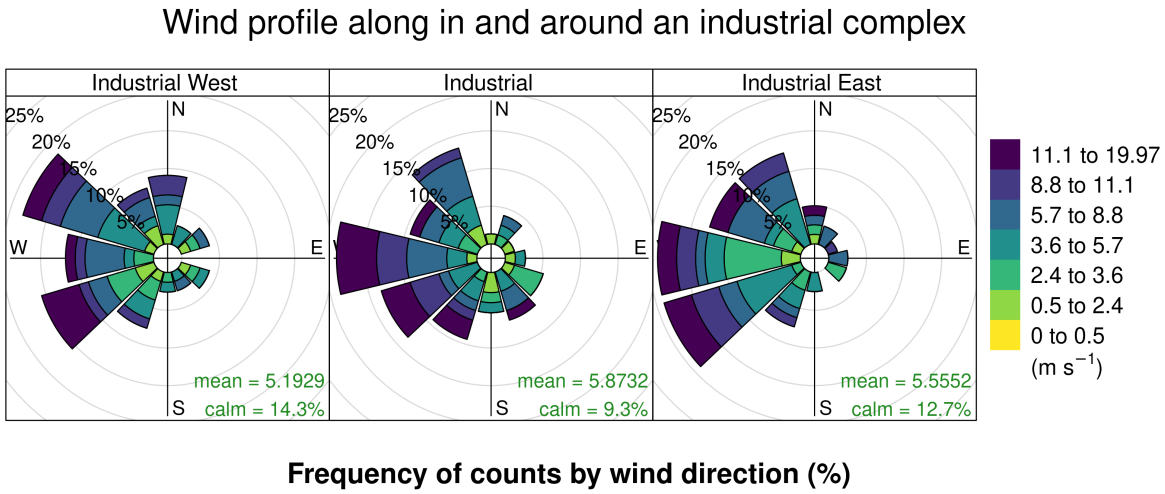

Figure 6.27: *The mean wind direction over the industrial site is shown above. Directly east of the power station, where the highest number of events is observed could be impacted by air pollution dispersion from the effective stack height over the region. Interestingly, there is lower number of storm events and less severe events over the industrial area.*

The mean rain rate over the industrial area is the highest (17 mm/hr) and lowest over the eastern area (14 mm/hr). The western area, as expected, has the highest maximum rain rate, 55 mm/hr, but a lower mean rain rate than the industrial complex. Storms east of the industrial complex are much less severe in the maximum (38 mm/hr), but as noted, this is where the highest frequency of storms are observed, indicating some enhancement of precipitation inhibition or delay in precipitation due to CCN loading downwind of the power station.

Finally, the lightning observations from the industrial and surrounding sites show the highest

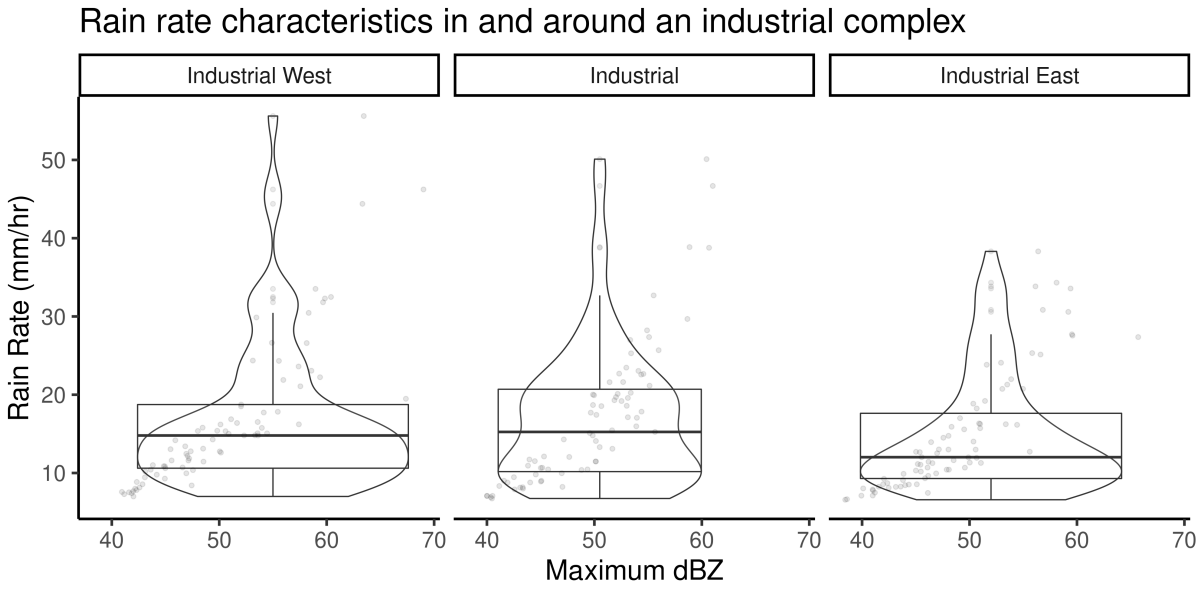

Figure 6.28: *The radar-derived rain rate, as a function of reflectivity, shows the highest mean rain rates west of the industrial complex (55 mm/hr). However, the mean rain rate is the highest over the industrial complex; interestingly, the lowest mean and max rain rate occur east of the power station where the most events are actually observed, indicating a possible convective inhibition process downwind the power station.*

frequency of events due east of the power station, similar to the radar observations (Figure 6.29). What is surprising is that the data contrasts the informal settlement (also east to west analysis), where we see an enhancement of storm activity right above the informal settlement. A detailed analysis of the CCN composition is necessary to explain this. There are other considerations, SO_2 (a highly hygroscopic particle) is released into the boundary layer where dispersion occurs. Individual storm events with increased lightning could impact the accumulated number of events over a region. As a function of the mean winds, this gets dispersed towards the east. This could result in increased CCN particles, smaller droplet concentrations and lower rainfall amounts. This does not necessarily explain why more storms occur east. Surface measurements would aid in the validation of ground precipitation, but within the scope of this study, we show an impact on storm dynamics does occur in the vicinity of an industrial complex (Heinzeller et al., 2016; Kerminen et al., 2012).

The mechanisms by which industrial sites, such as the power station mentioned above, impact aerosols and storm characteristics are incredibly complex. Mean wind direction has an impact on storms on the lee side of the industrial complex, however, the mechanisms are complex (Heinzeller et al., 2016). We attempted to limit natural variability by selecting only a small subset of data in a region, and close to each other. Although we focus subjectively on the aerosol's role as CCN as the main driver of storm occurrence, we cannot discount that the downwind aerosols might also result in tropospheric heating, which acts as a possible convection inhibitor is known to happen around fires (Tosca et al., 2015).

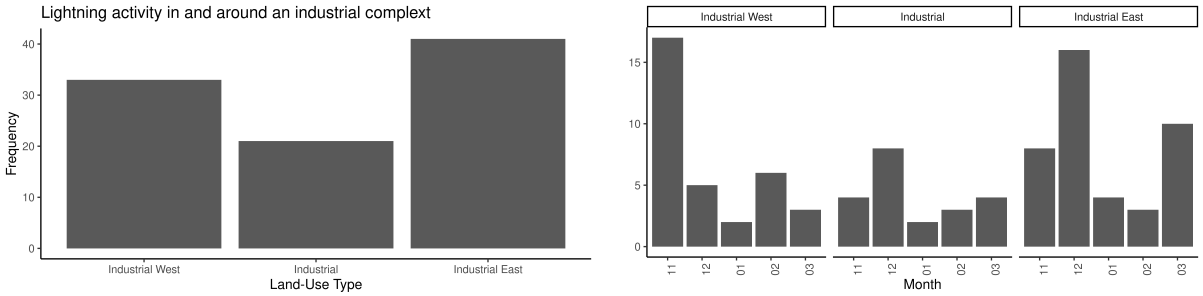

(a) *Cumulative Frequency* **(b)** *NDJFM Frequency*

Figure 6.29: *Lightning data from TRMM and ISS supports the above findings. The least number of storm events occur over industrial complexes. East of the industrial complex, we see the highest number of storms.*

Conclusion

In this chapter, the second objective of this study, i.e. ***Evaluating local scale anthropogenic and non-anthropogenic impacts on convective events***, is addressed. We examined this question using radar data from the Irene S-Band radar located in central Gauteng and supplemented this with lighting data from the LIS sensor onboard the TRMM and ISS missions. The SANLC dataset is applied in the land-use data analysis. The dataset initially contained 73 land-use categories and we reclassified them into five sensible categories for this analysis, i.e. rural, urban, suburban, informal, and industrial.

Regional climatology plays a significant part in storm occurrence within the radar range. We could not assume that a simple analysis of all the data within the radar range would yield meaningful results that apply to the general area. Secondly, the topography within the radar range varies vastly, from the high plateaus in the south to the varied terrain with mountain ranges in the North-West province. As a result of these observations, we first posed several questions related to topography and regional climatology by sub-setting various areas in the radar range in the hope of minimising biases that would occur if we examine the whole dataset as uniform. The first question we posed was, *what is the difference between simple and complex topography on storm dynamics?*. We chose two areas in close proximity to each other, one over flat terrain and one over the Pilanesberg area. We found that complex terrain enhances convective processes, most likely by orographic effects. Over complex terrain, higher cloud tops, higher mean and max dBZ, and a higher number of radar events was observed. This was supported by the lightning data, which indicated a higher number of lightning occurrences over the area. Chapter 3 discusses the occurrence of isolated events being mainly a mid-summer occurrence and in my opinion this is somewhat reflected in the lower lightning counts observed in January.

We examined *the impact of an orographic feature on the characteristics of storms*. Here, neighbouring storms to the west and east of the Magaliesberg mountain range was specifically examined. We found that the mountain range, although small, showed differing storms in each of the regions. The mean westerly wind direction played a role, and radar-derived storm dynamics indicate that although we experience storms with severe characteristics on the mountain's western side, more storms, albeit less severe, occur more frequently on the eastern (lee side) of the mountain.

Lightning data indicated a similar result. Although we cannot examine severity from the lightning data, there was more events on the lee side of the mountain. These two questions made it clear that any analysis on storm dynamics is highly complex, and separating small scale land-use from topography and orography is difficult.

After this, and with the knowledge of the topographical complexities, we examined the land-use impacts on storm dynamics. Similar to the first analysis, we broke down the data into various subsets to avoid various biases. The first bias was that the number of data points within the rural category far outweighed any other category because most of the area inside the radar range is rural. The second was finding areas most representative of informal, urban, suburban, and industrial areas. Each of these had to be analysed to remove any climatology bias and be close enough to make a valid comparison. We decided to break the analysis down into 1) rural-urban-suburban, 2) informal and neighbouring, and 3) industrial and neighbouring. In the rural-urban-suburban analysis, we examined the region around Johannesburg. We found an observable difference between storms due south, mainly within the rural area, compared to the urban and suburban areas. The latter shows indications that storms over urban and suburban areas are more severe and frequent; however, Johannesburg also has a complex topography making a conclusion about the sole impact of land-use complex. It was necessary to examine a large informal settlement and isolate its impacts to avoid any urban bias. Here we examined the impact of Ga-Rankuwa in northern Gauteng and an area directly east and west of it. Radar and lightning data showed indications of a higher frequency and more severe events directly over the settlement.

Finally, we isolated an area directly over the Kendall power station in Mpumalanga and examined storm characteristics directly east and west of this site. We once again chose this site to limit any urban or informal bias. The site also has a reasonably simple topography. Both radar and lightning derived data showed a lower number of events directly over the power station, and higher number of events east and west of the power station. Highly hygroscopic SO_2, could impact cloud characteristics downwind by increasing smaller droplet number concentration, decreasing droplet size and decreasing rainfall intensity.

The radar data used has various uncertainties that have to be taken into consideration. This uncertainty can be a function of topography, elevation, beam depletion, calibration, interference, and mechanical issues. In the above section, we assumed the impacts of topography was minimal, and due to the location of all the selected sites near Irene Radar, some issues would be avoided. The further the event being studied is, i.e. at the edge of the radar range, the more likely uncertainties accumulate. This is why modelling offers us a way to understand events on various scales, even with the added uncertainty of erroneous initial conditions. We can run and rerun a model various times with the benefit of changing and adapting the physical parameters.

On the scale of convection, we can consider a variety of impacts, on various scales, that affect storm characteristics. Our attempt to isolate these as a function of natural or artificial surface characteristics did not yield any single significant, easily quantifiable impact on storms over various areas. Instead, the answer is, it is complex. In the final section of this study, we examine the impact of aerosols on the cloud microphysics of a convective event over the Highveld by using an NWP and changing the aerosol composition and land-use characteristics. This allows

us to examine the impacts of aerosols under various pollution scenarios to better understand the small scale impacts in addition to the above analysis.

Chapter 7
CCN and land-use impacts on convective weather

"Models have their own particular problems that may rival those associated with estimating natural variability from real data, but they do offer an opportunity for a controlled experiment..."
Madden (1983)'s reply to critique on his Madden (1976) paper

In the previous sections the study showed that convective thunderstorms are highly sensitive to changes in land-use and topography even when in close proximity to each other. The next section builds on this knowledge and examines the changes in modelled storm dynamics and physics by running a high resolution, convective permitting simulation of a severe thunderstorm over the Johannesburg area. A new aerosol-aware parameterisation scheme is applied and we change the CCN concentration and land-use characteristics in the model to examine the effects on storm properties over Johannesburg.

Introduction

This final chapter, examines the impacts of varying CCN concentrations on severe convective weather using CPM scale NWP. WRF is used to simulate a severe case study on CPM scale where the land-use and CCN concentration is altered to examine changes in storm dynamics. The added value of CPM simulations has been discussed in Chapter 1 and in this introduction, a review some work related to CPM simulations in southern Africa is touched on. While the field of NWP has been well established since the mid 20th century, various limitations have existed. At first, observations (required to initialise models) and computation resources were limited (Bauer et al., 2015). Lewis Fry Richardson's original solution proposed a human forecast factory (Charlton-Perez and Dacre, 2011; Lynch, 2008). With time, computational resources became available, advanced observational platforms was easily accessible and systems became more reliable and accessible even in the most remote places of the world. These advances allowed accurate and timely initial conditions to NWP which improved numerical forecasts (Bauer et al., 2015). Still, some significant uncertainties exist as a function of parameterisation schemes used to represent various processes and improve model runtime. In the last decade, improvements in computing power and affordability, have allowed us some degree of freedom away from parameterisation schemes and the explicit simulation of convection, i.e. CPM (Pal et al., 2019; Prein et al., 2015, 2013).

CPM in SA and southern Africa, is still in its infancy. The first CPM simulations were conducted in 2015-2016 (Havenga, 2018) where five hail events over Gauteng were simulated with convection parameterisation turned off using WRF. We evaluated the modelled thermodynamics with Irene soundings and the results in this study were promising. WRF as a CPM captured diurnal

evolution of convection well over Gauteng. More recently, Engelbrecht et al. (2021); Keat et al. (2019); Stein et al. (2019) evaluated CPM using the MetUM model to simulate rainfall over SA. All three studies showed a marked improvement in the representation of precipitation over the region. However, the timing of convective initiation still remains a challenge in the model as noted by Keat et al. (2019); Stein et al. (2019). The drawback of the MetUM model is accessibility, an advantage of community models such as WRF. CPM simulations in southern Africa using WRF is not that common, although as noted by Bopape et al. (2019), WRF and Consortium for Small-scale Modeling (COSMO) are the two most used models in the region, after they surveyed various meteorological agencies in Africa. While many papers have explored the value of WRF for understanding meteorological processes and evaluated various parameterisation schemes (Crétat et al., 2012; De Lange et al., 2021a,b; Kuik et al., 2015; Maisha, 2014; Ratna et al., 2014) for southern Africa, only a few did so on CPM scale as seen in Molongwane et al. (2020); Somses et al. (2020). While various processes require parameterisation, there is indeed *added value* (Prein et al., 2013) in CPM simulations, as we will see in this study. The evaluations of parameterisation schemes are essential. However, the goal of this section is not to evaluate parameterisations schemes as this falls outside the scope of this study. Instead, we use WRF to capture storm day dynamics reasonably well and then alter the physics options to evaluate the variation from the typical dynamics as a function of land-use and CCN changes. Understanding the explicit impact of increased CCN and land-use changes will provide us with a valuable overview of the local scale changes storm dynamics.

Case study overview

Still recognised as the most costly hail event over SA, the November 28, 2013 hailstorm caused over ZAR 1 billion in damages, the most significant single-day loss for insurers. The event was well documented in media (Barry, 2014; Eliseev, 2013; Eye Witness News, 2013; Makhubu et al., 2013; Rahlaga, 2013; Sawdis, 2013), and scientific publications, (Ayob, 2019; Dyson et al., 2021; Havenga, 2018; Powell and Burger, 2014). Following the original METROMEX experiments methodology for the event day, we describe the:

- Synoptic weather conditions
  The dominating synoptic weather pattern over the subcontinent is examined and described using ERA5 reanalysis data (also used in the severe storm environments section).
- Precipitation processes
  The dominant precipitation process will be described from observations and also media reports.
- Surface and remote sensing measurements
  All storm day measurements will be examined to understand the local scale characteristics of the storm day; this includes radar data, surface observations (i.e. AWS), and radiosonde data. There must be a complete 24h radar scan and radiosonde data preceding - and after the event for a case to be considered.

- Case simulations
  All the aspects mentioned above are examined and detailed here. The storms are then simulated in WRF, where anthropogenic effects are incorporated and examined.

This study's scope is not to validate WRF and its various parameterisation schemes for operational use. We run idealised scenarios to examine the physical and dynamic changes in severe weather based on subjective changes in the CCN concentration (i.e. business as usual to worst-case). In the control run the case study and the model's ability to simulate the event with reasonable accuracy is detailed, and this run will form the basis of the modified simulations.

Synoptic weather conditions

Figure 7.1 shows the synoptic-scale circulation that was dominant over the subcontinent on November 28, 2013. On the surface, MSLP isobars from the ERA5 reanalysis data show a ridging anticyclone over the east coast of SA, while a well-defined continental tropical low wave was present in the northwest of central SA. Both these systems resulted in an influx of surface moisture from the warm Indian Ocean originating from tropical flow (←)[1] and the ITCZ, originating from north-easterly flow (↙), respectively. ERA5 cloud cover and the Meteosat infrared (IR) images (Figure 7.1a and b) show a tropical-extra tropical cloud band, or TTT, present. The TTT indicates the advection of moist air from the ITCZ, providing ample surface and low-level moisture when convection initiation occurred. Strong pressure gradients over central SA between the ridging high and the continental tropical low would have resulted in large scale mixing of air masses on the surface along the pressure gradient. At 500hPa, we can see that the trailing edge of a 500hPa trough was present over SA, driving the ridging anticyclone eastwards to extend over the eastern seaboard[2], Similarly, the flow at 500hPa would enhance rotation and the temperature gradient of the atmosphere, the impact of the westerly flow also enhances the freezing of hydrometeors. The freezing is also highly correlated with hail events as discussed in Figure 5.15). Furthermore, Figure 7.1a and b show that the new generation ERA5 data captures the synoptic scale features well (i.e. TTT) in comparison with the Meteosat data.

The performance of ERA5 data is even more evident on a lower scale. In Figure 7.1c and d, localised instability over central SA was reasonably low during the storm day (a detailed look into the localised thermodynamics will follow after this section). The thermodynamic diagram shown in Figure 7.1d is an overlay of the storm day vertical profile data from ERA5 (red and blue) and actual storm day observations (green and orange). Here we can see that the new generation of ERA5 data captures the vertical changes in the atmosphere with reasonable accuracy.

Local scale characteristics

Only one sounding for the storm day is available and was launched at 0900 UTC (1100 SAST) (Figure 7.2). The hodograph indicates surface winds from the north-east (↙) at the time of the sounding. This tropical flow results in the advection of moist tropical air along the strong pressure gradient. The hodograph indicates a strong rotational component in the lower levels

[1] ←indicates the direction the wind originates from
[2] under stable conditions, the South Atlantic High-pressure is located due west of Namibia

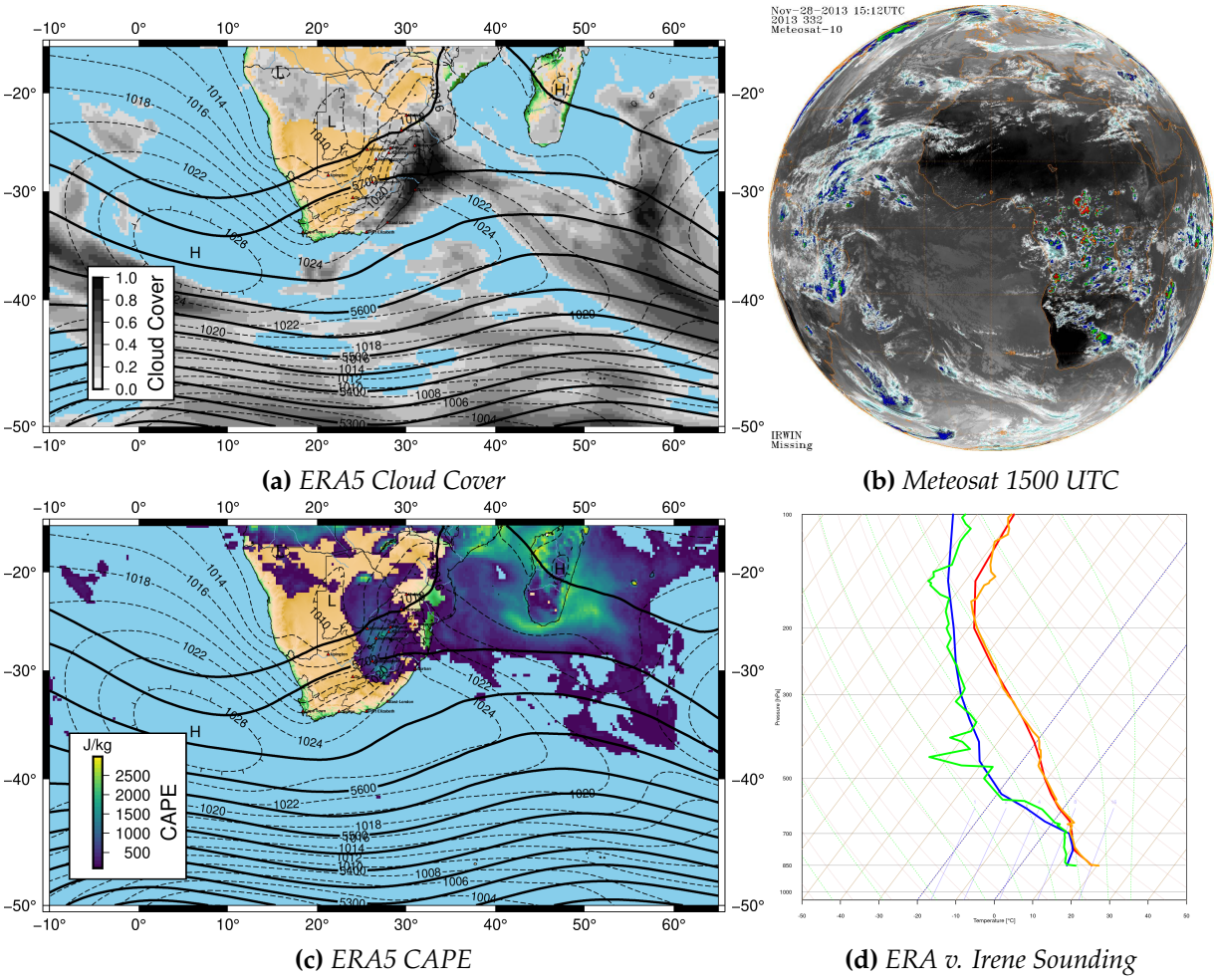

(a) *ERA5 Cloud Cover* **(b)** *Meteosat 1500 UTC*

(c) *ERA5 CAPE* **(d)** *ERA v. Irene Sounding*

Figure 7.1: *The above diagrams show the circulation dominant over SA during the country's most expensive storm day to date. Several distinct surface and upper-air features created conditions ideal for thunderstorm development and sustainability. A ridging high-pressure over the eastern seaboard and an continental tropical low extending over Botswana was observed at the surface (a, b and c). Both systems resulted in the surface advection of moist air from the Indian Ocean and ITCZ, respectively, apparent from the TTTseen in a and b. At 500hPa, the trailing end of a westerly wave trough was visible, creating cold upper-air conditions and enhancing the ice process. The differential winds between the surface and the 500hPa level would also favour rotation with increased height. A strong pressure gradient was observed across central SA, where CAPE over 2000 J/kg was observed (c). All in all, an abundance of low-level moisture, strong westerly flow at 500 hPa and strong pressure gradients created an ideal environment for enhanced uplift and rotation.*

(0-3 km) and bulk shear values of 14 m/s was observed. Similar to the mean shear described in Figure 5.18 for severe events. storm relative helicity (SRH) between 0-3 km indicated relatively strong rotation ($240 m^2/s^2$) associated with non-tornadic storms (Doswell and Evans, 2003; Moller et al., 1994). This rotational component favours fast-moving, rotation convective storms. In the upper air from 3 km and above, the dominant westerly flow ($\rightarrow$) is observed. The westerlies in the upper air were of extra-tropical origin, enhancing conditional instability and hail formation as a function of the lower freezing level (Figure 5.15).

In this paragraph the thermodynamic profile of the storm day is discussed. Thermodynamically, the event day was a typical summer day with a chance of thunderstorms, as is common

during early summer. CAPE values were high at 1727 J/k, high enough to indicate possible thunderstorm development. Interestingly CIN was 0 at the time of the sounding. Case studies from other regions of the world tell us that some CIN, that are caused by low-level inversions, are essential for storm development (Groenemeijer and Van Delden, 2007; Sherburn and Parker, 2014). Other thermodynamic indices also indicated possible thunderstorm development. The Significant Hail Parameter (SHIP), which is a function of CAPE, the lapse rate between 700-500 hPa and wind shear (Allen et al., 2015; Schemm et al., 2016; Tang et al., 2019), developed by NOAA to distinguish between small and large (>2 cm) hail, indicated the possibility of small hail with a value of 0.9 on this day. SHIP values over 1 are associated with hail > 2 cm in the USA.

The Supercell Composite Parameter (SCP) (Rae, 2014; Thompson et al., 2003), calculated as a function of CAPE, SRH between 0-3 km and wind shear, similarly indicated an environment favouring marginal rotation and instability. SCP values over 1 favour supercells, while severe rotating supercells associated with tornadoes have values over 4. Significant Tornado Parameter (STP) calculated as a function of CAPE, SRH and LCL, showed conditions favouring marginal rotation (Thompson et al., 2003). Apart from the 0 CIN value, all indices showed conditions favouring thunderstorm development. The thermodynamic parameters underestimated instability on the storm day, but this could be a function of the location and time of the Irene sounding in proximity to the areas of the highest instability. This fact highlights the spatial limitation of radiosonde, which was located far away from the area of most severe convection. There was an advantage of the Irene sounding location in this case as it provided us with information on the pre-convective environment and the storm inflow area.

As indicated in Figure 7.3, the highest accumulated 1 hour precipitation occurred over Johannesburg Botanical Gardens and Springs at 1400 UTC and 1500 UTC (1600 SAST and 1700 SAST). At both sites, over 10 mm accumulated precipitation was measured for the hour. The Irene station, where the sounding was located, had the lowest accumulated rain rate. Pretoria had peak accumulated rainfall at 1600 UTC (1800 SAST), as the storm moved towards the northern parts of Gauteng. In addition to the surface stations, social media provided a real-time report of the storm path from citizens affected. Eye Witness News (2013) contains various posts of damage in the greater Johannesburg area. Most reports were shared between 1500 and 1600 UTC (1700 SAST and 1800 SAST) on Twitter. Hail pictures from Johannesburg showed tennis ball sized hail, while users from other areas, such as Pretoria, shared images of smaller, golf ball sized hail.

Radar data from the Irene S-Band Radar provides the most detailed spatial-temporal observation of the storm. Further enhancements to the default TITAN algorithm is included here by incorporating the Irene sounding data into TITAN to improve the freezing level and winds aloft estimation. While the main benefit is improved tracking for now-casting purposes, we use it to improve storm day, radar-derived statistics. Currently, there is no indication in the literature that daily sounding is included in the SAWS TITAN algorithms.

Morning conditions, as seen in Figure 7.4 and 7.5, were calm directly over Johannesburg. There were convective storms developing to the north-east and south-east of the area of interest in the early morning. These storms mostly propagated north-east. By 1000 UTC (1200 SAST),

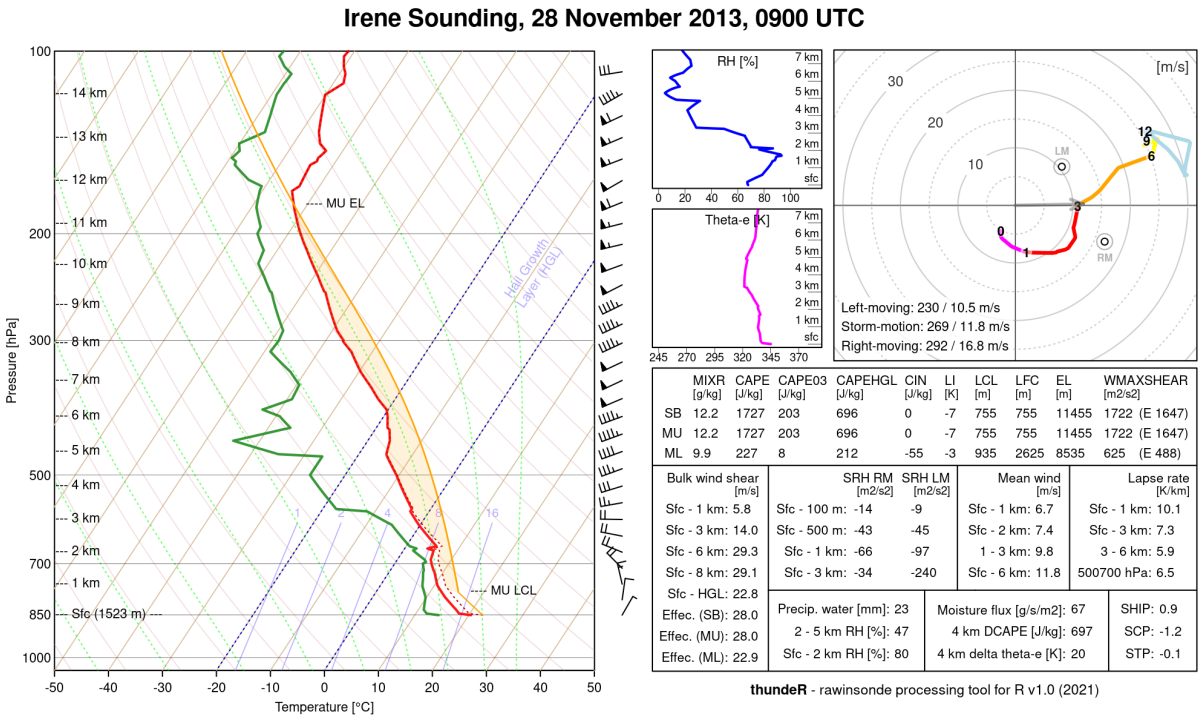

Figure 7.2: *The radiosonde data seen in the figure was collected at 0900 UTC on the storm day (1200 SAST). This sounding was not located within the immediate proximity of the storm but provided valuable information on the pre-convective environment. Severe storm indices such as CAPE and SRH indicated unstable conditions for the development of thunderstorms. Wind shear indicated rotation near the surface, while the upper air at 500hPa had a strong westerly component, both ideal for sustained thunderstorm events.*

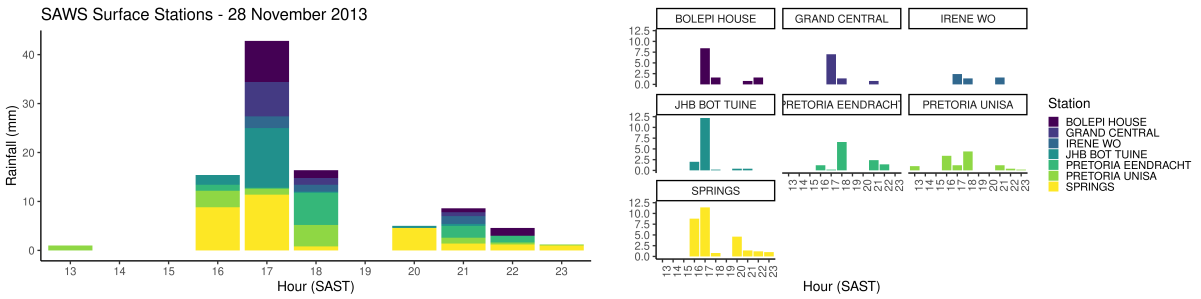

Figure 7.3: *SAWS weather stations in the vicinity of the storm showed peak accumulated hourly rainfall of over 10 mm at stations in Johannesburg and Springs at 1400 UTC and 1500 UTC. Stations north of these sites in Pretoria had significantly less rainfall, peaking about an hour later as the storm moved north.*

the first radar returns were observed due south-west of Irene, in the northern Free State. The maximum reflectivity was 67 dBZ and the storms speed was 14 m/s with a due 83°(east-north-east) heading (wind direction was 276°from the west). By 1100 UTC large areas with over 65 dBZ were visible in the volume scans, with mean storm speeds over 22 m/s, heading 66°(north-east), towards Gauteng.

By 1200 UTC, mean storm speed had increased to 24 m/s and cloud tops over 15 km were observed. Radar-derived hail mass aloft (kilotons) was above 140 k/tons, in the vicinity of Vereeniging. Mean storm motion stayed due east for the duration of the event, while storm

speed continued to increase up to a maximum mean of 29 m/s at 1600 UTC. The mean reflectivity between 1200 UTC and 1600 UTC was well over 50 dBZ during all scans, with maximum reflectivity of 75 dBZ observed during various scans between 1400 UTC and 1600 UTC when most of the severe hail reports occurred. During this time, the cloud top height was 16 km, but was possibly higher due to radar scan limitations. The height of the recorded maximum dBZ were at a 8 km, between 1300 UTC and 1400 UTC. The highest mean dBZ for the event day were only recorded 5 hours later at 1900 UTC. The height of the maximum dBZ plays a vital role in understanding the precipitation process, more so than just the overall dBZ. This is already known from the previously discussed FOKR index and can be observed here.

Further investigation of the radar data shows a strong Weak Echo Region (WER) in the inflow area at 1300 UTC close to Johannesburg. This is expected as the maximum WER will be most pronounced when hail mass aloft, as a function of the updraft strength, is at a maximum before significant precipitation occurs. This WER can be seen in Figure 7.7. Other radar derived severe storm indicators, such as the locally developed SSS, developed by Visser (2001), were also accurate in the prediction of severe storm regions. The SSS proves to be a handy operational indicator in severe storms as it takes into account the 3-dimensional structure of the storm. In contrast, the traditional radar display typically shows a 2-dimensional volume scan and users manually examine the reflectivity characteristics at various levels. The latter proves time-consuming in a high-pressure environment considering the lifetime of a typical thunderstorm at one point is less than 20 minutes (Wilson et al., 1998). On this day, Visser (2001)'s SSS accurately represented areas where dBZ were above 55 and most Vertically Integrated Liquid (VIL) above 6 km. The advantage was that no vertical sections needed to be examined and thus storm vertical structure could quickly be inferred. The SSS also allowed us to see that the most severe regions were on the storm's western flank. The inflow region to the north-east had a moderate severity rating, with hydrometeors distributed equally throughout the storm's mid-levels.

On November 28, 2013, Gauteng residents, particularly in Johannesburg, fell victim to one of the most devastating hailstorms ever recorded. The storm accured over ZAR 1.3 billion in damages. While the storm was unavoidable, accurate, seamless prediction across scales and targeted forecasts and warnings could have reduced damage in ideal circumstances. To improve this seamless forecasting across scales, especially for thunderstorm events, high-resolution numerical models have to be used operationally with accurate and timely initiation. Predictions and warnings can only be improved if the initial conditions driving the model are adequate. What should also be considered is the dynamical and physical effects of smaller-scale features, typically parameterised. The storm day radar data made it clear that a severe storm was developing and already damaging before it reached the greater Johannesburg area. The largest cell over 70 dBZ only developed once the storm was directly over urban areas (see 1400 UTC and 1500 UTC over Krugersdorp and the West Rand). Although randomness cannot be discounted, understanding and possibly implementing aerosol schemes and high-resolution land-use schemes can assist us in understanding the changes in storm dynamics. The November 28 event is an ideal case study due to the occurrence over a massive urban region and the availability of high-resolution data for comparison with model data. The following section runs several case studies of the November 28 event under varying conditions to examine these changes.

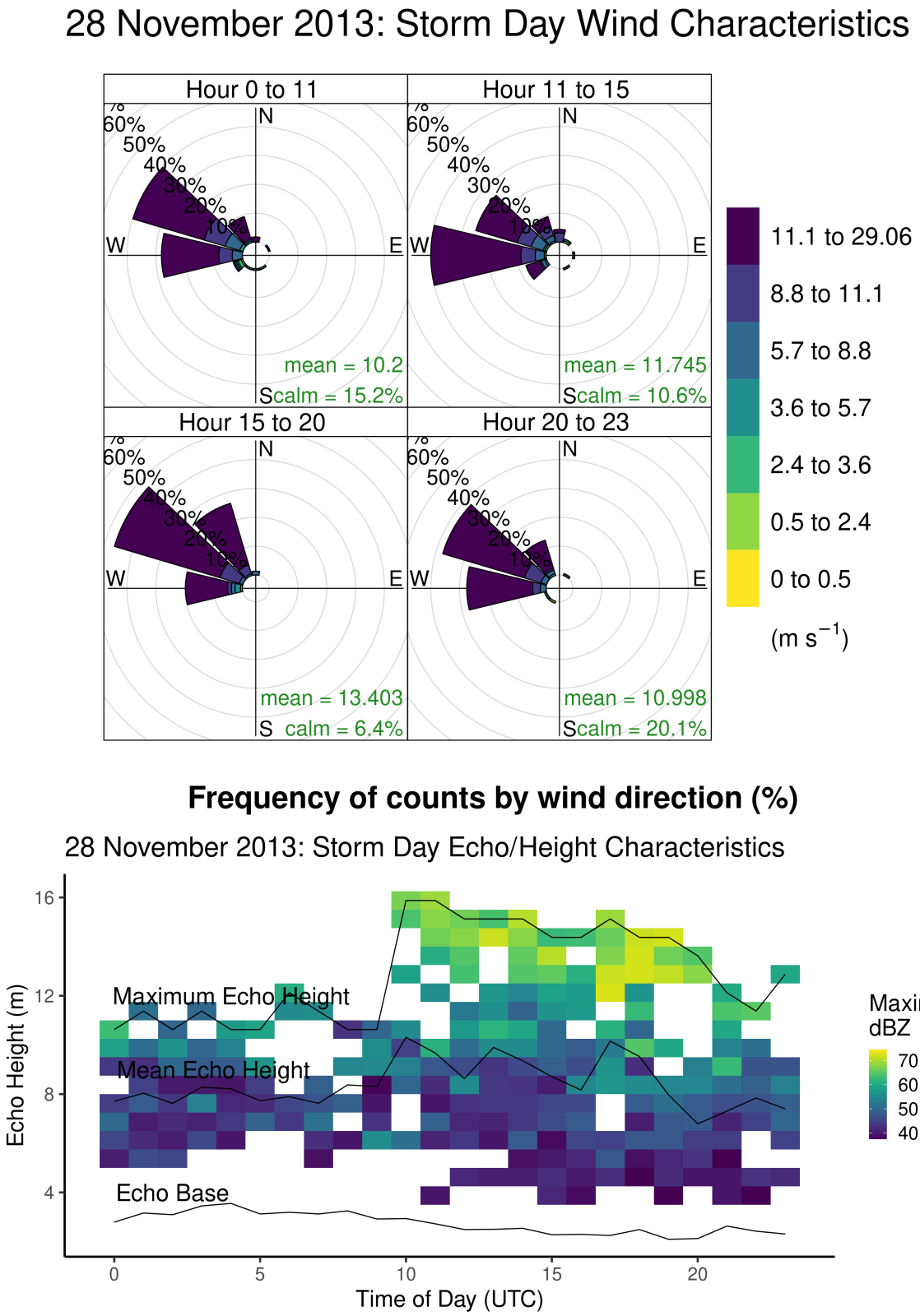

Figure 7.4: *Radar derived cloud and wind characteristics show that calm conditions prevailed until 1000 UTC when convective initiation occurred and storm rapidly grew with cloud tops of > 15 km observed not soon after. Mean wind direction was west (due east) during the storm most severe stage (1100 – 1500 UTC), with maximum wind speeds up to 30m m/s observed.*

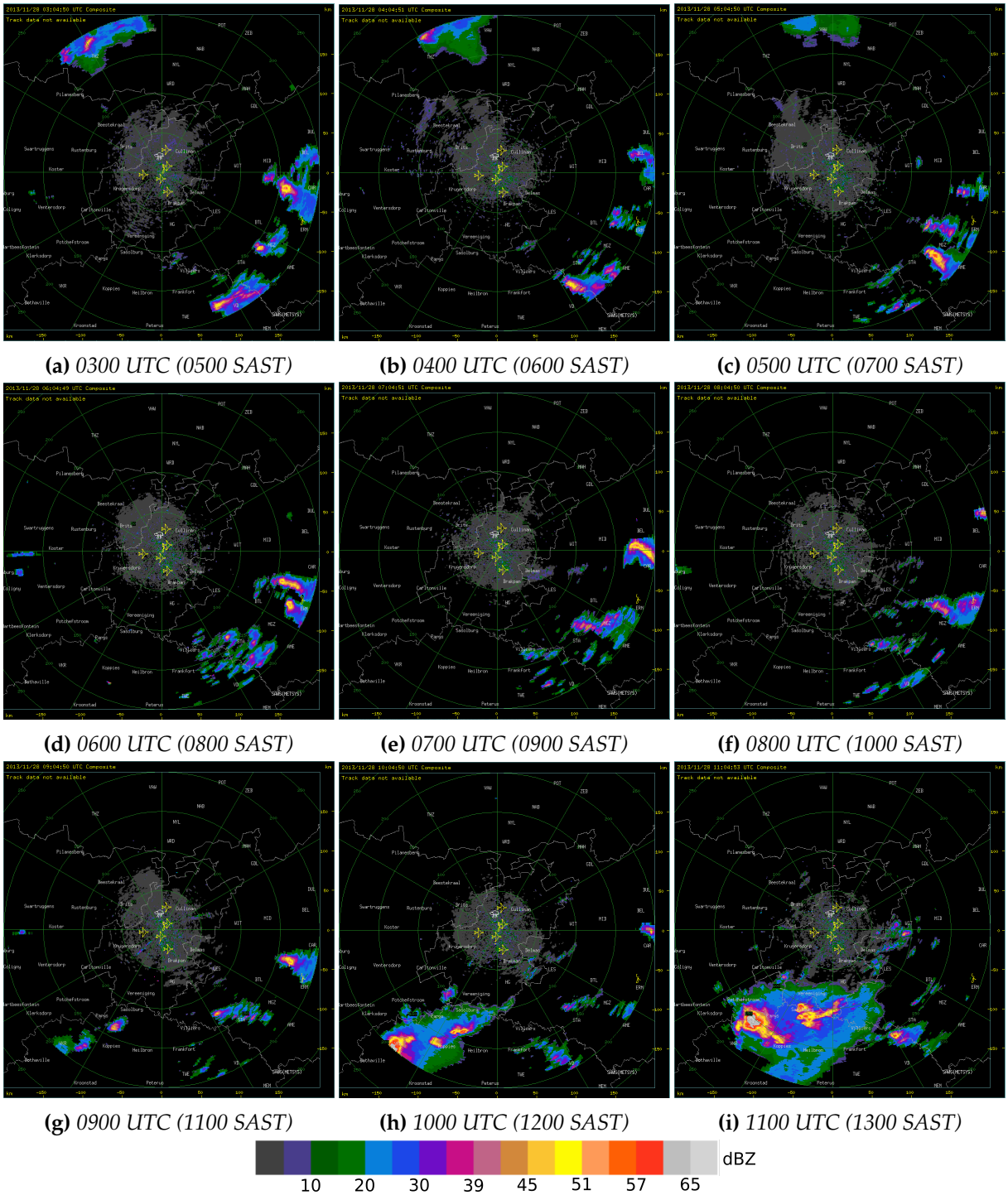

(a) *0300 UTC (0500 SAST)* **(b)** *0400 UTC (0600 SAST)* **(c)** *0500 UTC (0700 SAST)*

(d) *0600 UTC (0800 SAST)* **(e)** *0700 UTC (0900 SAST)* **(f)** *0800 UTC (1000 SAST)*

(g) *0900 UTC (1100 SAST)* **(h)** *1000 UTC (1200 SAST)* **(i)** *1100 UTC (1300 SAST)*

Figure 7.5: *On November 28, 2013, a severe hailstorm caused unprecedented destruction over much of the Gauteng province, impacting the greater Johannesburg area. Radar analysis for the morning of the storm day shows a reasonably calm morning over Gauteng, with some convective activity in the region. By 1100 SAST, SAWS released it's radiosonde at Irene (radar centre) when some convective activity began in the south-west, 200 km away. By 1200 SAST, the first significant indications of a storm with a due north-east heading at 10 m/s was visible on the radar and by 1300 SAST, large areas with reflectivity over 65 dBZ was visible, indicating a severe storm with large hail heading towards Gauteng.*

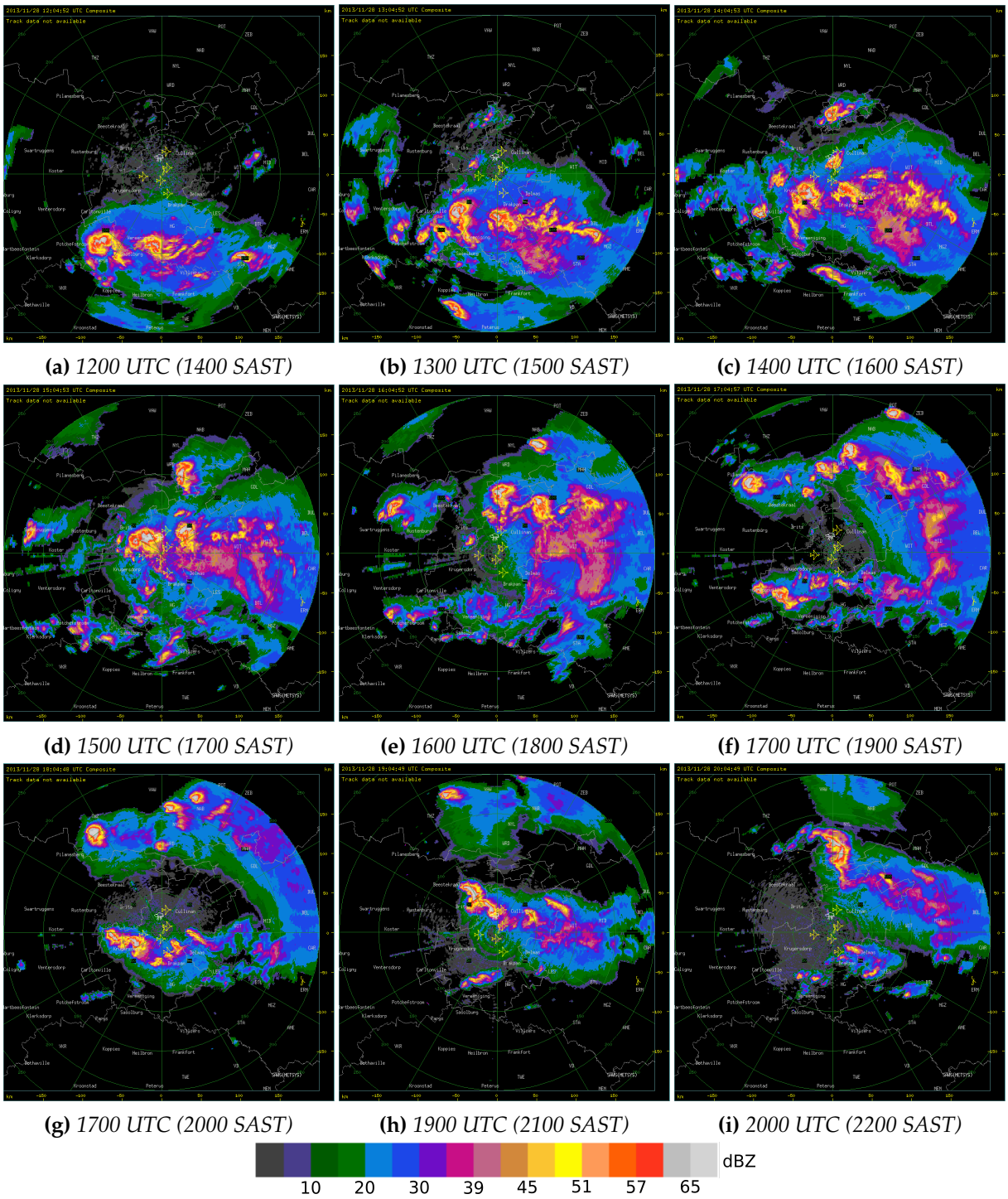

(a) *1200 UTC (1400 SAST)* **(b)** *1300 UTC (1500 SAST)* **(c)** *1400 UTC (1600 SAST)*

(d) *1500 UTC (1700 SAST)* **(e)** *1600 UTC (1800 SAST)* **(f)** *1700 UTC (1900 SAST)*

(g) *1700 UTC (2000 SAST)* **(h)** *1900 UTC (2100 SAST)* **(i)** *2000 UTC (2200 SAST)*

Figure 7.6: *The first signs of a fast-moving, severe convective storm was observed by the Irene radar at 1200 SAST. By 1400 SAST, storm cells over 70 dBZ developed south-east, south and south-west of Gauteng. The south-eastern cell was sustained and grew into a supercell. By 1600 SAST, it propagated north-east over the West Rand and Krugersdorp. During this time, the maximum storm speed reached 29 m/s and dBZ > 75 observed, where hail the size of golf balls caused large scale damage. At 1800 SAST, the storm started dissipating over Johannesburg and the West Rand and moved further north-east over Pretoria, where some severe hail was observed.*

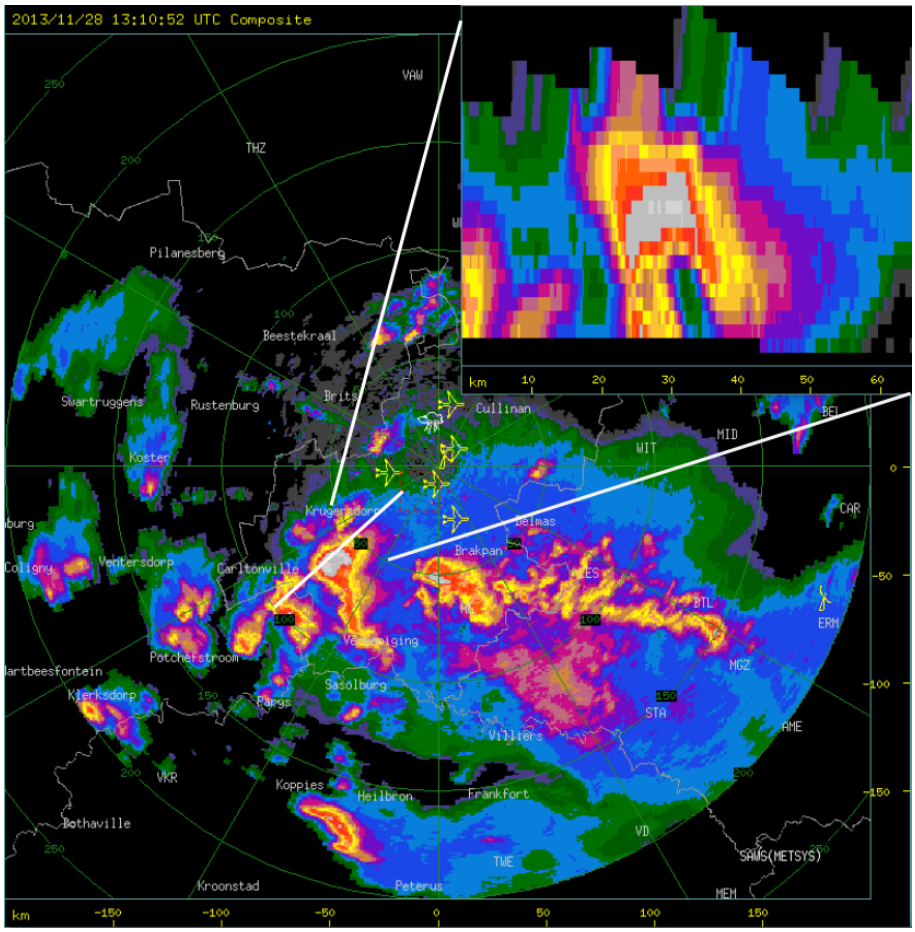

Figure 7.7: *A well defined weak echo region can be observed at 1300 UTC (1500 SAST) when most severe hail was recorded. A well defined WER indicates sustained hail aloft, which enhances growth. As the size and terminal velocity of the hailstones increases and overcome the updraft strength, the WER disappears and severe hail will precipitate.*

Simulation results

In this section the WRF setup and control run is evaluated. Under the setup, as described in the earlier section, WRF can capture convection on November 28 reasonably well. The following section will describe each run (i.e the control run, and the modified runs), changes in the land-use coefficients of each run, and the subsequent changes in storm dynamics separately. In the conclusion, the modelled impact and implications of small scale modifications to the land-use and CCN composition on surface precipitation and cloud composition is discussed.

Control run

The purpose of the control run is to examine if WRF captures severe convection with *reasonable* accuracy. The two main observational platforms that captured storm day convection was the Irene Sounding and the Irene S-Band radar. Using observational platforms allows us to compare the observed and simulated thermodynamic profile and the radar observation and reflectivity simulations. Regarding the reflectivity, the beam height limitations have to be considered when examining the region is close to the cone of silence, i.e. 20km around the radar.

The section begins by examining the synoptic-scale environment to evaluate if WRF captures the large scale features with accuracy. In Figure 7.1, the only observation platform of the storm day on this scale is from the Meteosat IR platform. ERA5 data is in good agreement with the storm day observations. Figure 7.8 visualises CAPE and radar reflectivity from WRF as proximity variables compared with the ERA5 and Meteosat data, respectively. Simulated CAPE and MSLP can capture the ridging anticyclone reasonably well on this day. Using reflectivity as proximity for cloud cover indicates that the model captures regions of high reflectivity along the east coast with reasonable accuracy.

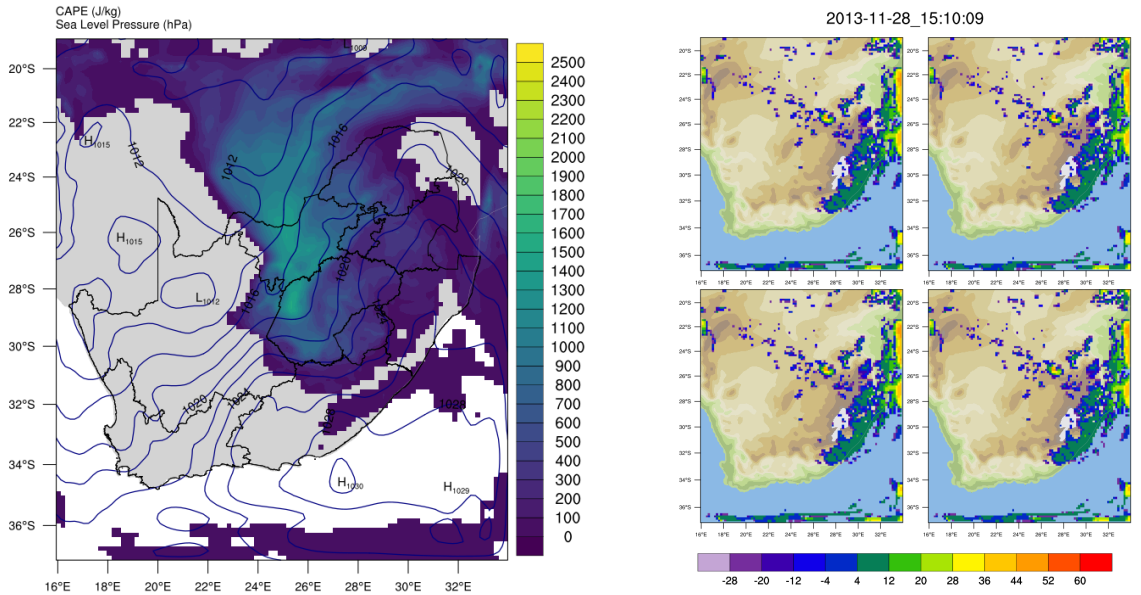

(a) *WRF Simulated CAPE* **(b)** *WRF Simulated dBZ*

Figure 7.8: *The WRF control simulation captures larges scale features, as seen in Figure 7.1 reasonably well. In Figure a, WRF captures the ridging anticyclone and major band of instability across central SA, as seen in the ERA5 synoptic map. In Figure b, radar reflectivity is used as a proxy for cloud cover and WRF captures areas of clouds cover well when compared to the Meteosat IR image.*

The simulated thermodynamic profile seen in Figure 7.9a is examined and compared with the observed at 0900 UTC (Figure 7.2 for Irene Sounding) in this section. ERA5 data, although used as a regional model, captures the storm day conditions reasonably well directly over Irene. However, the most unstable CAPE is underestimated at simulation time, 578J/kg compared to the sounding calculated 1727J/kg and overestimates the inversion layer lapse rate. The simulation accurately captures the simulated sounding's precipitable water (20 mm) compared to the 22 mm in the observation. The importance of differential winds means that it is essential that WRF captures directional and speed shear well and in the hodograph, we can see both are simulated accurately. On the surface, there are easterly winds in both the simulation and the observations, and directional steering in the upper levels agrees with the observation. WRF simulates the maximum instability slightly later. The 1130 UTC sounding from domain 3, where convection is turned off, represents the observed profile the best.

A cross-section of WRF simulated reflectivity and cloud cover, as seen in Figure 7.10, for the same section and time as seen in Figure 7.7, indicates that WRF captures storm formation, anvil position and areas of high reflectivity exceptionally well when compared to the observed radar

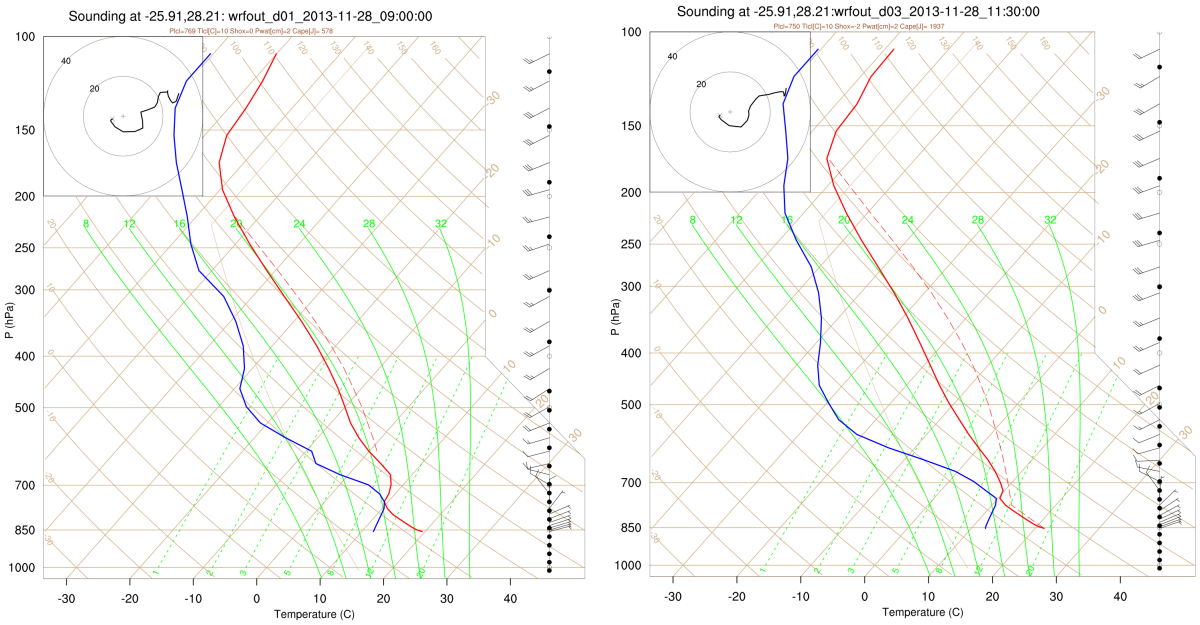

(a) *WRF Sounding D1, 0900 UTC* **(b)** *WRF Sounding D3, 1130 UTC*

Figure 7.9: *The above figure shows the simulated thermodynamic profile directly over Irene at 0900 UTC, as seen in Figure 7.2. The simulated profile compares well with the observations, however, instability (represented by CAPE) is less than what was observed. In the hodograph, we can see winds on the surface and aloft closely follows the observations. The control run captures the pre-convective profile within a reasonable degree of accuracy. Figure b, above, is from 1130 UTC in the convective permitting domain (domain 3). Instability is captured much more accurately in this profile and the wind profile matches the Irene profile. WRF simulates maximum instability later in this case but still represents the environment well.*

data cross-section. In the next section, we will examine the ice number concentration and rain number concentration for the control run, and compare these to the modified runs directly over the city of Johannesburg.

This section showed that WRF, with the control setup described, captures the storm day event with reasonable accuracy. On the synoptic-scale, WRF can represent the ridging high-pressure system over the eastern escarpment. Thermodynamically, WRF captures the vertical profile relatively well compared to observational time; however, the most accurate sounding is 2h30 hours later, indicating some delay in modelled convective initiation. The skew-t profiles also show that WRF accurately simulates winds at the surface and aloft. The hodograph shows storm directional steering, as also observed in the Irene sounding. The comparison to the radar data is promising and here we can see WRF represents the vertical motion and formation of the storm day event reasonably well. The anvil characteristics and regions of high and low reflectivity (WER) are well simulated. This allows us to use the control run setup to drive the next simulations, where we examine the changes in storm dynamics and physics with the inclusion of new parameters and land-use changes.

Modified aerosol and land-use simulations

The results of the modified event simulations are discussed here. WRF was run under a variety of differential CCN and land use scenarios. The first run, discussed previously, was a control

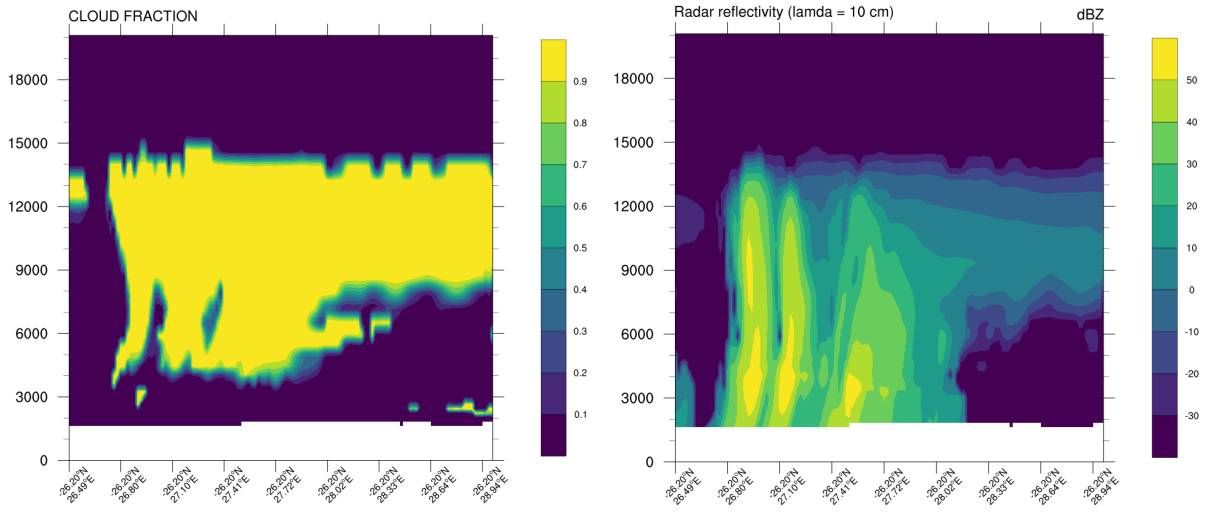

Figure 7.10: *In the convective permitting domain 3, WRF captures storm day features with reasonable accuracy compared to the Irene radar. Simulated storm formation, anvil position and high reflectivity represent the actual storm day environment. This data will enable us to compare the changes of storm day clouds when altering the model physics.*

run (Control Simulation Run (CNTRL)). Following this run there are 3 runs with a modified CCN concentration as indicated below:

1. A low CCN concentration run (**Aerosol Modified Simulation Run (AER)1**).
2. A moderate CCNconcentration similar to that observed by Ross et al. (2003) over the Highveld (**AER2**).
3. A run where an above-average CCN concentration is forced into the model, based on Ross et al. (2003)'s maximum observed CCN (**AER3**)).

Three runs are conducted to simulate a *green city* and two *polluted city* scenarios. In all cases, the CCN concentration the same as the AER1 to differentiate land-use impacts explicitly:

1. In the green city run (**GRNCITY**) the urban characteristics match a mixed forest type land-use and moderate albedo.
2. An urban area that has characteristics of a barren landscape, with high albedo (i.e. township) (**POLCITY1**)
3. An urban area that has characteristics of a western city landscape, with low albedo and low vegetation (i.e. traditional UHI) (**POLCITY2**)

More details on the specific changes can be found in Table 2.5.

The changes to the land-surface characteristics forced into the model, and directly over Johannesburg (-26.195, 28.034) is seen in Figure 7.11, and discussed here.

Surface emissivity as seen in Figure 7.11 refers to the effective radiation of a particle in relation to a black body (where a perfect emittance == 1 and a perfect reflector == 0). When a body is

a perfect emitter it absorbs energy efficiently, and all energy absorbed is directly released back into space (Sobrino et al., 2001). Perfect reflectors do not absorb any energy and it is directly reflected back into space. By default WRF-Modis applies a low surface emissivity over urban areas (Figure 7.11a). Changing the urban area to have the characteristics of a barren area (POLCITY) increases the emissivity slightly compared to the control runs. Increasing plant growth substantially to mimic that of a mixed forest area has the highest emissivity. Deriving emissivity of an urban environment is particularly challenging as the environment is less homogeneous than a vegetated area, and typically compromises high and low albedo surfaces, varied vegetation and soils in a close proximity to each other (Mitraka et al., 2012). Particularly challenging in the South African context is the legacy of apartheid spatial planning. Highly populated areas with little vegetation are often close to wealthy areas with many green spaces (Mudede et al., 2020).

Related to the changes in surface emissivity are the LAI and surface albedo, as seen in Figures 7.11a, b and c. Traditional UHI theories state that urban areas have a lower albedo and lower vegetation cover than surrounding rural areas (Kondo et al., 2001). However, in this study, we provide two albedo scenarios: a polluted city with less vegetation and higher albedo, i.e., more surfaces reflecting sunlight. Secondly, and in line with traditional UHI theories, a polluted city run with low albedo and vegetation cover. The motivation for these different runs will be discussed here as we have to consider some characteristics of African cities which might not be captured by models developed in the global north.

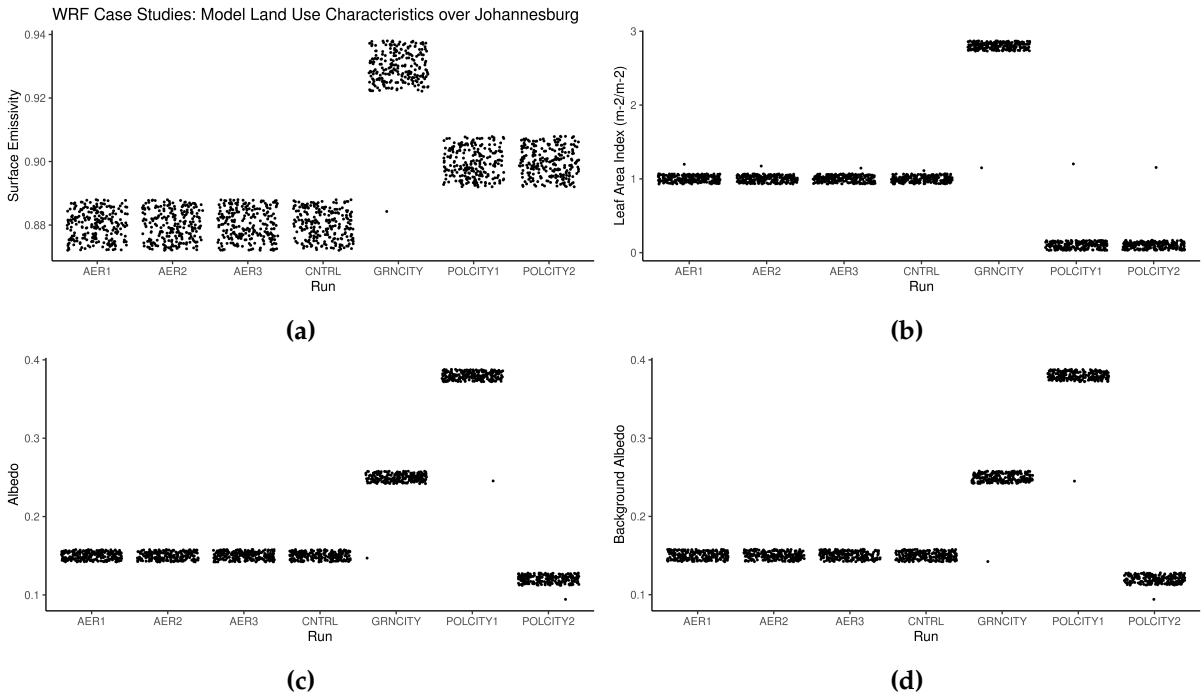

Figure 7.11: *In this study, three different land-use scenarios is examined related to the classic UHI theories. First, we use the WRF default land use in AER1 to 3. In the Green city (GRN) run, we simulate a sustainable city a high green fraction and vegetation cover (represented by the LAI). We then simulate two polluted city cases, the first one with a high albedo and low vegetation, to simulate corrugated iron as a building used in many areas of SA, and secondly a low albedo, low vegetation scenario similar to traditional UHI effects.*

The interaction between local scale climate, albedo and vegetation is complex. Sailor (1995) states that urban areas have a lower albedo than rural areas, but the same article refers to high albedo building materials with a reflective value of over 0.60. In SA, these building materials are prominent in low-income settlements where metal roofing material is the *de-facto* means to build a home (Mchunu and Nkambule, 2019). As we can see in Figure 7.12, Sandton, one of the continents wealthiest districts, has green spaces, large trees and houses that would be built with traditional building material (Sailor, 1995). In Alexandra, one of the poorest and most densely populated areas, there is little tree cover (Mudede et al., 2020). Most of the structures are built with corrugated iron - a highly reflective surface. Figure 7.12 also shows the vegetation cover between these two regions. Alexandra has little tree cover (less than 50 trees in the figure), while the neighboring Sandton is dense with vegetation. The vegetation (where LAI is used as a proxy for this in the figure below) can increase latent heat release due to transpiration (Sailor, 1995) or lead to additional cooling due to the evaporation cooling effect (Mudede et al., 2020). Both these effects are accurate and possibly leads to less variation in temperatures where there are well developed green spaces. Figure 7.12 is an example of a city with high albedo due to the fact that building material is typically highly reflective metal, the possibility that increased CCN can also increase reflectivity (refer back to Figure 1.12) also enhances the albedo over these regions, if pollution over townships is assumed to be higher than more affluent areas.

The next section examines the resulting meteorology of the each scenario directly above Johannesburg (-26.195, 28.034). Variables identified for analysis includes ice number concentration (QNICE), rain number concentration (QNRAIN), radar reflectivity (REFL10CM), specific humidity (QVAPOR), cloud water mixing ratio (QCLOUD), rain water mixing ratio (QRAIN) and ice water mixing ratio (QICE). The following formula is applied to convert model levels (Z) to altitude, $(PB + PHB)/9.8$, where PB is the base state geopotential, PHB perturbation geopotential and 9.8 is the acceleration of gravity (m/s). Converting model levels to altitude is valuable to understand the vertical profile of the model simulations in easily understandable terms.

Simulated dBZ is also examined. The advantage of simulating dBZ is that it allows a simple way to compare simulated storm intensity with radar data in the area. Figure 7.13, shows show that storm intensity is impacted in the model as a function of CCN concentration and land-use changes. In the CNTRL run, moderate storm characteristics are observed (45 dBZ). This reflectivity is observed from 1200 UTC to 1500 UTC, indicating convection was accurately captured compared to the actual event. When WRF is forced to run with Thompson and Eidhammer (2014)'s aerosol aware scheme and no changes to the land-use data, we can see an improvement in storm severity and convection timing. Between the three AER runs, AER1 has the lowest CCN concentration ($300cm^3$ at the surface, decreasing exponentially to $50cm^3$), and shows the closet representation of actual storm intensity, duration and timing. Increasing the CCN concentration as done in AER1 and 2, decreases storm severity between 1200 UTC and 1500 UTC.

In the GRNCITY we change the urban area to be more like a forest, with moderate albedo and more vegetation cover. In the GRNCITY case, WRF simulates the most severe convection of all cases, with the highest maximum reflectivity (58 dBZ) between 1200 UTC and 1500 UTC, when the storm was over Johannesburg and the most prolonged storm duration. Changing the land-use characteristics to represent a polluted city with high albedo and low vegetation

Figure 7.12: *The figure intends to show the differences in land-cover and how traditional UHI effects might not apply to densely populated township areas, where highly reflective material is used in construction (Mathee et al., 2021). On the left is Sandton, an affluent suburb of Johannesburg and on the right is Alexandra, one of the region's poorest and most densely populated townships. The difference in the surface characteristics is visible and applying traditional UHI effects to townships is complex as the albedo might be higher than the surrounding area. Map data: ©2018 Google, Maxar Technologies, Landsat/Copernicus. Images used under Google Earth attribution guidelines. These images can be used purposes such as research, education, film and nonprofit use without needing permission.*

(POLCITY1), and a traditional UHI example with low albedo and low vegetation decreases storm intensity and storm duration (maximum dBZ 38 and 40, respectively). To make more sense of the impact on the cloud composition, we will examine the simulated rain number and ice number concentration in detail for each respective run in the following sections.

Although this was not the study's intention, the GRNCITY run might be the most representative of Johannesburg's land-use and CCN concentration. The city has been known as an urban forest with many green spaces and a high density of trees in suburban areas. It could be that the default urban representation underestimated the green fraction, albedo, LAI, shade fraction and other land use properties of this city. This is motivation to improve model physics for specific cities in SA instead of relying on a generalised setup.

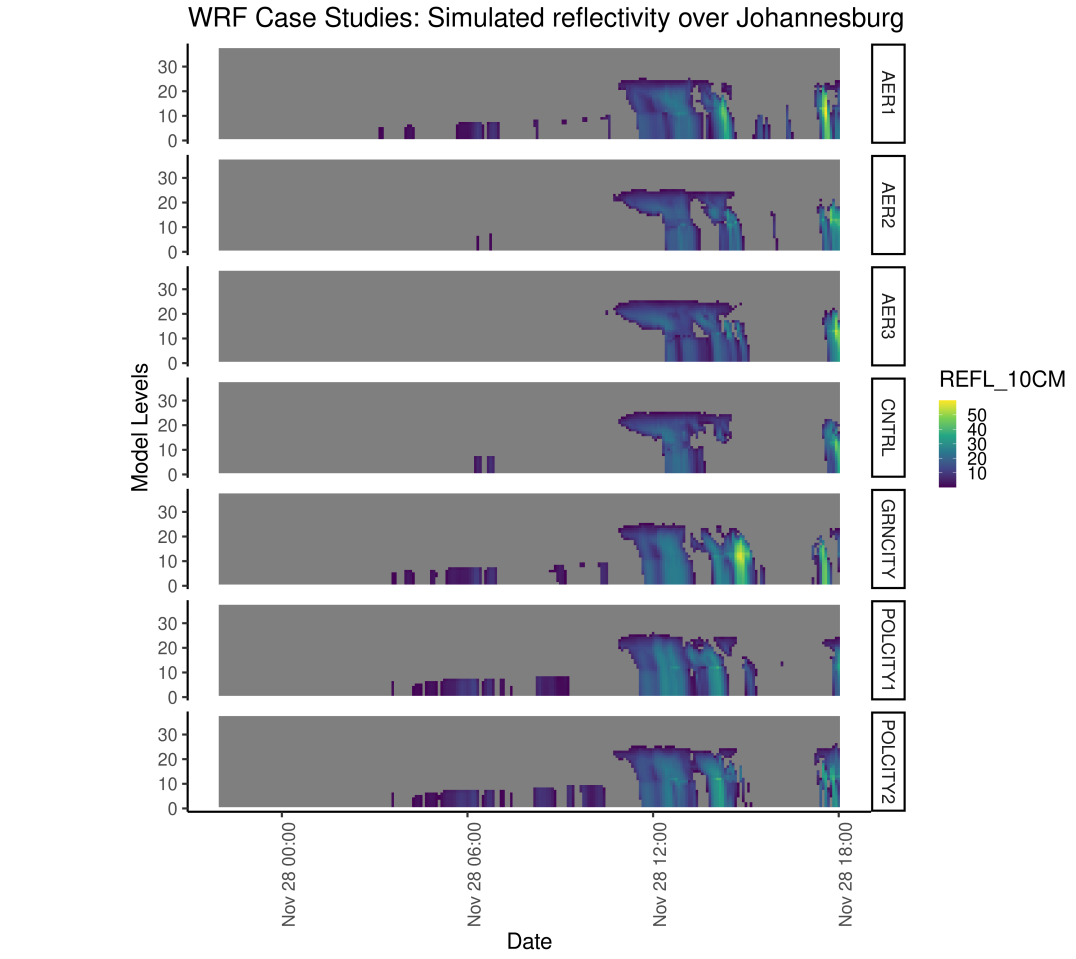

(a)

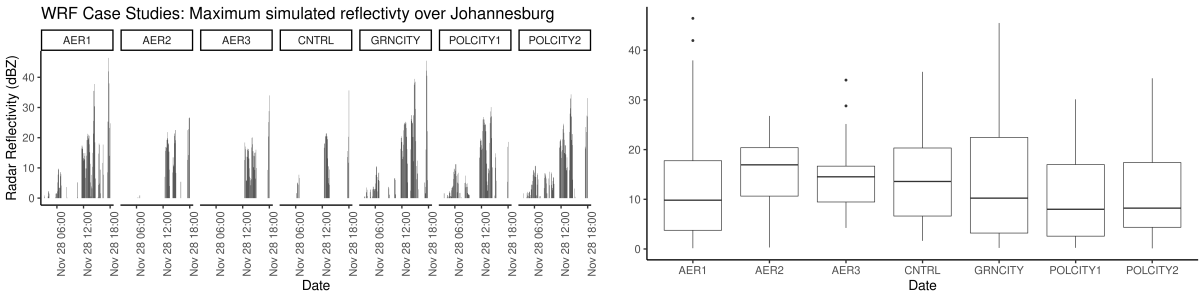

(b) **(c)**

Figure 7.13: *The results show the impact that changes to the CCN (AER1 to 3) and land-use (GRNCITY, POLCITY1 and 2) has on the simulated storm intensity as a function of reflectivity. The aerosol aware scheme improves the representation, duration and intensity of convection. The GRNCITY shows an increase in storm intensity, while both POLCITY cases show a decrease in storm intensity. We assume that WRF's default urban setup has underestimated the vegetation cover in Johannesburg and by applying the characteristics of a mixed forest, the event representation is improved.*

In the following section, we examine the rain and ice composition for the different simulations. We see that small scale changes to the urban land-use and CCN characteristics have significant implications for the composition of clouds. We extract the rain and ice number concentration for the whole column (from the surface to the model top in this section), but this is not a direct

representation of precipitation on the surface. First, we examine the rain number concentration as seen in Figure 7.14. The inclusion of the aerosol aware scheme increases the number concentration of rain particles in all cases. The timing of the highest rain number concentration is improved and better represents the event day rainfall. In AER1 to 3, the timing of rainfall during the actual event is much better representative than the CNTRL run. AER1 has the lowest mean rain number concentration and when increasing the CCN as done in AER2 and 3, the mean rain number concentration also increases (as seen in the box and whiskers plot in Figure 7.14b). By modifying AER1 land-use to simulate green and polluted cities, we significantly impact the rain number concentration. POLCITY1 and POLCITY2 capture the timing of rain number concentration better than the control run but mean and maximum rain number concentration is well below the AERruns and similar to the CNTRL run. Similar to what was observed in the reflectivity results, the GRNCITY shows the most rain number concentration in the column between 1200 UTC and 1500 UTC, when storm intensity over Johannesburg was the highest and we also see the highest maximum rain number concentration in this simulation. The mean rain number concentration is less than AER2 and 3, where a high CCN concentration was forced, but the timing, duration and peak are most accurately represented.

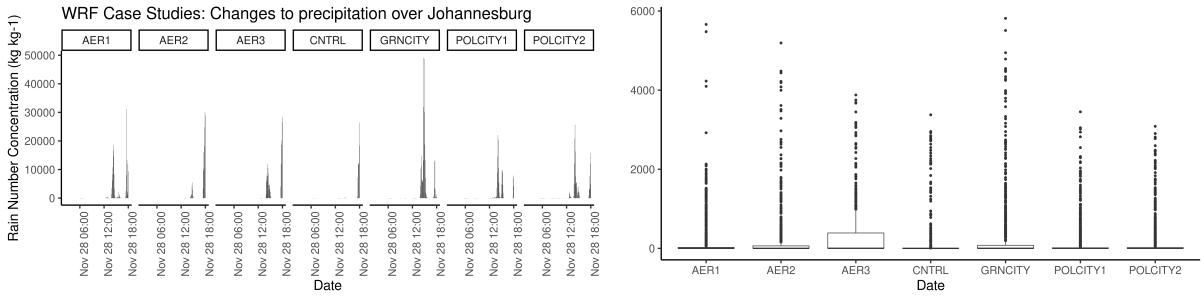

(a) **(b)**

Figure 7.14: *The inclusion of the aerosol aware scheme improves the rain number concentration in relation to the observed precipitation over Johannesburg on the storm day. Increasing CCN increases the mean rain number concentration. The inclusion of land-use changes shows that the simulated green city has a higher maximum and mean rain number concentration than polluted cities with the same CCN concentration.*

The ice number concentration indicates the instantaneous number of ice particles in the whole model column per time step and is not representative of surface hail but instead represents ice crystals in various forms within the model. In the next section hail and graupel is discussed. The results seen in Figures 7.15a and b show that the control simulation has the highest ice number concentration between all the simulations and the longest duration of simulated ice. The inclusion of the aerosol aware scheme decreases the maximum and the duration, of observable ice concentration. There is an observable difference between AER1, 2 and 3. In AER1 the maximum ice concentration is similar to the CNTRL run, but the duration of ice in the column is the lowest. With a simulated increase in CCN, the maximum number of ice particles is substantially lower than the AER1 run, but the duration of ice in the column is much longer. The lower ice concentration in AER1 and the higher rain concentration for the same simulation, seen in Figure 7.14, could indicate that the low CCN leads to the early onset of precipitation. In contrast, a high CCN scenario leads to delayed precipitation and increased ice concentration.

The GRNCITY and POLCITY 1 and 2 results are worth further investigation. In all three runs, the CCN concentration is the same as AER1. Land-use modification leads to lower peak ice concentrations in the column in comparison to AER1, but higher than AER2 and 3. POLCITY1 and POLCITY2 have a higher mean ice number concentration than the GRNCITY. Because the period between 1200 and 1600 UTC is the study's primary focus, we do not account for the convection observed at 1800 UTC. However, POLCITY1 and POLCITY2 capture the 1800 UTC cell in these runs (refer back to the 1800 UTC radar image in Figure 7.6). This could indicate a diurnal effect on convective storms as a function of vegetation. It should be considered is that these ice particles might not reach the surface, as we will see in the next analysis.

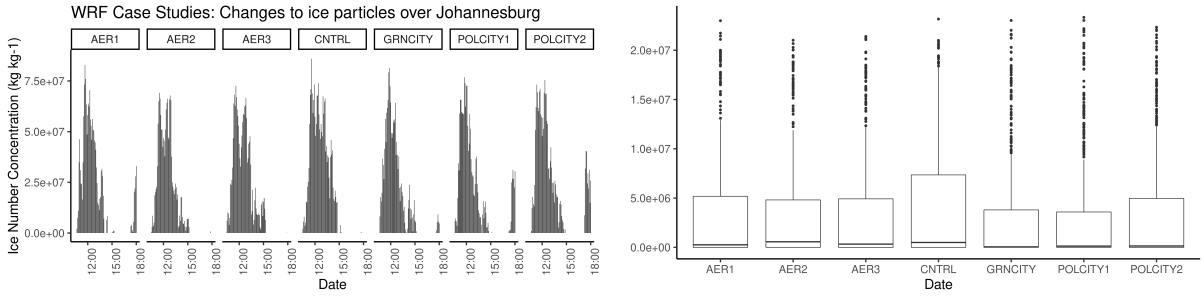

(a) **(b)**

Figure 7.15: *The ice number concentration shows the total number of ice particles from the surface to the model top. The CNTRL simulation has the highest number of simulated ice particles. The use of aerosol aware scheme decreases the ice number concentration overall and with an increase in the number of CCN particles, the number of ice particles decreases. The duration of particles in the column increases with CCN concentration, as seen in AER1, 2 and 3. When including land-use and vegetation changes, the GRNCITY run shows the highest peak ice concentration at 1200 UTC, representing the storm day event. The POLCITY1 and 2 run similarly captures ice concentration reasonably well. At 1800 UTC, the two POLCITY runs show an increase in ice particles, indicating a diurnal effect associated with low vegetation cover.*

The rain and ice number concentration provide valuable information about the atmospheric column characteristics, but these variables do not necessarily represent surface precipitation. The following section examines the modelled surface hail (graupel) and rainfall to examine the possible surface impacts of anthropogenic changes to observable weather. Figure 7.16a shows the largest hail concentration observed in the column before melting occurs. Simulated hail that reaches the surface for each respective run is seen in Figure 7.16b[3]. The aerosol aware runs better represent hail than the CNTRL. In AER1, 2 and 3, the duration of hail in the column is more prolonged. When CCN is increased, the number of simulated hail in the column also decreases and the duration of hail in the column. This is observed in the POLCITY runs, where hail concentration is lower than the GRNCITY run. The GRNCITY run has the highest hail concentration in the column and the highest peak hail concentration in the column between 1400 UTC and 1500 UTC – in good correlation with the actual storm day hail occurrence.

Hail that reaches the surface, as indicated in Figure 7.16b, show that only the aerosol aware schemes captured any hail between 1200 UTC and 1500 UTC. At 1800 UTC, the CNTRL, AER1, AER3 and POLCITY2 run capture surface hail. AER1 and AER3 have different CCN concentra-

[3]HAILMAX2D and HAILMAX1K in WRF files, respectively

tions. While the overall effect of increased CCN is decreased simulated surface hail, the AER3 run captures late afternoon hail and with a high concentration present in the AER3 column, which is not seen in AER2. Between POLCITY1 and 2, the only difference is the albedo, indicating that low local scale albedo could impact hail occurrence. However, the GRNCITY run simulates significantly more hail reaching the surface.

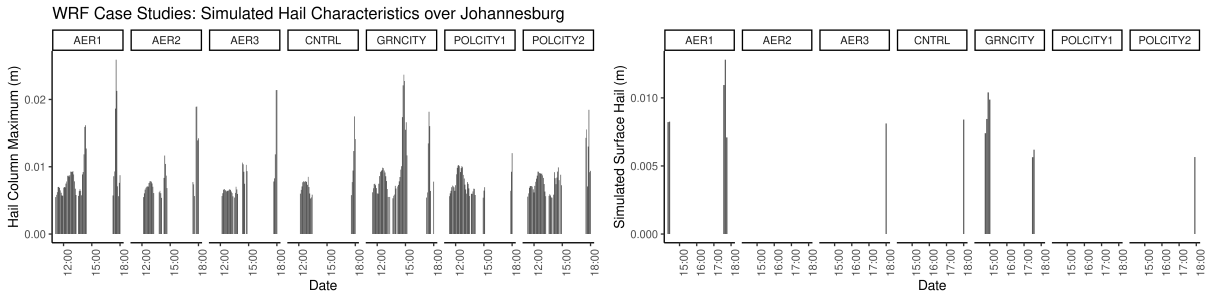

(a) *Column Simulated* **(b)** *Surface Simulated*

Figure 7.16: *Model simulated hail is derived from two variables indicating total hail in the column (sub figure a) and total hail reaching the surface after melting has taken place. There is simulated hail in the column in all cases, with GRNCITY having both the highest amount and most prolonged duration of simulated hail. With an increase in CCN (AER 2 and 3), the number of hail particles decreases. The GRNCITY run which simulates dense vegetation and high albedo, has the highest simulated accumulated hail, indicating that local-scale vegetation has a significant impact on local scale hail precipitation.*

Model accumulated rainfall reaching the surface is plotted in Figure 7.17a, and is compared against the storm day accumulated precipitation as discussed earlier (Figure 7.3). Note that times in this figure are in SAST format, i.e. UTC == SAST - two hours). For a direct comparison, the SAWS Botanical garden station (abbreviated JHB BOT) is examined. WRF could not capture the initial precipitation between 1400 and 1600 UTC (1600 SAST - 1800 SAST). The incorporation of an explicit CCN and land-use improved the local scale forecast in the GRNCITY run. AER1, GRNCITY, POLCITY1 and 2, where a low CCN concentration was simulated, captured realistic storm day precipitation. Using AER1 CCN concentration and a mixed forest type land-use (GRNCITY) increased accumulated precipitation and had the highest accumulated precipitation across all the simulations. Using the same CCN concentration with the polluted city scenarios decreases surface accumulated precipitation in this area. POLCITY1 and POLCITY2 have slight differences in the total precipitation as a result of albedo differences. POLCITY1 (low vegetation, high albedo) has higher accumulated precipitation, while POLCITY2 (low vegetation, low albedo) has the lowest accumulated precipitation between the AER1, GRNCITY and POLCITY runs which have the same CCN concentration.

Figure 7.17b shows accumulated graupel directly above Johannesburg. Models with low CCN concentration simulate surface graupel directly over Johannesburg, which is an improvement on the actual storm day simulation compared to the control run. The inclusion of aerosol aware scheme improves storm day representation and that changes to the CCN content can have local scale effects. POLCITY1 and 2 simulate the lowest accumulated graupel. AER1 captures the timing of hail well. The GRNCITY simulation indicates that high vegetation, high albedo surface would have a higher accumulated hail during the same time. However, the GRNCITY run does represent the timing of convection better in all cases. It indicates that more vegetation

and higher albedo surfaces would lead to increased precipitation and hail on a local scale. Both POLCITY runs have the lowest accumulated graupel. POLCITY1 (high albedo, low vegetation) shows a small accumulation from 1200 UTC. However, POLCITY2 (low albedo, low vegetation) only accumulates hail toward the end of the simulation.

The GRNCITY findings are supported by the analysis on storm characteristics in and around Johannesburg using radar data, as seen in Figure 6.19. In that analysis, rain rate, as a function of reflectivity, shows that severe rainfall is on average lowest over rural areas, whereas urban and suburban areas of Johannesburg have higher rainfall intensities.

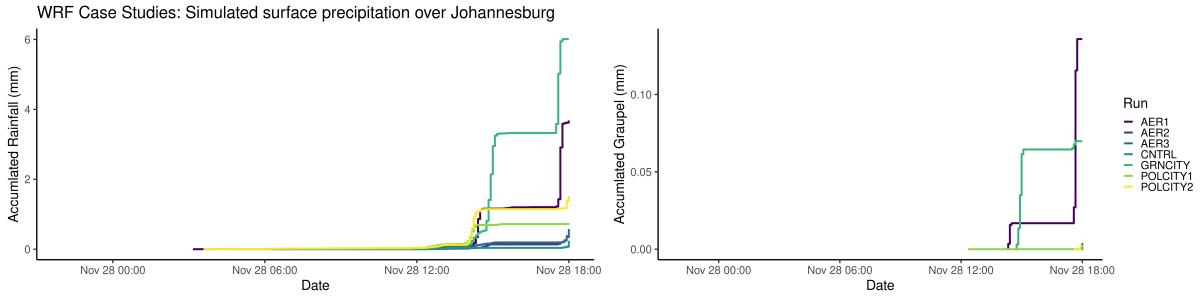

(a) *Accumulated Rainfall* **(b)** *Accumulated Graupel*

Figure 7.17: *Accumulated precipitation is improved with the inclusion of the aerosol aware scheme. However, high CCN concentrations (AER2 and 3) have shown lower precipitation than the low CCN run. With the inclusion of land-use changes, the accumulated precipitation changes dramatically. The GRNCITY run has the highest accumulated precipitation, while POLCITY1 and 2 with the same CCN concentration have significantly lower modelled precipitation. In sub figure b, the GRNCITY run is the only simulation indicating hail over the selected area and matches the storm day timing of hail over Johannesburg.*

Changes to the local thermodynamic environment

There is a well known link between the aerosol concentrations and the vertical temperature profile. On a large scale, aerosols can heat or cool the atmosphere, as seen in Chapter 1, Figure 1.12. The direct and indirect effect impact radiative forcing throughout the whole vertical profile, from the surface to the cloud top (Albrecht, 1989; Atwater, 1970; Myhre et al., 2013; Stocker et al., 2013; Twomey, 1974, 1977). And with all this said, the changes observed in the above section has to be examined in the context of the thermodynamic environment directly above the city – because the impact of local scale instability on thunderstorms is well known. On a local scale, Pante et al. (2021); Rosenfeld, Lohmann, Raga, O'Dowd, Kulmala, Fuzzi, Reissell and Andreae (2008); Solmon et al. (2021); Tosca et al. (2015) have shown that aerosols alter the thermodynamic profile, which in turn alters instability, timing of convection, differences in latent heat release and finally the amount of surface precipitation. The study does not examine the exact mechanism by which aerosols change the thermodynamic environment, but attempts to characterise the possible changes.

The following section examines the thermodynamic evolution for the simulated parcel of air directly above Johannesburg for each of the previously described scenarios. For this analysis 1000 UTC, 1200 UTC, 1400 UTC and 1600 UTC profiles are examined, these 2 hour intervals

capture the general storm environment and thermodynamic evolution reasonably well (refer to Figure 7.13). Particular attention is given to CAPE which represents instability, and inversion layers in the lower and mid troposphere which could show UHI or aerosol heating or cooling effects. Inversion layers can suppress convection if convective instability is not enough to overcome the stable layer, however, under the right conditions the deterioration of the stable layer during convective storms can result in the continued growth of severe convection.

At 1000 UTC the thermodynamic profile across all the simulations as seen in Figure 7.18 have some important differences. At the surface AER1 is significantly warmer than both AER2 and 3. At 700 hPa there is a stable layer visible, indicating strong CIN, in all the cases, however, this is most pronounced in AER3. At the Irene sounding (Figure 7.2), which is 35 km away from the simulated sounding, there is also a fairly weak stable layer visible at 700 hPa during this time. Thermodynamically this could indicate that low CCN concentrations do not inhibit convection and the stable layer is not as pronounced. At AER3, CCN above the surface could result in the warming of the lower tropospheric layers, either enhancing the UHI effect or directly absorbing heat at this level. CAPE is also significantly less than in all the other soundings over the region. These findings are similar to Tosca et al. (2015) findings on fire's in the tropical regions of west Africa where aerosols are stated to inhibit convection (Pante et al., 2021; Solmon et al., 2021). The three land-use scenarios show a fairly similar vertical profile to the AER1 run[4]. No significant difference in instability, or stable layers is visible, yet.

At 1200 UTC, and in all cases, convective clouds with a large structure (high reflectivity, high cloud top) is observed at this time step. All soundings have some characteristics that indicate favorable environments for severe storm development, this includes high CAPE, dry mid-levels and strong wind shear (Brooks et al., 1994). The thermodynamic profile, as seen in Figure 7.19 shows several key differences between each simulation. In the AER1 the stable layer dissipated rapidly, while AER2 and 3 still have a well defined stable layer. In AER1, we can assume convective instability overcame the stable layer to accelerate cloud development and rainfall, this is also seen in Figure 7.13 where heavy precipitation occurs earliest in the low aerosol runs. However, at the same time, in AER2 and 3, the persistent stable layer at 700 hPa could lead to enhanced convective triggering once the CIN is overcome. In the GRNCITY run, CAPE at 1200 UTC is significantly higher than all other runs. Due to increased latent heat from the dens vegetation type landscape in this simulation, this is not unusual. Several new studies on convective storms over irrigated farmlands have found that neglecting the added local moisture from these sources does have a significant impact on simulated convective storms (Qian et al., 2020). Similarly, neglecting the artificial increase in moisture from a man-made, urban forest like Johannesburg can have an impact on local scale thermodynamics, as seen here. In POLCITY1, the stable layer persists and will inhibit convection. Over POLCITY2, the stable layer has also dissipated, CAPE is the highest in this run at 1200 UTC, indicating that the UHI enhances convection, most likely due to surface heating.

At 1400 UTC the most severe convective regions of the storm is over the area of interest in all cases. In the previously discussed Figure 7.13, the GRNCITY simulation has the highest simulated reflectivity at this time. Thermodynamically, the 1400 UTC sounding shows that AER1

[4]all three runs used the same CCN concentration to the AER1 run

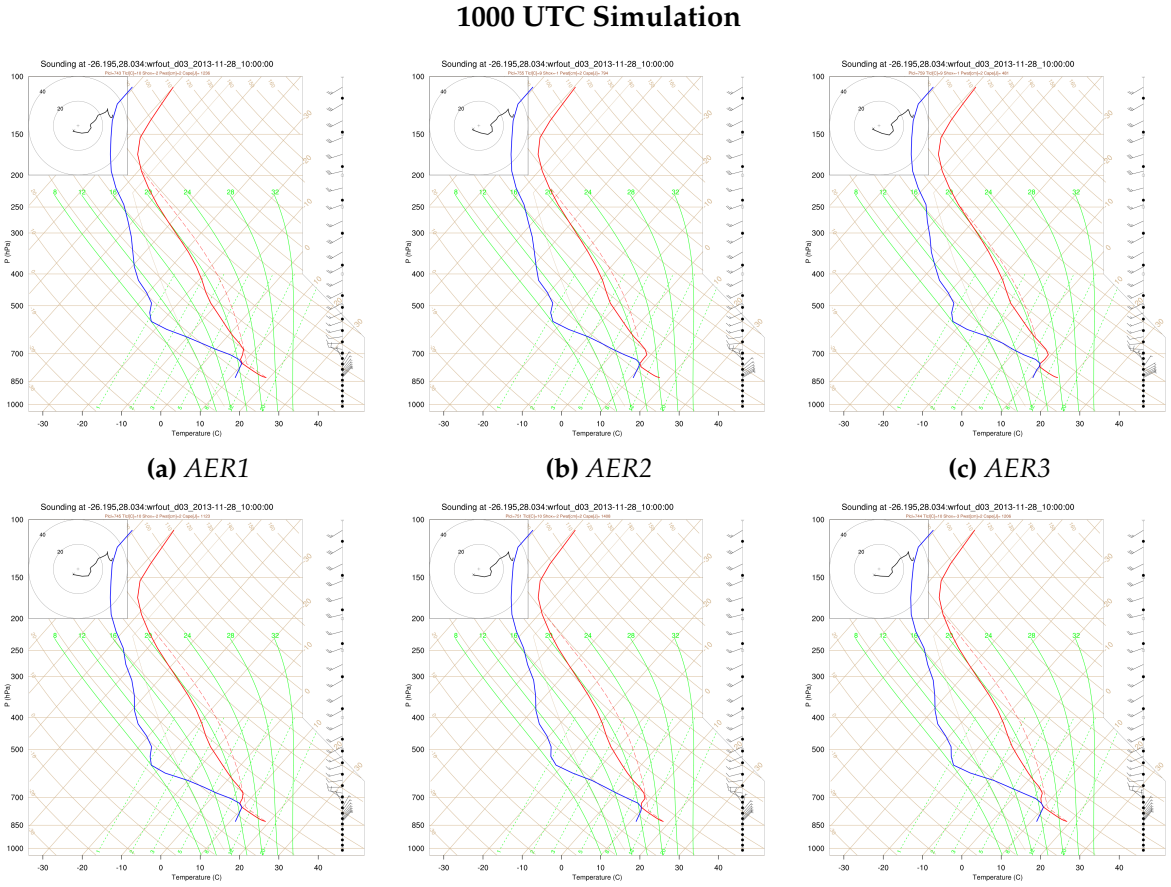

(a) *AER1* **(b)** *AER2* **(c)** *AER3*

(d) *GRNCITY* **(e)** *POLCITY1* **(f)** *POLCITY2*

Figure 7.18: *The 1000 UTC soundings show that with an increase in CCN the stable layer is stronger, and CAPE values well below severe storm numbers.*

and the GRNCITY and POLCITY2 is representative of an sounding in a convective cloud. In both cases CAPE is still significantly higher than the AER2 and 3 cases. Here it is clear that increased CCN has an significant effect on heating in the lower troposphere. The stable layer still persists, and convective processes is still inhibited and thunderstorms in this specific scenario is less severe, this also includes less surface precipitation reaching the ground and little ice processes occurring due to the inhibition of convective updrafts. It is also interesting to observe the dry mid-level in the AER2 sounding that persists, here the dry mid-level could enhance the possibility of severe convective events such as cloud burst (Brooks et al., 1994), however, from the reflectivity analysis it was seen that this was never realised. In the differential land use scenarios, some interesting changes has occurred from the 1200 UTC sounding. First, CAPE is significantly higher over the GRNCITY compared to POLCITY1 and 2. Interestingly, POLCITY 2 has shown an significant decrease in CAPE from the previous sounding. Due to local scale heating from low albedo surfaces, isolated showers might have occurred earlier than expected, resulting in a decrease in instability earlier. This is supported by the reflectivity analysis in Figure 7.13 in which we can see that POLCITY2 has consistent precipitation throughout the morning, more so than the other simulations. Convective initiation also occurs slightly earlier here than in the other scenarios. The results also show that POLCITY 2 had reasonably high accumulated precipitation, as seen in Figure 7.17, however, the lowest accumulated hail. This

1200 UTC Simulation

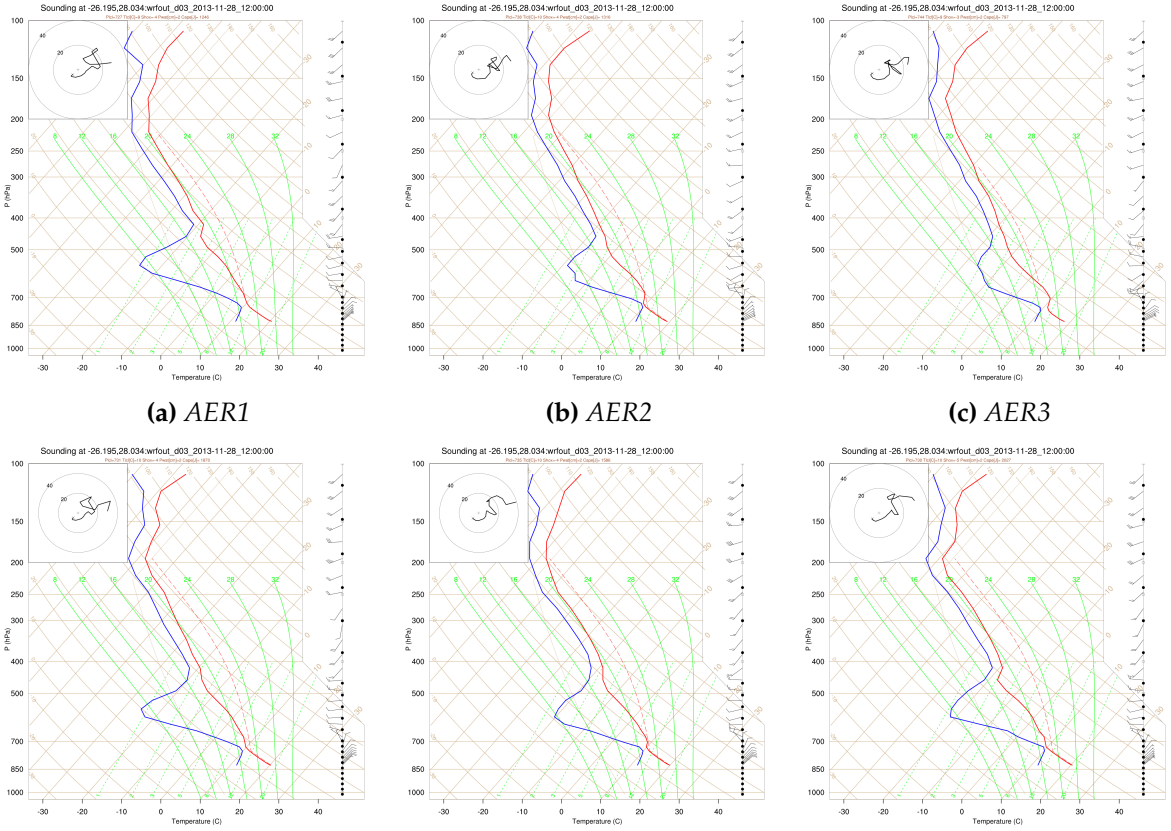

(a) *AER1* **(b)** *AER2* **(c)** *AER3*

(d) *GRNCITY* **(e)** *POLCITY1* **(f)** *POLCITY2*

Figure 7.19: *At 1200 UTC all soundings have some characteristics that indicate favorable environments for severe storm development, this includes high CAPE, dry mid-levels and strong wind shear. The AER1 and GRNCITY run's stable layer has dissipated in this sounding. In the GRNCITY run, CAPE is significantly higher. The increased moisture from the mixed forest landscape is expected to increase latent heat directly above the city area, invigorating thunderstorm development.*

possibly shows that increased convective heating did not result in deep Cumulonimbus formation, instead early convection, with only rainfall.

The final sounding analysis for this case study is at 1600 UTC, as seen in Figure 7.21. Here CAPE has decreased in all cases, AER1 and GRNCITY still show characteristics of a cloud sounding and there is still some convective instability in these scenarios. In the AER2 and 3 sounding the stable layer is still persistent and stronger than before, CAPE levels has slightly increased, but major storm development was never realised due to this stable layer during this time. This supports the theory that increased aerosols can result in heating of the lower troposphere and decrease convective instability. The exact mechanism for this is unclear and not explored in the study, The increase in CAPE is important and it is however noted that in the Figure 7.13, there is increased precipitation in the AER2 and 3 runs starting at 1800 UTC. At this time, the PBL would cool down a result of diurnal cooling, which allows the convective energy to finally overcome the stable layer and result in late afternoon precipitation – possibly severe due to the build up of CAPE during the afternoon. However, this study stops short in analysing the delayed precipitation and focussed on the time period when most severe hail occurred (1200

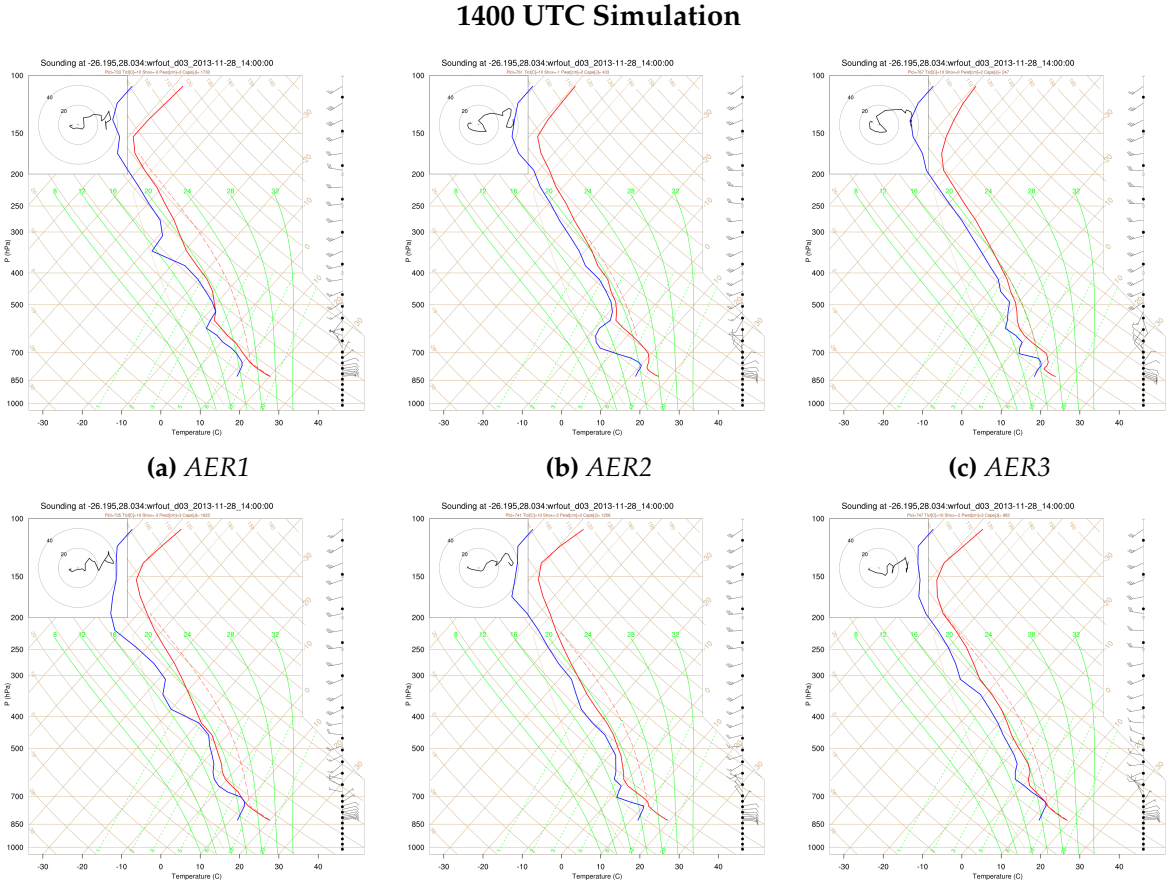

(a) *AER1* **(b)** *AER2* **(c)** *AER3*

(d) *GRNCITY* **(e)** *POLCITY1* **(f)** *POLCITY2*

Figure 7.20: *At 1400 UTC the some of the most intense moments of precipitation was simulated in all cases. Thermodynamically the AER1, GRNCITY and the POLCITY2 sounding shows characteristics of a in cloud sounding. CAPE is still high in both these soundings. In all other AER soundings, the stable layer persists at 700 hPa, indicating that CCN has major thermodynamic impact on the temperature profile of the atmosphere on a local scale. A dry mid-level feature persists in AER2, and this could enhance severe thunderstorm possibility, however, from previous analysis it was clear that this was never realised. This stable layer would decrease convective potential and storm development. CAPE remained the highest in the GRNCITY, while it decreased substantially in the UHI simulation, here precipitation occurred earlier, and no hail was simulated.*

UTC – 1600 UTC). In the POLCITY simulations there is a newly formed inversion at 700 hPa, with dry mid-levels and increased CAPE. This is especially prominent in POLCITY2, showing that surface heating plays an important role in convective development and can cause instability to rapidly change. Due to earlier precipitation in this simulation there could also be increased surface moisture that is parameterised back into the atmosphere increasing the latent heat in this case. In the GRNCITY simulation the sounding remains consistent with a cloud sounding, and possible precipitation occurring at this time still. By referring back to Figure 7.17 again, we can see that by this time the GRNCITY had the highest accumulated precipitation and hail. The sustained increase in latent heat and moisture from the artificial vegetation could explain the difference with the other two land use cases, where CAPE was high during certain times, but convection was less unstable and occurred more sporadically.

Changes in CCN concentration, vegetation and land-cover have a significant impact on cloud

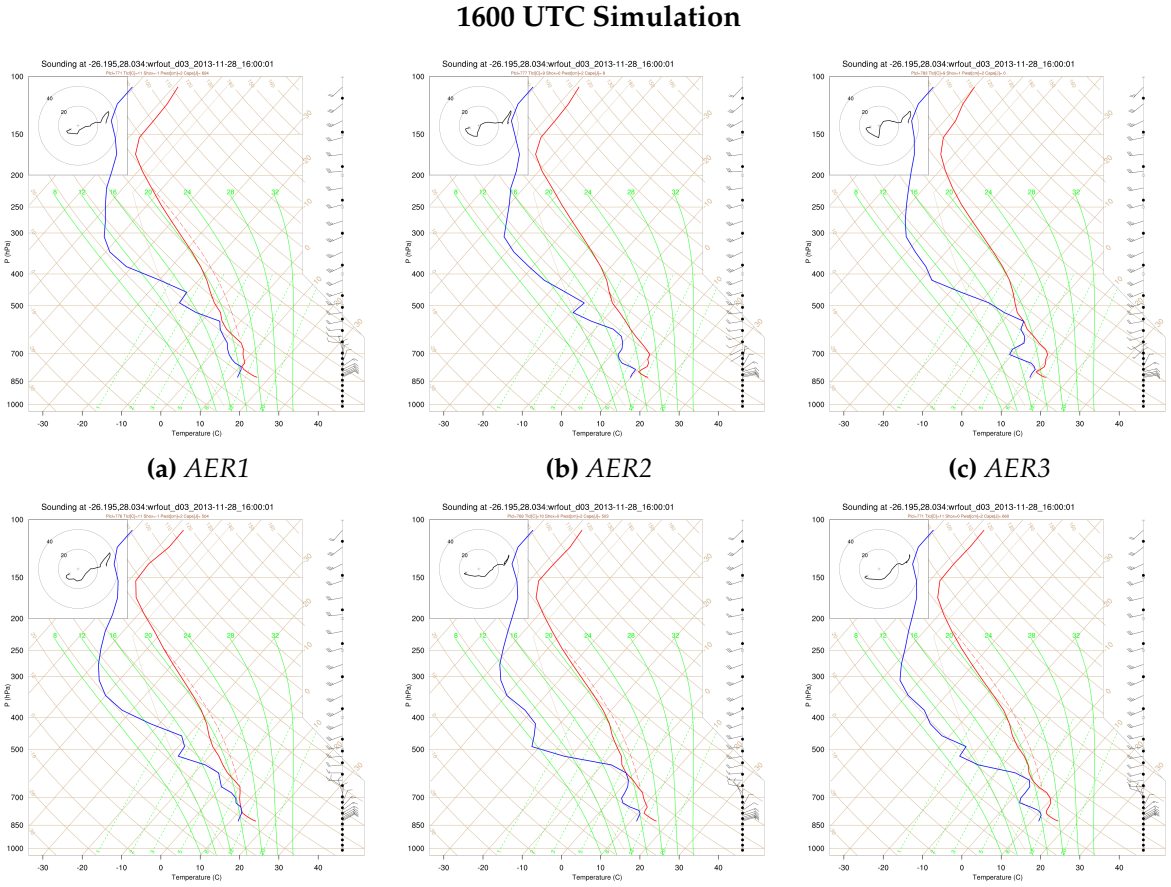

(a) *AER1* **(b)** *AER2* **(c)** *AER3*

(d) *GRNCITY* **(e)** *POLCITY1* **(f)** *POLCITY2*

Figure 7.21: *At 1600 UTC most severe hail was already recorded over the region of interest. The 1600 UTC sounding shows the continued presence of the stable layer in the AER2 and 3 sounding, and interestingly here CAPE increased. While this is not examined, it is clear from the reflectivity analysis that there was indeed delayed precipitation in these runs. There is a possible link to diurnal cooling which will weaken the stable layer and allow for the build up CAPE to initiate severe convection later in the day. In the land-use change scenario, the GRNCITY shows persistent cloud soundings, while the two polluted city soundings show a newly developed stable layer and increase in CAPE, indicating that convection might occur later in the day again as we did see occurring.*

composition and surface weather on a local scale. We started this analysis by showing that WRF could simulate the hail event of November 28, 2013. Simulating the event with reasonable accuracy allowed us to run a control case from which we can evaluate a few simple but important changes to the CCN and land-use characteristics in the model. We applied these changes based on traditional UHI theories where albedo and vegetation play a significant role in the weather and climate of cities. We completed seven runs with various configurations to this end. First, we forced WRF with CCN only changes, partly guided by Ross et al. (2003); Terblanche et al. (2000)'s studies on the CCN characteristics in the region. Here we provided three scenarios: a low CCN load, a medium CCN load and an extreme CCN load. Throughout the study, it became clear that the low CCN load simulations showed the most intense storms under these conditions and higher rainfall and hail/graupel amounts. We selected the AER1 CCN concentration to simulate different land-use and vegetation changes over the Johannesburg urban area. We theorised three scenarios, a green city where albedo was moderate, but increased the vegetation

of the urban area to give it the characteristics of a mixed forest. Then we created two polluted cities. First was a theorised township-type city where albedo was high due to building material (Figure 7.12 for an explanation of why this assumption was made). The second polluted city was more representative of the classic UHI effect, and we decreased vegetation and decreased albedo. The results show that under a green city rainfall and hail is the highest in this case, and instability remains the most consistent throughout the case. In the two POLCITY runs convective initiation occurs slightly earlier, but less rainfall and hail reaches the surface. The early precipitation means the highly unstable environment dissipates fairly quickly. In POLCITY2, which represents the UHI, it is apparent that an highly unstable environment develops quickly after the major rainfall event and that delayed storm development is likely.

The results show that increased CCN concentrations effect not only the number concentration of rain and ice particles over the urban area, but it also has a significant effect on the thermodynamic profile over the areas. The most significant finding is that green city scenarios has the highest hail and rainfall reaching the surface, and that convective processes is enhanced earlier in the day over this city. The second significant finding is that increased aerosol loading results in persistent stable layers over the urban area during noon to late after noon, during this time convective instability is inhibited, but later during the day, possibly as a result of diurnal cooling convective potential is finally realised and delayed severe precipitation occurs over the urban area. The section showed that small scale changes to land-use and vegetation can impact surface weather, and that South African cities need to be better represented in current NWP. It is also worth noting that these results support both Rosenfeld, Lohmann, Raga, O'Dowd, Kulmala, Fuzzi, Reissell and Andreae (2008) and Tosca et al. (2015) findings that increased aerosols (CCN) results in heating of the lower troposphere, as we saw in the thermodynamic profile in this case, there was a persistent inversion at 700 hPa. And further in support of Pante et al. (2021); Solmon et al. (2021); Tosca et al. (2015), this seems to delay initial precipitation. However, as Rosenfeld, Lohmann, Raga, O'Dowd, Kulmala, Fuzzi, Reissell and Andreae (2008) showed, the polluted environments might have delayed precipitation, which could also be more severe later on (refer back to Figure 1.11). The thermodynamics could be directly affected by the CCN concentrations, or it could be an indirect effect due to changes in the droplet number or size. The exact mechanism is not examined in this study.

Future convective environments over urban Gauteng

Under changing climatic conditions, the need to understand how convective environments have changed in the past is critical. By applying a linear regression analysis on CP commonly associated with severe storm development, i.e. CAPE, precipitable water, freezing height, and equilibrium level, as seen in Figure 7.22, it is observed that convective favouring environments for NDJFM months have been increasing over the last three decades. Of particular importance is the increase in CAPE and precipitable water, as these two variables are good indication of storm development. The freezing level, essential to hail formation, as we saw, also showed a slight increase over all months. The changes in the convective nature of the atmosphere over Gauteng can lead to a situation where events such as thunderstorms and flash flooding become more prevalent. In contrast, hail events could decrease because of an increasing freezing level,

and we expect higher surface temperatures to lead to longer time aloft. Wind shear, however, is decreasing, and this would have an impact on the storms experienced over the Highveld region. While wind shear is an important feature in supercell and MCC development, the lack there of can mean isolated convection will become more prominent over the region, where rainfall is all ready spatially and temporally rare.

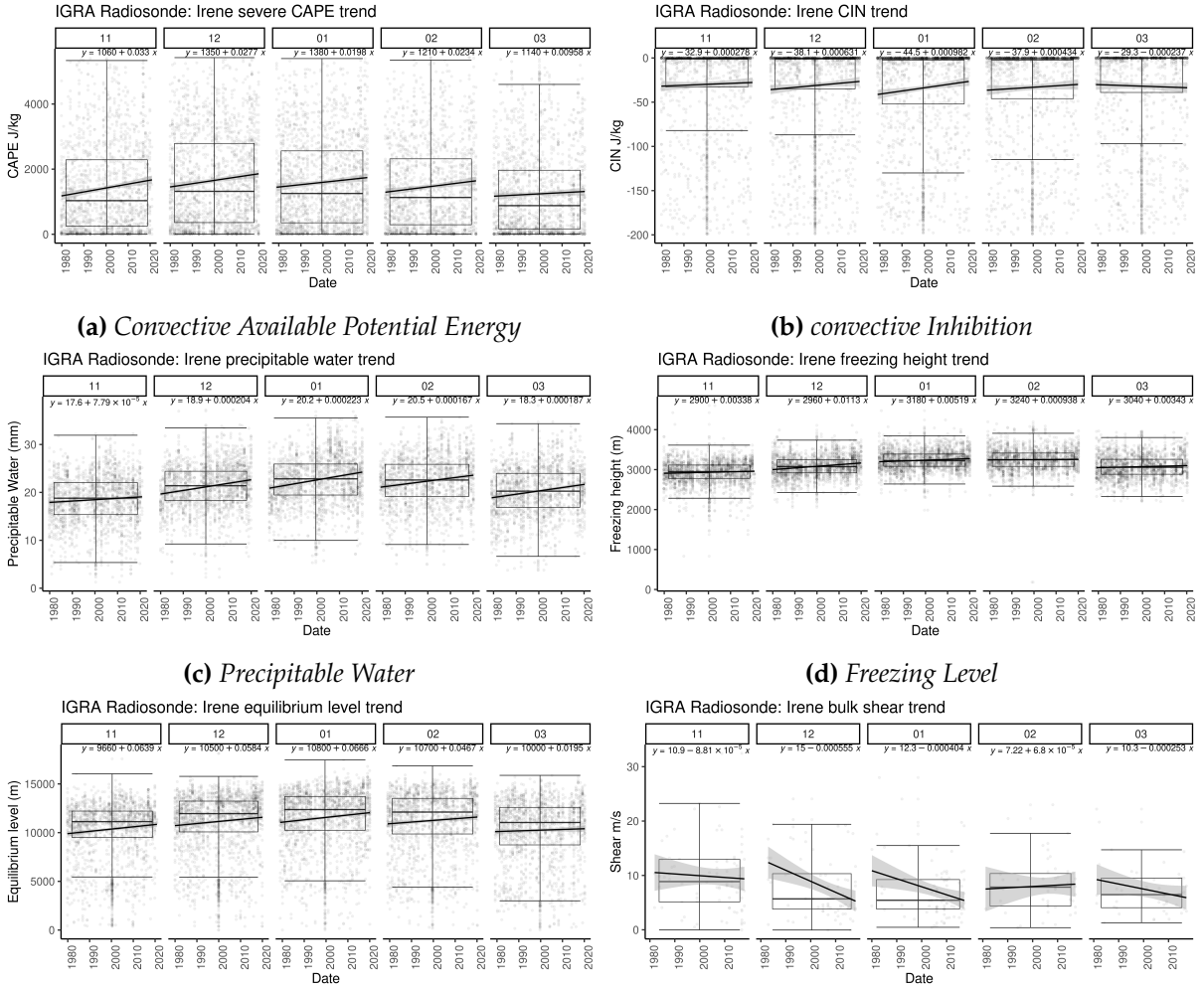

(a) *Convective Available Potential Energy*

(b) *convective Inhibition*

(c) *Precipitable Water*

(d) *Freezing Level*

(e) *Equilibrium Level*

(f) *Wind Shear (850hPa - 500hPa)*

Figure 7.22: *Long term data from 1979 shows an increase in CAPE from radiosonde observations over Irene, indicating an environment favouring severe convective storms over the Highveld. Also interesting to note here are the other variables (precipitable water, freezing level and equilibrium level) that indicate that the atmosphere is becoming more favourable to extreme weather events. As the atmosphere warms, we can look to the Clausius-Clapeyron equation and expect an atmosphere that can hold more moisture as temperatures increase. At the same time, a higher freezing level means that particles may remain suspended in the atmosphere for longer, while growing in size.*

Several studies have examined the changing atmospheric precipitable water content as a function of the well known Clausius-Clapeyron equation (Held and Soden, 2006; Mohr and Kunz, 2013; Trapp et al., 2007; Trenberth, 2012). The Clausius-Clapeyron equation described by (Held and Soden, 2006),

$$\frac{d \ln e_s}{dT} = \frac{L}{RT^2} = \alpha(T), \tag{7.1}$$

Warming can increase latent heat (L) of the atmosphere and subsequently the saturation vapour pressure (e_s) by 7% for every 1-kelvin increase in temperature. The increase in latent heat storage creates a positive feedback mechanism; as water vapour stores more latent heat and the saturation vapour pressure increases. This has considerable impacts on the storm environment and can also increase heavy precipitation.

Conclusion

The interaction between the urban CCN concentration, thunderstorm formation and surface precipitation is complex, as was evident from introduction (see *The aerosol and convective cloud life cycle on page 15*). CCN can either enhance or reduce precipitation as a function of size, concentration, lifetime and variety of other factors not necessarily accounted for in the simulations, or even in our current understanding of microphysics. Similarly, the effects of land-use in an urban climate is complex, from the moisture flux around plants, the albedo of township building materials (Mathee et al., 2021), to the topography in the region.

In this chapter we examined convective storm characteristics under a variety of scenarios. The results show that the inclusion of the new *aerosol aware* parameterisation scheme improves storm day simulations. More intense storms, higher rainfall, hail and graupel were simulated when this scheme was activated, regardless of CCN concentration. The results support the conclusions of Ross et al. (2003). Increased CCN results in less precipitation over the urban area. Changing the land-use characteristics significantly changes precipitation characteristics over the city further. Modelled hail and precipitation reaching the surface is the highest in a green city scenario while the two polluted city simulations show that decreasing the vegetation cover decreases the likelihood of hail. Thermodynamically, the GRNCITY consistently has the highest CAPE leading up to the severe storm occurrence, the increase in latent heat over the area will increase moisture availability, and enhance the convective lifting of the parcel. Both AER2 and 3 has a persistent stable layer, this is significant finding and indicates that increased CCN concentrations results in the heating of the lower troposphere and decreases convective instability. The mechanism of heating is complex, and the thermodynamics could be directly affected by the CCN concentrations, or it could be an indirect effect due to changes in the droplet number or size, however the mechanism for heating was not examined in the scope of this study.

Although it was not the purpose of the study, it is clear that the inclusion of localised CCN and land-use data will improve model results. In most cases, the default model coefficients for most physical parameters are generalised for North-American conditions. In practical terms this means that, for example, Kimberly and Johannesburg are both classified as urban areas, however, an understanding of South African geography will immediately allow the user to realise that these urban areas have vastly different land-use characteristics, and accounting for them in the same manner is not correct. There are also various other considerations that the user must account for. The impact convection on a barren surface might mean that a "less" severe weather event could have more impact than a sustainable city with enough vegetation that can absorb likely erosion and flash flooding. It is beyond the scope of this thesis to characterise this, but it has to be an important consideration when thinking about the nature of local-scale convection. This study could also be viewed from a different lens, i.e. *local-scale drought could be*

enhanced by urbanisation. Future case studies should invest in including high-resolution datasets specific to South African areas to better apply models to our local landscape. Fundamental to this is major observational research that must be undertaken regularly. This includes aerosol measurements, ice characterisation and land-use monitoring. This will have to occur during all seasons for accurate results. Improving our understanding of the local microphysics, CCN concentration, land-use and vegetation characteristics and model uncertainties will improve NWP on a very localised level and assist stakeholders in applying targeted interventions to mitigate weather-related risks.

Chapter 8
Summary and conclusions

This thesis attempted to improve the current knowledge of anthropogenic impacts on convective weather over the South African Highveld by building a novel climatology using radar-derived data, radiosonde data and media reports. We extended this to see if there is a difference between urban and rural storms by examining the spatial characteristics of storms in various land-use areas. Finally, the study modelled a severe storm event over Johannesburg using WRF and examined the effects of clean and polluted environments on storm characteristics by applying an aerosol aware parameterisation scheme and land-use modifications to various model runs. The following chapter summarises the findings of the research.

Using a suite of methods, the thesis characterised the nature of small-scale impacts on convective events over the Highveld. A first analysis of convective weather events as derived from the Irene radar, provided a detailed spatio-temporal characterisation of storms in the area. The radar data were used to examine observed changes to storm characteristics over different land-use and topographical areas. Using media reports we were able to understand the significance of convective weather to the region by classifying events according to their type and impact. This is the first study to examine the collection of convective reports over the Highveld. The conditions under which these significant events occurred in were examined from the synoptic to the thermodynamic scale. This was achieved using an objective clustering method which helped describe the complex number of synoptic conditions leading to convective events. The thermodynamic environment of these events was analysed using radiosonde data from the IGRA. Finally, the results from the simulations shows that small-scale modifications to an urban area can significantly modify the thermodynamic and precipitation characteristics of local scale convective events. Increasing the CCN number concentration results in the formation of inversion layers, which decreases and delays precipitation. Additionally, increasing the vegetation results in increases to the accumulated hail and rainfall over the region, possibly due to increased local moisture and instability. The final section examined future convective environment over the Highveld, showing that while instability is increasing, wind shear is decreasing, highlighting a possible shift to convective weather dominated by tropical forcing.

The overall conclusion of this thesis, is that humans can alter the nature of convective storms over an urban area through pollution and land use changes. In turn, these changes alter the local scale thermodynamics and aerosol profile, which plays a major role in the eventual characteristics of storms. The main contributions of the current study to convective weather research in SA are listed below:

The nature of convective weather events over the Highveld using radar data

The study used radar data to characterise convective events over Gauteng and parts of the Highveld.

- Convective events over the Highveld have a strong diurnal pattern, with convection peaking at 1500 UTC.
- There is a distinct difference in the dynamics between storms in early and mid-summer convective events. These differences manifest themselves in the storm speed, rain rate, hail probability and cloud structure, such as the cloud top.
- Fast-moving convective storms, with the highest maximum rain rate and hail probability occur most frequently in November (early summer).
- Slow-moving storms, characteristic of isolated thunderstorms, high mean rain rate and low probability of hail occur most frequently in January (mid-summer).
- Understanding the local scale nature of convective storms allows for adequate planning and mitigation of risks.

The significance of convective weather impacts over the Highveld

Using a database of reported weather events, this section characterised the significance of convective weather, economically and socially, over the region.

- Damage from these events are common, and over 75 reports mention livestock or human fatality, while over 20 events had reported damage over ZAR 1 million.
- There has been a continued increase in the number of significant weather reports over the region.
- November has the most severe and non-severe convective weather reports.
- There is a distinction between reported events during early- and mid-summer. Early summer reports are predominantly hail events, while mid-summer events are predominantly associated with heavy rainfall.
- The region experiences, on average, 5 – 10 severe hail events and 10 – 15 heavy rainfall events per year. and
- The trends of hail reports, even when accounting for increase in digital media, has remained fairly consistent since the 1980's. Rainfall reports have increased substantially since the 1980's. This supports later findings of an environment possibly favoring heavy rainfall events, characteristic of tropical circulation.

The synoptic and thermodynamic environment of significant convective events

The dates on which significant weather events, that had an economic or social impact, occurred on are used to examine the synoptic and thermodynamic environment associated with the event.

The synoptic environment of impactful events:

- Localised instability plays a major role in convective weather during mid-summer months. Tropical continental low and TTT are a major contributor to significant convective storms, and particularly to rainfall. The westerlies is displaced during heavy rainfall events indicating the tropical forcing dominating during this time.
- A ridging high over the eastern escarpment is another important feature for moisture advection over the Highveld, and is particularly prominent during early summer. This orographic feature can enhance convection over the eastern Highveld. At the same time, there is strong westerly wave at 500 hPa, enhancing wind shear and conditional instability.

The thermodynamic and wind profile of impactful events:

- The highest mean CAPE for all reported events is observed in November, while other CP's during this time also indicate the most favourable environment for severe storm development.
- CIN which plays a role in inhibiting convection is decreasing over the region, possibly favoring rapid storm development.
- There is a strong correlation between the height of the freezing levels and the occurrence of hail events. November events, predominantly hail, have a low freezing level and is associated with extra-tropical circulation.
- January events, dominated by rainfall, have a high freezing level and is associated with a tropical/convective environment.
- Hail and tornado events occur under high mean wind shear conditions. Thunderstorms and heavy rainfall occur under lower mean wind shear conditions.

Small scale anthropogenic and non-anthropogenic impacts on observed convective events

Radar data is used to characterise observed convective events over a variety of landscapes that include regions of complex topography, urban areas, informal areas and industrial areas. To support the radar data, lightning observations are extracted over the same regions.

- Topography plays a role in storm dynamics. Storms over complex terrain have higher dBZ and cloud tops suggests orographic enhancement over such areas in comparisons to areas with simple topography.
- Rural areas close to Johannesburg have fewer and less severe storms than the Johannesburg CBD and suburban areas.
- There is a higher storm frequency over an informal area than rural areas due west and east of it.
- Directly over a power station, there is a low frequency of convective storms compared to sites due east and west of the station.

Changes in significant storm event characteristics under different CCN and land use scenarios

WRF was employed to simulate a convective event under various land use and CCN concentrations. Changes in the thermodynamics, cloud characteristics and surface precipitation under these different scenarios were examined to understand the possible effects of unintended small-scale impacts.

- The section examined different urban development scenarios and the impact on convective storm characteristics.
- Increasing the CCN results in the presence of a persistent stable layer which inhibits convection.
- Under a low vegetation and high albedo scenario (characteristic of a sprawling informal settlement), the lowest surface rainfall and accumulated hail was simulated.
- Under a low vegetation and low albedo scenario (according to traditional UHI models), early and sporadic precipitation occurs.
- Cities with low vegetation cover, irrespective of albedo, have more sporadic rainfall and instability. Storms in these scenarios are characteristic of isolated convection, in which only warm cloud processes dominate.
- Under a green city with high vegetation cover (similar to affluent areas in Johannesburg) and moderate albedo, more intense storms, accumulated hail, and accumulated surface precipitation is simulated. This indicates that vegetation significantly affects storm severity, possibly due to increased surface moisture and latent heat, which also increases instability.

Long term changes in the nature of the convective environment over the Highveld

Using radiosonde data, the final chapter examines the changing nature of the convective storm environment over Gauteng.

- All thermodynamic indicators associated with instability show a significant increase in a convective favoring environment.
- Wind-shear, which is particularly important during the occurrence of hail, and an early summer feature, has decreased.
- The changes described above indicate that the environment is favoring tropical circulation, associated with convective instability, while the impact of extra-tropical features associated with conditional instability is decreasing.
- These observed changes are consistent with current projections of anthropogenic climate change.

Future research is required to examine the physical processes which results in formation of stable layers under high CCN scenarios. The thermodynamics could be directly affected by the CCN concentrations, or it could be an indirect effect due to changes in the droplet number or size. It would, in the context of this study, be valuable to conduct in-situ research campaigns to characterise the aerosol profile directly above Johannesburg, which would allow us to force models with accurate local conditions and improve our understanding of the storm dynamics over the region.

References

↑ refers back to in text citations

Abdelmotaleb, A., Järvinen, E., Duft, D., Hirst, E., Vogt, S., Leisner, T. and Schnaiter, M. (2016). PHIPS-HALO: the airborne Particle Habit Imaging and Polar Scattering probe. Part 1: Design and operation, *Atmospheric Measurement Techniques* . (↑8)

AghaKouchak, A., Chiang, F., Huning, L. S., Love, C. A., Mallakpour, I., Mazdiyasni, O., Moftakhari, H., Papalexiou, S. M., Ragno, E. and Sadegh, M. (2020). Climate Extremes and Compound Hazards in a Warming World, *Annual Review of Earth and Planetary Sciences* **48**. (↑2)

Alber, K., Zhou, L. and Raghavendra, A. (2021). A shift in the diurnal timing and intensity of deep convection over the Congo Basin during the past 40 years, *Atmospheric Research* **264**: 105869. (↑65)

Albrecht, B. A. (1989). Aerosols, cloud microphysics, and fractional cloudiness, *Science* **245**(4923): 1227–1230. (↑22), (↑23), (↑163)

Albrecht, R. I., Goodman, S. J., Buechler, D. E., Blakeslee, R. J. and Christian, H. J. (2016). Where are the lightning hotspots on Earth?, *Bulletin of the American Meteorological Society* **97**(11): 2051–2068. (↑121)

Allen, J. T. (2017). Atmospheric hazards: Hail potential heating up, *Nature Climate Change* **7**(7): 474. (↑33)

Allen, J. T., Tippett, M. K. and Sobel, A. H. (2015). An empirical model relating US monthly hail occurrence to large-scale meteorological environment, *Journal of Advances in Modeling Earth Systems* **7**(1): 226–243. (↑146)

AMS (2016). Glossary of Meteorology. (↑16)

Andreae, M. and Rosenfeld, D. (2008). Aerosol–cloud–precipitation interactions. Part 1. The nature and sources of cloud-active aerosols, *Earth-Science Reviews* **89**(1-2): 13–41. (↑15), (↑19)

Arghavani, S., Malakooti, H. and Bidokhti, A.-A. A. A. (2020). Numerical assessment of the urban green space scenarios on urban heat island and thermal comfort level in Tehran Metropolis, *Journal of Cleaner Production* **261**: 121183. (↑55)

Arnold, D. L. (2008). Severe deep moist convective storms: Forecasting and mitigation, *Geography Compass* **2**(1): 30–66. (↑17)

Atwater, M. A. (1970). Planetary albedo changes due to aerosols, *Science* **170**(3953): 64–66. (↑22), (↑163)

Ayob, N. (2019). Hail nowcasting over the South African Highveld. MSc dissertation, North West University Potchefstroom. (↑143)

Balashov, N. V., Thompson, A. M., Piketh, S. J. and Langerman, K. E. (2014). Surface ozone variability and trends over the South African Highveld from 1990 to 2007, *Journal of Geophysical Research: Atmospheres* **119**(7): 4323–4342. (↑25)

Barros, A. P. and Lettenmaier, D. P. (1994). Dynamic modeling of orographically induced precipitation, *Reviews of Geophysics* **32**(3): 265–284. (↑124)

Barry, H. (2014). Short-term insurers take a R1.6bn hammering, *Moneyweb* . (↑2), (↑6), (↑73), (↑143)

Barry, R. G. and Chorley, R. J. (2009). *Atmosphere, Weather and Climate*, Routledge. (↑6), (↑7)

Bauer, P., Thorpe, A. and Brunet, G. (2015). The quiet revolution of numerical weather prediction, *Nature* **525**(7567): 47–55. (↑142)

Betts, N. (2003). Analysis of an anomalously severe thunderstorm system over Northern Ireland, *Atmospheric Research* **67**: 23–34. (↑49)

Bhavika, B. (2007). The influence of terrain elevation on lightning density in South Africa. MSc dissertation, University of Johannesburg. (↑60), (↑122)

Blakeslee, R. J., Christian, H. J., Stewart, M., Mach, D., Bateman, M., Walker, T. D., Buechler, D., Koshak, W., O'Brien, S., Wilson, T. et al. (2014). Lightning Imaging Sensor (LIS) for the International Space Station (ISS): mission description and science goals, *XV Int. Conf. Atmos. Electricity*. (↑43)

Blakeslee, R. J., Lang, T. J., Koshak, W. J., Buechler, D., Gatlin, P., Mach, D. M., Stano, G. T., Virts, K. S., Walker, T. D., Cecil, D. J. et al. (2020). Three years of the Lightning Imaging Sensor onboard the International Space Station: Expanded global coverage and enhanced applications, *Journal of Geophysical Research: Atmospheres* **125**(16): e2020JD032918. (↑43)

Blamey, R., Middleton, C., Lennard, C. and Reason, C. (2016). A climatology of potential severe convective environments across South Africa, *Climate Dynamics* pp. 1–18. (↑11), (↑12), (↑13), (↑38), (↑45), (↑46), (↑85), (↑87)

Bopape, M.-J. M., Sithole, H. M., Motshegwa, T., Rakate, E., Engelbrecht, F., Archer, E., Morgan, A., Ndimeni, L. and Botai, J. (2019). A regional project in support of the SADC cyber-infrastructure framework implementation: Weather and climate, *Data Science Journal* . (↑143)

Brimelow, J. C., Burrows, W. R. and Hanesiak, J. M. (2017). The changing hail threat over North America in response to anthropogenic climate change, *Nature Climate Change* **7**(7): 516. (↑33)

Broccardo, S. (2015). Airborne DOAS Measurements over the South African Highveld. PhD thesis, University of Witwatersrand. (↑10)

Brooks, H. E. (2013). Severe thunderstorms and climate change, *Atmospheric Research* **123**: 129–138. (↑114)

Brooks, H. E., Doswell, C. A. and Cooper, J. (1994). On the environments of tornadic and non-tornadic mesocyclones, *Weather and Forecasting* **9**(4): 606–618. (↑18), (↑114), (↑164), (↑165)

Brooks, H. E., Lee, J. W. and Craven, J. P. (2003). The spatial distribution of severe thunderstorm and tornado environments from global reanalysis data, *Atmospheric Research* **67**: 73–94. (↑114)

Bruintjes, R. T. (1999). A review of cloud seeding experiments to enhance precipitation and some new prospects, *Bulletin of the American Meteorological Society* **80**(5): 805–820. (↑30)

Bühl, J., Seifert, P., Engelmann, R. and Ansmann, A. (2019). Impact of vertical air motions on ice formation rate in mixed-phase cloud layers, *NPJ Climate and Atmospheric Science* **2**(1): 1–5. (↑19)

Burgess, D. W., Magsig, M. A., Wurman, J., Dowell, D. C. and Richardson, Y. (2002). Radar observations of the 3 May 1999 Oklahoma City tornado, *Weather and forecasting* **17**(3): 456–471. (↑59)

Caelum (1991). History of notable weather events in South Africa 1500–1990. (↑43), (↑44), (↑45), (↑77)

Carte, A. and Held, G. (1978). Variability of hailstorms on the South African Plateau, *Journal of Applied Meteorology* **17**(3): 365–373. (↑2), (↑4), (↑5), (↑12), (↑43), (↑59), (↑60), (↑62), (↑117)

Cattell, R. B. (1966). The scree test for the number of factors, *Multivariate Behavioral Research* **1**(2): 245–276. (↑46)

Cecil, D. J., Buechler, D. E. and Blakeslee, R. J. (2014). Gridded lightning climatology from TRMM-LIS and OTD: Dataset description, *Atmospheric Research* **135**: 404–414. (↑43), (↑60), (↑121)

Cecil, D. J., Buechler, D. E. and Blakeslee, R. J. (2015). TRMM LIS climatology of thunderstorm occurrence and conditional lightning flash rates, *Journal of Climate* **28**(16): 6536–6547. (↑43), (↑60), (↑121)

Changnon, S. A. (1992a). Inadvertent weather modification in urban areas: lessons for global climate change, *Bulletin of the American Meteorological Society* **73**(5): 619–627. (↑3), (↑4), (↑31)

Changnon, S. A. (1992b). Temporal and spatial relations between hail and lightning, *Journal of Applied Meteorology and Climatology* **31**(6): 587–604. (↑61)

Changnon, S. A., Huff, F. A., Schickedanz, P. T. and Vogel, J. L. (1977). Summary of METROMEX, Volume 1: Weather anomalies and impacts. (↑3), (↑4), (↑31)

Chapman, S., Watson, J. E., Salazar, A., Thatcher, M. and McAlpine, C. A. (2017). The impact of urbanization and climate change on urban temperatures: a systematic review, *Landscape Ecology* **32**(10): 1921–1935. (↑31)

Charlton-Perez, A. and Dacre, H. (2011). Lewis Fry Richardson's forecast factory–for real, *Weather* **66**(2): 52–54. (↑28), (↑142)

Chidhindi, P., Belelie, M. D., Burger, R. P., Mkhatshwa, G. and Piketh, S. J. (2019). Assessing the impact of Eskom power plant emissions on ambient air quality over KwaZamokuhle, *Clean Air Journal* **29**(1): 29–37. (↑135), (↑136)

Chronis, T. and Koshak, W. J. (2017). Diurnal variation of TRMM/LIS lightning flash radiances, *Bulletin of the American Meteorological Society* **98**(7): 1453–1470. (↑43), (↑60), (↑121)

Collett, K. S., Piketh, S. J. and Ross, K. E. (2010). An assessment of the atmospheric nitrogen budget on the South African Highveld, *South African Journal of Science* **106**(5-6): 35–43. (↑34)

Cotton, W. R. (1982). Modification of precipitation from warm clouds – A review, *Bulletin of the American Meteorological Society* **63**(2): 146–160. (↑30)

Cover (2013). Mutual and Federal manages influx of claims, *Cover* .
URL: *https://www.cover.co.za/mutual-and-federal-manages-influx-of-claims/* (↑2), (↑6)

Craven, J. P., Brooks, H. E. and Hart, J. A. (2004). Baseline climatology of sounding derived parameters associated with deep, moist convection, *National Weather Digest* **28**(1): 13–24. (↑34), (↑38), (↑40), (↑104), (↑106), (↑107), (↑114)

Crétat, J., Pohl, B., Richard, Y. and Drobinski, P. (2012). Uncertainties in simulating regional climate of Southern Africa: sensitivity to physical parameterizations using WRF, *Climate Dynamics* **38**(3-4): 613–634. (↑51), (↑143)

Ćwik, P., McPherson, R. A. and Brooks, H. E. (2021). What Is a Tornado Outbreak?: Perspectives through Time, *Bulletin of the American Meteorological Society* **102**(4): E817–E835. (↑77)

DAbreton, P. (1991). A synoptic characterization of some South African tornadoes, *South African Journal of Science* **87**(1): 56–61. (↑13)

Dagan, G., Koren, I., Altaratz, O. and Heiblum, R. H. (2016). Aerosol effect on the evolution of the thermodynamic properties of warm convective cloud fields, *Scientific reports* **6**: 38769. (↑3), (↑19), (↑20)

Davies-Jones, R. (2015). A review of supercell and tornado dynamics, *Atmospheric Research* **158**: 274–291. (↑46)

De Coning, E. and Adam, B. (2000). The tornadic thunderstorm events during the 1998-1999 South African summer, *Water SA* **26**(3): 361–376. (↑13), (↑88), (↑89), (↑90), (↑118)

De Coning, E., Adam, B. and Banitz, L. (2000). A severe weather event on 29 December 1997: synoptic and mesoscale perspectives, *Water SA* **26**(2): 137–146. (↑118)

De Coning, E., Forbes, G. S. and Poolman, E. (1998). Heavy precipitation and flooding on 12-14 February 1996 over the summer rainfall regions of South Africa: Synoptic and isentropic analyses, *National Weather Digest* **22**: 25–36. (↑48), (↑83), (↑118), (↑119)

De Lange, A., Naidoo, M., Garland, R. M. and Dyson, L. L. (2021a). Sensitivity of meteorological variables on planetary boundary layer parameterization schemes in the WRF-ARW model, *Atmospheric Research* **247**: 105214. (↑51), (↑143)

De Lange, A., Naidoo, M., Garland, R. M. and Dyson, L. L. (2021b). The sensitivity of simulated surface-level pollution concentrations to WRF-ARW-model PBL parameterisation schemes over the Highveld of South Africa, *Atmospheric Research* **254**: 105517. (↑51), (↑143)

Dedekind, Z., Engelbrecht, F. A., Burger, R. P. and Piketh, S. (2013). Modelling the attibutes of rainfall over the eastern escarpment of South Africa, *29th Annual Conference of South African Society for Atmospheric Sciences*, p. 142. (↑7)

Department of Environment Forestry & Fisheries (2019). South African National Land-Cover 2018. (↑46)

Devara, P. and Manoj, M. (2013). Aerosol–cloud–precipitation interactions: A challenging problem in regional environment and climate research, *Particuology* **11**(1): 25–33. (↑15)

Dimitrova, R., Danchovski, V., Egova, E., Vladimirov, E., Sharma, A., Gueorguiev, O. and Ivanov, D. (2019). Modeling the impact of urbanization on local meteorological conditions in Sofia, *Atmosphere* **10**(7): 366. (↑31)

Dixon, M. and Wiener, G. (1993). TITAN: Thunderstorm identification, tracking, analysis, and nowcasting-A radar-based methodology, *Journal of Atmospheric and Oceanic Technology* **10**(6): 785–797. (↑42)

Doswell, C. A. (1991). A review for forecasters on the application of hodographs to forecasting severe thunderstorms, *National Weather Digest* **16**(1): 2–16. (↑114)

Doswell, C. A. and Evans, J. S. (2003). Proximity sounding analysis for derechos and supercells: An assessment of similarities and differences, *Atmospheric Research* **67**: 117–133. (↑145)

Doyle, J. D. and Durran, D. R. (2002). The dynamics of mountain-wave-induced rotors, *Journal of the Atmospheric Sciences* **59**(2): 186–201. (↑123)

Du Preez, R. G. (2017). Deployment, re-engineering and risk analysis of a C-band weather radar to build local capacity in South Africa. MSc dissertation, North West University Potchefstroom. (↑42)

Dudhia, J. (2014). Overview of WRF Physics, *University Corporation for Atmospheric Research, Boulder, CO, http://www2. mmm. ucar. edu/wrf/users/tutorial/201401/Physics_full. pdf* . (↑26)

Duong, T. et al. (2007). ks: Kernel density estimation and kernel discriminant analysis for multivariate data in R, *Journal of Statistical Software* **21**(7): 1–16. (↑47)

Dupilka, M. L. and Reuter, G. W. (2006). Forecasting tornadic thunderstorm potential in Alberta using environmental sounding data. Part I: Wind shear and buoyancy, *Weather and Forecasting* **21**(3): 325–335. (↑111), (↑114)

Durre, I., Vose, R. S. and Wuertz, D. B. (2006). Overview of the integrated global radiosonde archive, *Journal of Climate* **19**(1): 53–68. (↑37), (↑39)

Durre, I., Vose, R. S. and Wuertz, D. B. (2008). Robust automated quality assurance of radiosonde temperatures, *Journal of Applied Meteorology and Climatology* **47**(8): 2081–2095. (↑37)

Dyson, L. L. (2009). Heavy daily-rainfall characteristics over the Gauteng Province, *Water SA* **35**(5). (↑11), (↑12), (↑34)

Dyson, L. L. (2013). Atmospheric thermodynamics and circulation associated with heavy rainfall over the Gauteng Province, South Africa. PhD thesis, University of Pretoria. (↑11), (↑12), (↑18), (↑38)

Dyson, L. L. (2015). A heavy rainfall sounding climatology over Gauteng, South Africa, using self-organising maps, *Climate Dynamics* **45**(11-12): 3051–3065. (↑14), (↑34), (↑39), (↑67), (↑68), (↑85), (↑87), (↑107)

Dyson, L. L., Pienaar, N., Smit, A. and Kijko, A. (2021). An ERA-Interim HAILCAST hail climatology for southern Africa, *International Journal of Climatology* **41**(1): 262–277. (↑143)

Dyson, L. L., Van Heerden, J. and Sumner, P. D. (2015). A baseline climatology of sounding-derived parameters associated with heavy rainfall over Gauteng, South Africa, *International Journal of Climatology* **35**(1): 114–127. (↑34), (↑38), (↑40)

Eliseev, A. (2013). Parts of Tswane declared 'disasters areas', *Eye Witness News* . (↑2), (↑143)

ENCA (2013). Hail storm destroys shacks, *ENCA* .
URL: *https://www.enca.com/south-africa/shacks-destroyed-hailstorm* (↑6)

ENCA (2016). Tornado damages Tembisa Hospital, Phumulani Mall, *ENCA* .
URL: *https://www.enca.com/south-africa/roof-collapse-at-tembisas-phumulani-mall* (↑81)

Engelbrecht, C. J., Landman, W. A., Engelbrecht, F. A. and Malherbe, J. (2015). A synoptic decomposition of rainfall over the Cape south coast of South Africa, *Climate Dynamics* **44**(9-10): 2589–2607. (↑14)

Engelbrecht, C. J., Landman, W. A., Graham, R. and McLean, P. (2017). Seasonal predictive skill of intraseasonal synoptic type variability over the Cape south coast of South Africa by making use of the Met Office Global Seasonal Forecast System 5, *International Journal of Climatology* **37**(4): 1998–2012. (↑14)

Engelbrecht, E. H., Landman, W. A. and Landman, S. (2021). The Impact of High-Resolution Soil Moisture States on Short-Term Numerical Weather Prediction of Convective Initiation over South Africa, *arXiv preprint arXiv:2102.08523* . (↑143)

Eye Witness News (2013). Flood warnings for storm-hit Gauteng, *Eye Witness News* .
URL: *https://ewn.co.za/2013/11/28/Flood-warnings-for-storm-hit-Gauteng* (↑143), (↑146)

Fan, J., Rosenfeld, D., Zhang, Y., Giangrande, S. E., Li, Z., Machado, L. A., Martin, S. T., Yang, Y., Wang, J., Artaxo, P. et al. (2018). Substantial convection and precipitation enhancements by ultrafine aerosol particles, *Science* **359**(6374): 411–418. (↑3), (↑16), (↑20)

Fan, J., Wang, Y., Rosenfeld, D. and Liu, X. (2016). Review of aerosol–cloud interactions: mechanisms, significance, and challenges, *Journal of the Atmospheric Sciences* **73**(11): 4221–4252. (↑3), (↑16), (↑20)

Fitchett, J. M. (2018). Recent emergence of CAT5 tropical cyclones in the South Indian Ocean, *South African Journal of Science* **114**(11-12): 1–6. (↑10)

Foote, G. B., Krauss, T. W. and Makitov, V. (2005). Hail metrics using conventional radar, *Proc., 16th Conference on Planned and Inadvertent Weather Modification*. (↑73)

Freiman, M. and Piketh, S. (2003). Air transport into and out of the industrial Highveld region of South Africa, *Journal of Applied Meteorology* **42**(7): 994–1002. (↑34)

Frew, E. W., Argrow, B., Borenstein, S., Swenson, S., Hirst, C. A., Havenga, H. and Houston, A. (2020). Field observation of tornadic supercells by multiple autonomous fixed-wing unmanned aircraft, *Journal of Field Robotics* **37**(6): 1077–1093. (↑XV)

Fromm, M., Miller, S., Turk, J. and Lee, T. (2007). Pyroconvection and Climate Change, *Technical report*, Naval Research Lab. Washington, D.C. Defense Technical Information Center. (↑30)

Ganeshan, M., Murtugudde, R. and Strack, J. (2013). The role of negative buoyancy in surface-based convection and its representation in cumulus parameterization schemes, *Journal of Applied Meteorology and Climatology* **52**(12): 2887–2905. (↑104)

Garstang, M., Emmitt, G. and Kelbe, B. (1981). Rain augmentation in Nelspruit (RAIN), *Technical report*. (↑31)

Garstang, M., Tyson, P. and Emmitt, G. (1975). The structure of heat islands, *Reviews of Geophysics* **13**(1): 139–165. (↑31), (↑32), (↑46), (↑127), (↑128)

Geldenhuys, M., Dyson, L. L. and Van Der Mescht, D. (2020). Blocking, gap flow and mountain wave interaction along the coastal escarpment of South Africa, *Theoretical and Applied Climatology* **139**(3): 1291–1303. (↑123)

Gettelman, A., Seidel, D., Wheeler, M. and Ross, R. (2002). Multidecadal trends in tropical convective available potential energy, *Journal of Geophysical Research: Atmospheres* **107**(D21). (↑38)

Gijben, M. (2012). The lightning climatology of South Africa, *South African Journal of Science* **108**(3): 1–10. (↑60), (↑122)

Gijben, M. and De Coning, E. (2017). Using satellite and lightning data to track rapidly developing thunderstorms in data sparse regions, *Atmosphere* **8**(4): 67. (↑60), (↑122)

Gimeno, L. (2013). Grand challenges in atmospheric science, *Frontiers in Earth Science* **1**: 1. (↑33)

Goyette, S. (2011). Synoptic conditions of extreme windstorms over Switzerland in a changing climate, *Climate Dynamics* **36**(5): 845–866. (↑46), (↑57)

Groenemeijer, P. and Van Delden, A. (2007). Sounding-derived parameters associated with large hail and tornadoes in the Netherlands, *Atmospheric Research* **83**(2): 473–487. (↑40), (↑104), (↑105), (↑107), (↑146)

Hansen, J., Ruedy, R., Sato, M. and Lo, K. (2010). Global surface temperature change, *Reviews of Geophysics* **48**: RG4004. (↑37)

Hardy, C. and Nel, A. (2015). Data and techniques for studying the urban heat island effect in Johannesburg, *The International Archives of Photogrammetry, Remote Sensing and Spatial Information Sciences* **40**(7). (↑47), (↑132)

Hart, N., Reason, C. and Fauchereau, N. (2010). Tropical–extratropical interactions over southern Africa: three cases of heavy summer season rainfall, *Monthly Weather Review* **138**(7): 2608–2623. (↑118), (↑119)

Havenga, H. (2018). Characteristics of hailstorms over the South African Highveld. MSc dissertation, North West University Potchefstroom. (↑50), (↑51), (↑142), (↑143)

Heinzeller, D., Junkermann, W. and Kunstmann, H. (2016). Anthropogenic aerosol emissions and rainfall decline in southwestern Australia: Coincidence or causality?, *Journal of Climate* **29**(23): 8471–8493. (↑138)

Held, G. (1977). Description of the unusual behavior of a prefrontal squall line in South Africa, *Journal of Applied Meteorology* **16**(6): 651–653. (↑31)

Held, I. M. and Soden, B. J. (2006). Robust responses of the hydrological cycle to global warming, *Journal of Climate* **19**(21): 5686–5699. (↑170)

Hersbach, H., Bell, B., Berrisford, P., Biavati, G., Horányi, A., Muñoz Sabater, J., Nicolas, J., Peubey, C., Radu, R., Rozum, I. et al. (2018). ERA5 hourly data on single levels from 1979 to present, Copernicus Climate Change Service (C3S) Climate Data Store (CDS), *ECMWF* **147**: 5–6. (↑86)

Hersey, S., Garland, R. M., Crosbie, E., Shingler, T., Sorooshian, A., Piketh, S. and Burger, R. (2015). An overview of regional and local characteristics of aerosols in South Africa using satellite, ground, and modeling data, *Atmospheric Chemistry and Physics* **15**(8): 4259–4278. (↑132)

Hohl, R., Schiesser, H.-H. and Knepper, I. (2002). The use of weather radars to estimate hail damage to automobiles: an exploratory study in Switzerland, *Atmospheric Research* **61**(3): 215–238. (↑6)

Huff, F. A. (1973). Summary report of metromex studies, 1971–1972, *Technical report*, Illinois State Water Survey, Urbana (USA). (↑3)

Huff, F. and Changnon Jr, S. (1973). Precipitation modification by major urban areas, *Bulletin of the American Meteorological Society* **54**(12): 1220–1232. (↑31)

Insua-Costa, D., Lemus-Cánovas, M., Miguez-Macho, G. and Llasat, M. C. (2021). Climatology and ranking of hazardous precipitation events in the western Mediterranean area, *Atmospheric Research* **255**: 105521. (↑14)

IPCC (2007). *Climate Change 2007: Synthesis Report. Contribution of Working Groups I, II and III to the Fourth Assessment Report of the Intergovernmental Panel on Climate Change [Core Writing Team, Pachauri, R.K and Reisinger, A. (eds.)]*., Intergovernmental Panel on Climate Change. (↑3)

Jahn, M. (2015). Economics of extreme weather events: Terminology and regional impact models, *Weather and Climate Extremes* **10**: 29–39. (↑6)

Järvinen, E., Jourdan, O., Neubauer, D., Yao, B., Liu, C., Andreae, M. O., Lohmann, U., Wendisch, M., McFarquhar, G. M., Leisner, T. et al. (2018). Additional global climate cooling by clouds due to ice crystal complexity, *Atmospheric Chemistry and Physics* **18**(21): 15767–15781. (↑8), (↑22)

Kaltenböck, R., Diendorfer, G. and Dotzek, N. (2009). Evaluation of thunderstorm indices from ECMWF analyses, lightning data and severe storm reports, *Atmospheric Research* **93**(1): 381–396. (↑121)

Kapsch, M.-L., Kunz, M., Vitolo, R. and Economou, T. (2012). Long-term trends of hail-related weather types in an ensemble of regional climate models using a Bayesian approach, *Journal of Geophysical Research: Atmospheres* **117**(D15). (↑8)

Keat, W. J., Stein, T. H., Phaduli, E., Landman, S., Becker, E., Bopape, M.-J. M., Hanley, K. E., Lean, H. W. and Webster, S. (2019). Convective initiation and storm life cycles in convection-permitting simulations of the Met Office Unified Model over South Africa, *Quarterly Journal of the Royal Meteorological Society* **145**(721): 1323–1336. (↑9), (↑56), (↑60), (↑70), (↑143)

Kelbe, B. (1984). Cumulus cloud characteristics of the Eastern Transvaal Lowveld, *Water SA* **10**(2): 81–90. (↑43), (↑59), (↑60), (↑117)

Kerminen, V.-M., Chen, X., Vakkari, V., Petäjä, T., Kulmala, M. and Bianchi, F. (2018). Atmospheric new particle formation and growth: review of field observations, *Environmental Research Letters* **13**(10): 103003. (↑3)

Kerminen, V.-M., Paramonov, M., Anttila, T., Riipinen, I., Fountoukis, C., Korhonen, H., Asmi, E., Laakso, L., Lihavainen, H., Swietlicki, E. et al. (2012). Cloud condensation nuclei production associated with atmospheric nucleation: a synthesis based on existing literature and new results, *Atmospheric Chemistry and Physics* **12**(24): 12037–12059. (↑138)

Keywood, M., Kanakidou, M., Stohl, A., Dentener, F., Grassi, G., Meyer, C., Torseth, K., Edwards, D., Thompson, A. M., Lohmann, U. et al. (2013). Fire in the air: Biomass burning impacts in a changing climate, *Critical Reviews in Environmental Science and Technology* **43**(1): 40–83. (↑30)

Kingfield, D. M., Calhoun, K. M., de Beurs, K. M. and Henebry, G. M. (2018). Effects of city size on thunderstorm evolution revealed through a multiradar climatology of the central United States, *Journal of Applied Meteorology and Climatology* **57**(2): 295–317. (↑3), (↑4), (↑31)

Kondo, A., Ueno, M., Kaga, A. and Yamaguchi, K. (2001). The influence of urban canopy configuration on urban albedo, *Boundary-Layer Meteorology* **100**(2): 225–242. (↑55), (↑156)

Korolev, A. (2007). Limitations of the Wegener–Bergeron–Findeisen mechanism in the evolution of mixed-phase clouds, *Journal of the Atmospheric Sciences* **64**(9): 3372–3375. (↑19)

Krayenhoff, E. S., Moustaoui, M., Broadbent, A. M., Gupta, V. and Georgescu, M. (2018). Diurnal interaction between urban expansion, climate change and adaptation in US cities, *Nature Climate Change* **8**(12): 1097–1103. (↑31)

Kruger, A. C. and Nxumalo, M. (2017). Historical rainfall trends in South Africa: 1921–2015, *Water SA* **43**(2): 285–297. (↑14)

Kruger, A. and Sekele, S. (2013). Trends in extreme temperature indices in South Africa: 1962–2009, *International Journal of Climatology* **33**(3): 661–676. (↑3)

Kubheka, T. (2018). Sun City resumes operations following heavy hailstorm, *Eye Witness News* . (↑123)

Kuik, F., Lauer, A., Beukes, J., Van Zyl, P., Josipovic, M., Vakkari, V., Laakso, L. and Feig, G. (2015). The anthropogenic contribution to atmospheric black carbon concentrations in southern Africa: a WRF-Chem modeling study, *Atmospheric Chemistry and Physics* **15**(15): 8809–8830. (↑51), (↑143)

Kumar, A., Dudhia, J., Rotunno, R., Niyogi, D. and Mohanty, U. (2008). Analysis of the 26 July 2005 heavy rain event over Mumbai, India using the Weather Research and Forecasting (WRF) model, *Quarterly Journal of the Royal Meteorological Society* **134**(636): 1897–1910. (↑50)

Labbouz, L., van Baelen, J., Tridon, F., Reverdy, M., Hagen, M., Bender, M., Dick, G., Gorgas, T. and Planche, C. (2013). Precipitation on the lee side of the Vosges Mountains: Multi-instrumental study of one case from the COPS campaign, *Meteorologische Zeitschrift* **22**(4): 413–432. (↑123)

Laprise, R. (2008). Regional climate modelling, *Journal of Computational Physics* **227**(7): 3641–3666. (↑8)

Lee, L., Carslaw, K., Pringle, K. and Mann, G. (2012). Mapping the uncertainty in global CCN using emulation, *Atmospheric Chemistry and Physics* **12**(20): 9739–9751. (↑135)

Lekoloane, L. E., Bopape, M.-J. M., Rambuwani, T. G., Ndarana, T., Landman, S., Mofokeng, P., Gijben, M. and Mohale, N. (2021). A dynamic and thermodynamic analysis of the 11 December 2017 tornadic supercell in the Highveld of South Africa, *Weather and Climate Dynamics* **2**(2): 373–393. (↑13)

Lemus-Canovas, M., Lopez-Bustins, J. A., Martín-Vide, J., Halifa-Marin, A., Insua-Costa, D., Martinez-Artigas, J., Trapero, L., Serrano-Notivoli, R. and Cuadrat, J. M. (2021). Characterisation of extreme precipitation events in the Pyrenees: from the local to the synoptic scale, *Atmosphere* **12**(6): 665. (↑14)

Lemus-Canovas, M., Lopez-Bustins, J. A., Martin-Vide, J. and Royé, D. (2019). synoptReg: An R package for computing a synoptic climate classification and a spatial regionalization of environmental data, *Environmental Modelling & Software* **118**: 114–119. (↑46)

Lemus-Canovas, M., Lopez-Bustins, J. A., Trapero, L. and Martin-Vide, J. (2019). Combining circulation weather types and daily precipitation modelling to derive climatic precipitation regions in the Pyrenees, *Atmospheric Research* **220**: 181–193. (↑14), (↑46)

Li, F., Chavas, D. R., Reed, K. A. and Dawson II, D. T. (2020). Climatology of severe local storm environments and synoptic-scale features over North America in ERA5 reanalysis and CAM6 simulation, *Journal of Climate* **33**(19): 8339–8365. (↑86), (↑87)

Li, M., Zhang, Q. and Zhang, F. (2016). Hail day frequency trends and associated atmospheric circulation patterns over China during 1960–2012, *Journal of Climate* **29**(19): 7027–7044. (↑46)

Li, Z., Lau, W.-M., Ramanathan, V., Wu, G., Ding, Y., Manoj, M., Liu, J., Qian, Y., Li, J., Zhou, T. et al. (2016). Aerosol and monsoon climate interactions over Asia, *Reviews of Geophysics* **54**(4): 866–929. (↑15), (↑18), (↑21), (↑22)

Liang, X.-Z., Xu, M., Yuan, X., Ling, T., Choi, H. I., Zhang, F., Chen, L., Liu, S., Su, S., Qiao, F. et al. (2012). Regional climate-weather research and forecasting model, *Bulletin of the American Meteorological Society* **93**(9): 1363–1387. (↑50)

Lin, P.-F., Chang, P.-L., Jou, B. J.-D., Wilson, J. W. and Roberts, R. D. (2011). Warm season afternoon thunderstorm characteristics under weak synoptic-scale forcing over Taiwan Island, *Weather and Forecasting* **26**(1): 44–60. (↑6)

Liu, J. and Niyogi, D. (2019). Meta-analysis of urbanization impact on rainfall modification, *Scientific Reports* **9**(1): 1–14. (↑3), (↑4), (↑31)

Lynch, P. (2008). The origins of computer weather prediction and climate modeling, *Journal of Computational Physics* **227**(7): 3431–3444. (↑142)

Macron, C., Pohl, B., Richard, Y. and Bessafi, M. (2014). How do tropical temperate troughs form and develop over southern Africa?, *Journal of Climate* **27**(4): 1633–1647. (↑118), (↑119)

Madden, R. A. (1976). Estimates of the natural variability of time-averaged sea-level pressure, *Monthly Weather Review* **104**(7): 942–952. (↑142)

Madden, R. A. (1983). Reply, *Monthly Weather Review* **111**(3): 586–589. (↑142)

Mader, G., Neishlos, H., Saunders, M. and Carte, A. (1986). Some characteristics of storms on the Transvaal Highveld, *Journal of Climatology* **6**(2): 173–182. (↑43), (↑59), (↑60), (↑117)

Maisha, T. (2014). The influence of topography and model grid resolution on extreme weather forecasts over South Africa. Msc dissertation, University of Pretoria. (↑51), (↑143)

Makhubu, N., Mudzuli, K. and Venter, Z. (2013). Hailstorm wreaks havoc, *IolNews* . (↑143)

Markowski, P. and Richardson, Y. (2014). Tornado formation, *Physics Today* **67**(9): 26. (↑46)

Marshall, J., Hitschfeld, W. and Gunn, K. (1955). Advances in radar weather, *Advances in geophysics*, Vol. 2, Elsevier, pp. 1–56. (↑59)

Martins, J. A., Brand, V. S., Capucim, M. N., Felix, R. R., Martins, L. D., Freitas, E. D., Gonçalves, F. L., Hallak, R., Dias, M. A. S. and Cecil, D. J. (2017). Climatology of destructive hailstorms in Brazil, *Atmospheric Research* **184**: 126–138. (↑2), (↑43)

Mason, S. J. and Jury, M. (1997). Climatic variability and change over southern Africa: a reflection on underlying processes, *Progress in Physical Geography* **21**(1): 23–50. (↑85), (↑119)

Mathee, A., Moyes, J., Mkhencele, T., Kleynhans, J., Piketh, S., Moroe, E., Wafawanaka, F., Martinson, N., McMorrow, M., Tempia, S. et al. (2021). Housing Quality in a Rural and an Urban Settlement in South Africa, *International Journal of Environmental Research and Public Health* **18**(5): 2240. (↑47), (↑55), (↑132), (↑158), (↑171)

Mather, G. K. (1991). Coalescence enhancement in large multicell storms caused by the emissions from a Kraft paper mill, *Journal of Applied Meteorology and Climatology* **30**(8): 1134–1146. (↑31)

Mather, G., Terblanche, D., Steffens, F. and Fletcher, L. (1997). Results of the South African cloud-seeding experiments using hygroscopic flares, *Journal of applied meteorology* **36**(11): 1433–1447. (↑31)

Mathias, L., Ludwig, P. and Pinto, J. G. (2019). Synoptic-scale conditions and convection-resolving hindcast experiments of a cold-season derecho on 3 January 2014 in western Europe, *Natural Hazards and Earth System Sciences* **19**(5): 1023–1040. (↑45), (↑87)

Matwitz, J. (1972). The structure and motion of severe hailstorms. Part III: Severely sheared storms, *Journal of Applied Meteorology* **11**: 189–201. (↑111), (↑114)

Mchunu, K. and Nkambule, S. (2019). An evaluation of access to adequate housing: A case study of eZamokuhle township, Mpumalanga; South Africa, *Cogent Social Sciences* **5**(1): 1653618. (↑157)

McPhillips, L. E., Chang, H., Chester, M. V., Depietri, Y., Friedman, E., Grimm, N. B., Kominoski, J. S., McPhearson, T., Méndez-Lázaro, P., Rosi, E. J. et al. (2018). Defining extreme events: A cross-disciplinary review, *Earth's Future* **6**(3): 441–455. (↑5)

Menne, M. J., Durre, I., Vose, R. S., Gleason, B. E. and Houston, T. G. (2012). An overview of the global historical climatology network-daily database, *Journal of Atmospheric and Oceanic Technology* **29**(7): 897–910. (↑37)

Merino, A., García-Ortega, E., López, L., Sánchez, J. and Guerrero-Higueras, A. (2013). Synoptic environment, mesoscale configurations and forecast parameters for hailstorms in Southwestern Europe, *Atmospheric Research* **122**: 183–198. (↑38)

Mitchell, T. and Schultz, D. M. (2020). A Synoptic Climatology of Spring Dryline Convection in the Southern Great Plains, *Weather and Forecasting* **35**(4): 1561–1582. (↑13)

Mitraka, Z., Chrysoulakis, N., Kamarianakis, Y., Partsinevelos, P. and Tsouchlaraki, A. (2012). Improving the estimation of urban surface emissivity based on sub-pixel classification of high resolution satellite imagery, *Remote Sensing of Environment* **117**: 125–134. (↑156)

Mohr, S. and Kunz, M. (2013). Recent trends and variabilities of convective parameters relevant for hail events in Germany and Europe, *Atmospheric Research* **123**: 211–228. (↑38), (↑39), (↑43), (↑170)

Molinari, J., Moore, P. and Idone, V. (1999). Convective structure of hurricanes as revealed by lightning locations, *Monthly Weather Review* **127**(4): 520–534. (↑121)

Moller, A. R., Doswell, C. A., Foster, M. P. and Woodall, G. R. (1994). The operational recognition of supercell thunderstorm environments and storm structures, *Weather and Forecasting* **9**(3): 327–347. (↑145)

Molongwane, C., Bopape, M.-J. M., Fridlind, A., Motshegwa, T., Matsui, T., Phaduli, E., Sehurutshi, B. and Maisha, R. (2020). Sensitivity of Botswana Ex-Tropical Cyclone Dineo rainfall simulations to cloud microphysics scheme, *AAS Open Research* **3**(30): 30. (↑143)

Morris, C. and Simmonds, I. (2000). Associations between varying magnitudes of the urban heat island and the synoptic climatology in Melbourne, Australia, *International Journal of Climatology: A Journal of the Royal Meteorological Society* **20**(15): 1931–1954. (↑46), (↑57)

Mudede, M. F., Newete, S. W., Abutaleb, K. and Nkongolo, N. (2020). Monitoring the urban environment quality in the city of Johannesburg using remote sensing data, *Journal of African Earth Sciences* **171**: 103969. (↑156), (↑157)

Musungu, K., Motala, S. and Smit, J. (2012). Using multi-criteria evaluation and GIS for flood risk analysis in informal settlements of Cape Town: the case of Graveyard Pond, *South African Journal of Geomatics* **1**(1): 92–108. (↑132)

Myhre, G., Shindell, D., Bréon, F.-M., Collins, W., Fuglestvedt, J., Jianping, H., Koch, D., Lamarque, J.-F., Lee, D. et al. (2013). Anthropogenic and Natural Radiative Forcing, *Climate Change 2013: The Physical Science Basis. Contribution of Working Group I to the Fifth Assessment Report of the Intergovernmental Panel on Climate Change*, Cambridge University Press, pp. 659–731. (↑22), (↑23), (↑24), (↑163)

Naidoo, S., Piketh, S. J. and Curtis, C. (2014). Quantification of emissions generated from domestic burning activities from townships in Johannesburg, *Clean Air Journal* **24**(1): 34–41. (↑132)

Nastos, P. and Matsangouras, I. (2014). Analysis of synoptic conditions for tornadic days over western Greece, *Natural Hazards and Earth System Sciences* **14**(9): 2409–2421. (↑46), (↑57)

National Academies of Sciences. (2016). *Attribution of Extreme Weather Events in the Context of Climate Change*, National Academies Press. (↑10), (↑11)

Nature (2019). It's time to talk about ditching statistical significance, *Nature* **567**: 283. (↑XIV)

Ndarana, T., Rammopo, T. S., Reason, C. J., Bopape, M.-J., Engelbrecht, F. and Chikoore, H. (2021). Two types of ridging South Atlantic Ocean anticyclones over South Africa and the associated dynamical processes, *Atmospheric Research* p. 105897. (↑18), (↑95), (↑116)

News24 (2008). Tornado kills teen in Eastern Cape, *News24* .
URL: *https://www.news24.com/news24/tornado-kills-teen-in-e-cape-20080220* (↑89)

Ngulani, T. and Shackleton, C. (2020). The degree, extent and value of air temperature amelioration by urban green spaces in Bulawayo, Zimbabwe, *South African Geographical Journal* **102**(3): 344–355. (↑132)

Nicholson, S. E. (2000). The nature of rainfall variability over Africa on time scales of decades to millenia, *Global and Planetary Change* **26**(1-3): 137–158. (↑11)

Nuzzo, R. (2014). Scientific method: statistical errors, *Nature News* **506**(7487): 150. (↑XIV)

Orlanski, I. (1975). A rational subdivision of scales for atmospheric processes, *Bulletin of the American Meteorological Society* **56**: 527–530. (↑VII), (↑6), (↑8)

Ortiz, L. E., González, J. E., Horton, R., Lin, W., Wu, W., Ramamurthy, P., Arend, M. and Bornstein, R. D. (2019). High-resolution projections of extreme heat in New York City, *International Journal of Climatology* **39**(12): 4721–4735. (↑31)

Otte, I., Detsch, F., Mwangomo, E., Hemp, A., Appelhans, T. and Nauss, T. (2017). Multidecadal trends and interannual variability of rainfall as observed from five lowland stations at Mt. Kilimanjaro, Tanzania, *Journal of Hydrometeorology* **18**(2): 349–361. (↑40)

Pal, S., Chang, H.-I., Castro, C. L. and Dominguez, F. (2019). Credibility of convection-permitting modeling to improve seasonal precipitation forecasting in the southwestern United States. (↑8), (↑51), (↑142)

Pante, G., Knippertz, P., Fink, A. H. and Kniffka, A. (2021). The potential of increasing man-made air pollution to reduce rainfall over southern West Africa, *Atmospheric chemistry and physics* **21**(1): 35–55. (↑21), (↑163), (↑164), (↑169)

Paruk, B. and Blackwell, S. (1994). A severe thunderstorm climatology for Alberta, *National Weather Digest* **19**(1): 27–33. (↑43)

Penner, J. E., Andreae, M., Annegarn, H., Barrie, L., Feichter, J., Hegg, D., Jayaraman, A., Leaitch, R., Murphy, D., Nganga, J. et al. (2001). Aerosols, their direct and indirect effects, *Climate Change 2001: The Scientific Basis. Contribution of Working Group I to the Third Assessment Report of the Intergovernmental Panel on Climate Change*, Cambridge University Press, pp. 289–348. (↑22)

Peterson, D. A., Fromm, M. D., Solbrig, J. E., Hyer, E. J., Surratt, M. L. and Campbell, J. R. (2017). Detection and inventory of intense pyroconvection in western North America using GOES-15 daytime infrared data, *Journal of Applied Meteorology and Climatology* **56**(2): 471–493. (↑30)

Peterson, D. A., Hyer, E. J., Campbell, J. R., Fromm, M. D., Hair, J. W., Butler, C. F. and Fenn, M. A. (2015). The 2013 Rim Fire: Implications for predicting extreme fire spread, pyroconvection, and smoke emissions, *Bulletin of the American Meteorological Society* **96**(2): 229–247. (↑30)

Piketh, S., Annegarn, H. and Tyson, P. (1999). Lower tropospheric aerosol loadings over South Africa: The relative contribution of aeolian dust, industrial emissions, and biomass burning, *Journal of Geophysical Research: Atmospheres* **104**(D1): 1597–1607. (↑24)

Piketh, S., Formenti, P., Annegarn, H. and Tyson, P. (1999). Industrial aerosol characterisation at a remote site in South Africa, *Nuclear Instruments and Methods in Physics Research Section B: Beam Interactions with Materials and Atoms* **150**(1-4): 350–355. (↑24)

Piketh, S., Vogel, C., Dunsmore, S., Culwick, C., Engelbrecht, F. and Akoon, I. (2014). Climate change and urban development in southern Africa: The case of Ekurhuleni Municipality (EMM) in South Africa, *Water SA* **40**(4): 749–758. (↑3), (↑13)

Powell, C. L. and Burger, R. P. (2014). The severe Gauteng hailstorms of 28 November 2013, South African Atmospheric Society (SASAS). (↑143)

Powers, J. G., Klemp, J. B., Skamarock, W. C., Davis, C. A., Dudhia, J., Gill, D. O., Coen, J. L., Gochis, D. J., Ahmadov, R., Peckham, S. E. et al. (2017). The weather research and forecasting model: Overview, system efforts, and future directions, *Bulletin of the American Meteorological Society* **98**(8): 1717–1737. (↑27), (↑50)

Prein, A. F., Holland, G. J., Rasmussen, R. M., Clark, M. P. and Tye, M. R. (2016). Running dry: The US Southwest's drift into a drier climate state, *Geophysical Research Letters* **43**(3): 1272–1279. (↑8), (↑14)

Prein, A. F., Langhans, W., Fosser, G., Ferrone, A., Ban, N., Goergen, K., Keller, M., Tölle, M., Gutjahr, O., Feser, F. et al. (2015). A review on regional convection-permitting climate modeling: Demonstrations, prospects, and challenges, *Reviews of Geophysics* **53**(2): 323–361. (↑8), (↑51), (↑142)

Prein, A. F., Liu, C., Ikeda, K., Trier, S. B., Rasmussen, R. M., Holland, G. J. and Clark, M. P. (2017). Increased rainfall volume from future convective storms in the US, *Nature Climate Change* **7**(12): 880. (↑14), (↑28), (↑29), (↑32)

Prein, A., Gobiet, A., Suklitsch, M., Truhetz, H., Awan, N., Keuler, K. and Georgievski, G. (2013). Added value of convection permitting seasonal simulations, *Climate Dynamics* **41**(9-10): 2655–2677. (↑8), (↑51), (↑142), (↑143)

Punge, H. and Kunz, M. (2016). Hail observations and hailstorm characteristics in Europe: A review, *Atmospheric Research* **176**: 159–184. (↑6)

Qian, Y., Yang, Z., Feng, Z., Liu, Y., Gustafson, W. I., Berg, L. K., Huang, M., Yang, B. and Ma, H. Y. (2020). Neglecting irrigation contributes to the simulated summertime warm-and-dry bias in the central United States, *NPJ Climate and Atmospheric Science* **3**(1): 1–10. (↑9), (↑164)

Quagraine, K. A., Hewitson, B., Jack, C., Pinto, I. and Lennard, C. (2019). A methodological approach to assess the co-behavior of climate processes over southern Africa, *Journal of Climate* **32**(9): 2483–2495. (↑14)

Rae, K. (2014). A Modified Supercell Composite Parameter for Supercell thunderstorms over the Gauteng Province, South Africa. MSc dissertation, University of Pretoria. (↑118), (↑146)

Rahlaga, M. (2013). Power failures in Gauteng after storms, *Eye Witness News* . (↑2), (↑6), (↑143)

Ratna, S. B., Ratnam, J., Behera, S., Ndarana, T., Takahashi, K., Yamagata, T. et al. (2014). Performance assessment of three convective parameterization schemes in WRF for downscaling summer rainfall over South Africa, *Climate Dynamics* **42**(11-12): 2931–2953. (↑51), (↑143)

Reason, C. and Keibel, A. (2004). Tropical cyclone Eline and its unusual penetration and impacts over the southern African mainland, *Weather and Forecasting* **19**(5): 789–805. (↑11), (↑33)

Rodríguez, O. and Bech, J. (2020). Tornadic environments in the Iberian Peninsula and the Balearic Islands based on ERA5 reanalysis, *International Journal of Climatology* . (↑87)

Rose, W. I., Delene, D., Schneider, D., Bluth, G., Krueger, A., Sprod, I., McKee, C., Davies, H. and Ernst, G. G. (1995). Ice in the 1994 Rabaul eruption cloud: implications for volcano hazard and atmospheric effects, *Nature* **375**(6531): 477. (↑30)

Rosenfeld, D., Andreae, M. O., Asmi, A., Chin, M., de Leeuw, G., Donovan, D. P., Kahn, R., Kinne, S., Kivekäs, N., Kulmala, M. et al. (2014). Global observations of aerosol-cloud-precipitation-climate interactions, *Reviews of Geophysics* **52**(4): 750–808. (↑3), (↑16)

Rosenfeld, D. and Lensky, I. M. (1998). Satellite-based insights into precipitation formation processes in continental and maritime convective clouds, *Bulletin of the American Meteorological Society* **79**(11): 2457–2476. (↑15)

Rosenfeld, D., Lohmann, U., Raga, G. B., O'Dowd, C. D., Kulmala, M., Fuzzi, S., Reissell, A. and Andreae, M. O. (2008). Flood or drought: How do aerosols affect precipitation?, *Science* **321**(5894): 1309–1313. (↑20), (↑21), (↑163), (↑169)

Rosenfeld, D. and Woodley, W. L. (2000). Deep convective clouds with sustained supercooled liquid water down to -37.5°C, *Nature* **405**(6785): 440. (↑18), (↑19)

Rosenfeld, D., Woodley, W. L., Lerner, A., Kelman, G. and Lindsey, D. T. (2008). Satellite detection of severe convective storms by their retrieved vertical profiles of cloud particle effective radius and thermodynamic phase, *Journal of Geophysical Research: Atmospheres* **113**(D4). (↑18)

Ross, K., Piketh, S., Bruintjes, R., Burger, R., Swap, R. and Annegarn, H. (2003). Spatial and seasonal variations in CCN distribution and the aerosol-CCN relationship over southern Africa, *Journal of Geophysical Research: Atmospheres* **108**(D13). (↑15), (↑21), (↑22), (↑24), (↑25), (↑54), (↑155), (↑168), (↑171)

Sailor, D. J. (1995). Simulated urban climate response to modifications in surface albedo and vegetative cover, *Journal of Applied Meteorology and Climatology* **34**(7): 1694–1704. (↑55), (↑157)

Satterthwaite, D., Archer, D., Colenbrander, S., Dodman, D., Hardoy, J., Mitlin, D. and Patel, S. (2020). Building resilience to climate change in informal settlements, *One Earth* **2**(2): 143–156. (↑132)

Sawdis (2013). Real Time Storm Observation: Krugerdorp, *S.A. Weather and Disaster Information Service (SAWDIS)* .
URL: *https://saweatherobserver.blogspot.co.za/2011/10/real-time-storm-observation-krugerdorp.html* (↑6), (↑143)

SAWS (2018). SAWS Infrastructure.
URL: *http://www.weathersa.co.za/about-us/overview/* (↑35)

Scheifinger, H. and Held, G. (1997). Aerosol behaviour on the South African highveld, *Atmospheric Environment* **31**(21): 3497–3509. (↑34)

Schemm, S., Nisi, L., Martinov, A., Leuenberger, D. and Martius, O. (2016). On the link between cold fronts and hail in Switzerland, *Atmospheric Science Letters* **17**(5): 315–325. (↑146)

Schnaiter, M., Järvinen, E., Ahmed, A. and Leisner, T. (2018). PHIPS-HALO: the airborne Particle Habit Imaging and Polar Scattering probe. Part 2: Characterization and first results, *Atmospheric Measurement Techniques* **11**(1): 341. (↑8)

Schoeman, F., Newby, T., Thompson, M. and Van den Berg, E. C. (2013). South African national land-cover change map, *South African Journal of Geomatics* **2**(2): 94–105. (↑46)

Schultz, D. M., Schumacher, P. N. and Doswell, C. A. (2000). The intricacies of instabilities, *Monthly Weather Review* **128**(12): 4143–4148. (↑17), (↑18)

Schulze, B. (1965). Hail and thunderstorm frequency in South Africa, *Notos* **14**: 67–71. (↑13), (↑45), (↑48), (↑85)

Scott, A. A., Misiani, H., Okoth, J., Jordan, A., Gohlke, J., Ouma, G., Arrighi, J., Zaitchik, B. F., Jjemba, E., Verjee, S. et al. (2017). Temperature and heat in informal settlements in Nairobi, *PloS One* **12**(11): e0187300. (↑132)

Scovronick, N., Lloyd, S. J. and Kovats, R. S. (2015). Climate and health in informal urban settlements, *Environment and Urbanization* **27**(2): 657–678. (↑132)

Segele, Z. T., Leslie, L. M. and Lamb, P. J. (2013). Weather Research and Forecasting Model simulations of extended warm-season heavy precipitation episode over the US Southern Great Plains: data assimilation and microphysics sensitivity experiments, *Tellus A: Dynamic Meteorology and Oceanography* **65**. (↑50)

Seinfeld, J. H., Bretherton, C., Carslaw, K. S., Coe, H., DeMott, P. J., Dunlea, E. J., Feingold, G., Ghan, S., Guenther, A. B., Kahn, R. et al. (2016). Improving our fundamental understanding of the role of aerosol- cloud interactions in the climate system, *Proceedings of the National Academy of Sciences* **113**(21): 5781–5790. (↑9), (↑18)

Sequera, P., González, J. E., McDonald, K., LaDochy, S. and Comarazamy, D. (2016). Improvements in land-use classification for estimating daytime surface temperatures and sea-breeze flows in Southern California, *Earth Interactions* **20**(16): 1–32. (↑54)

Sherburn, K. D. and Parker, M. D. (2014). Climatology and ingredients of significant severe convection in high-shear, low-CAPE environments, *Weather and Forecasting* **29**(4): 854–877. (↑18), (↑114), (↑146)

Sheridan, S. C. and Lee, C. C. (2011). The self-organizing map in synoptic climatological research, *Progress in Physical Geography* **35**(1): 109–119. (↑14)

Simpson, L.-A. and Dyson, L. L. (2018). Severe weather over the Highveld of South Africa during November 2016, *Water SA* **44**(1): 75–85. (↑83), (↑111), (↑114), (↑118)

Sindhu, K. D. and Bhat, G. (2019). Storm characteristics and precipitation estimates of monsoonal clouds using C-band polarimetric radar over Northwest India, *Theoretical and Applied Climatology* **138**(1-2): 237–248. (↑73)

Sisodiya, A., Pattnaik, S., Baisya, H., Bhat, G. and Turner, A. (2019). Simulation of location-specific severe thunderstorm events using high resolution land data assimilation, *Dynamics of Atmospheres and Oceans* **87**: 101098. (↑46), (↑87)

Smuts, J. C. (1926). *Holism and Evolution*, Macmillan and Co. (↑XIII)

Sobrino, J., Raissouni, N. and Li, Z.-L. (2001). A comparative study of land surface emissivity retrieval from NOAA data, *Remote Sensing of Environment* **75**(2): 256–266. (↑156)

Solmon, F., Elguindi, N., Mallet, M., Flamant, C. and Formenti, P. (2021). West African monsoon precipitation impacted by the South Eastern Atlantic biomass burning aerosol outflow, *npj Climate and Atmospheric Science* **4**(1): 1–7. (↑21), (↑163), (↑164), (↑169)

Somses, S., Bopape, M.-J. M., Ndarana, T., Fridlind, A., Matsui, T., Phaduli, E., Limbo, A., Maikhudumu, S., Maisha, R. and Rakate, E. (2020). Convection Parametrization and Multi-Nesting Dependence of a Heavy Rainfall Event over Namibia with Weather Research and Forecasting (WRF) Model, *Climate* **8**(10): 112. (↑45), (↑143)

Squires, P. (1958a). The microstructure and colloidal stability of warm clouds, *Tellus A: Dynamic Meteorology and Oceanography* **10**(2): 262–271. (↑15), (↑16)

Squires, P. (1958b). The microstructure and colloidal stability of warm clouds: Part II - The causes of the variations in microstructure, *Tellus A: Dynamic Meteorology and Oceanography* **10**(2): 262–271. (↑15), (↑16)

Starzec, M., Mullendore, G. L. and Kucera, P. A. (2018). Using radar reflectivity to evaluate the vertical structure of forecast convection, *Journal of Applied Meteorology and Climatology* **57**(12): 2835–2849. (↑42), (↑43)

Stein, T., Keat, W., Maidment, R., Landman, S., Becker, E., Boyd, D., Bodas-Salcedo, A., Pankiewicz, G. and Webster, S. (2019). An evaluation of clouds and precipitation in convection-permitting forecasts for South Africa, *Weather and Forecasting* **34**(1): 233–254. (↑9), (↑42), (↑43), (↑60), (↑143)

Stocker, T. F., Qin, D., Plattner, G.-K., Tignor, M., Allen, S. K., Boschung, J., Nauels, A., Xia, Y., Bex, V., Midgley, P. M. et al. (2013). *Climate Change 2013: The Physical Science Basis. Contribution of Working Group I to the Fifth Assessment Report of the Intergovernmental Panel on Climate Change*, Cambridge University Press, Cambridge, United Kingdom and New York, NY, USA. (↑22), (↑23), (↑24), (↑163)

Stolz, D. C., Businger, S. and Terpstra, A. (2014). Refining the relationship between lightning and convective rainfall over the ocean, *Journal of Geophysical Research: Atmospheres* **119**(2): 964–981. (↑43)

Stull, R. B. (2018). *Practical Meteorology: An Algebra-based Survey of Atmospheric Science*, University of British Columbia. (↑61)

Swain, D. L., Singh, D., Touma, D. and Diffenbaugh, N. S. (2020). Attributing extreme events to climate change: A new frontier in a warming world, *One Earth* **2**(6): 522–527. (↑10), (↑11)

Takayabu, Y. N. (2006). Rain-yield per flash calculated from TRMM PR and LIS data and its relationship to the contribution of tall convective rain, *Geophysical Research Letters* **33**(18). (↑43), (↑60), (↑121)

Taljaard, J. J. (1981). *Upper-air circulation, temperature and humidity over southern Africa*, Weather Bureau, Department of Transport. (↑45), (↑85)

Tang, B. H., Gensini, V. A. and Homeyer, C. R. (2019). Trends in United States large hail environments and observations, *NPJ Climate and Atmospheric Science* **2**(1): 1–7. (↑146)

Taszarek, M., Allen, J. T., Groenemeijer, P., Edwards, R., Brooks, H. E., Chmielewski, V. and Enno, S.-E. (2020). Severe convective storms across Europe and the United States. Part I: Climatology of lightning, large hail, severe wind, and tornadoes, *Journal of Climate* **33**(23): 10239–10261. (↑46), (↑87), (↑121)

Taszarek, M., Allen, J. T., Marchio, M. and Brooks, H. E. (2021). Global climatology and trends in convective environments from ERA5 and rawinsonde data, *NPJ Climate and Atmospheric Science* **4**(1): 1–11. (↑13)

Taszarek, M., Allen, J. T., Púčik, T., Hoogewind, K. A. and Brooks, H. E. (2020). Severe convective storms across Europe and the United States. Part II: ERA5 environments associated with lightning, large hail, severe wind, and tornadoes, *Journal of Climate* **33**(23): 10263–10286. (↑46), (↑86), (↑87)

Taszarek, M., Kendzierski, S. and Pilguj, N. (2020). Hazardous weather affecting European airports: Climatological estimates of situations with limited visibility, thunderstorm, low-level wind shear and snowfall from ERA5, *Weather and Climate Extremes* **28**: 100243. (↑18), (↑45), (↑46), (↑86), (↑87)

Taylor, C. M., Belušić, D., Guichard, F., Parker, D. J., Vischel, T., Bock, O., Harris, P. P., Janicot, S., Klein, C. and Panthou, G. (2017). Frequency of extreme Sahelian storms tripled since 1982 in satellite observations, *Nature* **544**(7651): 475–478. (↑88)

Terblanche, D., Mittermaier, M., Burger, R., Piketh, S. and Bruintjes, R. (2000). The Aerosol Recirculation and Rainfall Experiment (ARREX): An initial study on aerosol-cloud interactions over South Africa, *South African Journal of Science* **96**(1). (↑16), (↑24), (↑54), (↑168)

Terblanche, D., Pegram, G. and Mittermaier, M. (2001). The development of weather radar as a research and operational tool for hydrology in South Africa, *Journal of Hydrology* **241**(1-2): 3–25. (↑118)

Tessendorf, S. A., Bruintjes, R. T., Weeks, C., Wilson, J. W., Knight, C. A., Roberts, R. D., Peter, J. R., Collis, S., Buseck, P. R., Freney, E. et al. (2012). The Queensland cloud seeding research program, *Bulletin of the American Meteorological Society* **93**(1): 75–90. (↑30)

Thompson, G. and Eidhammer, T. (2014). A study of aerosol impacts on clouds and precipitation development in a large winter cyclone, *Journal of the Atmospheric Sciences* **71**(10): 3636–3658. (↑27), (↑28), (↑54), (↑157)

Thompson, G., Field, P. R., Rasmussen, R. M. and Hall, W. D. (2008). Explicit forecasts of winter precipitation using an improved bulk microphysics scheme. Part II: Implementation of a new snow parameterization, *Monthly Weather Review* **136**(12): 5095–5115. (↑27), (↑54)

Thompson, G., Tewari, M., Ikeda, K., Tessendorf, S., Weeks, C., Otkin, J. and Kong, F. (2016). Explicitly-coupled cloud physics and radiation parameterizations and subsequent evaluation in WRF high-resolution convective forecasts, *Atmospheric Research* **168**: 92–104. (↑26)

Thompson, R. L., Edwards, R., Hart, J. A., Elmore, K. L. and Markowski, P. (2003). Close proximity soundings within supercell environments obtained from the Rapid Update Cycle, *Weather and Forecasting* **18**(6): 1243–1261. (↑146)

Thompson, R. L., Mead, C. M. and Edwards, R. (2007). Effective storm-relative helicity and bulk shear in supercell thunderstorm environments, *Weather and Forecasting* **22**(1): 102–115. (↑114)

TimesLive (2013). Ekurhuleni medics on severe weather stand by, *Times Live* .
URL: *http://www.timeslive.co.za/local/2012/11/09/ekurhuleni-medics-on-severe-weather-stand-by* (↑2)

TimesLive (2018). Almost 200 hotel rooms damaged by severe storm at Sun City, *Times Live* .
URL: *https://www.timeslive.co.za/news/south-africa/2018-12-16-almost-200-hotel-rooms-affected-by-severe-storm-at-sun-city/* (↑122)

Tippett, M. K., Allen, J. T., Gensini, V. A. and Brooks, H. E. (2015). Climate and hazardous convective weather, *Current Climate Change Reports* **1**(2): 60–73. (↑6), (↑44)

Tomsett, A. C. and Toumi, R. (2000). Diurnal temperature range and rainfall probability over the United Kingdom, *Geophysical research letters* **27**(9): 1279–1282. (↑65)

Tosca, M., Diner, D., Garay, M. and Kalashnikova, O. (2015). Human-caused fires limit convection in tropical Africa: First temporal observations and attribution, *Geophysical Research Letters* **42**(15): 6492–6501. (↑21), (↑135), (↑138), (↑163), (↑164), (↑169)

Trapp, R. J., Diffenbaugh, N. S., Brooks, H. E., Baldwin, M. E., Robinson, E. D. and Pal, J. S. (2007). Changes in severe thunderstorm environment frequency during the 21st century caused by anthropogenically enhanced global radiative forcing, *Proceedings of the National Academy of Sciences* **104**(50): 19719–19723. (↑170)

Trenberth, K. E. (2012). Framing the way to relate climate extremes to climate change, *Climatic Change* **115**(2): 283–290. (↑170)

Twomey, S. (1974). Pollution and the planetary albedo, *Atmospheric Environment (1967)* **8**(12): 1251–1256. (↑22), (↑23), (↑163)

Twomey, S. (1977). The influence of pollution on the shortwave albedo of clouds, *Journal of the Atmospheric Sciences* **34**(7): 1149–1152. (↑22), (↑23), (↑163)

Tyson, P. D. (1986). *Climatic Change and Variability in Southern Africa*, Oxford University Press, USA. (↑45)

Tyson, P. D. and Preston-Whyte, R. A. (2000). *The Weather and Climate of Southern Africa*, Oxford University Press. (↑10), (↑11), (↑12), (↑13), (↑17), (↑18), (↑19), (↑45), (↑87), (↑111)

Tyson, P., Du Toit, W. and Fuggle, R. (1972). Temperature structure above cities: review and preliminary findings from the Johannesburg urban heat island project, *Atmospheric Environment* **6**(8): 533–542. (↑31), (↑32), (↑46), (↑127), (↑128)

Van Den Heever, S. C. and Cotton, W. R. (2007). Urban aerosol impacts on downwind convective storms, *Journal of Applied Meteorology and Climatology* **46**(6): 828–850. (↑28)

Van Der Mescht, D. (2012). Mountain wave turbulence in the lee of the Hex River Mountains. Msc dissertation, Stellenbosch University. (↑123)

Van Der Mescht, D. and Eloff, P. (2013). Mountain wave-induced rotors in the lee of the Hex River Mountains, *South African Geographical Journal* **95**(1): 117–131. (↑123)

Van Schalkwyk, L. and Dyson, L. L. (2013). Climatological characteristics of fog at Cape Town International airport, *Weather and Forecasting* **28**(3): 631–646. (↑14)

Varga, Á. J. and Breuer, H. (2020). Sensitivity of simulated temperature, precipitation, and global radiation to different WRF configurations over the Carpathian Basin for regional climate applications, *Climate Dynamics* **55**(9): 2849–2866. (↑52)

Varghese, M., Prabha, T. V., Malap, N., Resmi, E., Murugavel, P., Safai, P., Axisa, D., Pandithurai, G. and Dani, K. (2016). Airborne and ground based CCN spectral characteristics: Inferences from CAIPEEX–2011, *Atmospheric Environment* **125**: 324–336. (↑54)

Visser, P. J. (2001). The Storm-Structure-Severity method for the identification of convective storm characteristics with conventional weather radar, *Meteorological Applications* **8**(1): 1–10. (↑73), (↑148)

Von Storch, H., Kiladis, G. and Madden, R. (2004). Interview with Harry van Loon on 4 September 2004, *Niels Bohr Library & Archives, American Institute of Physics, College Park, MD USA* . (↑87)

Vonnegut, B. (1947). The nucleation of ice formation by silver iodide, *Journal of Applied Physics* **18**(7): 593–595. (↑30)

Voormansik, T., Müürsepp, T. and Post, P. (2021). Climatology of Convective Storms in Estonia from Radar Data and Severe Convective Environments, *Remote Sensing* **13**(11): 2178. (↑59)

Waldvogel, A., Federer, B. and Grimm, P. (1979). Criteria for the detection of hail cells, *Journal of Applied Meteorology* **18**(12): 1521–1525. (↑73)

Wallace, J. M. and Hobbs, P. V. (2006). *Atmospheric Science: An Introductory Survey*, Vol. 92, Elsevier. (↑14), (↑15), (↑16), (↑17)

Wang, X., Tolksdorf, V., Otto, M. and Scherer, D. (2021). WRF-based dynamical downscaling of ERA5 reanalysis data for High Mountain Asia: Towards a new version of the High Asia Refined analysis, *International Journal of Climatology* **41**(1): 743–762. (↑52)

Warren, R. A., Ramsay, H. A., Siems, S. T., Manton, M. J., Peter, J. R., Protat, A. and Pillalamarri, A. (2020). Radar-based climatology of damaging hailstorms in Brisbane and Sydney, Australia, *Quarterly Journal of the Royal Meteorological Society* **146**(726): 505–530. (↑73)

Washington, R. and Howard, E. (2019). Dry-lines in Southern Africa: Rediscovering the Congo Air Boundary, *Journal of Climate* **32**(23). (↑88), (↑90)

Wasserstein, R. L., Schirm, A. L. and Lazar, N. A. (2019). Moving to a world beyond "p< 0.05". (↑XIV)

WEF (2018). *The Global Risks Report 2018*, World Economic Forum. (↑2), (↑3)

Wheatley, D. M. and Stensrud, D. J. (2010). The impact of assimilating surface pressure observations on severe weather events in a WRF mesoscale ensemble system, *Monthly Weather Review* **138**(5): 1673–1694. (↑8)

Wilson, J. W., Crook, N. A., Mueller, C. K., Sun, J. and Dixon, M. (1998). Nowcasting thunderstorms: A status report, *Bulletin of the American Meteorological Society* **79**(10): 2079–2100. (↑148)

Wolski, P., Jack, C., Tadross, M., van Aardenne, L. and Lennard, C. (2018). Interannual rainfall variability and SOM-based circulation classification, *Climate Dynamics* **50**(1): 479–492. (↑14), (↑95)

Wright, C. Y., Kapwata, T., Du Preez, D. J., Wernecke, B., Garland, R. M., Nkosi, V., Landman, W. A., Dyson, L. and Norval, M. (2021). Major climate change-induced risks to human health in South Africa, *Environmental Research* **196**: 110973. (↑2)

Yano, J.-I., Ziemiański, M. Z., Cullen, M., Termonia, P., Onvlee, J., Bengtsson, L., Carrassi, A., Davy, R., Deluca, A., Gray, S. L. et al. (2018). Scientific challenges of convective-scale numerical weather prediction, *Bulletin of the American Meteorological Society* **99**(4): 699–710. (↑8), (↑9)

Yarnal, B. (1993). *Synoptic Climatology in Environmental analysis: A Primer*, Belhaven. (↑46), (↑57)

Yin, J., Zhan, X., Zheng, Y., Hain, C. R., Ek, M., Wen, J., Fang, L. and Liu, J. (2016). Improving Noah land surface model performance using near real time surface albedo and green vegetation fraction, *Agricultural and Forest Meteorology* **218**: 171–183. (↑55)

Yu, H., Kaufman, Y., Chin, M., Feingold, G., Remer, L., Anderson, T., Balkanski, Y., Bellouin, N., Boucher, O., Christopher, S. et al. (2006). A review of measurement-based assessments of the aerosol direct radiative effect and forcing, *Atmospheric Chemistry and Physics* **6**(3): 613–666. (↑22)

Zan, B., Yu, Y., Dong, L., Li, J., Zhao, G. and Zhang, T. (2020). Numerical Study of the Impact of Complex Terrain and Soil Moisture on Convective Initiation, *Atmosphere* **11**(8): 871. (↑52)

Zhang, Y., Hemperly, J., Meskhidze, N. and Skamarock, W. C. (2012). The global Weather Research and Forecasting (GWRF) model: model evaluation, sensitivity study, and future year simulation, *Atmospheric and Climate Sciences* **2**(3): 231–253. (↑50)

Appendix

Chapter 3: Cluster analysis mslp and zg500 supporting data

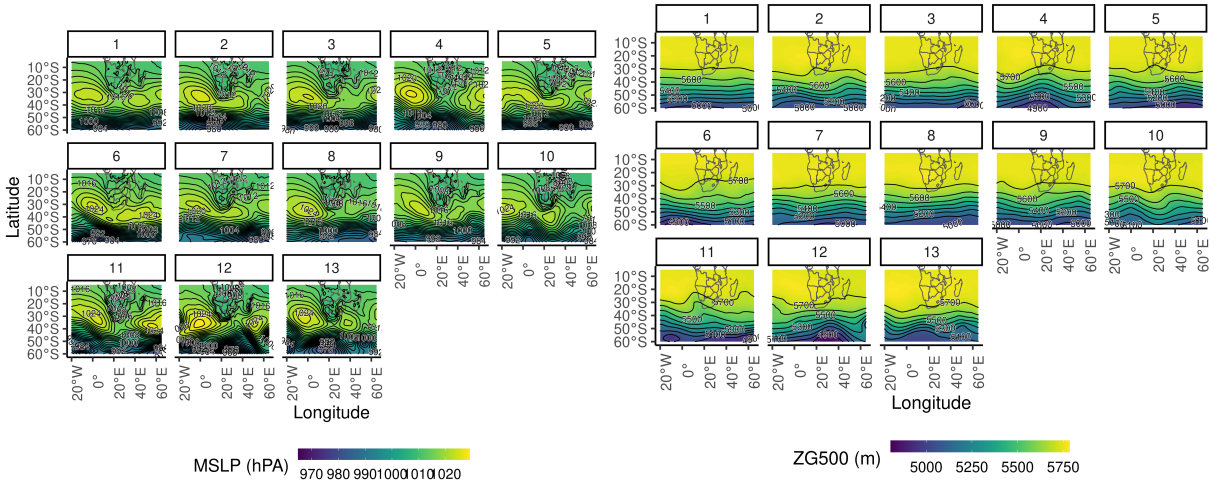

Figure 1: *MSLP and ZG500 of significant hail events*

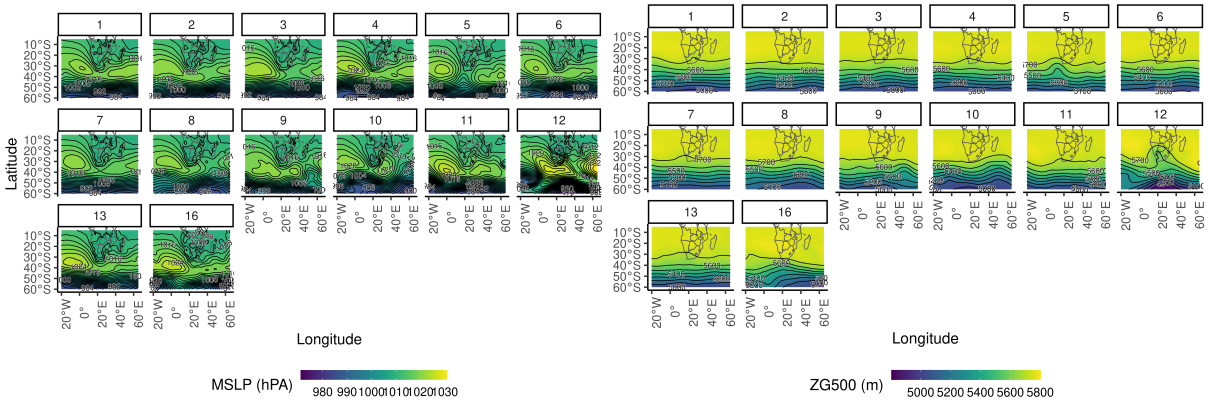

Figure 2: *MSLP and ZG500 of significant rain events*

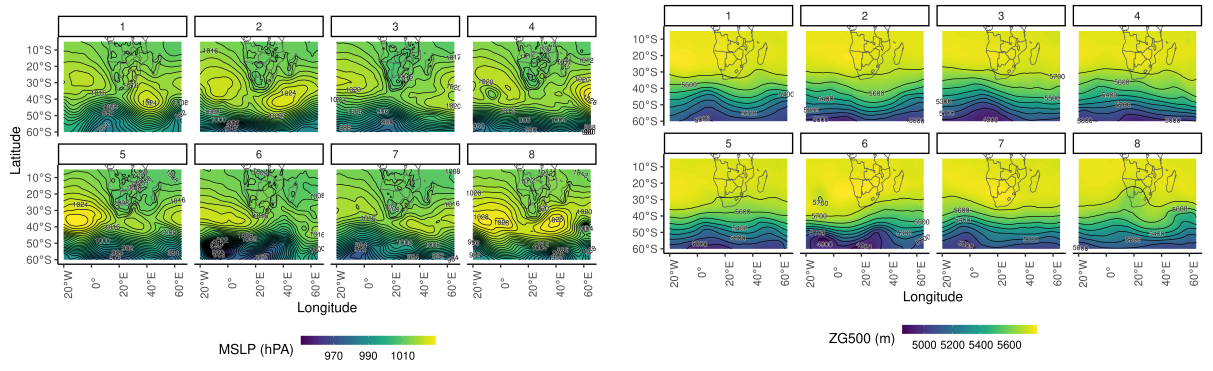

Figure 3: *MSLP and ZG500 of significant thunderstorm events*

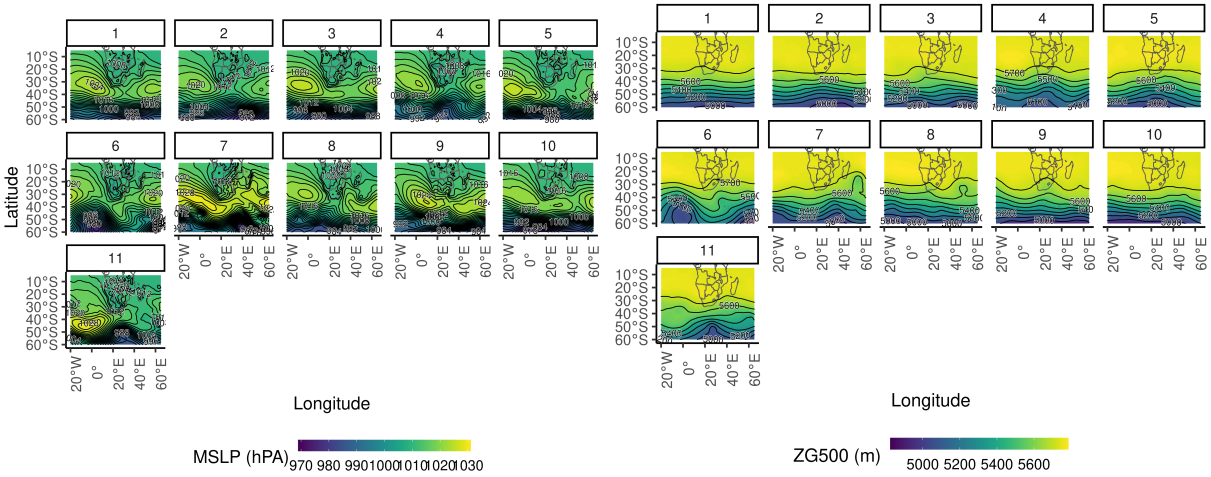

Figure 4: *MSLP and ZG500 of significant lightning events*

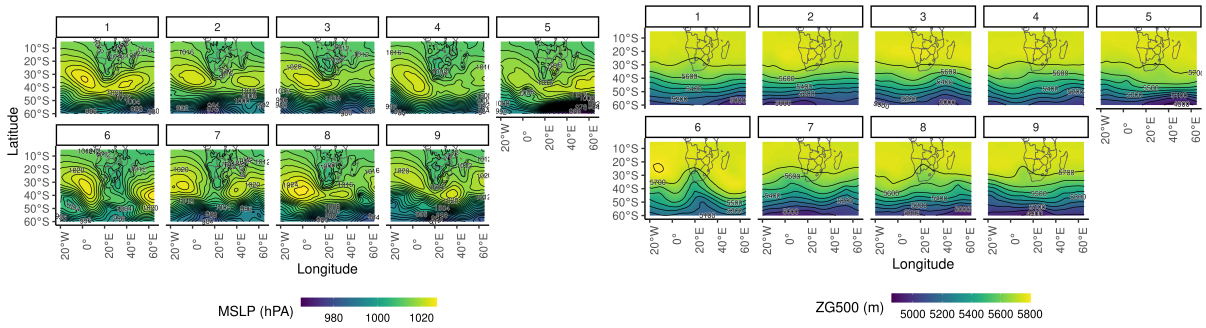

Figure 5: *MSLP and ZG500 of significant tornado events*

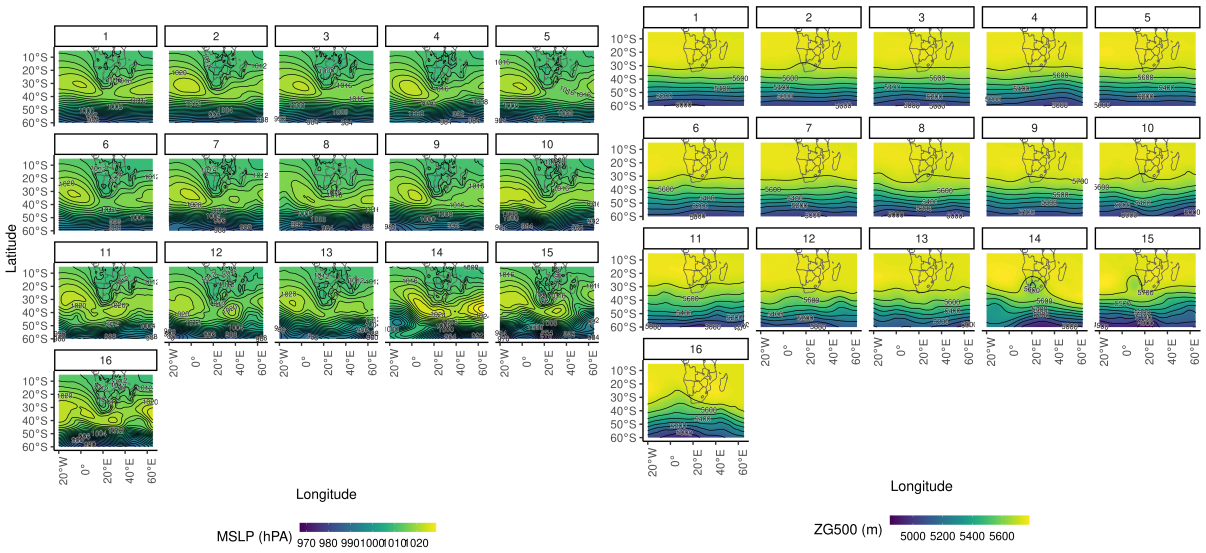

Figure 6: *MSLP and ZG500 of all significant convective events*